New Redox Active Ion Sensors :

Synthetic, Electrochemical, Spectroscopic and Guest Binding Studies

Hilary Jean Noelle Hartigan

PhD Thesis

University of Edinburgh

2002

Declaration

Except where specific reference is made to other sources, the work contained in this thesis is the original work of the author. It has not been submitted in whole or in part, for any other degree

Hilary Hartigan

Dedication

This thesis is dedicated in its entirety, to my Mum and Dad without whom, I would never have seen my dreams come true.....

with all my love

"The Great Tragedy of Science ;
The slaying of a beautiful hypothesis by an Ugly Fact"

Thomas H. Huxley, 1825-1895

Acknowledgements

My very special thanks go to my two supervisors Dr. Neil Robertson and Dr. Andy Mount, for their constant support and encouragement and their un-ending enthusiasm. A special thank-you to Neil for his friendship over the last four, very eventful years.

This thesis would also not be possible without the help of those who have supported the work, most especially throughout the final year. A very special thank-you to Dr. Lesley Yellowless for allowing me endless access to her lab and equipment and also the many chats, both work and non-work related. Dr Simon Parsons and Dr Andy Parkin are owed a special thank-you for their patience with my 'crystals'. The final stages of this work were made easier with the added support of Prof.s Peter Tasker and Steve Chapman. A special thank-you also goes to Donald Robertson who gave me every support especially in the closing stages of the lab work.

To everyone, past and present, in the Robertson and Mount groups especially Lorna, Lee, Sarah, Dave, Madeline and Chris who helped me over the last few years, and made the last year in the lab a lot easier. Also thanks go to Georg Seeber, who is responsible for some of the initial lab-work in this area.

A special thank-you goes to all my friends to whom I owe so much – to Lizzie, Ken and Andy, with whom I have shared so much over the last three years – some memorable (and some best forgotten) moments – but all good. To Jen, for her constant cheerfulness and life-long friendship and to Liam and John who have always been very 'amusingly' honest with me - always managing to make me smile. To Alex and Mel – 'Harri' has grown on me after 3 years...

A very special thank-you also to Bryony, my cousin and my friend, who probably 'knows this thesis better than I do'.

Finally, to my entire family, especially to my mum and dad, without whom, this thesis would never have become a reality. I owe you both more than I can ever repay. This thesis is dedicated to you.

Abstract

The preparation of two new [18]ane S_4N_2 macrocycles with conjugated links to redox-active Co centres has been achieved [$(CpCo)_2$ S_4N_2 and (CpCo) S_4N_2 via reaction of an [18]ane S_4N_2 bisthione macrocycle with CpCoLL, LL = COD or $(CO)_2$. Optimisation of this reaction has lead to a high yielding and selective route to the ligand containing one Co centre The characterisation of these complexes is described in detail and includes a study of the spectro-electrochemical, electrochemical, EPR and UV-Vis spectroscopic data.

The second section of this thesis concentrates on complexation studies of these redox-active cobalt macrocycles with a variety of transition metal ions. The metal ions are a mixture of late transition metal and heavy metal ions and include possible pollutant species present within aqueous environmental systems. They include, Ag^{I}, Fe^{II}, Co^{II}, Ni^{II}, Cu^{I}, Cu^{II}, Pb^{II}, Cd^{II}, Hg^{II}, and Sn^{II}. The studies were carried out in a variety of solvent systems and complexations were followed by modifications in electrochemical behaviour and UV/Vis spectroscopy. Strong interactions were observed, between the Co centre and the guest metal ion in the macrocycle in several cases and encouraging results are reported indicating the use of these systems in Ion Sensing. In particular the complexation study carried out with Ag^{I} and Ni^{II} proved to be the most significant. A route to the method of complexation of the ions, Ag^{I}, Fe^{II}, Co^{II}, Ni^{II}, Cu^{I}, and Cu^{II} is proposed with a suggestion for an alternative pathway for the complexation of the heavier metals, Sn^{II}, Pb^{II}, Hg^{II} and Cd^{II} is also given.

The final section of the thesis deals with the variety of other routes employed in the deprotection of the [18]ane S_4N_2 thione- and analogous ketone macrocycles. A successful route to the deprotection of the [18]ane S_4N_2 ketone macrocycle using photochemical techniques is described and is used to synthesise two new macrocycles with conjugated links to redox-active Ni centres. Characterisation of these species involved UV-Vis spectroscopy and cyclic voltammetry. Other routes

towards the deprotection of the thione and ketone macrocycles are also discussed and include a variety of reactions involving base deprotection with NaOMe, H_2O, TMAOH and $Cs(OH)_2$.

Abbreviations

[18]ane S_4N_2 donor macrocycle 18 membered macrocycle with 4 S donor and 2 N donor atoms. See page xx for structure

Chemicals, Ligands, Radicals etc.

Ac	acetyl, CH_3CO
AIBN	azoisobutyronitrile
Ar	aryl or arene
aq	aquated, H_2O
bipy	2,2'-dipyridine, or bipyridine
Bu	butyl
COD	cycloocta-1,5-diene
Cp	cyclopentadienyl, C_5H_2
DMF	dimethylformamide
DMSO	dimethylsulphoxide, Me_2SO
dppe	1,2-bis(diphenylphosphino)ethane
en	ethylenediamine, $H_2NCH_2CH_2NH_2$
Et	ethyl
Me	methyl
Py	pyridine
R	alkyl or aryl group
TCNQ	7,7,8,8-tetracyanoquinodimethane
THF	tetrahydrofuran

Micellaneous

asym	asymmetric
bp	Boiling point
CFSE	Crystal field stabilisation energy
C_i	concentration of the i^{th} ion

c_∞	bulk concentration
cm^{-1}	wavenumber
CT	charge transfer
CV	cyclic voltammetry
D_i	diffusion coefficient, i
E	potential
$E_{1/2}$	half-wave potential
e^-	an electron
E_a	activation energy
E_p^{ox}	potential peak for an oxidation process
E_p^{red}	potential peak for a reduction process
EPR	Electron paramagnetic resonance
eV	Electron volt
F	Faraday's constant (96485 C mol^{-1})
G	Gibbs free energy (kJ mol^{-1})
g	g-values
H	enthalpy (kJ mol^{-1})
h	Plancks Constant (6.626 x10^{-34} J s)
HOMO	highest occupied molecular orbital
Hz	hertz, s^{-1}
I	current (A)
i_p^{ox}	current peak for an oxidation process
i_p^{red}	current peak for a reduction process
ir	Infrared
(l)	liquid state
K_{obs}	observed equilibrium constant

K	rate constant
k_{obs}	observed rate constant
LFSE	ligand field stabilisation energy
LMCT	ligand to metal charge transfer
LUMO	lowest unoccupied molecular orbital
MLCT	metal to ligand charge transfer
MO	molecular orbital
mp	melting point
mnt	$[S_2C_2(CN)_2]^{2-}$
n	electron number
nmr	Nuclear magnetic resonance
OTTLE	optical transparent thin layer electrode
Q	charge (C)
R	gas constant (8.31451 J K^{-1} mol^{-1})
S	entropy (J $K^{-1}mol^{-1}$)
(s)	solid state
SCE	saturated calomel electrode
Sym	symmetrical
T	temperature (K)
uv	ultraviolet
z	charge of a complex ion
Å	Angstrom
Δ_o	ligand field splitting parameter
ε	molar extinction coefficient (cm^{-1} mol^{-1} dm^3)
μ	ionic strength
ν	reaction rate; scan rate (V s^{-1})

Table of Contents

Chapter One Introduction

Chapter Two Experimental Techniques

Chapter Three Preparation of Redox-Active Macrocycles

Chapter Four Complexation Studies of Guest Metal Ions with the Cobalt Macrocycle [6]

Chapter Five Photochemical Reaction

Chapter Six Other attempted routes to alternative redox-active macrocycles

Appendices

List of Compounds

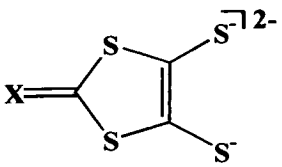

X = S [1]; O [2]

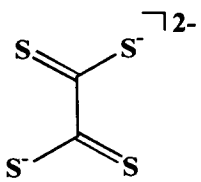

[3]

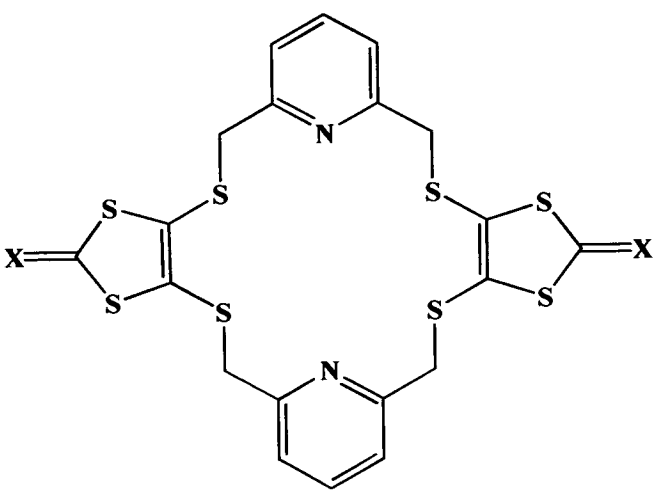

X = S [4]; O [5]

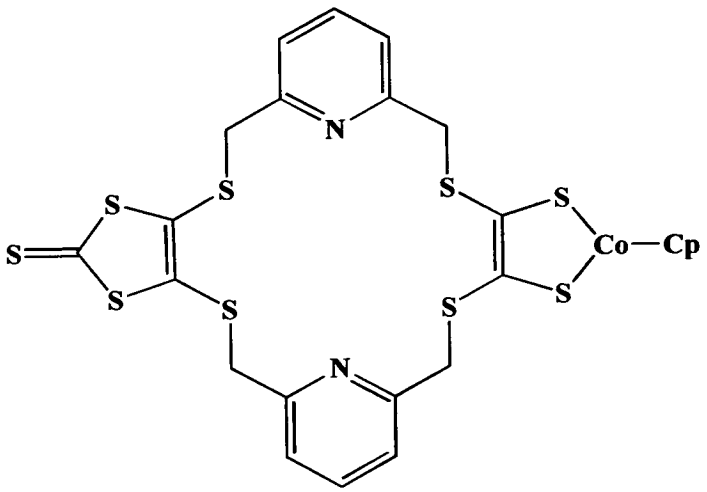

[6]

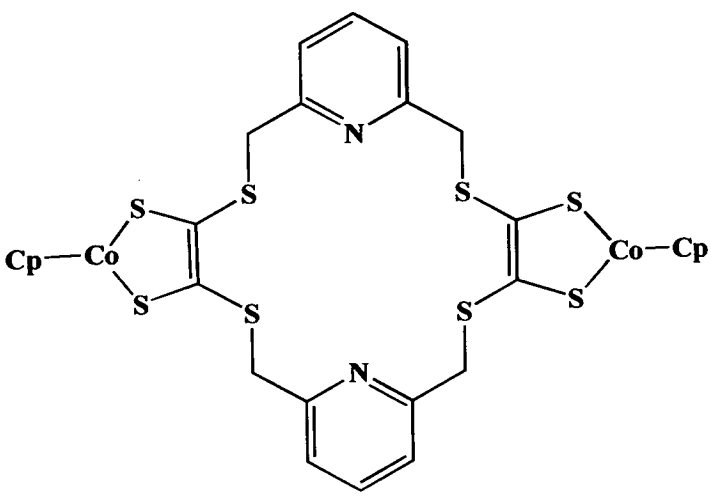

[7]

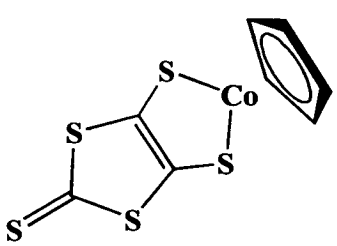

[8]

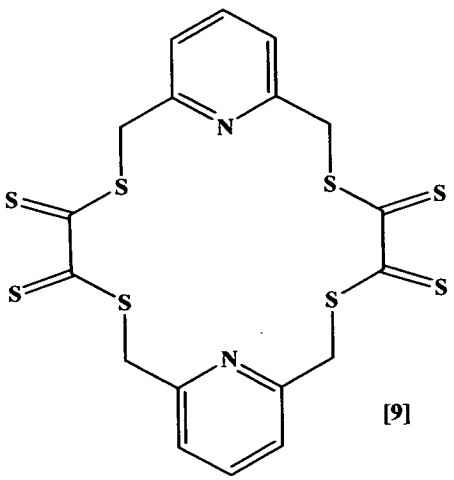

[9]

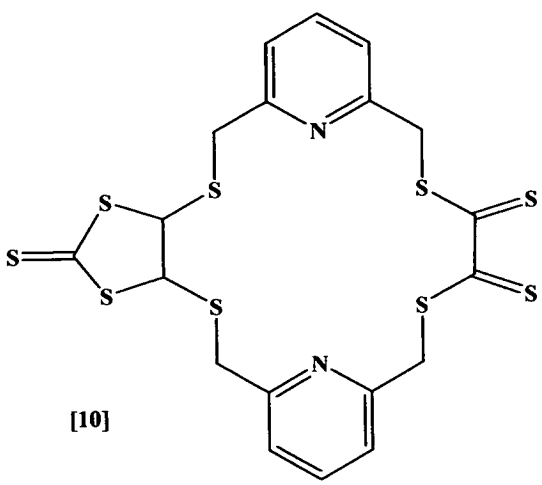

[10]

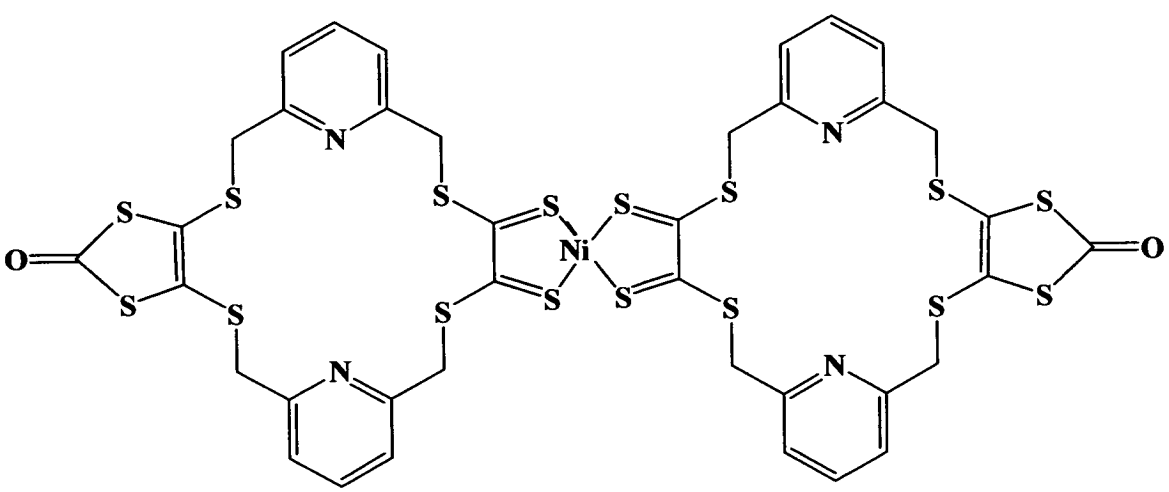

[11]

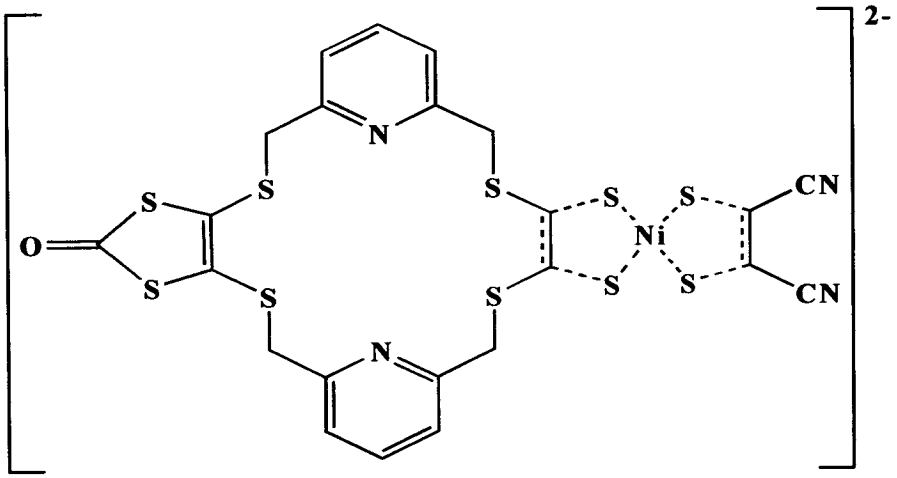

[12]

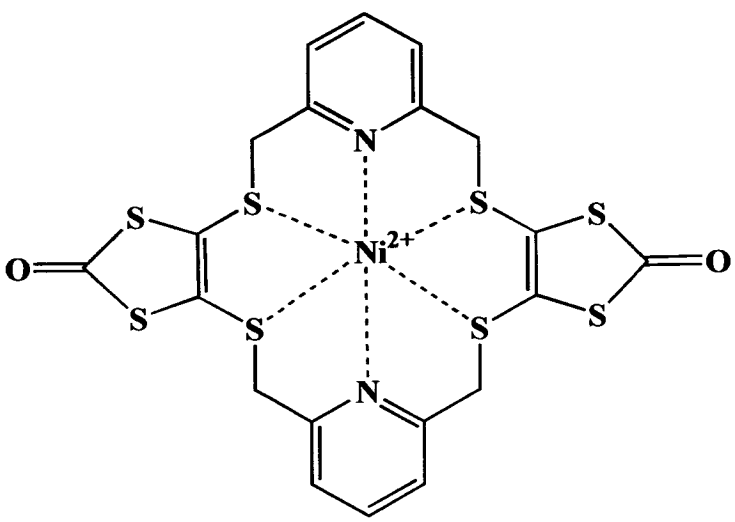

[13]

[14] Product of the reaction of the product of the irradiation of [5] with ` $[NEt_4]_2[Pd(mnt)_2]$

[15] Product of the reaction of the product of the irradiation of [5] with $[NEt_4]_2[Zn(dmit)_2]$

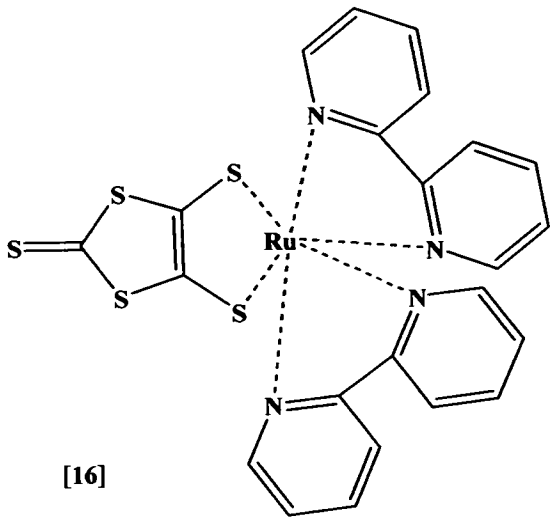

[16]

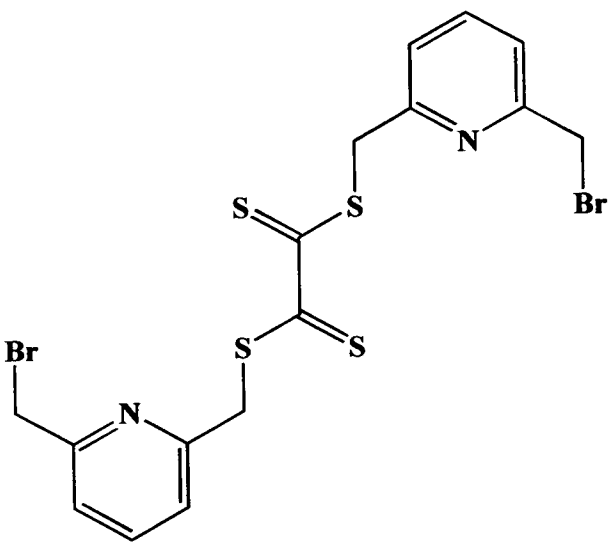

[17]

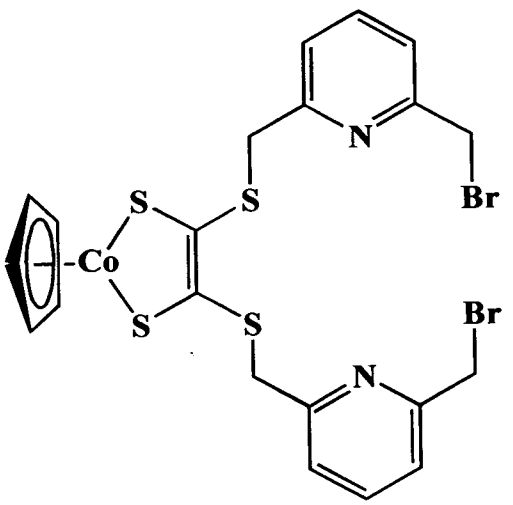

[18]

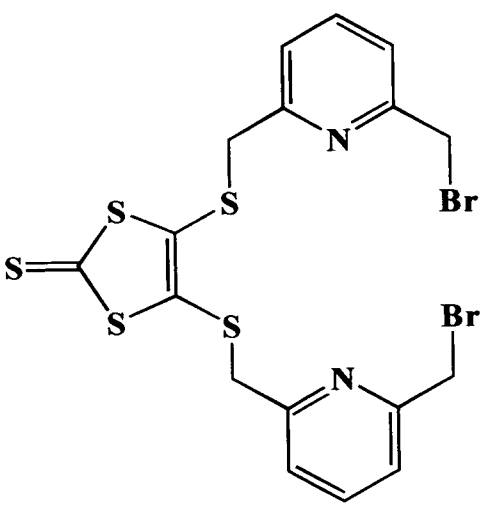

[19]

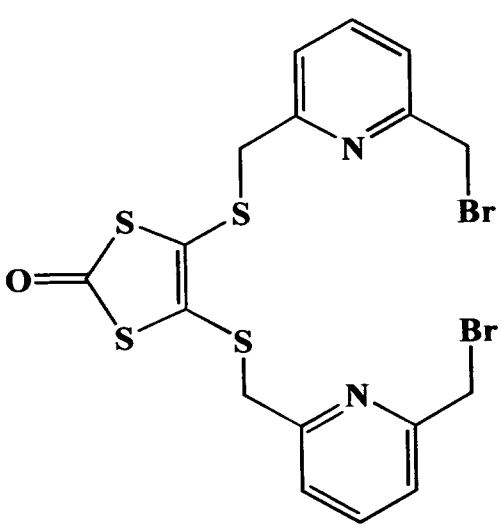

[20]

Table of Figures

Table of Schemes

Table of Tables

Chapter One

Introduction

Introduction

1.0 Introduction

Interest in the metal complexes of sulfur donor ligands over the past two decades has been stimulated by the discovery of several novel properties, intrinsic to these types of systems. In metal-*bis*-1,2-dithiolene chemistry for example, the extensive delocalisation of the HOMO and LUMO makes these systems ideally suited to their application as conducting materials. Some metal complexes of systems such as 1,3-dithiole-2-thione-4,5-dithiolate (dmit dianion) [**1**] and 1,3-dithiole-2-one-4,5-dithiolate (dmid dianion) [**2**] have also been shown to exhibit metallic and even super-conducting properties under pressure [1]. Other compounds of this type have been shown to exhibit potential as third order non-linear optical materials [2] and more recently a novel molecular ferromagnet based on a dithiolene ligand has been discovered [3].

Synthesis and characterisation of new macrocyclic systems incorporating one type or a mixture of chalcogen donor atoms, O, S, Se or Te, has been of considerable interest in areas of contemporary organic and advanced materials chemistry. In particular there has been a distinct surge in sulfur-based chemistry and the development of new sulfur-based macrocycles.

In this chapter, attention will be paid to the properties exhibited by these types of sulphur-donor systems. In specific, a detailed description of the synthetic routes to, and the properties of, the key precursor materials, the 1,3-dithiole-2-thione-4,5-dithiolate [**1**] and the tetrathiooxalate dianion [**3**], will be described. From this discussion, the suitability of these compounds for the development of a soft-donor

macrocycle, for application in the area of ion sensor technology should become apparent.

Leading on from these precursor materials, a brief overview of the area of host-guest chemistry will be given. Emphasis will be on thioether and mixed sulfur-nitrogen based systems; however a brief overview, for comparison purposes, of the area of hard-donor nitrogen, oxygen and mixed nitrogen-oxygen donor systems will be made. Finally, the area of 'responsive' macrocycles i.e. macrocycles which are able to alter their physical properties, upon binding of a guest ion species to the macrocyclic cavity will be discussed. In this section, particular attention will be paid to redox-active systems and their application as amperometric sensory devices.

1.1 Sulfur-based precursors

1.1.1 1,3-dithiole-2-thione-4,5-dithiolate [1]

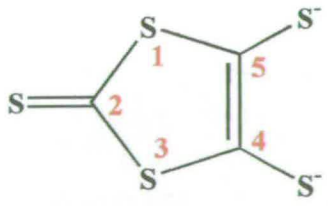

Figure 1.1 1,3-dithiole-2-thione- 4,5-dithiolate [**1**] with numbering convention

1.1.1.1 Introduction

The 1,3-dithiole-2-thione-4,5-dithiolate ligand, dmit [**1**] [4] and its analogues have recently received prominence in the chemistry of new materials [5], particularly as a major component of conducting solids. The discovery of metallic conductivity within molecular materials has proven extremely important in the progress of materials chemistry. In particular a series of $[M(dmit)_2]^{2-}$ complexes have been prepared and studied by Robertson et al [6]. The chemistry of these sulfur containing systems, either as the free dithiolate ligand, or incorporated into heterocyclic systems, has proven extremely interesting, mainly because of the exceptionally rich redox chemistry and the polarisability of the sulfur atoms.

When presenting these compounds as likely precursors for the development of donor macrocycles, the wide-ranging chemistry that is possible is an important consideration. The thiocarbonyl group of the 1,3-dithiole-2-thione-4,5-dithiolate dianion [**1**], contains a relatively nucleophilic sulfur atom and a similarly electrophilic carbonyl carbon. The dual reactivity of this group provides the basis for several general reaction types, which can be performed on most alkylated or acylated derivatives of dmit and related compounds.

1.1.1.2 Methods of Preparation

Fetkenheuer *et al* [7]discovered the dmit dianion [**1**] Figure 1.1, in 1927 during an unsuccessful attempt to prepare the di-anionic tetrathiaoxalte compound $[C_2S_4]^{2-}$ [**3**]. Since then, many preparative methods have been proposed for the preparation of the dmit-class of systems.

Possibly the most widely used of the routes reported is the direct formation of the dmit precursor by reduction of carbon disulphide using alkali metals in dimethylformamide, as described in Scheme 1.1 below. This pathway, was first described by Hoyer et al, in 1979 [8]. The reaction is believed to involve a transient tetrathiaoxalate intermediate $[C_2S_4]^{2-}$ **[3]**, and will be discussed in greater detail in the next section.

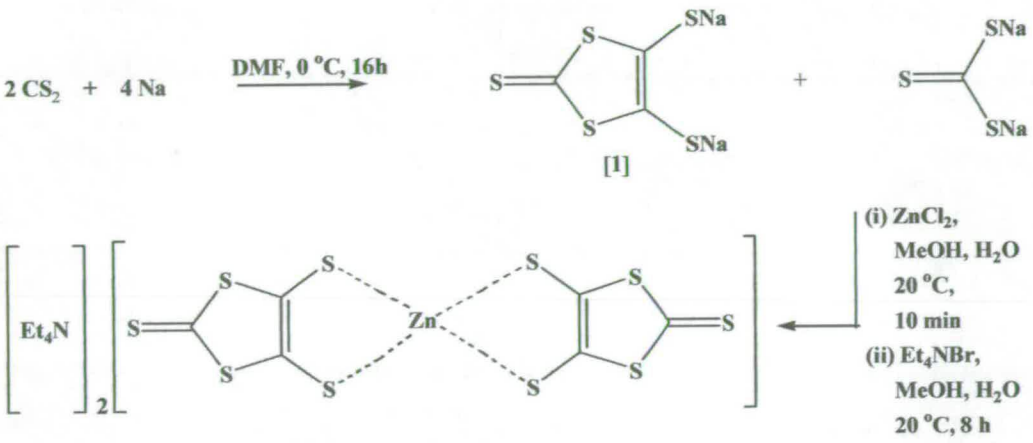

Scheme 1.1 Na reduction of CS_2 towards the formation of 1,3 dithiole,2-thione, 4,5- dithiolate **[1]**

As a result of the chelation of the dmit ligand **[1]** to zinc, this route has the advantage of producing a far more stable derivative of dmit than that of the lithium, sodium or potassium salt of the free $[C_3S_5]^{2-}$ dianion **[1]**. The derivatisation of the dithiolate at the 4- and 5- positions (Figure 1.1) may be carried out using a variety of reactions, which lead to derivatives of the dmit, stable over long periods of time.

1.1.1.3 Chemistry of the 1,3-dithiole-2-thione-4,5-dithiolate dianion [1]

1.1.1.3a Introduction

The wide-ranging chemistry associated with the 1,2-dithiole-2-thione-4,5-dithiolate dianion [1] makes it a versatile precursor for the preparation of sulfur containing marocyclic systems. Modes of reaction involve thermal and photochemical rearrangements and synthetic transformations (e.g. transchalcogenation, alkylation, and reactions with phosphorus reagents such as PCl_5) [9, 10, 11]. To consider in detail, the entire range of chemical transformations which are possible is however out-with the scope of this chapter. The reactions relevant to the work described in the remainder of this thesis will therefore be described.

Occasionally, the need arises to block the 4,5-dithiolate functionalities of [1], especially when transformations carried out on the thione group may cause alterations to the dithiolate sulfurs. One such side-reaction is the complexation of these sulfurs to any transition metal involved in the transformation. An example is the transchalcogenation reaction of the thione group, using $Hg(OAc)_2$ (Section 1.1.1.3c) where coordination to the Hg atom may take place unless the thiolate sulfurs at the 4 and 5 positions are protected.

1.1.1.3b Derivatisation and Deprotection of the dmit dianion [1]

As well as preventing the formation of unwanted side-products, one of the main functions of protecting the 4- and 5- thiolate position, is to enable the long-term storage of these compounds. One of the more common forms for long-term storage of the precursor is prepared from the Zn complex $[NEt_4]_2[Zn(dmit)_2]$ produced in

Scheme 1.1. From this complex, a route derived by Rauchfuss in 1990 [12] involved the treatment of an acetonitrile solution of the zinc salt with a solution of sulfuryl chloride (SO_2Cl_2) at –40 °C. From the resulting yellow solid product, the dmit dimer product [5] could be isolated in 46 % yield by extraction with carbon disulphide.

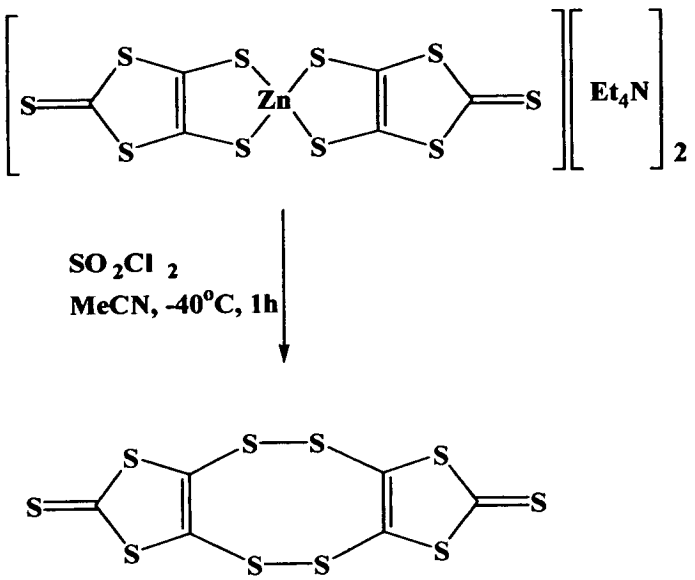

Scheme 1.2 Preparative route to the dmit dimer [12]

Acyl derivatives of dmit have been considerably less explored in comparison to their alkyl analogues. However of those produced, the benzoyl derivative of the dmit dianion precursor, Scheme 1.3, is most easily prepared. Reaction of the $[NEt_4]_2[Zn(dmit)_2]$ with benzoyl chloride in acteone at room temperature yields the acylated derivative in 76 % yield. Another frequently used protecting group is the 2-cyanoethyl group [13].

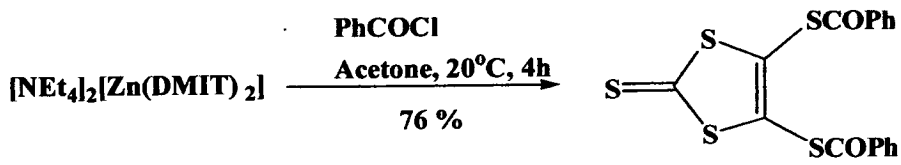

Scheme 1.3 Acylation of the 1,3-dithiole,2-thione-4,5-dithiolate dianion [1] using PhCOCl in acetone

The products of these reactions i.e. the benzoylated and cyanoethyl- protected compounds, can easily be used to regenerate the dithiolate by reaction of the chosen precursor with 2 equivalents of base. A base such as NaOMe is sufficient in the case of the benzoylated derivative, however a strong base or hydroxide is required in the case of the 2-cyanoethyl derivative, where the reaction is carried out in a solvent other than Methanol or Ethanol. Despite the fact that only a few acylated derivatives of the dmit dianion have been prepared, they, along with the cyanoethyl- derivative, have proven to be important starting materials for the synthesis of other derivatives of dmit [1].

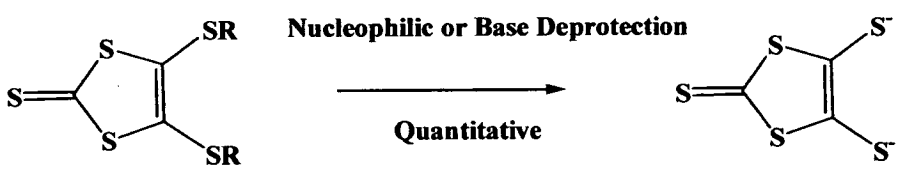

R = -COPh; -CH_2CH_2CN

Scheme 1.4 Nucleophilic deprotection of the protected 4,5-dithiolate functionalities

In the cases where mono-deprotection is required, 1 equivalent of caesium hydroxide hydrate may be employed and the resulting caesium salts may be isolated and stored in the solid state for months without any evidence of decomposition.

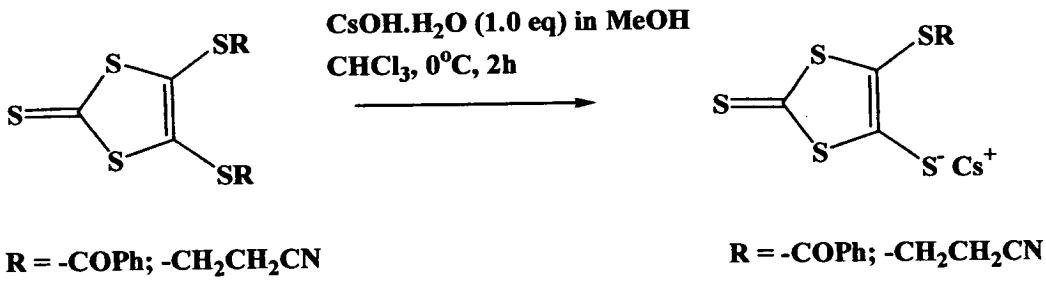

R = -COPh; $-CH_2CH_2CN$ R = -COPh; $-CH_2CH_2CN$

Scheme 1.5 Selective deprotection of the 4,5-dithiolate functionalities of dmit [1]

While deprotection may easily be carried out with base, Neilands *et al* [14] reported the photochemically induced rearrangement of 4,5-bis(alkylthio)-1,3-dithiole-2-thiones to the corresponding 4,5-bis(alkylthio)-1,2-dithiole-3-thiones.

The general rearrangement is outlined in Scheme 1.7. One such reaction involved the irradiation of an ethanol solution of 4,5-ethylenedithio-1,3-dithiole-2-thione for 1 hour using a high pressure mercury lamp. The product of this reaction was collected as the 4,5-ethylenedithio-1,2-dithiole-3-thione in 93 % yield..

The use of mercury irradiation in photochemical rearrangements is not limited to the preparation of 4,5-bis(alkylthio)-1,2-dithiole-3-thiones, as described above. In fact, in contrast to these observations, the alkylated derivatives of the 4,5-dithiolate-1,3-dithiol-2-one species do not undergo this type of reaction. Instead, the decarbonylation reaction has been reported [9], where upon irradiation with a medium-pressure mercury lamp, the dialkyl derivative of tetrathiaoxalate is formed, Scheme 1.6

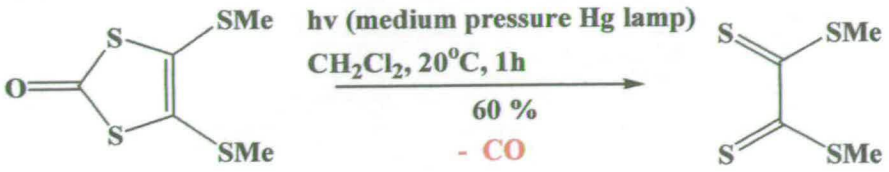

Scheme 1.6 Irradiation of the alkylated derivatives of 4,5-bis(methylthio)-1,3-dithiol-2-one [1] using Hg irradiation

The reaction apparently only proceeds for simple linear alkyl derivatives, since irradiation of 4,5-ethylenedithio-1,3-dithiol-2-one as well as of 4,5-propylenedithio-1,3-dithiol-2-one produced only carbon monoxide, elemental sulfur and polymeric material. A more in-depth discussion of irradiation experiments is given in Chapter 5.

1.1.1.3c Transchalcogenation Reactions

In terms of functional group inter-conversion, the transchalcogenation of 4,5-bis(alkylthio)-1,3-dithiol-2-ones to 4,5-bis(alkylthio)-1,3-dithiol-2-ones, is probably the most well known of all tranchalcogenation reactions reported [9]. The reaction involves the conversion of the readily attainable 1,3-dithiole-2-thiones to their more reactive 2-one analogue.

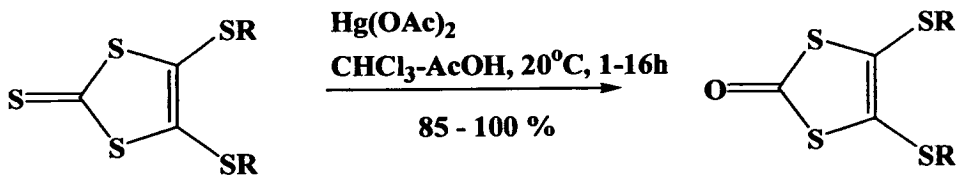

Scheme 1.7 Transchalcogenation of an alkylated 1,3-dithiole,2-thione-4,5-alkylthiolates to 1,3-dithiole,2-one-4,5-alkylthiolates

The reagent used for this inter-conversion is mercuric acetate in a $CHCl_3$-glacial acetic acid solution. Dichloromethane has also been successfully used in place of chloroform with good results, as has pure acetonitrile. By-products are present in low concentration and work-up is generally very straightforward, making this the method of choice when carrying out the conversion of a 2-thione to a 2-one species.

1.1.1.3d Binding of 1,2-dithiolate ligands to Transition Metal Units

Transition metal complexes incorporating 1,2-dithiolenes as the co-ordinating ligand have been extensively studied over a number of years [15]. The significant interest in these types of compounds arises from the interesting properties they exhibit. Consisting of one transition metal atom, two co-ordinated sulfur atoms and two unsaturated carbon atoms, a metalladithiolene ring is a unique metal chelate system [15c, 16, 17]. The ring is a conjugated system with 6-π electrons and this means metalladithiolene rings tend to be aromatic in nature. As a result of this extended delocalisation, a variety of different resonance forms of the complex may be written which incorporate the metal in a range of formal oxidation states Scheme 1.9.

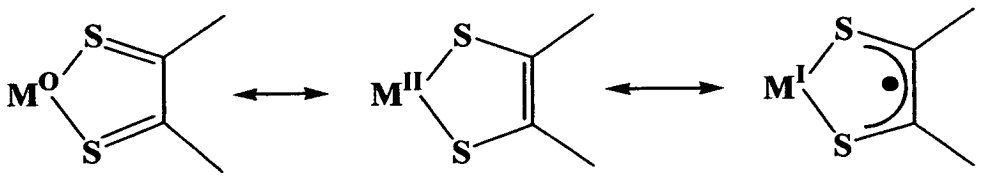

Scheme 1.8 Extended delocalisation allows the metal to be assigned several well-defined formal oxidation states

This class of complex can be characterised by a variety of properties, which can ultimately be used in the development of new materials. For the metal-*bis*-1,2-dithiolene complexes where M = Ni, Pd, and Pt, these properties may be summarised as follows :-

(a) They have the ability to exist in several well defined, but inter-convertible charged states. This interconversion produces the neutral, mono- and di-anionic species, for example for Ni, Pd and Pt, Scheme 1.9, and can be attained by chemical or electrochemical means.

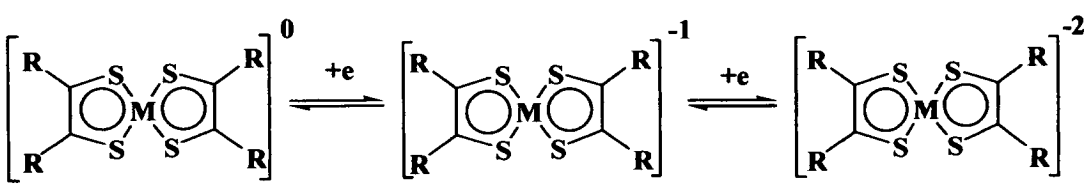

M = Ni, Pd, Pt

Scheme 1.9 The interconvertible states of metal-*bis*-1,2-dithiolenes

(b) The presence of an intense low energy absorption band corresponding to the HOMO ($2b_{1u}$) to LUMO ($3b_{2g}$) transition is normally observed. This property has been exploited in the area of third order non-linear optical materials [18] and is also used commercially in laser dyes [19].

(c) The presence of an unpaired electron within the delocalised LUMO of the mono-anionic salt can result in co-operative magnetic properties for the solids [16c, 20].

(d) The system is tuneable, both in terms of the redox behaviour and the position of the low energy HOMO to LUMO transition. One aspect of this fine-tuning is the ability to substitute electron withdrawing and donating groups on the ligand. In this way, changes to the electronic nature of the central metal may be made which makes these systems ideal candidates to act as precursors for the synthesis of a wide variety of sulfur-based materials [15c].

The aromaticity of the metalladithiolene rings has long been discussed and the properties utilised in the development of new functional materials. Schrauzer first pointed out the unusual electronic structure of the metalladithiolene ring: the bonding is characterised by extensive delocalisation of electrons [15a]. ^{1}H NMR studies revealed the existence of ring currents ascribed to the aromaticity of the metalladithiolene ring [21]. A further discussion of the bonding of sulfur donor atoms to metal species is given in Section 1.2.3.

1.1.2 Tetrathiaoxalate dianion $[tto]^{2-}$ [3]

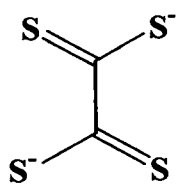

Figure 1.2 The tetrathiaoxalate dianion [3]

1.1.2.1 Methods of Preparation

The first claim for tetrathiaoxalate goes back to 1927, where the formation of 4,5-bis(methylthio)-1,3-dithiole-2-thione (Me_2dmit) was reported by the chemical reduction of CS_2 (Equation 1.1) and subsequent methylation. From the elemental analysis, the product was thought to be the tetrathiaoxalate dianaion $[tto]^{2-}$ [3]. The reduction was repeated using different reductants and media (e.g. electrochemically in DMF [22], but in all cases reported, the dimethylthioether Me_2dmit was formed preferentially to Me_2tto.

$$2\ CX_2 \quad 2\ e^- \longrightarrow \left[C_2X_4\right]^{2-} \qquad \textbf{Equation 1.1}$$

In 1981, a reliable route to the synthesis and X-ray characterisation of the tetrathiaoxalate dianion was reported [23]. The mechanism involved the electrochemical reduction of CS_2 over a liquid mercury cathode, while in the presence of a quaternary ammonium or phosphonium salt (Equation 1.2).

$$2\ CS_2 \xrightarrow[Et_4NCl]{-2\ V\ vs\ NHE} (Et_4N)_2C_2S_4$$

Equation 1.2

Also in 1981, Lodmell et al, proved conclusively by HPLC experiments that $[tto]^{2-}$ is indeed formed during the two-electron reduction of two 16-electron CS_2 molecules. In the course of the reaction these two monomers dimerize to form the red crystalline salts of $[NEt_4]_2[C_2S_4]$ [24]. It was reported that the two electrons may be provided by chemical means i.e. Na reduction of CS_2 or by electrochemical reduction. In the course of the electrochemical reduction of CS_2, applying a potential slightly more negative than the reduction potential of CS_2 (-1.15 V vs SCE) to an acetonitrile solution of CS_2 and $[Et_4N][Br]$, the corresponding $[C_2S_4]^{2-}$ salt [**3**] was formed.

In this reaction, precipitation results in the stabilisation of the product salt $[NEt_4]_2[C_2S_4]$, which prevents any further reactions e.g. the production of the $[C_3S_5]^{2-}$ dianion, Scheme 1.10

As previously discussed (Section 1.1.1.2), the sodium reduction of CS_2 has been found to be the most effective preparative route for the dmit dianion $[C_3S_5]^{2-}$ [**1**] where $[C_2S_4]^{2-}$ [**3**] has been proven to be an important intermediate in the reaction mechanism. The isolation of the tetrathiaoxalate dianion [**3**] from such reaction methods has proven problematic, with low yields achieved due to the constant possibility of over-reaction to give $[C_3S_5]^{2-}$ [**1**] and $[CS_3]^{2-}$.

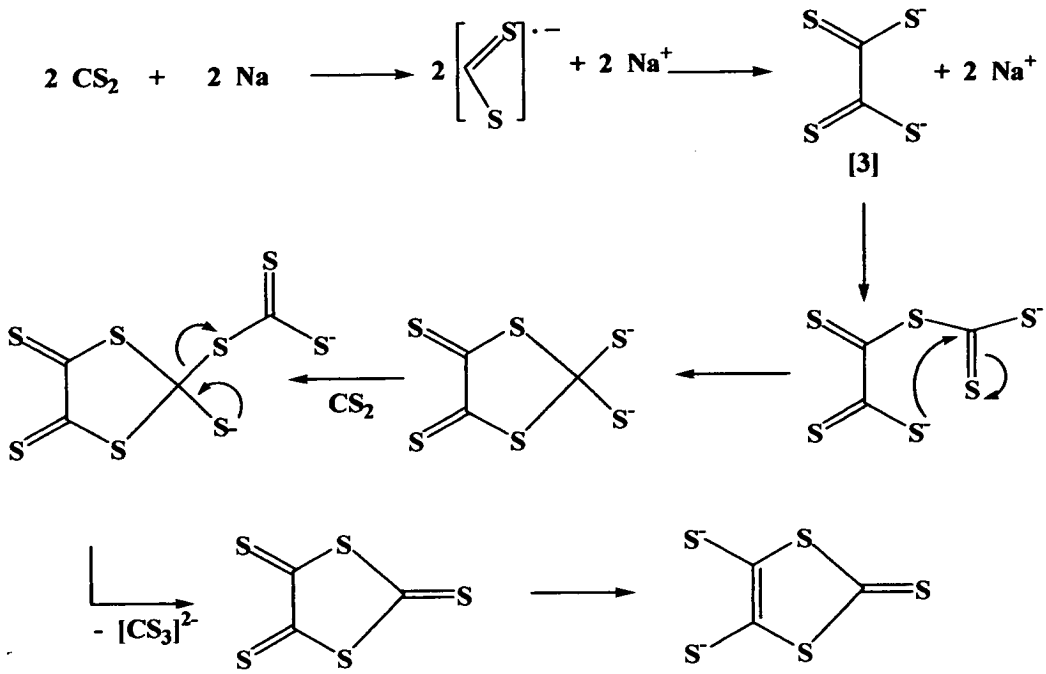

Preparative route to the formation of tetrathiaoxalate dianion $[C_2S_4]^2$ [3]

Further reaction of the resultant tetrathiaoxalate dianion $[C_2S_4]^{2-}$ [3] to the dianion $[C_3S_5]^{2-}$ [1]

Scheme 1.10 Preparative mechanism for the formation of $[C_3S_5]^{2-}$ [1], showing the importance of $[C_2S_4]^{2-}$ [3] as an intermediate

Two noticeable improvements for the direct preparation of $[C_2S_4]^{2-}$ [3], have been reported more recently [25]. The first involves the reaction of $Na_2S.9H_2O$ with C_2Cl_4 in a mixture of MeOH and MeCN. Pure tetrathiooxalate [3] is collected, though in quite low yield (≈ 29 %).

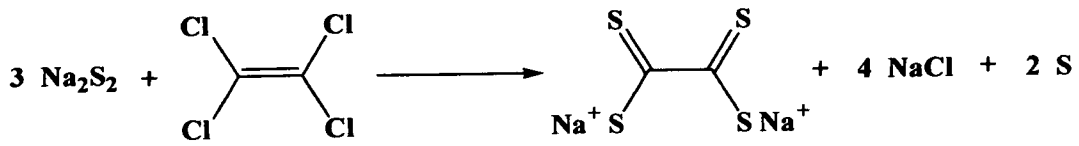

Scheme 1.11 Equation for the preparation of tetrathiooxalate [3] from Na_2S_2

The second and probably the most effective route, involves the initial preparation of Na_2S_2 by sodium reduction of sulfur flowers in liquid ammonia. This more reactive precursor is reacted with C_2Cl_4 at 70 °C for 30 minutes (Scheme 1.11). While a significant work-up is involved, the yield of the product $[NEt_4]_2[C_2S_4]$ [3], as red crystals was found to be significantly higher (≈ 45 %). The structure of the tetraethylammonium salt has been reported [8b, 23a, 26].

In the latter case, prolonged reaction of C_2Cl_4 with Na_2S_2 has been found to result in dark solutions which, upon investigation by UV-Vis spectroscopy, have been shown to contain $[C_4S_6]^{2-}$, Scheme 1.12 [27]. The formation of this species has been shown to be a result of the reaction of the preformed $[C_2S_4]^{2-}$ [3] product toward elemental sulfur, which is formed in the course of the reaction.

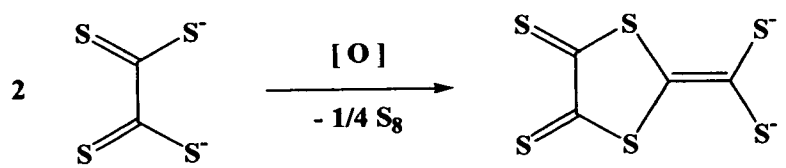

Scheme 1.12 Susceptibility of $[NEt_4]_2[C_2S_4]$ [3] to oxidation

The oxidative nature of this pathway has been confirmed by the treatment of $[C_2S_4]^{2-}$ [3], with 0.5 equivalents of I_2 followed by heating, which gave $[C_4S_6]^{2-}$ in quantitative yield.

It has also been shown that some transition metal centres favour the dimerization of carbon disulfide [28], despite the fact that no similar metal promoted dimerisation has ever been observed for carbon dioxide.

1.1.2.2 Bonding and Structure

The tetraanionic (ethylenetetrathiolate : ett) form of $[C_2S_4]$ though it has not actually been isolated, is generally considered to be another stable form of $[C_2S_4]$ when bonded to a metal system [29]. In this particular case a carbon-carbon double bond is seen to form. The weakness of the C-C σ bond in the case of ethylenetetrathiolate becomes less crucial because of the co-operating C-C π bond.

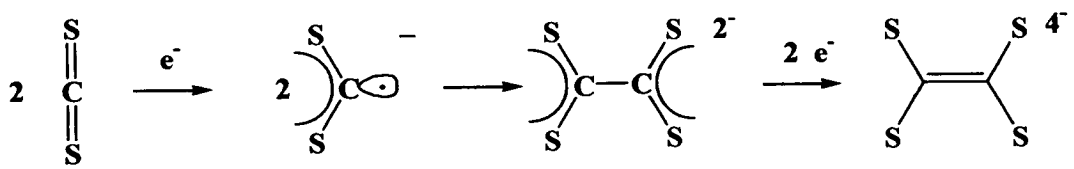

Scheme 1.13 Schematic of the coupling of two CS_2 molecules to give the $[C_2S_4]^{2-}$ dianion [3] and its reduction to form the inherently unstable tetraanionic form of $[C_2S_4]$, $[tto]^{4-}$, ethylenetetrathiolate.

Comparison of the $[C_2S_4]^{2-}$ dianion [**3**], with its oxygen analogue highlights an inherent instability in the case of the former species. This instability is explained as being a direct result of the electronegativity difference of the C-X bond, due to the replacement of the oxygen atoms with sulfur atoms. The shape of the Fragment Molecular Orbital (FMO) of the CX_2 species {X = O, S}, which is used to form the C-C bond in $[C_2X_4]^{2-}$, changes (as shown in Figure 1.4) for increasing ΔE_{C-X} (E=Electronegativity).

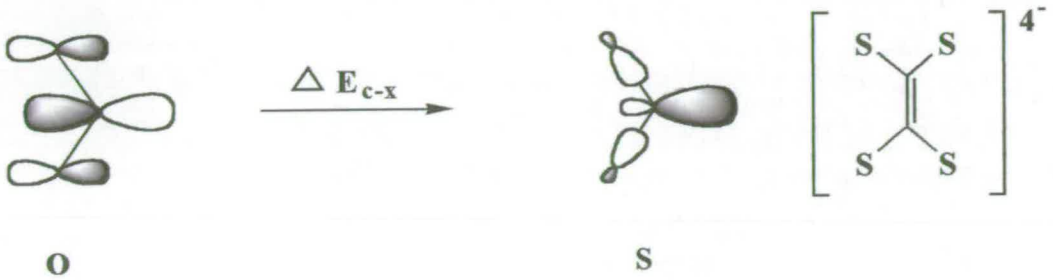

Figure 1.3 Changing shape of the Fragment Molecular Orbital due to the electronegativity increase on going from Oxygen to Sulfur

Since the larger hybrid orbitals at each carbon, is consistent with a better overlap, the argument agrees with the larger stability of the oxalate anion. Another source of instability is the enhanced direct repulsion of the sulfur lone pairs, which are far more diffuse than the corresponding oxygen lone pairs of $[C_2O_4]^{2-}$.

1.1.2.3 Coordination of the tetrathiooxalate dianion $[C_2S_4]^{2-}$ [3] to metals

Much work in the preparation of new dithiolene-containing molecules has been focussed on producing systems, which extend the delocalising ability of the overall complex. In making a larger delocalised system we have the ability to reduce any coulombic repulsions and also increase the possibility of intermolecular interactions. Most importantly however, in regard to the work reported here, systems have been produced with the aim to achieve lower energy absorptions in the visible spectrum.

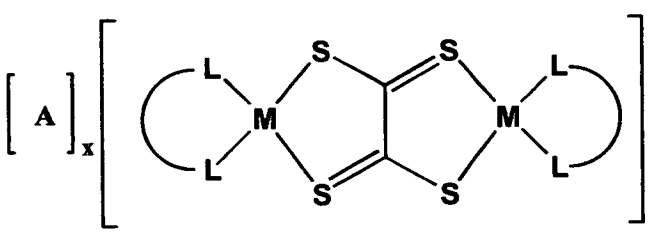

Figure 1. 4 Schematic structure a dinuclear system containing a tetrathiaoxalate bridge

The general structure of the systems in question is described in Figure 1.4. Consideration of the bridging tetrathiaoxalate ligand [3], and the effect that this will have on the properties of the multimetallic species is of considerable relevance to the work described in this thesis.

The extensive polarisability of the sulphur atoms and the delocalisation within the system allows for interaction between the two metal sites. For example, study of the magnetic properties of $[AsPh_4]_2[Cu_2(C_2S_4)(dmit)_2]$ shows a very strong anti-ferromagnetic coupling between the S = 1/2 Cu^{II} centres, mediated by the $[C_2S_4]$ bridge with $|J| > 800$ cm^{-1}. The very strong interaction is significant for the use of these types of ligands, in the synthesis of soft-donor macrocycles with application to ion sensing.

Some species, which have been prepared to date, are described in Table 1.1

Table 1.1 A sample of some of the multinuclear species using $[C_2S_4]^{X-}$ bridges with their structure defined by Figure 1.5

M	L	Charge (X)	Cation (A)	Ref
Cu	dmit	2-	$AsPh_4$	30
Cu	tto	2-	PPh_3	31, 32, 33, 34
Ni	dmit	2-	NBu_4	35
Ni	dmit	2-	NMe_4	36
Ni	dmit	2-	NEt_4	36, 37
Ni	dmit	2-	$N(Ph_3P)_2$	38
Ni	$S_2C_2S_2C_2(CO_2Me)_2$	2-	$AsPh_4$	39
Ni	$S_2C_2S_2C_2(CO_2Me)_2$	0	NBu_4	39
Au	tto	2-	PPh_3	40, 41, 42
Rh	tto	2-	PPh_3	40, 41, 42, 43
Ag	tto	2-	PPh_3	40, 41, 42

The synthesis [44], structures [45] and vibrational spectra [46] of alkaline salts of other thio-oxalates, namely the trithiooxalates (trto) and 1,1-dithiooxalate (*i*-dto), were reported already in the 1970s. In contrast however, little is known of their ligand properties [47]. One reason for that might be the high tendency of these ligand types to form coordination polymers. In more recent times structures containing these types of ligands have been more frequently researched and reported.

1.1.2.4 Conclusions

While much has been learned about transition metal dithiolenes, [15c, 16a, b, 48] a significantly smaller amount of detail is known about the ligand properties and coordination chemistry of $[C_2S_4]^{n-}$ containing precursors.

From the work reported in the literature, the capacity of these molecules to act as coordination ligands to transition metal units is evident. The sulfur lone pairs allow these systems to play a considerable role in soft donor coordination chemistry with transition metals. They also have a highly delocalising π-system, which will later be shown to make these compounds ideal for development of new sensor molecules.

1.2 Thioether based Donor Macrocycles and their Application in Transition Metal Ion Sensing

1.2.1 Introduction

As has already been mentioned, less work has been done in the area of ion complexation with soft thioether and mixed thio-donor host sites in comparison to hard donor oxygen systems. There has, however been some development of new sulfur donor systems, which show a significant capacity for complexation of transition metal ions; interestingly, they also show *selectivity* towards specific ions within a multi-ion containing system[49].

1.2.2 Preparation of sulfur based donor macrocycles

1.2.2.1 Sulfur donor macrocycles

The synthesis of sulfur-based macrocycles is of interest in many areas of chemistry. In particular the synthesis and chemistry of polythioethers has been the subject of extensive reviews [50]. The lack of safe, general, high-yielding routes to sulfur based ligands has, up until recent times, severely impeded work on crown thioethers. The synthesis of these types of systems was first reported in 1920 with [9]ane S_3 crown thioether (notation pg. viii) produced from $BrCH_2CH_2Br$ and alcoholic KSH saturated with H_2S, Scheme 1.14 [51].

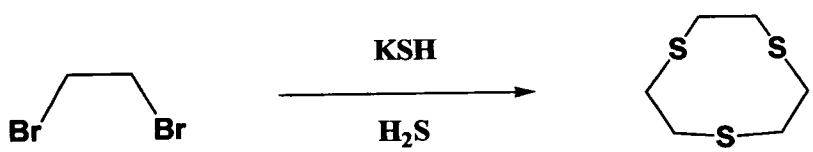

Scheme 1.14 Preparation of [9]ane S_3 crown thioether [51]

This was followed by a report of the isolation of [18]ane S_6 crown thioether in very low yield (< 2 %) from the reaction between the dimercaptan and $BrCH_2CH_2Br$ in the presence of KSH in 1934 by Meadow and Reid, Scheme 1.15 [52]. In 1974, Ochrymowycz and co-workers improved the yield to 32.8 %, but the route required the use of mustard gas [53].

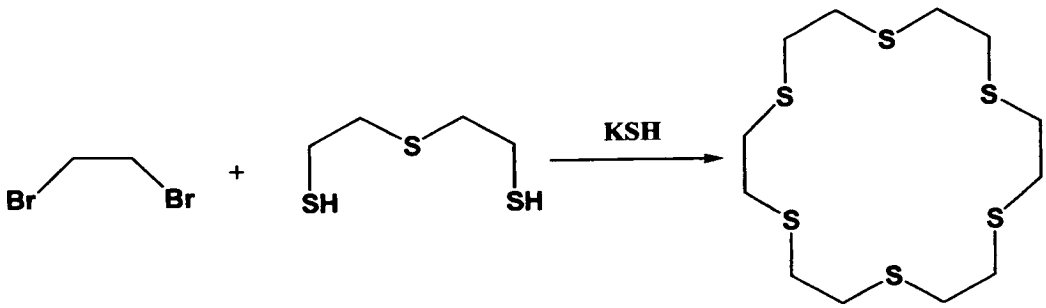

Scheme 1.15 Isolation of [18]ane S_6 macrocycle

Since then the use of caesium salts in the cyclisation reaction, an innovation introduced by Kellogg and co-workers [54, 55], has improved yields, giving the macrocycle [18]ane S_6 thio crown ether in approximately 80 % yield. The caesium ion is thought to influence the reactivity of the crucial halo-thiolate intermediate produced by the first nucleophilic displacement, through which both cyclisation and polymer formation must proceed. Caesium probably promotes this reaction by forming weak ion pairs with RS^- anions, which would make them exceptionally nucleophilic. Under high dilution conditions this enhanced reactivity would favour intra- over inter- molecular S_{N2} reaction of the open chain halo-dithiolate intermediate.

1.2.2.2 Mixed Sulfur-Nitrogen donor macrocycles

A number of macrocycles have been reported incorporating both sulfur and nitrogen donor atoms. Approaches involving both (a) alkylation and (b) acylation, followed by amide reduction, have been employed to obtain a series of crown compounds containing mixed sulfur-nitrogen donor atoms.

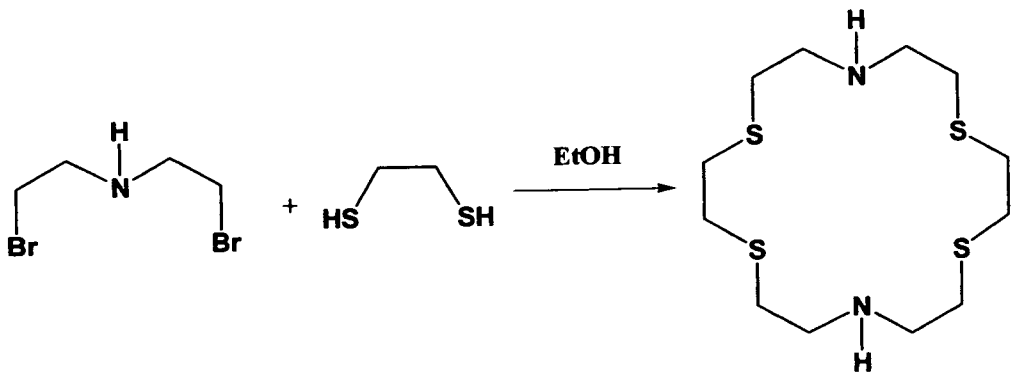

Scheme 1.16 Preparative route to the [18]ane S_4N_2 macrocycle

The mixed nitrogen and sulfur [18]ane S_4N_2 system has been isolated [56] from the reaction shown in Scheme 1.16, between the dibromide and ethanedithiol in ethanol under high dilution conditions. More recently, an acylation reduction sequence has afforded better overall yields of this ligand and related crown compounds [57].

The incorporation of a pyridine ring into these systems has been studied in some detail together with the metal complexes formed by such ligands. [58] In the preparation of such pyridine containing macrocycles, the key starting material has been 2,6-bis(bromomethyl)pyridine.

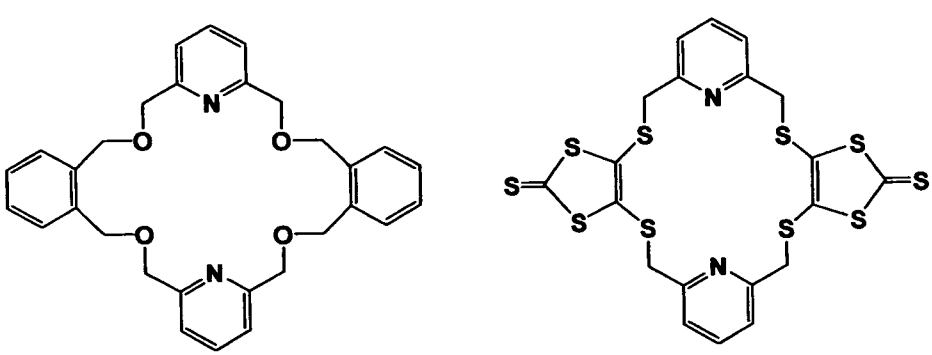

[4]

Figure 1.5 Incorporation of a pyridyl unit into a macrocyclic system

In 1973, Newkome and Robinson [59] isolated 22-, 33-, 44- and 55-membered ring compounds after reaction of this dibromide with 1,2-di(hydroxymethyl)benzene in $MeOCH_2CH_2OMe$ with NaH as base.

Since then, a novel macrocycle incorporating the 1,3-dithiole-2-thione-4,5-dithiolate unit was prepared [60] from a reaction of bis(bromomethyl)pyridine and the dmit dianion. The product macrocycle was collected in 76 % yield as a yellow microcrystalline solid. Excellent yields in this reaction are due to the rigid nature of the starting dithiolate in contrast to the dithiol species normally used. On reaction with the equally rigid 2,6-bis(bromomethyl)pyridine, the dominant product is the 2+2 addition product. No evidence for any polymeric material is seen.

Due to the rigidity of the starting materials the need for high dilution conditions are eliminated, producing a very high yield of the final product. Also important, is the absence of any mustard compounds from the preparative scheme.

1.2.3 Complexation to Transition Metals : Structure and Bonding Information

The outer electron configuration of sulfur in the ground state is $3s^2 3p^4 3d^0$. In dialkyl compounds, two of these valence electrons are involved in bonding to the alkyl groups, leaving four electrons retained in non-bonding orbitals on the chalcogen. The orbitals on chalcogens vary a great deal through the group, however concentrating on sulphur donor systems we can simplify to a situation where sulfur is generally considered to involve sp^3-hybridisation with two lone pairs. One or both of these lone pairs may donate electron density in order to form a link with an electron acceptor such as a guest metal ion.

In almost all sulfur containing thiolate [C-S]$^-$ bonds, the bond angles about sulfur are approximately tetrahedral, consistent with the presence of one lone pair of electrons in an orbital that can roughly be described as sp^3. Distortions from the ideal tetrahedral angle would be expected and are indeed found where the metal and sulfur atoms form part of a ring. Most M-S-C angles lie below rather than above the tetrahedral angle, Figure 1.6. This is an observation that can be attributed either to the large steric effect of the sulfur lone pair or to a less than complete involvement of the s orbital in any orbital hybridisation.

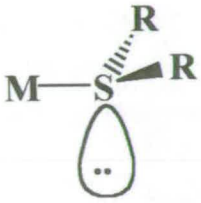

Figure 1.6 The sp^3 hybridised lone pair of tetrahedral sulfur

If only one lone pair is involved in bonding, the other lone pair may either (i) remain non-bonding, in which case it will result in stereo-electronic repulsion, or (ii) take part in π–donation by re-hybridisation to sp^2. This is followed by π–donation of the lone pair from a p-orbital on the chalcogen to the electron acceptor.

Figure 1.7 Metal-thioether bonding assuming sp^2 hybridisation at sulfur

In the case of complexation to a metal, the Dewar-Chatt model, which was developed for P→M σ-donation in phosphine→metal coordination, becomes ambiguous. With only one lone pair of R_2S involved in σ-bonding to the metal centre (assuming sp^3 hybridisation), the second lone pair is capable of π-donation to the metal. In addition the S-donor has empty d orbitals that may be of the correct symmetry and energy to act as π-acceptor orbitals. In principle therefore, thioether based systems are capable of acting as π-acceptors or π-donors, Figure 1.7 [61]. π-donation might be anticipated with the earlier transition metals as they have empty d-orbitals of appropriate symmetry to act as acceptors. This can be attributed to the repulsion of the lone pair on the chalcogen and the electrons on the acceptor.

The ability of electron donors to take part in strong σ-bonding depends on the effective electronegativity of the donor as well as its size (for matching of orbital energies and orbital overlap with the electron acceptor), dipole moment and polarizability. Of these factors electronegativity and size are generally the most important.

In addition to the filled valence orbitals, all the chalcogens have empty nd orbitals, some of which, have the correct symmetry to take part in π back-donation from metal to ligand. Whenever there are orbitals of correct symmetry available for bonding there is always a possibility of such bonding occurring depending on the degree of overlap and relative energies of the orbitals concerned.

Non-covalent interactions play an important role in the recognition and binding of a guest by a synthetic receptor. A host is a molecule, which can non-covalently interact with and bind a guest. Hosts may be cyclic, macrocyclic or oligomeric, and possess cavities or clefts into which the guest fits. The host may be pre-organised for binding or may organise itself during the interaction with the guest. It is normally found that the host is large in comparison to the guest, and the binding sites may interact with the guest by a combination of all non-covalent interactions available,

including coordinate bonds, hydrogen bonding, ion-dipole, ion-ion, π, van der Waals, electron donor-acceptor and hydrophobic interactions.

Guests on the other hand are molecules or atoms which may be ionic or neutral and whose area of binding presents sites complementary in charge and steric requirements to the host. Typical guests have included metal ions, the ammonium ion, polar neutral species such as acetonitrile, hydrogen-bonding compounds, aromatic substrates, diazonium salts, halides, biological molecules and many others.

Complexation of cations in the cavity of donor systems, such as crowns, relies on the type of donor atoms, hard or soft [62], and also on the type of cation that is being complexed. In general hard donor atoms such as oxygen tend to complex to alkali/alkaline earth cations and the lanthanide metal ions. Work in this area has been extensive. In contrast, the softer sulfur donor atoms preferentially complex transition metal cations. This stabilising effect is further enhanced by the moderate π-acidity of thioethers [61] (intermediate between that of amines and that of phosphines) which may act to stabilise lower oxidation states (e.g. +1or +2) of metal ions to yield complexes with unusual reactivity. Despite this interesting chemistry, work to date with soft donor macrocycles has been severely hampered by poorer synthetic routes to their preparation than for analogous oxygen-donor systems. Nitrogen has mixed donor properties being able to complex both hard and soft ion species. More detail of these complexation properties is given in Chapter 4.0.

1.3 Introduction to Ion Sensors

1.3.1 Introduction

In 1974, when Cram coined the use of the term Host-Guest chemistry [63] to describe the then relatively new field of synthetic complexation chemistry, which at the time was exemplified by crown ethers and cryptands, Host-Guest chemistry was primarily concerned with elucidating the 'rules of non-covalency'. The coordination chemistry of sulfur donor ligands is not as extensive as that of the oxygen and nitrogen donor systems and those of the group 15 atoms [64]. There are many reviews on the various types of chalcogen containing ligands [15c, 16a, 49e, 65].

1.3.2 Physical Properties

The central purpose of synthesising most hosts is to determine how they associate with guests. Consequently, measurement and interpretation of the kinetics and thermodynamics of Host-Guest interactions is key in Host-Guest chemistry and has received much attention [66].

The equilibrium expression for complexation of a guest (G) by a host (H) is deceptively simple, Figure 1.8. However, many factors influence this equilibrium, such as conformational changes in both host and guest before and during the complexation and the reorganisation of the solvent throughout the binding process.

$$H_{solv} + G_{Solv} \underset{k_{-1}}{\overset{k_1}{\rightleftharpoons}} (H:G)_{solv}$$

$$K_a = \frac{k_1}{k_{-1}}$$

Figure 1.8 Equilibrium expression for the complexation of a guest (G) by a host (H)

A significant increase in the binding ability is usually seen for a macrocycle in comparison with its acyclic analogue. This is known as the 'Macrocyclic Effect', which, together with complementarity and pre-organisation, is one of the key contributing factors in determining the overall binding ability of the host. It is difficult to obtain qualitative understanding of the origin of the macrocyclic effect, however, a favourable entropy term has been entirely attributed to the differential solvation of macrocyclic and open-chain ligands.

In a study carried out [67] comparing the coordination of Cu^{II} to the macrocyclic structure [x]aneN_4 {x = 12, 13, 14, 15} with that of coordination studies with open chain structures containing such coordinating groups as :NH_2 and :NHMe, a number of results were found. The first is that both the entropic and enthalpic effects favour the macrocyclic complex. The hole-size is also observed with maximum stability at the 13-membered ring in [13]aneN_4 and finally, that alklyated ligands provide a better model for the ligands than NH_2 groups.

The concept of complementarity states that for optimum binding, the area of binding of the guest must fit the recognition site of a host as exactly as possible in terms of size, electronic match and steric compatibility with nearby groups. A host is said to be pre-organised, if bound and unbound conformations closely resemble each other

[68]. The more highly the hosts are organised for binding the lower the ability of the solvent molecules to solvate the systems during the complexation process. This results in a higher binding constant for interaction of the system with a guest.

Pre-organisation is distinct from, but complementary to, the macrocycle effect, in that there are acyclic hosts which are pre-organised and macrocyclic hosts which are not. Although the macrocyclic effect and complementarity are important to the binding ability of a host, the degree of pre-organisation must also be considered as an important contributing factor to the major differences in binding ability seen between host classes.

1.3.3 Complexation Studies

As discussed, a considerable amount of work has been done to date on the theory of ion complexation. The majority of the work reported involves studies on the complexations of hard cations e.g. Na^+ and K^+ and other Group 1 and Group 2 Alkali and Alkaline Earth metals. In the course of these studies, complexing hosts generally comprised of hard-donor atoms such as oxygen or a mixture of oxygen and nitrogen. A significant amount of work has also been carried out in the preparation of 'soft' donor systems based on sulfur or mixed sulfur-nitrogen donor systems. Studies into their complexation with transition metal ions have also been vast though comparatively less frequently reported than the cases involving hard donor systems.

One of the most widely studied systems is the [18]ane N_2S_4 crown ether species and its derivatives, which has been studied extensively in all aspects of host-guest chemistry. It is an example of a system, which has inherent flexibility in the mechanics of complexation. This can be seen when comparison of the resultant geometry within the crystal structure is made in the case of the bound and unbound systems, Figure 1.9. The unbound conformation has C_i symmetry, with a centre of

inversion at the central point in the cavity. The bound conformation is octahedral and attains D_{2h} symmetry upon complexation, completely 'rearranging' in order to attain the most stable environment for the guest species.

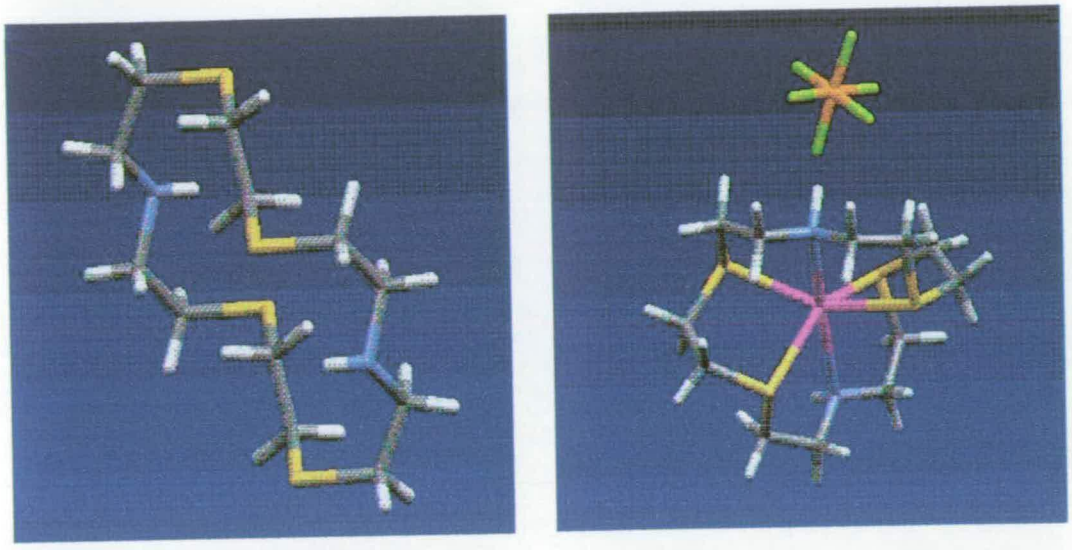

Figure 1.9 Comparison of the conformations for the bound and unbound [18]ane S_4N_2 mixed donor macrocycle [69]

Similar effects are seen for all other donor systems with donor sets such as O_4N_2, S_4N_2, etc. where oxygen has been replaced by sulfur and/or nitrogen, shown in Figure 1.9, is the effect of complexation on the conformation of the mixed nitrogen-sulfur [18]ane S_4N_2 macrocycle.

Selectivity is of vital importance in the development of any host system and the size, shape and nature (hard or soft donor atoms) of the cavity all need to be considered carefully.

1.3.4 Responsive Macrocyclic Systems

1.3.4.1 Redox Active Hosts

We have seen how simple organic host systems (i.e. containing only C, H, O, N and S) are governed by a variety of effects, which determine successful binding of the guest to the host cavity. Other more complicated types of donor systems have been of interest more recently however and these systems include redox active macrocyclic systems. These are systems, which show an electrochemical response upon the binding of a guest metal ion in the host cavity. In order to show a reasonable electrochemical response to ion complexation, these systems should adhere to one or both of the following features :

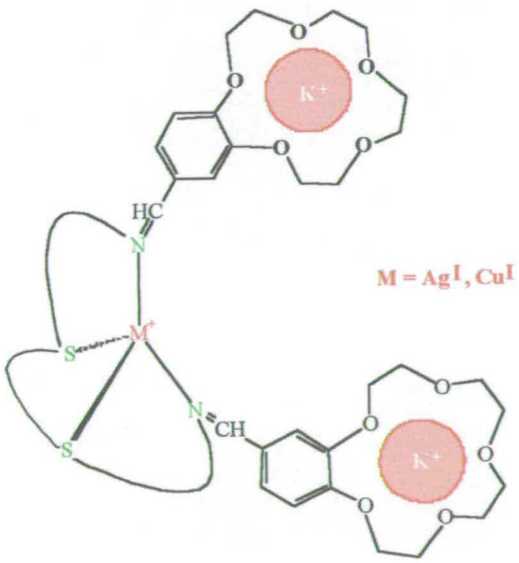

Figure 1.10 A system arranged for redox response upon guest binding [70]

(i) The host redox unit and the host cavity (guest binding site) should be in close proximity in order that communication between the two sites allows a significant perturbation in the potential of any redox process of the host upon binding of the guest metal ion.

(ii) This may be achieved by close proximity of the host redox unit and the guest-binding site or should be linked by a suitably delocalised system to enhance the perturbation on binding of the guest ion. This means that as well as sensing the binding through the structural backbone, through-space interactions should also be possible. Each of these factors therefore, contributes to the sensitivity of the redox sensing of binding.

One example of this approach involves air and moisture-stable diamagnetic alkoxides, amides and thiolates of the type [ML(NO)Y] {M = Mo or W; L = tris(3,5-dimethylpyrazolyl)-borate; Y = OR (alkyl or aryl), NHR (alkyl or aryl), or SR (R = alkyl or aryl)} are redox active, undergoing a 1-electron reduction to a paramagnetic species [71]. Bimetallic complexes containing the redox-active moieties [ML(NO)X] can be constructed using ligands such as $[C_6H_4O]^{2-}$, $[NHC_6H_4CH_2C_6H_4NH]^{2-}$ or $[Fe(\eta\text{-}C_5H_4S)_2]^{2-}$. These species undergo two 1 electron reductions and an analysis of the electrochemical data shows that the 2-redox-active units {MoL(NO)Y} may be bound to the periphery of or directly into crown ether rings, and addition of Na^+ to these redox-active guest macrocycles causes significant shifts in the measured $E_{1/2}$ values

Steps have been made to develop the concept of redox active systems further with the development of a redox active macrocycle designed for direct attachment to electrode surfaces. A compound containing a redox-switchable ferrocene unit, a cation binding site (crown ether), a hydrophobic tail, and a functional group suitable for conversion into an electrode anchor has been synthesised [72]. Its properties were studied using mass spectrometric and electrochemical techniques. The effect of cation binding on the properties of the compound were reported. These techniques

demonstrate cation-mediated co-operativity between the redox centre and the host-binding site.

Macrocycles containing a redox-active tetrathiafulvalene unit combined with a variety of receptors have been prepared. One example involves a phenanthroline ligand and these are able to respond to the binding of different metal ions (e.g. Cu^{I}, Ag^{I} and Li^{I}) when part of a precatenate complex. Thus Cu^{I} (R = Me), Min (M = Ag^{I}, Li^{I}, Ni^{II}; R = hexyl) and Cu^{II} were reported [73]. The complexes were characterised by cyclic voltammetry and differential pulse voltammetry where it was found that the Cu^{I} complex (R = Me) exhibits 3 reversible redox potentials assigned to the oxidation of Cu^{I} and 2 oxidations of the tetrathiafulvalene moiety.

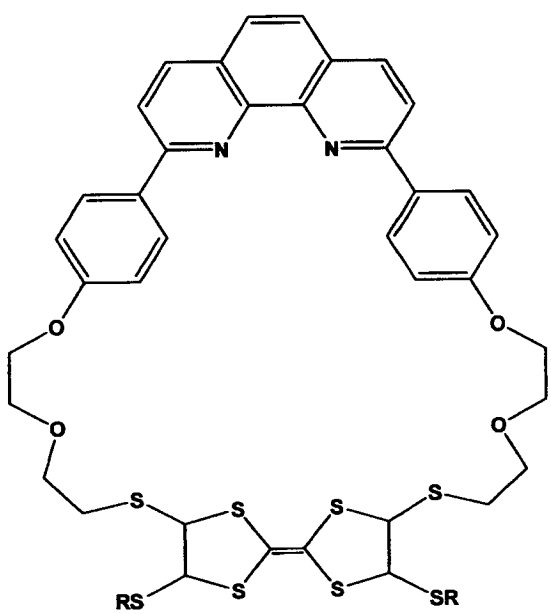

Figure 1.11 General Structure of the Phenanthroline-tetrathiafulvalene macrocycle which is used as a redox active sensor for metal ions.

The Ag^{I} complex also exhibits 2 tetrathiafulvalene redox potentials. The appearance of the 2 tetrathiafulvalene redox potentials for the Cu^{I} and Ag^{I} complexes demonstrates the advantage of employing such macrocycles as possible redox responsive sensors for transition metal ions with distinctive shifts observed for the complexation of each of Cu^{II} and Ag^{I}.

Selectivity studies of these types of systems has proven to be an important topic of study with an investigation [74] of the interaction of Co^{II}, Ni^{II}, Cu^{II}, Zn^{II}, Cd^{II}, Pb^{II} and Ag^{I} with two N,N'-dibenzylated nitrogen-oxygen mixed donor macrocyclic ligands. It was found that both ligands formed stable complexes with only the Cu^{II} and the Ag^{I} ion. While both complexes were formed however, transport measurements in a bulk liquid membrane system demonstrated a very high selectivity of the Ag^{I} ion over the other metal ions used.

1.3.4.2 Fluorescent Macrocycles

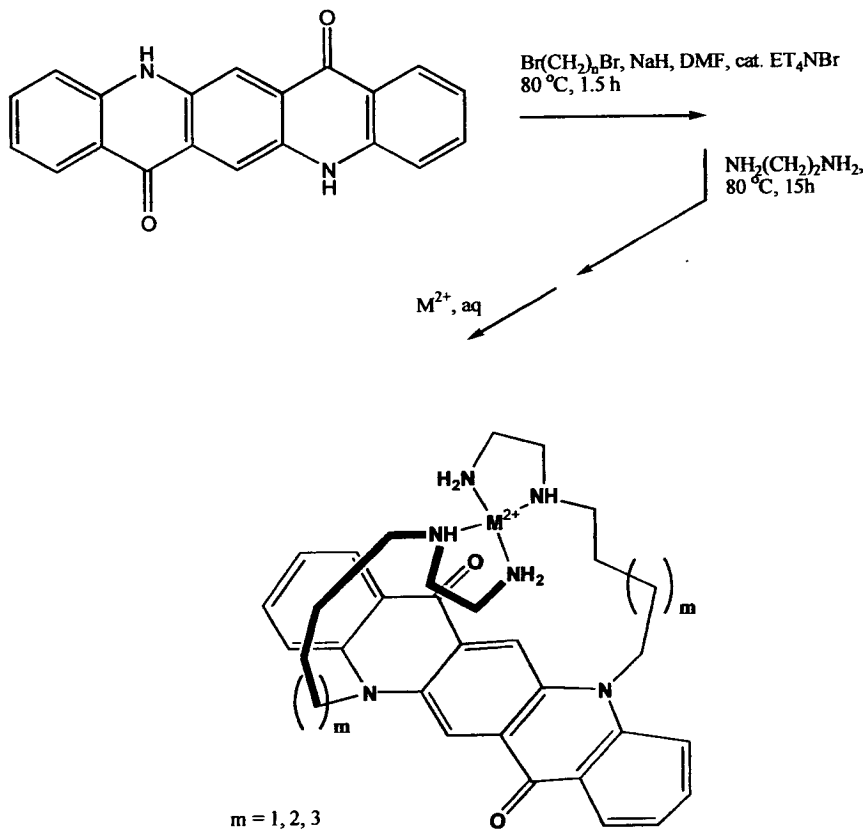

Scheme 1.17 Synthesis of quinacridone ligands from quinacridone. Complexation with co-ordinating metal ions (M = Cu, Hg, Z, Ni, Co) leads to a macrocycle in which the metal is placed above the aromatic unit.

Other transduction methods have also been investigated for measuring host-guest binding. A fluorescent metal-ion sensor based on chelation has been reported, Scheme 1.17 [75]. The light-emitting component is based on quinacridone, a red

organic pigment used in the dye industry and structurally related to acridone. Acridone has also been used to develop sensors for organic ligands [76].

In this work, a pair of chelating groups such as ethylenediamines, were attached via a linker to each nitrogen of the quinacridone. The linker was chosen to be long enough to ensure that the protonation-state of the chelating groups does not influence the fluorophore. Most importantly, the long linker also allows a co-ordinating metal ion to bind simultaneously at both groups in which the metal is in close proximity to the quinacridone chromophore.

Such an arrangement allows for fluorescence quenching, and this has been found to be particularly strong for metal ions such as copper and nickel [77]. Fluorescence titration curves show a 1:1 stoichiometry of complexation with Cu^{II} suggesting ML, M_2L_2 or M_nL_n modes of complexation.

1.3.4.3 Conclusions

The area of responsive macrocyclic chemistry has developed to become an important area of coordination chemistry. Redox active, Fluorescent and Chromogenic systems have all been reported. However, in most of the literature references in the area of responsive macrocycles, the work has related almost entirely to hard donor systems i.e. systems containing oxygen and nitrogen donor atoms. Few examples have been reported in the literature in which soft donor systems have been used.

1.4 Conclusions

From the details reported in this chapter, the extent of the work reported in the literature based on both hard and soft donor ligand systems and their complexation with metal ions is considerable, most particularly in the case of the hard donor systems. However, when we consider the developments made in the preparation and development of responsive macrocyclic systems, the emphasis has been placed largely on hard donor systems and their capacity to bind Group 1 and Group 2 metal ions. Comparatively little work has been done on responsive soft donor systems in this area. Based on these findings, the key focus of attention in this work turns to the preparation and development of responsive soft donor systems, which contain a mixed sulfur and nitrogen donor cavity capable of complexing transition metal ions.

In order to achieve this, we aim to incorporate a dithiolene precursor capable of introducing extended delocalistion into the system e.g. $[tto]^{2-}$ [3]. This would act to improve the communication between the responsive metal unit and the guest-binding site.

The systems developed will be applied as soft-donor sensors co-ordinating the metal ions to the right hand side of the transition metal series e.g. Fe – Zn. Also included, as guest ions are some heavier metal ions such as Cd^{II}, Hg^{II} and Pb^{II}. An interaction between the guest ion and the redox-active site of the host molecule is proposed to significantly alter the electrochemical and spectroscopic properties of the host metal unit upon complexation of the guest metal ion.

1.5 References

1 P. Cassoux, L. Valade, H. Kobayashi, A. Kobayashi, R. A. Clark and A. E. Underhill, *Co-ord. Chem. Rev.*, 1991, **110**, 115

2 C. S. Winter, S. N. Oliver, R. J. Manning, J. D. Rush, C.A. S. Hill and A. E. Underhill, *J. Mater. Chem.*, 1992, **2**, 443

3 M. L. Allan, A. T. Coomber, I. R. Marsden, R. H. Friend, A. Charlton and A. E. Underhill, *Synth. Met.*, 1993, **55-57**, 3317

4 N. Svenstrup, J. Becher, *Synthesis*, 1995, 215

5 T. K. Hansen, J. Becher, *J. Adv. Mater.*, 1993, **5**, 288 and *references therein*

6 N. Robertson, L. Cronin, *Coordination Chem. Rev.*, 2002, **227**, 1, 93

7 B. Fetkenheuer, H. Fetkenheuer, H. Lecus, *Chem. Ber.* 1927, **60**, 2528

8 (a) G. Steimecke, R. Kirmse, E. Hoyer, *Z. Chem.*, 1975, **15**, 28; (b) G. Steimecke, H–J Sieler, R. Kirmse, E. Hoyer, *Phosphorus Sulphur* 1979, **7**, 49

9 K. Hartke, T. Kissel, J. Quante, R. Matusch, *Chem. Ber.*, 1980 **113**, 1898

10 (a) P. R. Moses, J. Q. Chambers, *J. Am. Chem. Soc.*, 1974, **96**, 945; (b) J. Röhrich, K. Mullen, *J. Org. Chem.*, 1992, **57**, 2374; (c) A. J. Moore, M. R. Bryce, *Tetrahedron Lett.*, 1992, **33**, 1373

11 E. Fanghanel, K.-H Kuhnemund, A. M. Richter, *Synthesis*, 1984, 319

12 X. Yang, T. B. Rauchfuss, S. R. Wilson, *J. Chem. Soc., Chem. Commun.*, 1990, 34

13 N. Svenstrup, K. M. Rasmussen, T. K. Hansen, J. Becher, *Synthesis,* 1994, 809

14 V.Yu Khordorkovsky, Ya.Ya Katsens, O.Ya. Neilands, *Khim. Geterotsikl. Soedin,* 1986, 1568

15 (a) G. N. Schauzer, V. P. Mayweg, *J. Am. Chem. Soc.,* 1962, **84**, 3221; (b) H. B. Gray, R. Williams, I. Bernal, E. Billig, *J. Am. Chem. Soc.,* 1962, **84**, 3596; (c) J. A. McCleverty, *Prog. Inorg. Chem.,* 1968, **10**, 49

16 (a) G. N. Schrauzer, *Acc. Chem. Res.*, 1969, 2, 72; (b) R. P. Burns, C. A. McAuliffe, *Adv. Inorg. Chem. Radiochem*, 1979, **22**, 303; (c) U. T. Mueller-Westerhoff and B. Vance, in "Comprehensive Coordination Chemistry", ed

by G. Wilkinson, R. Gillard and J. A. McCleverty, Pergamon Press, New York, 1987, Vol. 2, p. 545

17 (a) A. Suigimori, M. Kajitani, *Kagaku (Kyoto)Zokan*, 1988, No 15, p. 113; (b) A. Suigimori, Yuki Gosei Kagaku Kyokai Shi, 1990, **8**, 788; (c) A. Suigimori, *Organomet.* News., 1990, No. 1, 1; (d) A. Suigimori, *Kokagaku (Photochemistry)*

18 C. S. Winter, S. N. Oliver, J. D. Rush, C. A. S. Hill, A. E. Underhill, *Mol. Cryst. Liq. Cryst,* 1993. **235**, 181

19 H. Wong, T. Meyer-Friedrichsen, T. Farrell, C. Mecker, J. Heck, *Eur. J. Inorg. Chem.*, 2000, **4**, 631

20 R. S. McLean, *Abstr. Pap. Am. Chem. S.*, 1992, **204 5-TECH**, Part 1

21 (a) S. Boyde, C. D. Garner, J. A. Joule and D. J. Rowe, *J. Chem. Soc., Chem. Commun.*, 1987, 800; (b) D, Argyropoulos, E, Lyris, C. A. Mitsopoulou and D. Katakis, *J. Chem. Soc., Dalton. Trans.*, 1997, 615

22 S. Wawzonek and S. M. Heilmann, *J. Org. Chem.*, 1974, **39**, 511

23 (a) P. Jeroschewski, *Z. Chem.*, 1981, **21**, 412; (b) P. Jeroschewski, P. Hansen, *Sulfur Rep.*, 1986, **7**, 1

24 J. C. Lodmell, W. C. Anderson, M. F. Hurley and J. Q. Chambers, *Anal. Chim. Acta,* 1981, **129**, 49

25 J. G. Breitzer, J–H Chou, T. B. Rauchfuss, *Inorg. Chem.*, 1998, **37**, 2090

26 A detailed discussion of the synthesis and head-to-head coupling mechanism of CS_2 is given by: E. Hoyer, *Comments Inorg. Chem.*, 1983, **2**, 261. For the structure of $(Ph_4P)_2C_2S_4$ see H. Lund, E. Hoyer, R. G. Hazell, *Acta Chem. Scand., Ser. B*, 1982, **B36**, 207

27 (a) L. F. Szczepura, C. P. Galloway, Y. Zheng, P. Han, A. L. Rheingold, S. R. Wilson, T. B. Rauchfuss, *Angew. Chem., Int. Ed. Engl.*, 1995, **34**, 5220

28 (a) J. J. Maj, A. D. Rac, L. F. Dahl, *J. Am. Chem. Soc.*, 1982, **104**, 4278; (b) P.V. Broadhurst, B. F. Johnson, J. Lewis, P. R. Rathby, *J. Chem. Soc., Chem. Commun.*, 1982, **140**; (c) H. A. Harris, A. D. Rac, L. F. Dahl, *190th National Meeting of the American Chemical Society Chicago, IL*, 1985

[29] B. M. Gimarc, In *Molecular Structure and Bonding*, Academic Press: New York, 1979, 187-192

[30] R. Vincente, J. Ribas, S. Alvarez, A. Segui, X. Solans, M. Verdaguer, *Inorg. Chem.*, 1987, **26**, 4004

[31] (a) K. Hartke, T. Kissel, J. Quante and G. Hessen, *Angew. Chem.* 1978, **90**, 1016; (b) K. Hartke, J. Quante and T. Kampchen, *Justus Liebigs Ann. Chem.*, 1980, 1482;

[32] K. Hartke, T. Kissel, J. Quante and R. Matusch, *Chem. Ber.*, 1927, **60**, 2528

[33] P. Strauch, W. Dietzsch and E. Hoyer, *Z. Chem.*, 1983, **23**, 448

[34] L. K. Hansen, J. Sieler, P. Strauch, W. Dietzsch and E. Hoyer, *Acta Chem. Scand. Ser. A*, 1985, **39**, 571

[35] J. Piotraschke, A. E. Pullen, K. A. Abboud, J. R. Reynolds, *Inorg. Chem.*, 1995, **34**, 4011

[36] A. E. Pullen, R.-M. Olk, S Zeltner, E. Hoyer, K. A. Abboud, J. R. Reynolds, *Inorg. Chem.*, 1997, **36**, 4163

[37] T. L. Sheng, X. T. Wu, Q. M. Wang, P. Lin, *Chinese Journal of Structural Chemistry*, 2001, **20**, 537

[38] U. Geiser, M. L. Mercuri, J. P. Parakka, *Acta. Crystallogr. C.*, 1999, **55**, 1253

[39] X. G. Yang, D. D. Doxsee, T. B. Rauchfuss, S. R. Wilson, *J. Chem. Soc., Chem. Commun*, 1994, 821

[40] K. Hartke, T.Kissel,J. Quante, G. Hessen, *Angew. Chem.*,1978, **90**, 1016; K. Hartke, J. Quante, T. Kampchen, *Justus liebigs Ann. Chem.*, 1980, 1482

[41] K. Hartke, T. Kissel, J. Quante, R. Matusch, *Chem. Ber.*, 1927, **60**, 2528

[42] P. Strauch, W. Dietzsch, E. Hoyer, *Z. Chem.*, 1983, **23**, 448

[43] J. Rheinhold, G. Stich, R. Strauch, R. Benedix, J. Siedler, E. Hoyer, *Z. Chem.*, 1987, **27**, 29

[44] W. Stork, R. Mattes, *Angew. Chem.*, 1975, **87**, 452

[45] (a) R. Mattes, W. Meschede, *Chem. Ber.*, 1976, **109**, 1832; (b) W. Meschede, R. Mattes, *Chem. Ber.*, 1976, **109**, 1832

46 R. Mattes, W. Stork, J. Kahlenberg, *J. Spectrchim. Acta*, 1977, **33A**, 643

47 W. Dietzch, P. Strauch, E. Hoyer, *Coord. Chem. Rev.*, 1992, **121**, 43

48 (a) J. A. Iibers, L. J. Pace, J. Marinsen, B. M. Hoffman, *Struct. Bonding (Berlin)*, 1982, **50**, 1; (b) E. Hoyer, W. Dietzch, W. Schroth, *Z. Chem.*, 1971, **11**, 41; (c) R. Eisenberg, *Prog. Inorg. Chem*, 1970, **12**, 295, (d) D. Coucouvanis, *Prog. Inorg. Chem.* 1970, **11**, 233 (e) L. F. Lindoy, *Coord. Chem. Rev.* 1969, **4**, 4; (f) L. Alcácer, H. Novais, In "*Extended Linear Chain Compounds*"; J. S. Miller, Ed, Plenum Press: New York, 1983; Vol. 3, Chapter 6

49 K. R. Adam, D. S. Baldwin, P. A. Duckworth, L. F. Lindoy, M. McPartlin, A. Bashall, H. R. Powell, P. A. Tasker, *J. Chem. Soc., Dalton Trans.*, 1995, **7**, 1127

50 (a) J. S. Bradshaw, J. Y. K. Hui, *J. Heterocyclic Chem.*, 1974, **11**, 649, (b) S. R. Cooper, *Acc. Chem. Res.*, 1988, **21**, 141; (c) A. J. Blake, M. Schroder, *'Advances in Inorganic Chemistry'*, Academic Press. Inc., 1990, Vol. 35.

51 P. C. Rây, *J. Chem. Soc.*, 1920, 1090

52 J. R. Meadow, E. E. Reid, *J. Am. Chem. Soc.*, 1934, **56**, 2177

53 L. A. Ochrymowycz, C–P Mak, J. D. Michna, *J. Org. Chem.*, 1974, **39**, 2079

54 K. Butler, R. M. Kellogg, *J. Chem. Soc., Chem. Commun.*, 1980, 466

55 J. Butler, R. M. Kellogg, *J. Org. Chem.* 1981, **46**, 4481

56 D. St. C. Black, I. A. McLean, *J. Chem. Soc., Chem. Commun.*, 1970, 1055

57 I. Tabushi, H. Okino, Y. Juroda, *Tet. Lett.*, 1976, 4339; D. Pelissard, R. Louis, *Tet. Lett,* 1972, 4589

58 (a) C. A. Salata, D. Van Engen and C. J. Burrows, *J. Chem. Soc., Chem. Commun.*, 1988, 579; (b) A. Carroy and J. -M Lehn, *ibid.*, 1986, 1232; (c) D. Parker, J.–M Legn and J. Rimmer, *J. Chem. Soc., Dalton. Trans.*, 1985, 1517; (d) M. J. Gunter, L. N. Mander, K. S. Murray and P. E. Clark, *J. Am.*

Chem. Soc., 1981, **103**, 6784; (e) J.–M. Lehn, *Pure Appl. Chem.*, 1980, **52**, 2441

59 G. R. Newkome and J. M. Robinson, *J. Chem. Soc., Chem. Commun.*, 1973, 831

60 H. F. Dare, J. A. K. Howard, U. P Massimino, F. G. A. Stone, J. Szameitat. *J. Chem. Soc., Chem. Commun*, 1989, 1409

61 S. G. Murray, F. R. Hartley, *Chem. Rev.*, 1981, **81**, 365

62 T.–L Ho., *Chem. Rev.*, 1975, **75**, 1; T.–L. Ho, *Hard and Soft Acids and Bases Principle in Organic Chemistry*, Academic Press, New York-San Francisco-London, 1977

63 D. J. Cram, J. M. Cram, *Science*, 1974, **183**, 803

64 (a) C. A. McAuliffe, Ed., "Transition Metal Complexes of Phosphines, Arsines and Stilbines", Macmillan, London, 1973; (b) W. Levason and C. A. McAuliffe, *Adv. Inrog. Radiochem.*, 1972, **14**, 173

65 (a) (b) J. A. McCleverty, *Prog. Inorg. Chem.*, 1968, **10**, 49; (c) M. A. Ali and S. E. Livingstone, *Coord. Chem. Rev.*, 1974, **13**, 101; (d) L. F. Lindoy, Coord. *Chem. Rev.*, 1969, **4**, 41

66 (a) G. W. Liesengang and E. M. Eyring, *In Synthetic Multidentate Macrocyclic Compounds*, Eds R. M. Izatt and J. J. Christensen, Academic Press, New York, 1978, pp245; (b) E. M. Eyring, M. M. Farrow, L. J. Rodriquez, L. B. Lloyd, R. P. Rohrbach and E. L. Allred, *NATO Adv. Study Inst. Ser., Ser. C*, 1979, **50**, 355; (c) F. Vögtle, *Pure Appl. Chem.* 1980, **52**, 2405; (d) S. L. Bazter and J. S. Bradshaw, *J. Heterocyclic Chem.* 1981, **18**, 233; (e) R. M. Izatt, J. S. Bradshaw, S. A. Nielsen, J. D. Lamb, J. J. Christensen and D. Sen. *Chem. Rev,* 1985, **85**, 271

67 In '*Coordination Chemistry of Macrocyclic Compounds*', E. C. Constable, Oxford, Chemistry Primers No. 72, Oxford Science Publications, Oxford University Press, 1998, p54-58

68 D. J. Cram, *Angew. Chem., Int. Ed. Engl.*, 1986, **25**, 1039

69 M. A. Ahearn, J. Kim, A. J. Leong, L. F. Lindoy, O. A. Matthews, G. V.

Meehan, *J. Chem. Soc., Dalton Trans*, 1996, **17**, 3591

[70] P. D. Beer, *Adv. Inorg. Chem.*, 1992, **39**, 79

[71] J. A. McCleverty, *Proc. Indian. Natl. Sci. Acad., Part A*, 1986, **52(4)**, 796

[72] J. C. Medina, B. C. Lynn, M. T. Rojas, G. W. Gokel, A. E. Kaifer, *Supramol. Chem.*, 1993, **1(2)**, 144

[73] K. S. Bang, M. B. Nielsen, R. Zubarev, J. Becher, *J. Chem. Soc., Chem. Commun*, 2000, **3**, 215

[74] J. Kim, T–H Ahn, M. Lee, M. Cho, S–J Kim, *J. Korean Chem. Soc.*, 1999, **43(2)**, 167

[75] G. Klein, D. Kaufmann, S. Schurch and J–L Reymond, *J. Chem. Soc., Chem. Commun.*, 2001, 561

[76] (a) J–L Reymond, T. Koch, J. Schroer and E. Tierney, *Proc. Natl. Acad. Sci.* USA, 1996, **93**, 4251; (b) N. Bahr, E. Tierney and J–L Reymond, *Tetrahedron Lett*, 1997, **38**, 1489; (c) P. Geymayer, N. Bahr and J–L Reymond, *Chem. Eur., J.*, 1999, **5**, 1006; (d) J. H. Roothman and W. C. Still, *Biorg. Med. Chem. Lett.*, 1999, **9**, 509

[77] F. Bolletta, H. Costa, L. Fabbrizzi, M. Licchelli, M. Montalti, P. Pallavicini, L. Prodi and N. Zaccheroni, *J. Chem. Soc., Dalton Trans.*, 1999, 1381

Chapter Two

Experimental Techniques

Experimental Techniques

2.0 Introduction

Throughout the course of this project a number of electrochemical, spectroelectrochemical and spectroscopic techniques were used to study both the systems prepared and the complexation of metals to these systems. This chapter outlines the various techniques employed and discusses the advantages and disadvantages of each technique.

2.1 Chemicals and Instrumentation

The solvents dichloromethane, CH_2Cl_2 {99.6% A.C.S. spectrophotometric grade}, dimethylformamide, DMF {99%}, tetrahydrofuran, THF {99.9%, inhibitor free HPLC grade} acetonitrile MeCN (A.C.S. spectrophotometric grade) and hexane (A.C.S. spectrophotometric grade) were obtained from Acros for the duration of this work. All reagents were of AnalaR quality or equivalent and unless otherwise stated, were used as received either from Sigma Aldrich or Acros.

All electrochemical and spectroscopic experiments were carried out in either dichloromethane or dimethylformamide, or tetrahydrofuran distilled from sodium and benzophenone. In the case of the electrochemical studies, background electrolytes were prepared using either tetrabutylammonium tetrafluoroborate $[NBu_4][BF_4]$ (0.1 M), or tetrabutylammonium hexafluorophosphate $[NBu_4][PF_6]$ (0.1 M) (see Section 3.5).

Electrochemical studies were controlled by a PST AT20 potentiostat and the experimental results manipulated using a DELL 466DL personal computer with General Purpose Electrochemical System (GPES) Version 4.5 software. The combined system is an Autolab system. All of the electrochemical techniques used a three-electrode configuration, consisting of a working electrode, a reference electrode and a counter (auxiliary) electrode. Potentials were applied between the working electrode and the reference electrode with currents being monitored between the working electrode and the counter electrode.

Elemental microanalysis data were either obtained using a Perkin-Elmer 2400 Elemental Analyser at the University of Edinburgh or a Carlo Erba CE 1108 elemental analyser operated by University of London Microanalytical Service. Electron impact mass spectrometry (EIMS) was carried out on a Kratos MS50TC spectrometer. Fast atom bombardment Mass Spectrometry (FABMS) was carried out using a Kratos MS50TC spectrometer with a 3-nitrobenzyl alcohol (NOBA) or thioglycerol matrix. Infra-red spectra were obtained as potassium bromide discs or solution spectra (solvent as specified) using a Perkin Elmer Paragon 1000 FT-IR spectrometer. All experiments involving ultraviolet spectroscopy were recorded on a lambda-9 spectrophotometer (Perkin Elmer), controlled by a Datalink PC running UV Win Lab software (version 2.70.01).

2.2 Electrode Properties [1, 2]

2.2.1 Working Electrode properties

The form of the working electrode depends on the electrochemical technique used. In all media, platinum electrodes tend to be generally employed, as they are

chemically inert over a wide potential range. A micro-working electrode was used which consists of a platinum disc, 0.5mm in diameter.

2.2.2 Electrode Processes

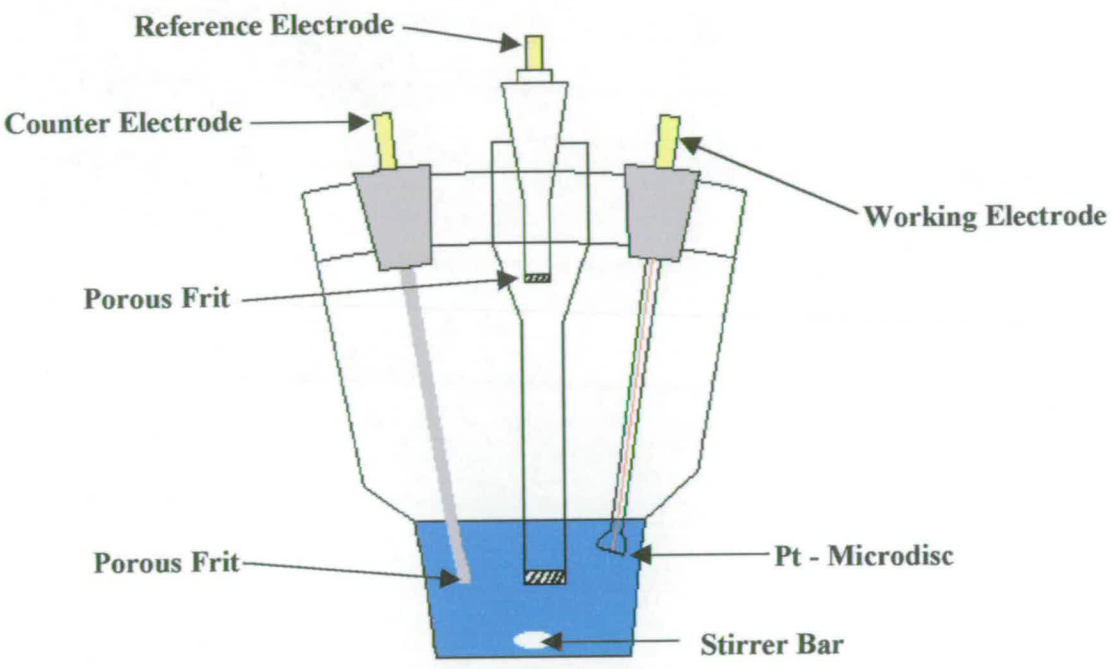

Figure 2.1 A typical cell for conventional electrochemical methods.

A typical experimental configuration for the electrochemical experiments in this thesis is shown in Figure 2.1 consisting of a Reference, Working and Counter electrode.

An electrode process involves the transfer of an electron between the electrode metal (m) and a redox species in the solution (s). If ϕ_s is the solution potential and the

metal potential is ϕ_m, then the potential drop across the electrode/solution interface $\Delta\phi_{m/s}$ controls the electron transfer rate. This is given by

$$\Delta\phi_{m/s} = \phi_m - \phi_s \qquad \textbf{Equation 2.1}$$

and is controlled by the applied voltage. However, direct measurement of $\Delta\phi_{m/s}$ is not feasible. For this reason a reference electrode is introduced into the system.

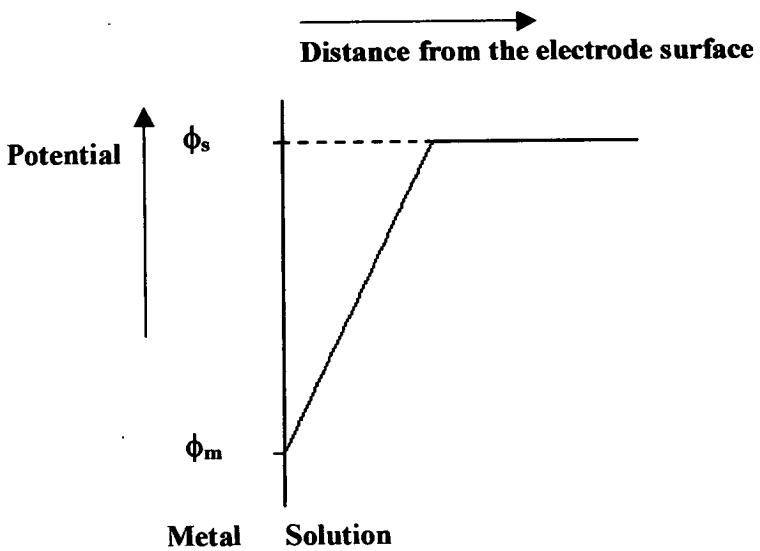

Figure 2.2 Schematic diagram of the potential drop across the metal/solution interface

A potential difference (or voltage) is applied between the working electrode and the reference electrode. Background electrolyte is added to the solution to ensure the potential drop, Figure 2.2, is as close to the electrodes as possible. Those ions at high electrolyte concentrations of 50-100 mM, form a thin double layer at the electrode surface, allowing the redox species to travel through the solution by diffusion to the electrode in order to react. The reaction is governed by $\Delta\phi_{m/s}$, which is varied by

changing the applied voltage, E as the reference electrode maintains a constant potential drop $\Delta\phi_{m/s}$ across its interface, Figure 2.3. The voltage, E can also be thought of as the potential of the working electrode with respect to the reference electrode.

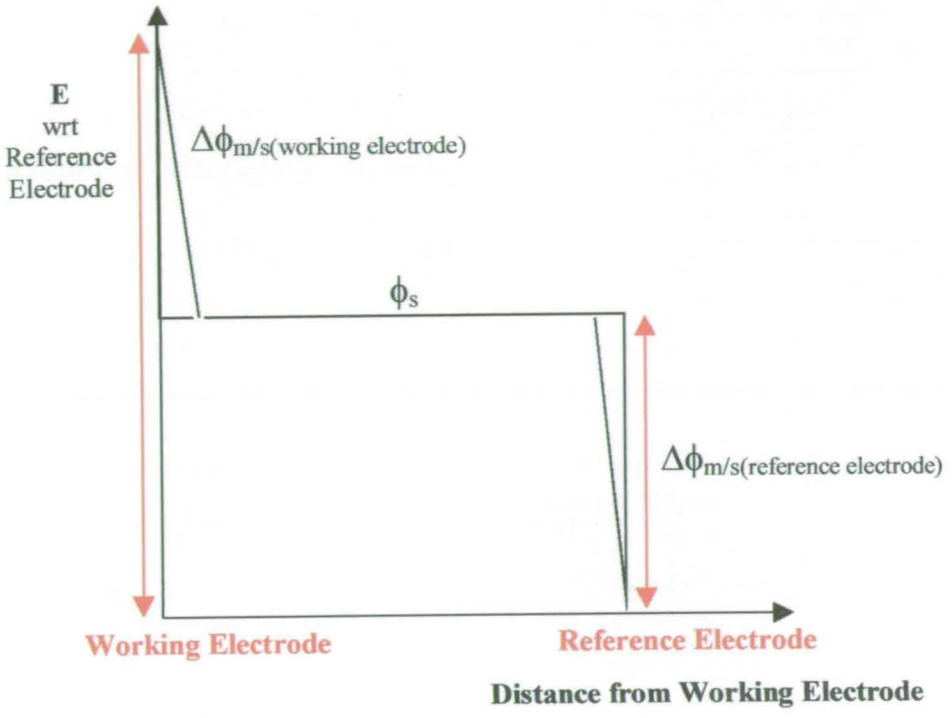

Figure 2.3 Control of changes in $\Delta_{\phi m/s\ (working\ electrode)}$ by changing the applied potential, E

This means that

$E = \Delta\phi_{m/s\ (working\ electrode)} - \Delta\phi_{m/s\ (reference\ electrode)}$ **Equation 2.2**

where $\Delta\phi_{m/s(reference\ electrode)}$ is constant, so the changes in the applied potential cause changes only in $\Delta\phi_{m/s(working\ electrode)}$, and hence changes to the working electrode reaction rate, Figure 2.3.

2.2.3 Reference and Counter Electrode Properties

When considering the suitability of the reference system, a number of issues need to be addressed

The internal resistance of this component should be not be high compared to the other electrodes. In fact, the reference electrode is designed to be able to take a large current without altering $\Delta\phi_{m/s(\text{Reference Electrode})}$. The reference electrode should use an electrochemically reversible redox couple, containing large amounts of oxidant and reductant in order to ensure a stable potential. In the case of the work described in this thesis, the reference electrode used here is Ag/AgCl in a 0.45M $[NnBu_4]BF_4$, 0.05M $[NnBu_4]Cl$ dichloromethane solution against which, the ferrocenium/ferrocene couple was measured at +0.550 V.

The reference solution must also not cause contamination of the test solution or be contaminated itself. In order to prevent this a porous frit is generally employed to separate the reference system from the electrochemical solution. In this particular work a double junction reference electrode is employed which reduces the influence of any changes in the redox potential (see Figure 2.1) by introducing a junction potential, which remains constant which further minimises any contamination.

The counter electrode used in the course of electrochemical experiments is usually constructed of an inert material, most commonly platinum, and should have a much larger surface area than the working electrode. This is to ensure that the working electrode reaction is rate limiting and determines the overall current. The counter electrode used in this work is a platinum rod.

2.3 Electrochemical Experimental Considerations[1, 2]

2.3.1 Solvent choice

When choosing a suitable solvent for the sample, the stability of the redox system in the solvent and of course its solubility, dictate the eventual choice. Other features of the solvent also to be considered in this regard include its effectiveness as an electrochemical solvent i.e. it must possess a wide electrochemical window, an accessible temperature range, a low viscosity and an ease of purification. Attention should also be paid to whether the solvent has any donor or co-ordination properties, as preferential coordination of selected oxidation states can cause shifts in the measured redox potentials. The dielectric constant of the solvent should also be high in order to minimise field effects and aggregation.

2.4 Electrochemical Techniques[1, 2]

2.4.1 Cyclic Voltammetry

Cyclic Voltammetry uses stationary electrodes in an unstirred solution. The lack of stirring in the test solution results in negligible mass transport of the sample species by migration and convection. As a result, diffusion is the predominant means of mass transport of the sample to the working electrode surface.

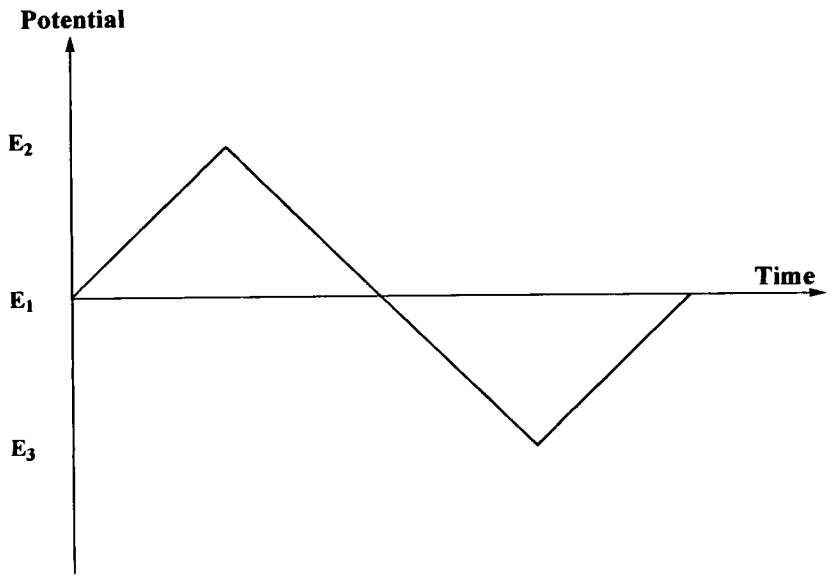

Figure 2.4 Triangular waveform of the first cycle of a Cyclic Voltammogram – Linear Sweep Voltammetry.

The potential of the working electrode is ramped linearly with time between two potentials. A cyclic voltammogram involves a triangular wave-form, (Figure 2.4). The potential is typically ramped from the starting potential E_1 to E_2, where the potential is then switched in the opposite direction until it reaches E_3 from where it finally cycles back to the starting potential to complete the cycle. Repeated cycling is used in Cyclic Voltammetry however, the first cycle of a cyclic voltammogram is often termed a Linear Sweep Voltammogram.

The scan-rate, ν, is constant and is typically between 0.02 and 0.5 V s^{-1}. The current, I, which flows at the working electrode, is measured as a function of the potential of the working electrode, E, and a cyclic voltammogram (of I versus E) is typically plotted.

2.4.2 Electrochemical Reversibilty

Electroactive species, which exhibit electron transfer at an electrode, fall into one of three classes.

(i) Electrochemically Reversible –

For the general reaction

$$O_{electrode} + e^- \underset{\leftarrow K}{\overset{\rightarrow K}{\Leftrightarrow}} R_{electrode} \qquad \textbf{Equation 2.3}$$

If both $\vec{K}$ and $\overleftarrow{K}$ are large, the rates of the reactions, Equation 2.3, will be fast compared to the rate of diffusion of the electroactive species to the electrode. As such, Equation 2.3 will be in equilibrium. In this case, a reduction process, the surface concentration of O and R can be calculated using the Nernst Equation. Such electrode reactions are termed *electrochemically reversible.*

The Nernst equation is

$$E_{eq} = E^{\theta} + \frac{RT}{nF} \ln \frac{a_O}{a_R} \qquad \textbf{Equation 2.4}$$

where E_{eq} is the equilibrium potential of the electrode (V); E^{θ} is the standard electrode potential of the redox reaction (V); a_O is the activity of the oxidised species and a_R is the activity of the reduced species at the electrode surface.

In background electrolyte the ionic strength of the solution can be considered to constant and so the Nernst equation becomes

$$E_{eq} \approx E^{\theta} + \frac{RT}{nF} \ln \frac{[O]}{[R]}$$ **Equation 2.5**

where [O] and [R] are the concentrations of oxidised and reduced species at the electrode surface. When [O] = [R], then $E_{eq} = E^{\theta}$.

The peak current at a maximum, i_{pa}, is directly proportional to the square root of the sweep rate ν, as given by Equation 2.4

$$i_p = (2.69 \times 10^5) n^{3/2} A D_O^{1/2} \upsilon^{1/2} C_O^*$$ **Equation 2.6**

at 25 °C

Where i_p is the peak current, n is the number of electrons, A is the area of the electrode (cm^2), C_O^* is the bulk concentration of the species O (mol cm^{-3}), ν is the scan rate and $D_O^{1/2}$ is the diffusion coefficient of the species O (cm^2 s^{-1}).

In linear sweep voltammetry of a fully electron transfer reaction, there is no change in peak position with sweep rate. Peak width is E_p-$E_{(p/2)}$ which is equal to 28.5/n mV for all scan rates. The peaks are separated by 56/n mV at 25 °C and E^{θ} lies midway between E_{pa} and E_{pc} (see Figure 2.5) where $E_{(pa/2)} = E_{pc}$ and $E_{(pc/2)} = E_{(pa/2)}$. The peak current ratio i_{pa}/i_{pc} = 1.0 at 25 °C for all scan rates where the effects of natural convection can be neglected and the peak current increases linearly as a function of the square root of the scan rate

The shape of the current response for a linear sweep voltammetry experiment, for the reduction of a species in solution is shown in, Figure 2.5. At the start of the experiment, the bulk solution contains only the reduced form of the redox couple (R) so that at potentials lower than the redox potential, i.e. the initial potential, there is no net conversion of R to O, the reduced form (point A).

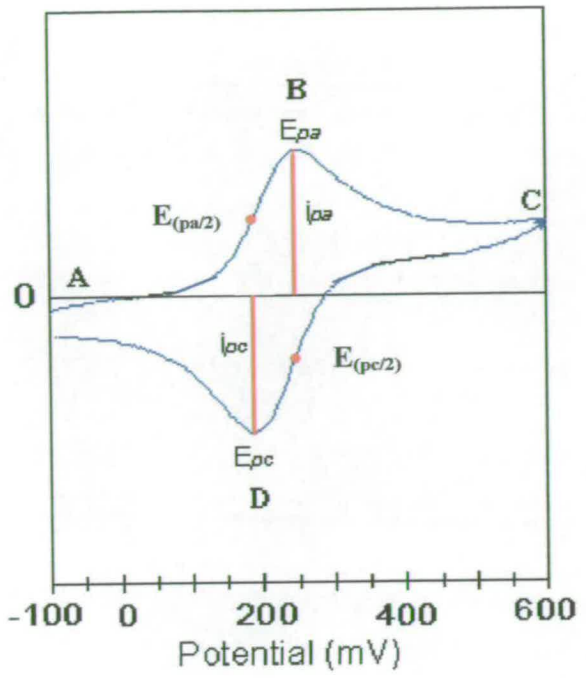

Figure 2.5 Typical Cyclic Voltammogram showing a fully reversible 1-electron reduction wave for the reduction of O to R. $E^0 = +230$ mV

As the standard electrode oxidation potential for the redox reaction is approached, there is a net anodic current, which increases exponentially with potential due to oxidation of R, depleting the concentration of R species near the electrode surface. When this depletion is large enough, the current reaches a peak (B) and then falls, as the e^- transfer becomes diffusion controlled. R is rapidly converted into O at the electrode and concentration gradients are set up which diffuse R to the electrode. Depletion of R extends further in the solution as this occurs, and transport becomes less efficient so the current falls. Eventually a pseudo steady state current is obtained at C where natural convection in the solution, which is impossible to eliminate, controls the mass transport.

When the sweep rate is reversed at C, the product O, formed at the electrode, is reduced. A return peak is therefore observed at a more negative potential than for the forward peak. The shape of this peak is governed by similar electron-transfer and diffusion rate factors as discussed above.

The parameters obtained from a linear sweep voltammogram can be used to determine the nature of a particular charge transfer reaction. These parameters, for an electrochemically reversible system are the anodic and cathodic peak currents and potentials, that is i_{pa}, i_{pc}, E_{pa} and E_{pc} respectively. These are shown in Figure 2.5. The average potential of E_{pa} and E_{pc} is the half wave potential, $E_{1/2}$ for the redox process under investigation where

$$E_{1/2} = E^{\theta} + \frac{RT}{nF} \ln \frac{D_R^{1/2}}{D_O^{1/2}} \qquad \textbf{Equation 2.7}$$

and for most systems where $D_o \approx D_R$

$$\ln \frac{D_R^{1/2}}{D_O^{1/2}} \approx 0 \qquad \textbf{Equation 2.8}$$

and $E_{1/2} = E^{\theta}$

(ii) ***Electrochemically Irreversible*** :- In this case, dynamic equilibrium is not established at the electrode surface. The electron-transfer rate is instead determined by the height of the energy barrier to the electron-transfer reaction.

Peaks show separations greater than 56.5/n mV and $|E_p-E_{p/2}| = (47.7/\alpha n)$ mV at 25 °C (α_{ox} is the transfer coefficient for an oxidation and α_{red} is the transfer coefficient for a reduction and $\alpha_{ox} = 1-\alpha_{red}$). From Equation 2.3 the reaction is now governed by the forward reaction only.

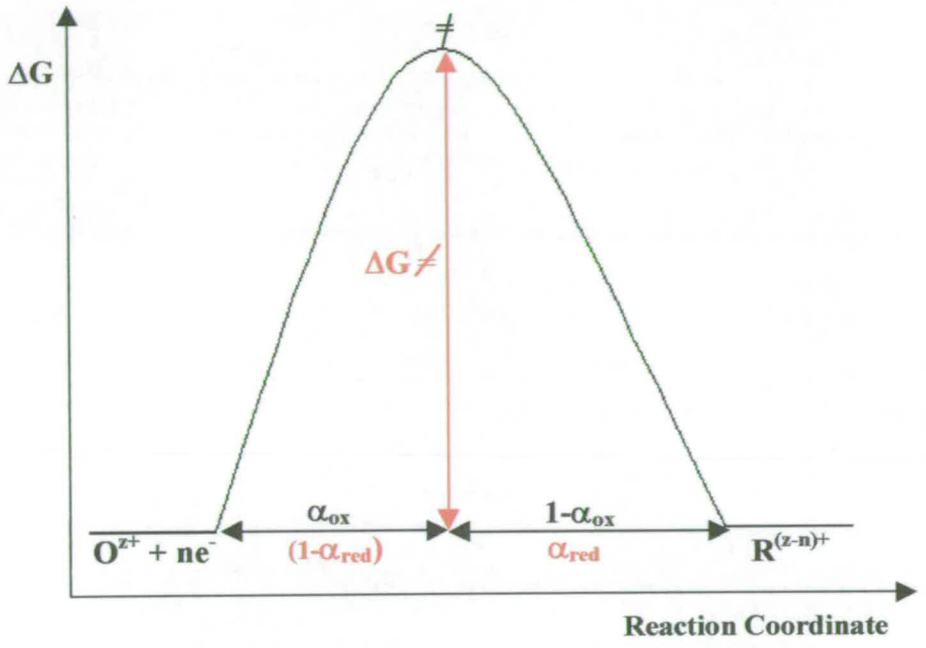

Figure 2. 6 Reaction profile for an irreversible reaction

In the case of an irreversible electrochemical reaction the peak current in linear sweep voltammetry is given by

$$i_p = (2.99x10^5)n(\alpha n_a)^{1/2} AC_O^* D_O^{1/2} \upsilon^{1/2} \qquad \textbf{Equation 2.9}$$

i_p is the peak current, n is the number of electrons, α is the transfer coefficient, n_a is the number of electrons involved in the rate determining step, A is the area of the electrode

(cm^2), C_O^* is the bulk concentration of the species O (mol cm^{-3}), ν is the scan rate and $D_O^{1/2}$ is the diffusion coefficient of the species O (cm^2 s^{-1}).

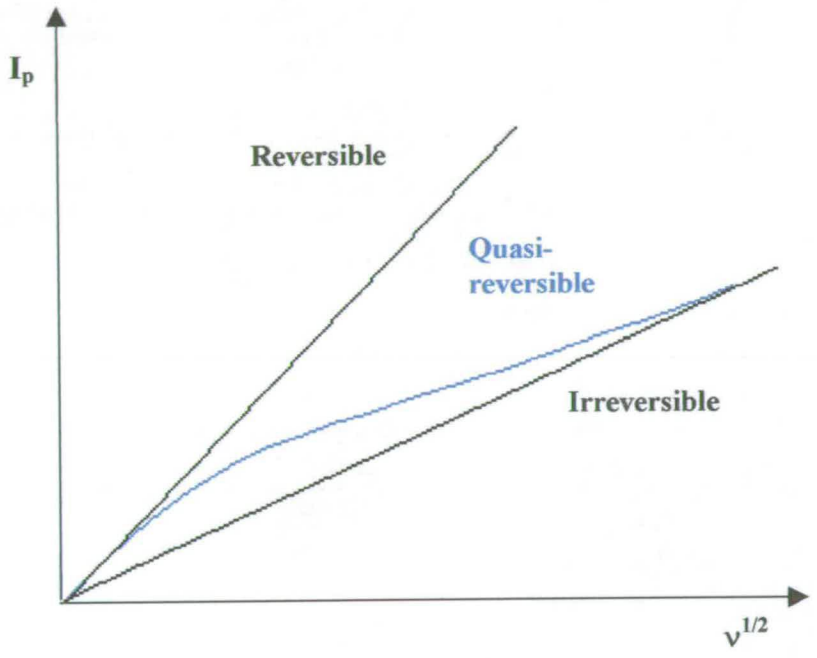

Figure 2. 7 Transition from a reversible system to an irreversible system on increasing sweep rate

For totally irreversible waves, i_p is proportional to C_O^* and $\nu^{1/2}$ and also E_p is a function of scan rate shifting positive (oxidation) and negative (reduction) by an amount $30/\alpha n_a$ mV at 25 °C for each tenfold increase in ν. A plot of ln (i_p) versus $E_p - E^\theta$ (E^θ is the standard potential of the electrode) determined at different scan rates should have a slope of $-\alpha n_a f$ (f = F/RT) and an intercept proportional to k^o.

(iii) ***Quasi-reversible*** :- For a quasi reversible system the electrochemical kinetics are intermediate between those of a reversible and irreversible system (Figure 2.7). Generally, the extent of irreversibility increases with increase in sweep rate, while at the same time there is a decrease in the peak current relative to the reversible case and an increasing separation between the anodic and cathodic peaks.

2.4.3 Chemical Irreversibility

Chemically irreversible reactions involve bonds breaking and a chemical reaction occurring (usually after electrochemical reactions), which often generate an electroinactive species i.e.

$$A + ne^- \leftrightarrow B$$ **Equation 2.10**

$$B(+C) \rightarrow D(+E)$$ **Equation 2.11**

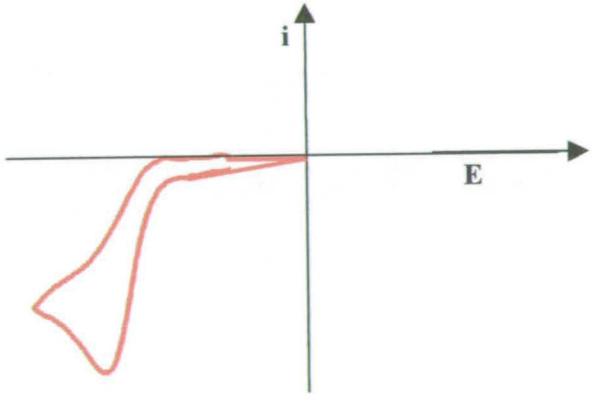

Figure 2. 8 Cyclic Voltammogram of a chemically irreversible reduction reaction

If D is electroinactive (Equation 2.11), in the limiting case when the chemical reaction is rapid then no back oxidation peak will occur (e.g. Figure 2.8) for the oxidation of B, as no B is left. However the reduction of A may be electrochemically reversible, and a sharp reduction peak may be observed.

2.4.4 Potential Step Chronoamperometry

In potential step chronoamperometric experiments the potential of the working electrode is changed instantaneously, and the current-time (chronoamperometric) response is recorded.

Assuming that the electrode reaction is as described by Equation 2.3, and that initially only R is present in solution, then a potential-time profile, as shown in Figure 2.9, is applied to the working electrode. E_1 is chosen such that no oxidation of R, or indeed any other electrode reaction, occurs. Then at time t = 0, the potential is instantaneously changed to a new value E_2, where the oxidation of R occurs at a diffusion controlled rate.

Ficks Second law, Equation 2.12, models the change in concentration of species, i with time at any point due to diffusion.

$$\frac{\partial c_i}{\partial_t} = D_i \frac{\partial^2 c_i}{\partial x^2} \qquad \textbf{Equation 2.12}$$

where, D_i is the diffusion coefficient of species i ($cm^2\ s^{-1}$) , c_i is the concentration of the species i (mol cm^{-3}), t is the time (s) and x is the distance from the point (m)

At the electrode surface, chosen as x = 0 at t = 0, c_i is instantaneously switched from its bulk value c_i^* to $c_i = 0$ as E_2 is chosen to be sufficiently large that the reaction is under diffusion control. Integration of Equation 2.12 with respect to x and t, with the

further boundary condition that as $x \rightarrow \infty$, $c_i \rightarrow c_i^*$ leads to the generation of $c_i(x,t)$. As $I = \pm nFAj$ where j is the flux of I at the electrode surface then

$$I = \pm nFADc\left(\frac{\partial c_i}{\partial x}\right)_{x=0} \qquad \textbf{Equation 2.13}$$

as, from Ficks first law

$$j = -D_i\left(\frac{\partial c_i}{\partial x}\right)_{x=0} \qquad \textbf{Equation 2.14}$$

then, the Cottrell equation relating i to t can be derived, Equation 2.15.

$$i = \frac{nFAD^{1/2}c_o^*}{\pi^{1/2}t^{1/2}} \qquad \textbf{Equation 2.15}$$

where i, is the current passed (A); n is the no of electrons passed; F is the Faraday constant (C mol^{-1}). D is the diffusion coefficient of the species O in the bulk solution ($cm^2\ s^{-1}$), A is the area of the electrode (cm^2), c_O^* is the concentration of the species O in the bulk solution (mol cm^{-3}), and t is the time (s).

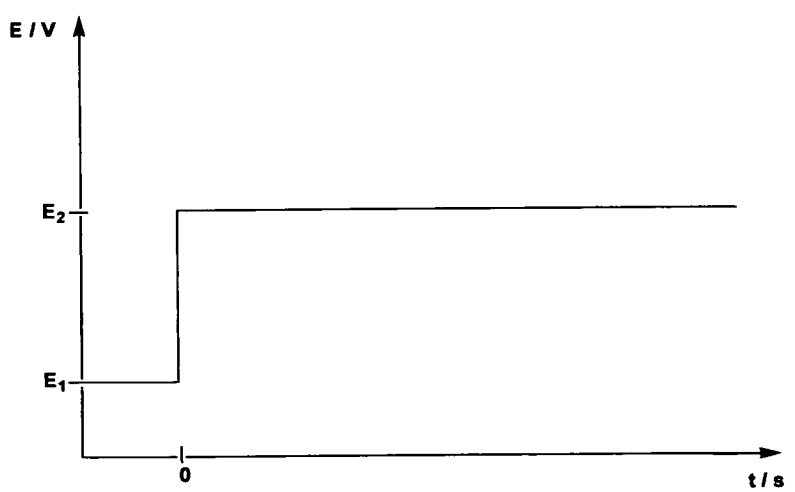

Figure 2. 9 Potential-Time profile for a single potential step chronoamperometric experiment.

A plot of I versus $t^{-1/2}$ should therefore be linear, passing through the origin, from which the diffusion coefficient D_i, can be found from the gradient of the straight-line plot as long as c_∞ is known. When measuring t, the shortest time for a reliable measurement will be determined by the time for the double layer to charge, which usually takes of the order of a few hundred microseconds for the microelectrode used in this work. The longest time is determined by the growing importance of natural convection. Even without taking special precautions, a value of a few seconds should easily be possible. Hence data over the range 1 ms to 10 s is normally plotted.

2.4.5 Bulk Electrolysis – Coulometry – Electrosynthesis

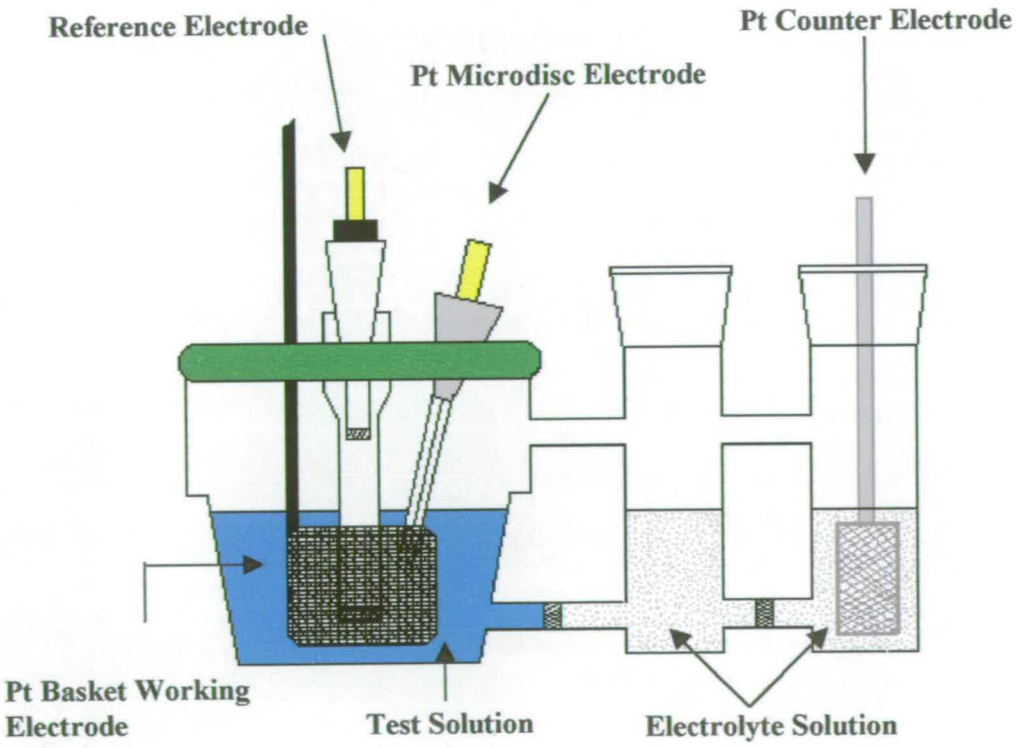

Figure 2.10 H-type cell used for potentiostatic electrolysis

There are two types of electrolysis; Potentiostatic, where the potential is fixed and the current is monitored with time and Galvanostatic, where a chosen current is forced to flow through the cell and the potential is monitored with time. Potentiostatic electrolysis was used throughout this work, as this is more suited to experiments where complete conversion of redox species in solution is required.

In bulk electrolysis a chosen potential is applied to a large working electrode (a platinum basket electrode was employed here) and the complete sample of electroactive species is reduced or oxidised in the stirred solution. The reference electrode is placed in the centre of the basket electrode and a Pt micro-disc electrode is also present in this compartment to facilitate the study of the redox properties of the electroactive species and the electrolysis products. In order to avoid the counter electrode reaction being simply the reverse of the electron transfer process, it is placed in a compartment separated from the working electrode by a glass frit (Figure 2.10). This also prevents the contamination of the test solution with any counter electrode products, which may be produced during the electrolysis. This set-up is commonly known as a H-cell.

In order to ensure complete conversion of a redox active species at the working electrode, it is a rule of thumb that, for an oxidation, the potential applied must be at least 60 mV more positive of the E^{θ} value (or more negative than E^{θ} for a reduction). The reason for this can clearly be seen from the Nernst Equation, Equation 2.5.

In a system where n = 1, a value of $E - E^{\theta} = 60$ mV corresponds to a ratio of [O]/[R] of 10 whereas a value of $E - E^{\theta} = -60$ mV corresponds to a ratio of [O]/[R] = 0.1. An applied potential of 60 mV greater or less than E^{θ} would therefore correspond to 91 % conversion of the reactants when equilibrium is established Applying a potential greater than 60 mV would therefore ensure complete conversion.

The current which flows and its' integral with time can be measured and the charge, Q can be calculated. Assuming 100 % efficiency, this charge can be related to the

amount of material, which has reacted and hence from the total amount of redox active species the number of electrons, n, involved in the electron transfer step can be calculated using

$$n = \frac{QM}{FW}$$ **Equation 2.16**

where Q is the total charge passed (C), M is the molecular mass of electroactive species (g mol^{-1}), F is the faraday constant (C mol^{-1}), W is the mass of sample used (g)

Following complete reduction or oxidation, the product can be investigated using Linear Sweep and Cyclic Voltammetry using the Pt micro-disc electrode and its electrochemical characteristics investigate using the electrochemical techniques outlined above (Section 2.4.1).

2.5 Electronic Spectroscopy – Ultraviolet Spectroscopy [4, 5]

Three main types of electronic transitions are usually found. These are categorised as metal based, charge transfer or ligand based in origin. Each transition type is considered separately, however the selection rules [2], which govern these transitions, are discussed together below.

2.5.1 Selection Rules

The intensity of a band in electronic spectroscopy is determined largely from selection rules, with more intense bands arising from transitions which are both spin and orbitally allowed. There are primarily three selection rules, which govern whether an electronic transition will be allowed and hence the value of the extinction coefficient.

(i) The first selection rule that is $\Delta l = \pm 1$. This rule means that an electronic transition, which involves a change in the quantum number l by one, is formally allowed. l = 0 corresponds to an s orbital, $l = 1$ corresponds to a p orbital, $l = 2$ a d-orbital and $l = 3$ are f-orbitals etc.. From this we can say that s→p; p→d; d→f transitions are allowed. Also from this rule we can say that transitions from orbitals of the same l quantum number (i.e. d→d transitions) are formally forbidden. There are however cases where d-d transitions may be observed. These conditions are discussed later (Section (iii)).

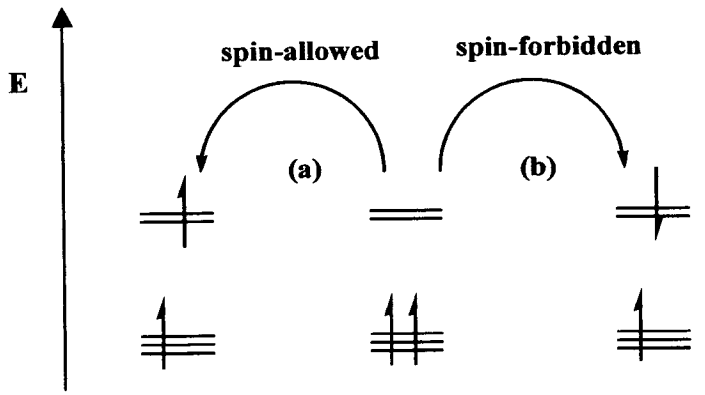

Figure 2.11 Spin Multiplicity Rule

(ii) The second selection rule to be considered is based on spin-multiplicity of the transition states. Transitions are allowed between states of the same multiplicity but not between those of different multiplicity, Figure 2.11. For example, transitions of $^3T \rightarrow {}^1E$ are formally forbidden, as there is a change in spin multiplicity whereas transitions such as ^2T to ^2E are formally allowed.

(iii) The third selection rule is based on the symmetry of the complex. When a system possesses a centre of inversion, as in the case of octahedral complexes, this selection rule forbids transitions between energy levels with the same symmetry with respect to the centre of inversion e.g. transitions between gerade (g) or ungerade (u) orbitals are formally forbidden. This selection rule is referred to as 'Laporte's rule'. These transitions are often observed however with reduced ε, as quite often a complex is not totally symmetric due to the coordination of different ligands or because the molecule vibrates and distorts, temporarily removing the centre of symmetry. This is called *vibronic coupling*.

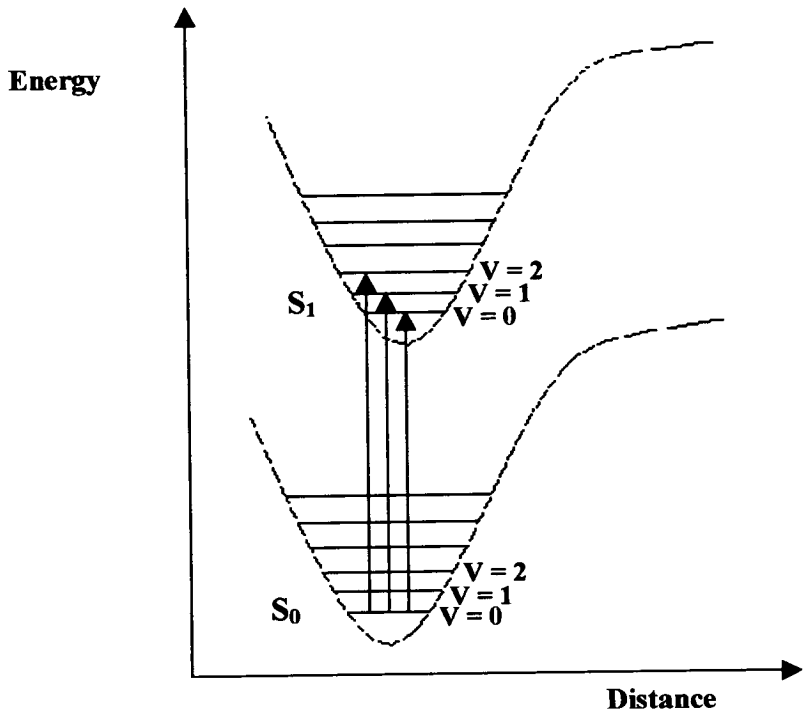

Figure 2.12 The source of vibrational fine structure on electronic bands

Electronic transitions are extremely rapid, typically occurring in a timescale of 10^{-15} seconds. Since molecules are constantly vibrating, it means that when an electronic transition is induced, molecules will be present in a variety of different vibrational states and therefore a range of energies will be absorbed (Figure 2.12) in transitions from the ground state (S_0) to the excited state (S_1). By scanning a range of λ the absorptions of in the UV-Vis spectral range are probed and measuring the peak positions observed, it is possible to estimate the vibrational frequency of the excited state responsible for the fine structure.

Depending on the solvent used and the change of dipole, the excited state may be either stabilised or destabilised with respect to the ground state and the absorption

band will move to lower or higher energy respectively. The displacement of an absorption or emission band in solvents of various dielectric constants is known as a solvatochromic shift. An important effect of this shift is the crossing of states of different electron distributions according to the polarity of the solvent, which can result in an alternative electronic state becoming the lowest excited state.

In the case of polar solvents, electronic states of large dipole moments are stabilised with respect to states of small dipole moments. When two excited states of differing dipole moments, are close in energy, an inversion of their order can take place when the polarity of the solvent is changed. As the photophysical and photochemical properties of most systems rely on the nature of the lowest excited state, the properties can show marked variations with solvent polarity.

The strength of a band is measured by its extinction coefficient, ε (M^{-1} cm^{-1}) which is calculated according to Equation 2.17.

$$\varepsilon = \frac{A}{cx}$$ **Equation 2.17**

where $A = \log_{10}\left[\frac{I_o}{I}\right]$ is the Absorbance, c is the concentration (mol dm^{-3}), x is the path length of the cell (cm). I is the intensity of the transmitted light and I_o is the intensity of the incident light. ε, (M^{-1} cm^{-1}).

2.5.2 Metal based or d-d transitions

The colours associated with transition metal complexes usually arise from transitions between different energy levels corresponding to a redistribution of electrons in the partially filled d-orbitals. Such transitions are referred to as d-d transitions and are

weak, having relatively small extinction typically of the order of 50 - 400 M^{-1} cm^{-1}, governed by selection rules (i) and (iii), which are discussed in Section 2.5.1. d-d bands are formally forbidden by (i) and often forbidden by (iii) however (i) can be overcome by the Heavy Atom Effect and (iii) is often overcome by vibronic coupling. These d-d transitions tend to occur in the near I.R. or visible region of the spectrum.

2.5.3 Charge Transfer Transition.

Absorption bands, due to charge transfer transitions, involve the transfer either of an electron from a molecular orbital based mainly on the metal to one based mainly on the ligand, i.e. a metal to ligand charge transfer band (MLCT), or vice versa i.e. a ligand to metal charge transfer band (LMCT).

Charge transfer transitions are usually observed at the blue end of the visible spectrum i.e. >11,000 cm^{-1}, or in the Ultra-Violet region ($200 < \lambda < 300$ nm). Nearly all of these charge transfer transitions are fully allowed and as such they tend to be very intense, with ε of the order 10^3-10^4 M^{-1} cm^{-1}.

2.5.4 $\pi \rightarrow \pi^*$ Transitions

Some ligands, particularly those containing π-bonds, will have electronic transitions arising from promotion of electrons from a low-lying filled bonding molecular orbital to an anti bonding or non-bonding orbital. An electronic transition can occur from an occupied orbital localised on the ligand to this low-lying unoccupied orbital also on the ligand.

These UV to visible transitions usually occur in the high-energy region of the spectrum, (the UV region) and are fully allowed with extinction coefficients of the order of 10^3–10^6 M^{-1} cm^{-1}. The energy of these transitions depends on the nature of the metal centre since the π-orbitals found on the ligand are sensitive to changes in the charge density of the metal (often brought about by changes in the oxidation state).

2.6 Spectroelectrochemical Techniques

Spectroelectrochemical experiments have long been an important tool in the investigation of organic and inorganic compounds [3]. The experiments are particularly helpful in the characterisation of short-lived reaction intermediates or in the characterisation of species, which are stable for long periods of time but only in the absence of air e.g. $[CpCoL]^-$.

To date, the most used solution spectroscopic technique combined with the electrochemical experiment is UV-visible spectroscopy, due to the simplicity of this experimental set-up. To a much lesser extent, IR spectroscopy has also been used, although this is often complicated by solvent adsorption.

Using the cell shown in Figure 2.13 the products of a bulk electrolysis experiment can be monitored *in-situ* by UV-Vis absorption spectroscopy. The optically transparent Thin Layer electrode (OTTLE) cell consists of a Pt/Rh gauze working electrode fitted into a quartz cell with a path length x, of 0.5 mm. A quartz extension is fitted to the cell, which acts as a reservoir for the sample solution. To complete the conventional three-electrode system a Pt wire counter electrode and Ag/AgCl reference electrode are placed into this reservoir, with both reference and counter electrodes separated from the sample solution by porous frits.

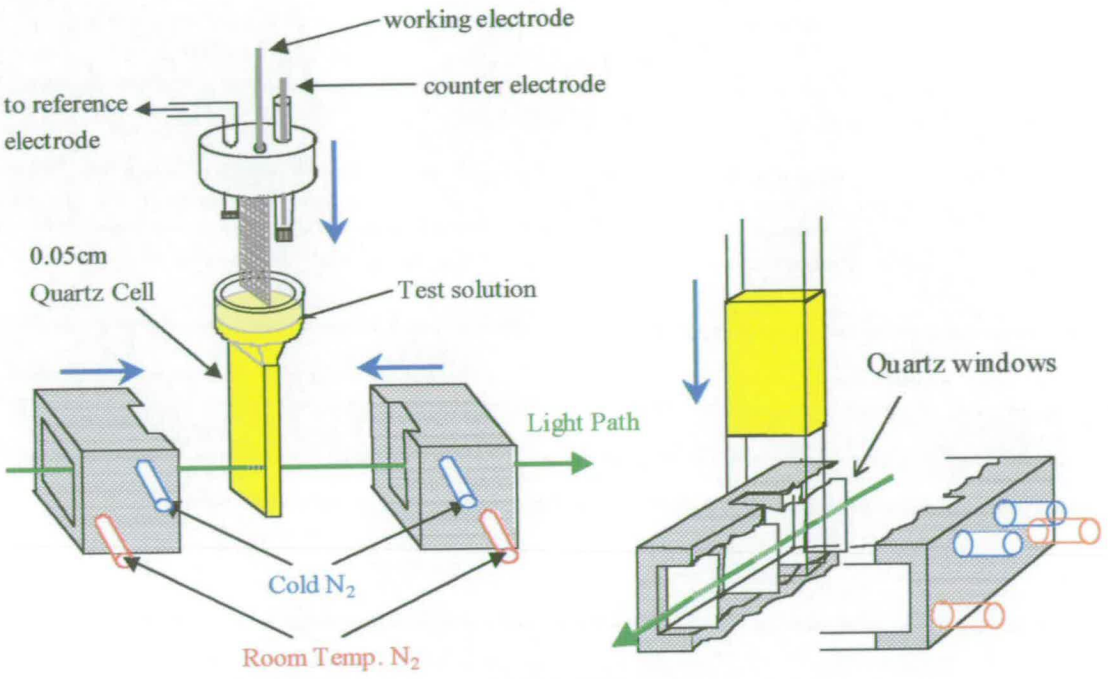

Figure 2.13 Spectroelectrochemical experimental setup

The cell assembly is then placed into a PTFE block, which is inserted into the spectrometer. Control of the temperature is achieved by passing dry, pre-cooled N_2 between the inner pair of quartz windows of the cell. The temperature is monitored using a thermocouple connected to a digital thermometer. To prevent the inner pair of quartz windows from fogging, N_2 is passed between the inner and outer quartz windows and through the sample chamber of the spectrometer.

During bulk Electrolysis (Section 2.4.5) the spectrum was recorded every five minutes. Once complete the potential electrolysis is reversed to regenerate the starting material. If the electron transfer process is chemically reversible the spectrum of the starting material is regenerated unchanged.

2.7 References

1 C. M. A. Brett, M. O. Brett, in *Electrochemistry Principles, Methods and Applications*, Oxford Science Publications, Oxford University Press, 1993

2 A. J. Bard, L. R. Faulkner, in Electrochemical Methods, Fundamentals and Applications, John Wiley and Sons Publications, 1980

3 A.B.P. Lever, *Inorganic Electronic Spectroscopy*, Elsevier, Amsterdam, 1968

4 I. Piljac, M. Tkalcec, B. Grabaric, *Anal. Chem.* 1975, **47**, 8, 1369

5 P. Suppan, *Chemistry and Light*, The Royal Society of Chemistry, 1994

Chapter Three

Preparation of Redox Active Macrocycles

Preparation of New Redox-Active Macrocycles

3.0 Introduction

In the area of ion sensor macrocycles and their applications in sensor technology, research has predominantly been based on complexation studies involving the binding of alkaline earth and alkali metal ions to hard donor system. (i.e. crown ethers and mixed O and N – donor systems) [1]. There are also examples of the binding of transition metals ions to these types of hard donor macrocycles reported in the literature [2], with the complexation of Ni^{II}, Co^{II}, Cu^{II}, Zn^{II} Mn^{II} and Ag^{I} perchlorates to [15]ane O_5 crown ether cavities and some derivatives of the crown system. With respect to 'redox-active' macrocycles [Section 1.3.4.1], a number of systems chemically bound to a redox active unit, have been developed which are capable of co-complexing other metal cations. However, once again this work is based almost entirely on hard donor systems and organic ligands, with the complexation of alkali metal ions and alkaline earth metal ions the most commonly reported [3].

A much smaller amount of the research in this area, has concerned the complexation behaviour of transition metal ions to soft donor redox-active macrocycles [1, 4, 5, 6, 7]. These types of systems have significant industrial relevance, as they can sense environmentally toxic metals [8]. Of these, one sulfur-based redox-active macrocycle has been prepared quite recently [9], using a tetrathiafulvalene–phenanthroline precatenate complex and successful complexation of Cu^{I}, and Ag^{I} has been reported.

In order to develop further 'redox-active' systems with soft donor atoms, we report here the preparation and development of two new cobalt based redox-active macrocycles based on the [18]ane S_4N_2 thione macrocycle [4] [10]. By incorporating

dithiolene ligands into the system we aim to achieve the high degree of delocalisation vital for the successful interaction of the host and guest metal ions.

The preparation of new cobalt-based macrocycles was achieved using the literature preparation described in Figure 3.1 [11]. The reaction describes the elimination of the thione group at the 2- position, by coordination of a CpCo- unit. The method reports the use of CpCoCOD {COD = cyclooctadienyl; Cp = cyclopentadienyl} as the 'CpCo'- source, toluene as the reaction solvent and a reaction time of 48 hours at reflux.

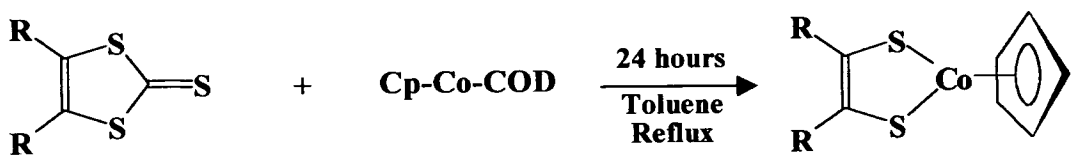

Figure 3.1 Literature reaction of CpCoCOD with compounds containing 1,3-dithiole-2-thione moieties

Electrochemical and spectroscopic complexation studies of the cobalt-based macrocycles prepared using this method are presented and discussed in detail in Chapter 4.

3.1 Reaction of the [18]ane S_4N_2 thione macrocycle [4] with CpCoR (Cp = cyclopentadienyl; R =COD (cyclococtadienyl); $(CO)_2$}

Optimum conditions for the formation of new cobalt based redox active macrocycles have been found. Reaction of the [18]ane S_4N_2 thione macrocycle [**4**] with 2 equivalents of $CpCo(CO)_2$ for three hours in THF, led to the successful formation of the new cobalt-based, redox active soft donor macrocycles [**6**], Scheme 3.1. Purification methods involved simple chromatographic separation on a silica column eluting with 2:1, Hexane:CH_2Cl_2 to give the mono- substituted CpCo- [18]ane S_4N_2 donor macrocycle [**6**] as a dark green microcrystalline powder, in 62 % yield. There was no evidence for the formation of the di-substituted CpCo- [18]ane S_4N_2 macrocycle [7] in the reaction.

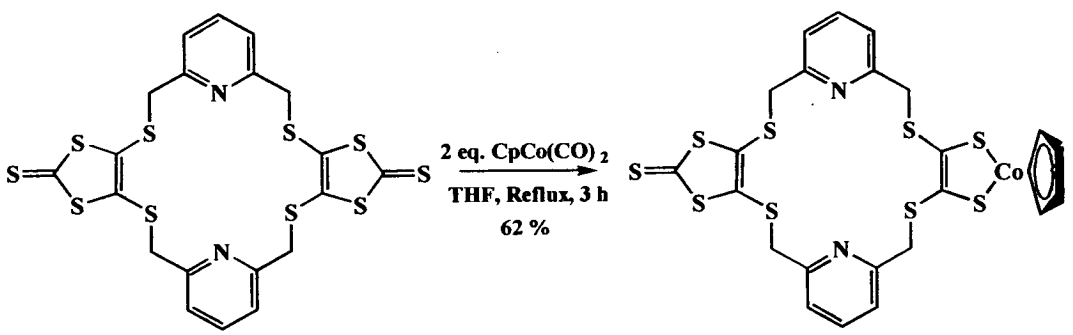

[4] [6]

Scheme 3. 1 Selective preparation of the monosubstituted CpCo- [18]ane S_4N_2 donor macrocycle [6]

Initial application of the literature preparation described above [11], to the [18]ane S_4N_2 thione macrocycle [**4**], led to the formation of a mixture of the mono- and di-substituted CpCo- macrocyles [**6**] (8 %) and [7] (10 %). The reaction had proceeded

via mechanisms identical to that observed previously i.e. displacement of the chelating di-olefin from CpCoCOD and also elimination of the thiocarbonyl group of [4] to form characteristically blue/green materials of $CpCo^{III}$ dithiolene complexes. The two materials [6] and [7] were separated using chromatographic techniques. The reaction involving [4] is described in Figure 3.3, above however it was also carried out for the [18]ane S_4N_2 ketone macrocycle [5] {prepared in a similar method to [4] using the keto analogue [2]} where elimination of the carbonyl group takes place followed by coordination of the CpCo group. Similar results were observed.

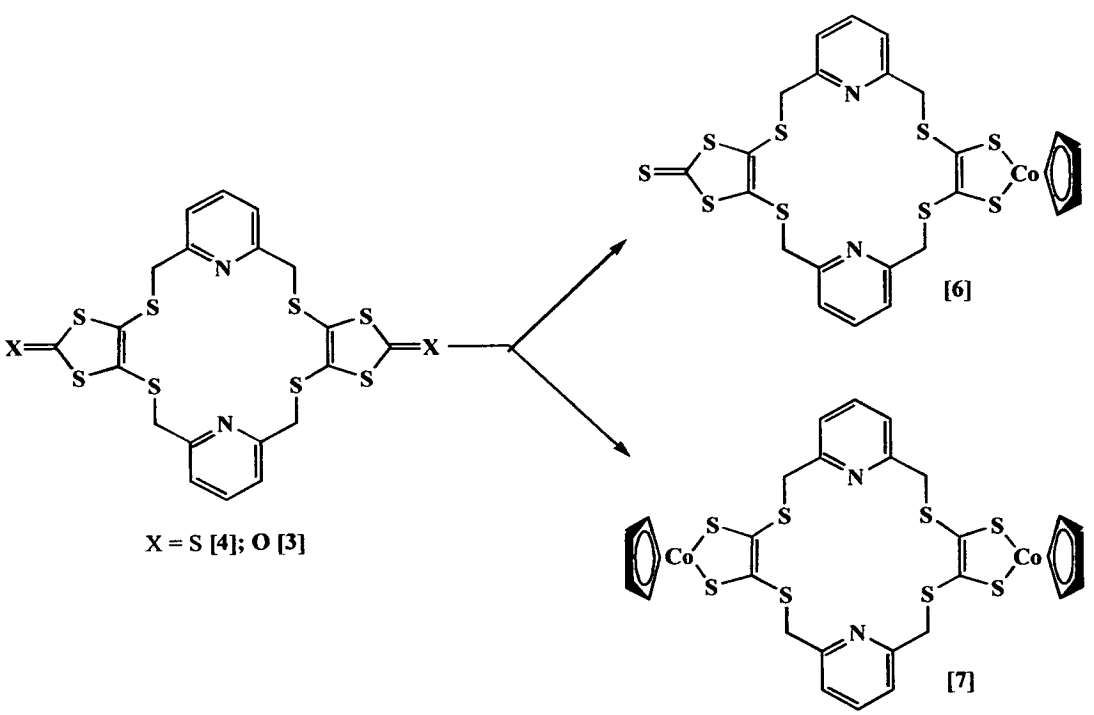

Figure 3. 2 Preparation of new mono- and di- substituted CpCo-containing macrocycles [6] and [7]. Table 3.1 and corresponding text describes full details of variations carried out in the course of this work

Many suggestions have been proposed for the mechanism by which the reaction takes place. The first proposes a dithiete intermediate [12]. Following the loose

coordination of the cobalt to the sulphurs at position 1 and 3 of the 1,3-dithiole-2-thione ring, a rearrangement has been proposed which results in a highly reactive four membered ring intermediate. This four-membered ring then readily rearranges to the five-membered metallacyclic product. In the coordination of the CpCo- group to the sulfur nucleophiles, the formal oxidation-state of the Co is found to oxidise from Co^{I} to Co^{III}. This is coupled with the formal reduction of the sulfur donor atoms.

In the second pathway proposed [12], it is proposed that rearrangement results in two thione groups, which are *trans* to each other, one of which is bound to the cobalt. The second thione sulphur then readily coordinates to the cobalt once again to close the ring and form the metallacyclic product. While this reaction mechanism has been proposed for simple dithiolene systems which are substituted at the 4 and 5 position with completely independent substituents, the macrocyclic system presented here could not geometrically allow for the trans geometry proposed for the two resultant thione groups before cyclisation occurs. It is possible however that complete trans geometry is not attained and cyclisation occurs at a considerably faster rate. Whichever mechanism is employed the result is the same, with the direct coordination of the now deprotected 1- and 3- positioned sulphurs to the cyclopentadienyl cobalt group.

In order to improve the yields of [**6**] and [**7**] a variety of different experimental conditions were applied. The variations are detailed in Table 3.1. One particular variation was a lower reflux temperature. It was proposed that refluxing toluene (b.p. 111 °C) was too harsh for the sensitive nature of the macrocycle and THF (b.p. 67 °C) was instead employed. However, the reaction appeared to proceed with a very different mechanism to that observed previously [11]. In one reaction we observed the preferential displacement of the Cp group from cyclopentadienyl cobalt cyclooctadiene under these conditions and the formation of the di- substituted $(CODCo)_2$- donor macrocycle {COD = cyclooctadienyl}. Mass spectrometric data was obtained which, together with the distinct absence of the characteristic Cp

proton signal in the ^1H NMR, adds weight to our proposal. Unfortunately this reaction seems to be irreproducible and no further characterisation has been possible. In this reaction no evidence for [**6**] or [**7**] was seen. In another variation to the reaction conditions, $CpCo(CO)_2$ was used in preference to CpCoCOD in order to minimise the effects of these competing reactions.

All other experiments reported in Table 3.1, gave mixtures of [**6**] and [**7**], which were collected as pure green microcrystalline materials in varying yields following chromatographic separation. A significant improvement was observed in the yield of [**6**], as it was found to form preferentially in all cases and in good yield. As a result of the increased yields of [**6**], a more detailed characterisation was possible. This included spectroelectrochemical, cyclic voltammetric measurements and epr data, which will be described in the next section.

Table 3.1 Experimental variations and yields for the reaction of [18]ane S_4N_2 thione macrocycle [**4**] with CpCoCOD and $CpCo(CO)_2$. Note that in all cases an N_2 inert atmosphere was applied.

CpCoCOD Reactions				$CpCo(CO)_2$ Reactions			
n^1	Solvent	Temp. / °C	Yield [6] / %	m^2	Solvent	Temp. /°C	Yield [6] / %
0.8	THF	67 (24 h)	30	1	THF	25	45
2	THF	67 (24 h)	52	2	THF	25 (3 d)	53
3	THF	67 (24 h)	40	2	THF	67 (3 h)	62
2	THF	25 (3 d)	51	4	THF	67 (2 h)	46
2	Toluene	67 (24 h)	30	2	Toluene	111 (3 h)	41
2	Toluene	111 (24 h)	32				

Note **1** : Number of equivalents of CpCoCOD added; **2** : Number of equivalents of $CpCo(CO)_2$ added

As well as the mono-substituted CpCo- donor macrocycle **[6]**, these reactions also gave the di-substituted CpCo- donor macrocycle **[7]**. Equally poor yields as those observed in the initial reaction with CpCoCOD were found however, and these yields are not included. Basic characterisation is reported in the analytical and experimental section, Section 3.2, for this species.

From the results reported in Table 3.1, we can draw some interesting conclusions. Of note are the reactions carried out in toluene (b.p. 111 °C). These reactions are based on the literature method of analogous species (Figure 3.1) and the range of yields observed was between 30 – 62 %.

In contrast, by introducing the lower boiling point solvent THF, we see a marked improvement in the yield to 52 %. This seems to indicate the sensitivity of the mono-substituted CpCo- donor macrocycle **[6]** to high temperatures over prolonged periods of time.

If we secondly consider the differences observed between the reactions with CpCoCOD and $CpCo(CO)_2$ we see higher yields of **[6]** from the latter. There are a number of reasons, which may be proposed for this. Firstly, the reactivity difference between the reagents should be considered. CpCoCOD is less reactive than $CpCo(CO)_2$ due to the necessity for the displacement of the coordinating di-olefin from CpCoCOD. The elimination of the carbonyl ligands from the cobalt coordination sphere is thermodynamically more favourable than the elimination of the coordinating di-olefin. The result of using $CpCo(CO)_2$ is greatly reduced reaction time in the case of $CpCo(CO)_2$, from the 48 hours reported previously to 3 hours. This coupled with the incorporation of THF as the reflux solvent, which is compatible with a thermally fragile product, results in greatly improved yields of **[6]** to 62 %.

3.2 Spectroscopic and Electrochemical analysis of the mono- and di-substituted CpCo- [18]ane S_4N_2 macrocycles [6] and [7]

3.2.1 UV-Vis Spectroscopy of macrocycles [4], [6] and [7]

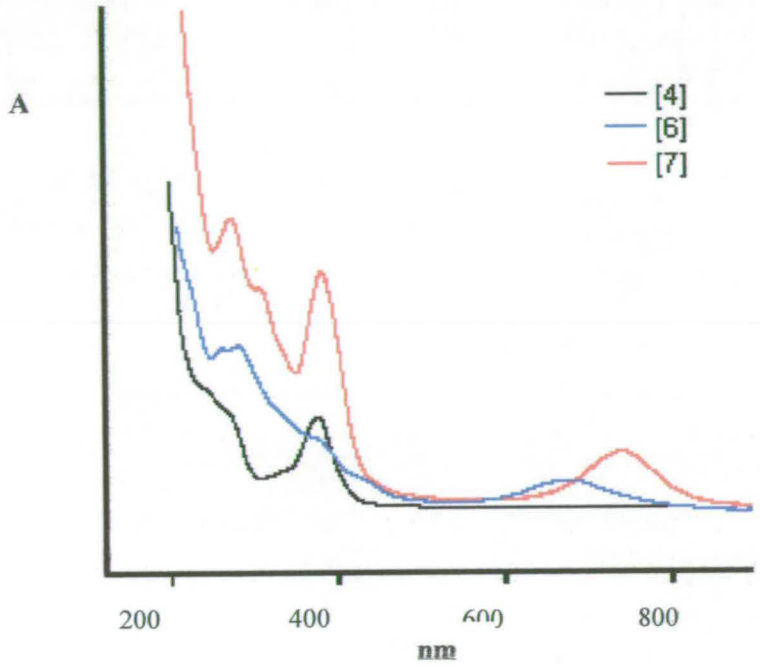

Figure 3. 3 UV-Vis spectra of the [18]ane S_4N_2 thione macrocycle [**4**], and the mono- and di-substituted macrocycles [**6**] and [**7**]. Spectra recorded in THF

In Figure 3.3, the UV-Vis spectra of the [18]ane S_4N_2 thione macrocyclic ligand [**4**] and the mono- and di- substituted redox active macrocycles [**6**] and [**7**], are illustrated. The most noticeable feature observed in these spectra is the presence of new bands at 675 nm and 740 nm in the case of the mono- and di- substituted macrocycles [**6**] and [**7**] respectively. These bands are characteristic of CpCo-dithiolene based transitions. The nature of this band is discussed below. Firstly, to be

noted is the distinct absence of bands of this type in the case of the [18]ane S_4N_2 thione macrocyclic ligand [**4**].

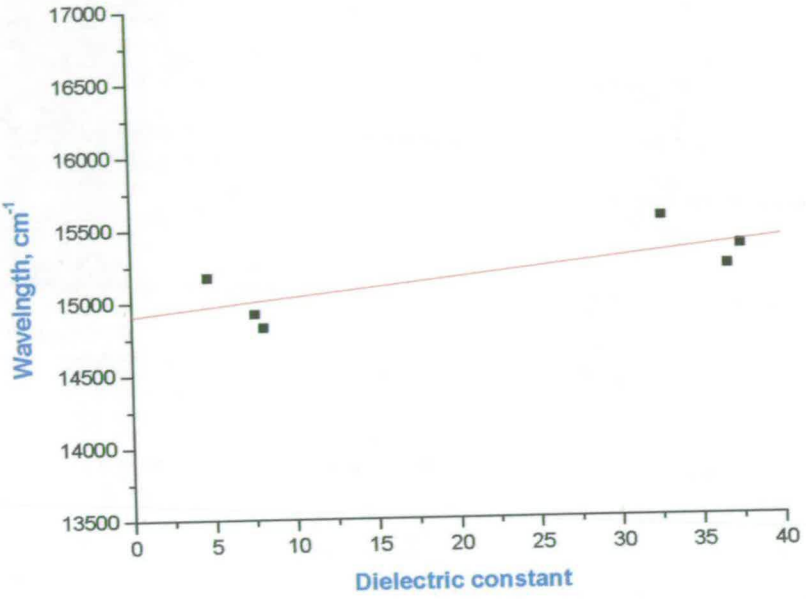

Figure 3. 4 Plot of the variation in dielectric constant against the wavelength (cm^{-1}) to determine solvatochromic shift within the macrocycle [**6**].

The variations in the wavelength of the band at 675 nm in [**6**] (THF) were measured by varying the solvent. Solvents with various dielectric constants were used including dichloromethane (CH_2Cl_2), dimethylformamide (DMF), dimethylsulphoxide (DMSO), tetrahydrofuran (THF), acetonitrile (MeCN) and methanol (MeOH). The lack of variation in wavelength indicates no significant solvatochromic shift. From this we can deduce that the absorbance at 675 nm is not a charge transfer band but is instead a $\pi^* \leftarrow \pi$ transition involving delocalised orbitals that may have both metal and ligand character.

Macrocyclic based absorbances are also observed at lower wavelengths. These again are $\pi^*\leftarrow\pi$ transitions, which occur within the macrocyclic ligand and in the case of [**4**], [**6**] and [**7**] are assigned as pyridyl based.

Table 3.2 Assignment of transitions observed in Figure 3.4

[4] / nm	Assign	[6] / nm	Assign	[7] / nm	Assign
280	Macrocycle $\pi^*\leftarrow\pi$	263	Macrocycle $\pi^*\leftarrow\pi$: $\varepsilon = 32756\ M^{-1}\ cm^{-1}$	275	Macrocycle $\pi^*\leftarrow\pi$ $\varepsilon = 23137\ M^{-1}\ cm^{-1}$
380	Macrocycle $\pi^*\leftarrow\pi$	370	Macrocycle $\pi^*\leftarrow\pi$: $\varepsilon = 11747\ M^{-1}\ cm^{-1}$	382	Macrocycle $\pi^*\leftarrow\pi$ $\varepsilon = 20342\ M^{-1}\ cm^{-1}$
		420	Macrocycle $\pi^*\leftarrow\pi$: $\varepsilon = 13328\ M^{-1}\ cm^{-1}$		
		670	ML_{FO} $\pi^*\leftarrow\pi$: $\varepsilon = 17620\ M^{-1}\ cm^{-1}$	740	ML_{FO} $\pi^*\leftarrow\pi$ $\varepsilon = 14942\ M^{-1}\ cm^{-1}$

Note **ML** indicates frontier orbitals involved in the unit CpCo-dithiolene possessing both metal and ligand character

3.2.2 Electrochemical analysis of the mono- and di-substituted macrocycles [6] and [7]

3.2.2.1 Cyclic Voltammetry of the mono substituted macrocycle [6]

The cyclic voltammogram of [**6**] in Figure 3.5 shows a reversible one-electron reduction wave at $E_{1/2}$ = -0.29 V. This has an anodic to cathodic peak separation ΔE_p of 63 mV.

Formally the reduction is a Co^{III}/Co^{II} reduction. However, as a result of the extent of delocalisation within the system (made possible by the direct coordination of a cyclopentadiene and dithiolene ligand to the cobalt) it is not chemically meaningful in this respect to refer to formal oxidation states. For this reason the reaction is best described as follows [13].

$$[CpCo(S_2C_2R)_2] + e^- \rightleftharpoons [CpCo(S_2C_2R)_2]^-$$

Further discussions in this thesis, however, will use the oxidation state formalism to aid in the clarity of the electron counting.

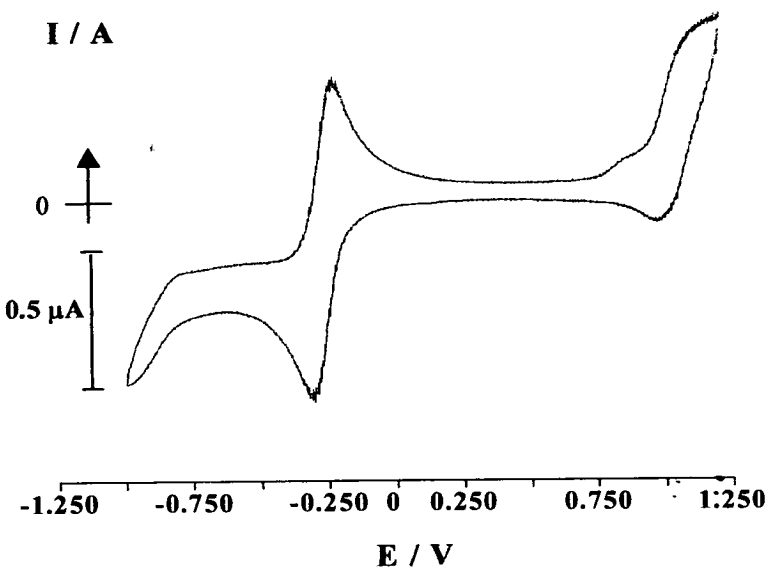

Figure 3. 5 Cyclic Voltammogram of [6] carried out in CH_2Cl_2 using $TBABF_4$ as electrolyte. Scan rate 100 mVs^{-1}

Coulometry at -0.42 V resulted in a colour change from dark green to a reddish/brown colour and confirmed a one-electron transfer. Electrogeneration at 0 V, re-generated the dark green Co^{III} species once again. The reversibility of the Co^{III}/Co^{II} couple was examined using varying scan rates and was shown to be completely electrochemically reversible.

3.2.3 Spectroelectrochemistry of [6]

Optically Transparent Thin Layer Electrochemistry (OTTLE) [14] uses *in situ* techniques to observe the UV-Vis spectra of species, which are air-sensitive in a given oxidation state which may not otherwise be observable and also allows spectra

of short-lived reaction intermediates to be collected when redox reaction products are unstable.

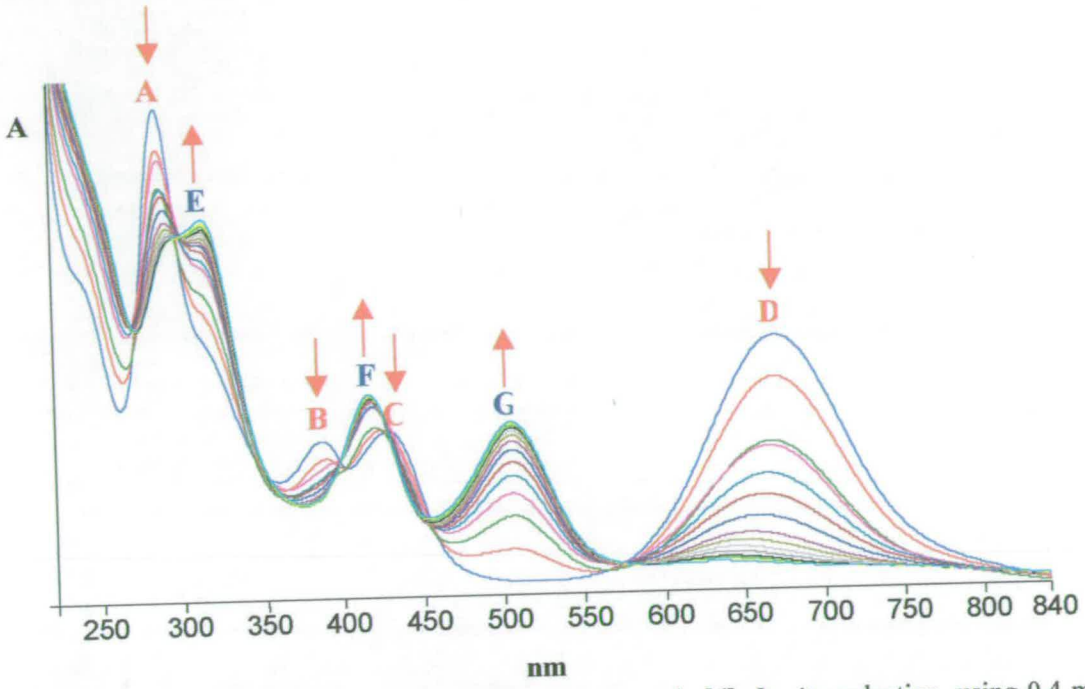

Figure 3.6 OTTLE of the mono-substituted macrocycle [**6**]. *In-situ* reduction, using 0.4 mol dm^{-3} $TBABF_4$/dichloromethane.

In situ reduction of the Co^{III} low spin compound [**6**] was carried out to the low spin Co^{II} compound $[\mathbf{6}]^-$ and was followed using spectroelectrochemcial techniques. A gradual decrease in the absorbance intensity of [**6**], {A, B, C and D} was observed, with corresponding sequential growth of those due to $[\mathbf{6}]^-$ {E, F and G}. The values of ε for each absorbance are reported in Table 3.3. These results give information on the orbital structure of the CpCo-dithiolene moiety and also some information on the transitions occurring within the molecule. These results are discussed together with the epr results obtained on $[\mathbf{6}]^-$ described, in the next section.

Table 3.3 UV-Vis absorbances of **[6]** and **[6]**$^-$. Included are extinction coefficients, wavelengths and the relevant transition involved in each absorbance.

Co^{III}, **[6]**				Co^{II}, **[6]**$^-$			
	Assignments	**λ / nm**	**ε / M^{-1} cm^{-1}**		**Assignments**	**λ / nm**	**ε / M^{-1} cm^{-1}**
A	π*←π	280	32756	**E**	π*←π	325	21009
B	π*←π	373	11747	**F**	π*←π	423	12651
C	π*←π	428	13328				
D	ML π*←π	674	17620	**G**	ML π*←π	505	11973

Higher energy absorbances between 200 and 450 nm which are present in the UV-Vis spectra of the mono-substituted CpCo- [18]ane S_4N_2 donor macrocycle **[6]** and its reduced species **[6]**$^-$ are also present in the [18]ane S_4N_2 thione macrocyclic ligand **[4]**. Based on this observation we can propose that all higher bands are based on π*←π transitions within the macrocyclic ligand.

3.2.4 Electron Paramagnetic Resonance (epr) and the Electronic Structure of the Co^{II} species **[6]**$^-$

Following bulk coulometry, an epr spectrum was obtained at room temperature and at 77 K for the reduced, Co^{II} species **[6]**$^-$. The room temperature spectrum showed the expected ^{59}Co (I = 7/2) octet. The eight hyperfine lines (Figure 3.7), were found to be equally spaced (J = 38.49 G) and the g-value was 2.1048. The frozen-solution spectrum of **[6]**$^-$ is also shown (Figure 3.7) together with a computer-simulated spectrum based on parameters described in Table 3.4.

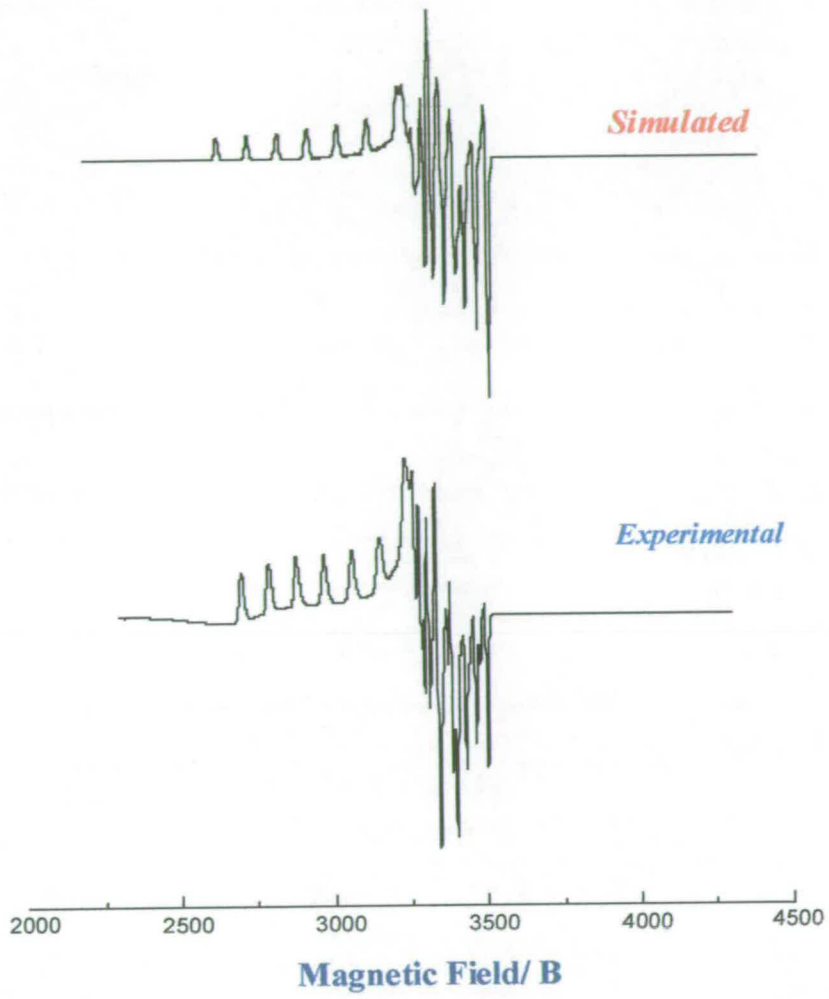

Figure 3.7 Experimental epr spectrum of mono-reduced, mono substituted macrocycle $[\mathbf{6}]^-$ in CH_2Cl_2 / 0.5 M $TBABF_4$ at 77K; Frequency 9.47GHz

In general the spectra (Figure 3.7) show 7 well-defined parallel features, which are evenly spaced. The eighth line is overlapping at the centre. In total three features g_x, g_y and g_z are observed indicating a rhombic system where $x \neq y \neq z$.

Table 3.4 Epr results. Data collected at 77 K

g-values	A-values / G	Linewidth / G
2.246	89	12
2.043	15.5	10
1.993	30	8

Some useful information (Table 3.4) may be obtained from the value of the coupling constant involved with complex being studied. It has been established that lower coupling constants, such as those observed here for [**6**] where A_{iso} = 38.49 G, are characteristic of a system in which the unpaired electron is delocalised over both the metal and the ligand environment [15, 16, 17].

Such small coupling constants are typical of Co^{II}-dithiolene based compounds which have previously been reported in the literature [15] such as nitrosyl based systems e.g. $\{Co(NO)[S_2C_2(CF_3)_2]_2\}^-$ where A_{iso} is reported as 32.9 G and g_{av} as 2.059 and $\{Co(NO)(S_2C_2Ph_2)_2]^-$ [16] which was observed as having A_{iso} of 29.4 G and a g_{av} of 2.050. A wide range of other Co^{II} compounds have also been studied. Some of these are described in Table 3.5 as a brief introduction to this work on the redox active macrocycle [**6**].

Table 3. 5 Summary of example epr results on $^{59}Co^{II}$ based systems related to this work

No.	Ion	g_{av}	g-values	A_{iso} / G	A-values / G
A^{18}	αCo-phthalocyanine	-	2.007, 2.422		116, 66
B^{18}	βCo-phthalocyanine	-	1.89, 2.94		150, 280
C^{21}	$[CpCoSCH_3]_2^-$	2.120	-	-	-
D^{21}	$[CpCoSCH_3]_2^+$	2.107	-	-	-
E^{15}	$[CpCoS_2C_2(CF_3)_2]^-$	2.454	-	41	-
F^{21}	$\{Co[S_2C_2(CF_3)_2]_2\}^{2-}$	-	2.04, 2.71, 2.04		
G^{19}	$[Co(S_2C_2Ph_2)]^{2-}$	2.33	-	-	-
H^{21}	$\{Co_2[S_2C_2(CF_3)_2]_4\}^-$	2.042	-	-	-
I^{20}	$Co(MNT)_2]^{2-}$	2.255	1.977, 2.798, 2.025	-	23, 50, 28

Note **mnt** = $(CN)_2C_2S_2$

Possibly one of the more important of these complexes in terms of comparisons to [**6**] is one reported by Dessy *et al* [15, 21] involving the tri-fluoromethyl dithiolene complex (Complex E in Table 3.5, Figure 3.8). In this complex the hyperfine coupling constant to ^{59}Co was found to be 41 G, which is very low and comparable to the coupling constant of 38.49 G obtained for [**6**]$^-$.

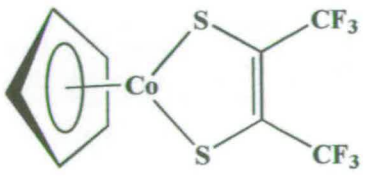

Figure 3. 8 Structure of [CpCo $S_2C_2(CF_3)_2$]

The high degree of delocalisation available within such systems acting through the Cp, d-orbitals on the Co^{II} centre and also the highly delocalised dithiolene unit, allows for extensive delocalisation of the unpaired electron which in turn results in the lower coupling constants observed.

With the confirmation of this delocalisation (based on the low coupling constant value), the application of these new Co-based macrocycles is evident. A high degree of communication between the cavity of the macrocycle and the cobalt centre is anticipated via delocalisation of the frontier orbitals onto sulfur atoms that form part of the donor set of the macrocyclic ring. Coordination of a guest ion to the host cavity is therefore expected to alter significantly the electrochemical behaviour of the Co centre. The different electronic nature of each possible guest ion may result in different effects upon the electronic properties of the Co centre.

Coupled with the change in the redox potential of the cobalt centre, variations in the spectroscopic properties of the CpCo-dithiolene unit, are also proposed. These are again based on the change in the electronic nature of the system made possible by this high degree of delocalisation. From these observations, the potential of this system to act as a sensor based on its redox and spectroscopic properties is clear.

3.3 Crystal structure determination

All attempts to crystallise the mono- substituted CpCo- macrocycle [**6**] were unsuccessful with crystals of a decomposition product [**8**], (Figure 3.9), formed instead. It should be noted at this point that there is no evidence for [**8**] in any of the analytical data collected for [**6**]. It appears to form as a result of the decomposition of the macrocyclic ring following prolonged lengths of time in solution. Attempts were also made to try to crystallise the macrocycle [**6**] at lower temperatures (–80 °C) however while no decomposition product was obtained no crystals of [**6**] were found to form either.

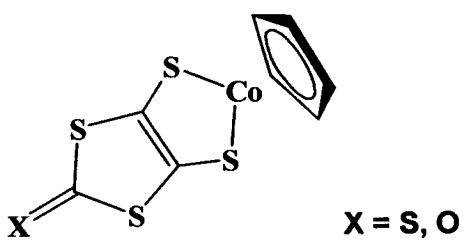

Figure 3.9 Structure of the degradation product [**8**] formed upon attempted crystallisation of the mono- substituted CpCo- macrocycle [**6**]

The instability of the macrocycle has previously been seen in the preparation of [**6**] where prolonged exposure of the system to both solvent room temperature and solvent at reflux temperatures resulted in significantly decreased yields of the resultant product. A further reference and discussion of the susceptibility of the ring to degradation is made in Chapters 5 and 6.

Two different sets of data were collected. **[A]** Figure 3.10, was collected from crystals, which were obtained from the slow evaporation of CH_2Cl_2 from a solution of **[6]** in a mixed solvent system of 1:1 of CH_2Cl_2 and hexane. Crystals were also obtained following slow evaporation from THF, **[B]**, Figure 3.11.

The crystals obtained under conditions, **[A]**, gave a structure **[8]** which was found to have $P2_1/c$ symmetry. This particular form of the compound has previously been reported in the literature, where it was formed and crystallised intentionally [22]. Crystallisation in THF gave **[B]**, which proved to be the ketone analogue of **[8]**. Based on the final final structural parameters of these crystals, and considering that the starting material in both cases was the S_4N_2 thione macrocycle **[4]**, we propose once again the degradation of the macrocycle ring and rearrangement to form the resultant crystal species.

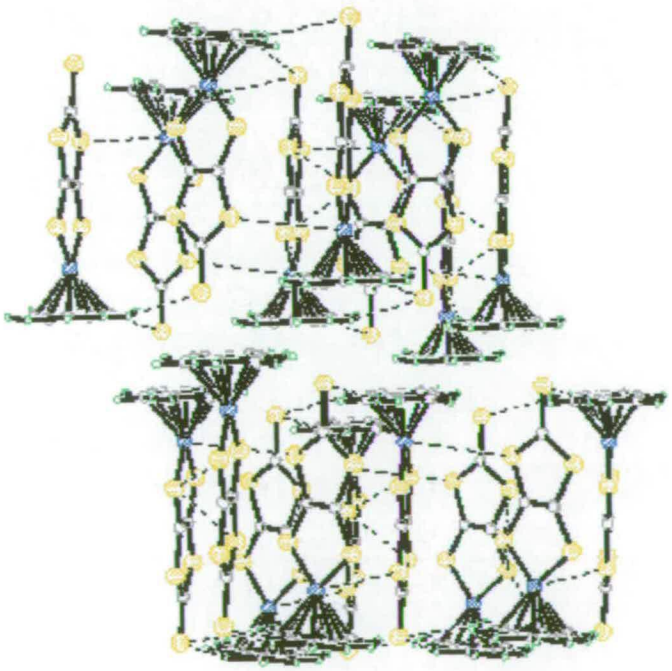

Figure 3.10 Packing diagram of the structure **[B]** of the decomposition product, **[8]** crystallised from 1:1 CH_2Cl_2:Hexane. Space Group is orthorhombic, $P2_1/c$

The two analogues of [**8**] which we observe are orthorhombic Pbcn [**A**] and monoclinic $P2_1/c$ [**B**]. The details of the structures are given in the Appendix 1.

While no crystals of the redox active macrocycle [**6**] were found, useful information may still be obtained from the crystal data and structure refinement of the sulphur and ketone analogues of [**8**]. As suggested one of the main features of this type of redox responsive macrocycle is the excellent communicating ability of the host and guest metal sites, which is made possible only by extensive delocalisation through the dithiolene C_2S_4 ligand. From examination of the crystal data collected in the case of the sulphur analogue of [**8**] in particular, we find evidence for this delocalisation within the bond lengths of the 2 five membered rings i and ii, Figure 3.11.

Table 3.6 Comparison of values for relevant bond lengths of [**8, X=S**]

Bond Lengths [8] {X = S} (P21/c)	
Co-S(1)	2.1273(10) Å
Co-S(5)	2.1223(9) Å
C(1)-S(1)	1.709(3) Å
C(1)-S(2)	1.732(3) Å
C(1)-C(3)	1.381(4) Å
C(2)-S(2)	1.728(3) Å
C(3)-S(4)	1.739(3) Å
C(3)-S(5)	1.704(3) Å

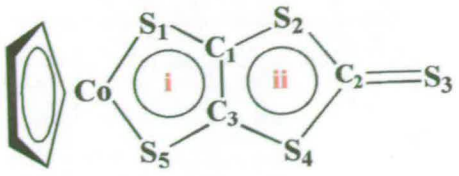

Figure 3.11 Schematic of the structure of [**8**] in order to show number system involved in aromatic regions of dithiolene ligand

Based on the numbering system laid out in Figure 3.11 we can the relevant bond lengths in order to show the extent of the delocalisation between the redox active site and the guest-binding site. This effect can be seen by consideration of the differences between the bond lengths from the reported single and double bond lengths and those experimental bond lengths observed here. When we consider first of all the central C(1)-C(3) bond and compare it to a normal aromatic bond length of 1.384(4) Å we see that the length is quite similar indicating that the central C-C bond has aromatic character.

Moving on to the Co-S bonds within [**8, X = S**] we see that in comparison to other reported Co-S bond lengths of 2.253(5) Å within Co-dithiolene systems, the bond lengths in our case of approximately 2.1 Å are considerably shorter. This is possibly due to the differing electronic nature of the groups attached to C(1) and C(3), however they are sufficiently comparable to indicate that they exist as similar types of bond with extended delocalisation into the CpCo- unit.

Comparing the C-S bonds directly attached to the central C(1) and C(3) carbons to those of normal single and double bonds we do indeed find evidence for aromatic behaviour in [**8, X=S**]. Normally C-S bonds are estimated to be 1.817(7) Å and C=S bond lengths 1.671(2) Å. When we consider the values of the bond lengths within [**8,**

X=S] we find that they lie almost exactly half way between normal C-S single and double bond length values. In fact considering thiophene C-S bond lengths, which are reported as 1.712 Å, we find further confirmation of the fact that the system is aromatic and highly delocalised in nature.

The final evidence for the delocalisation of the metal-dithiolene unit **[8]** is based on the bond lengths associated with the C(2)-S(2) and C(2)-S(4) bond lengths which, once again, when compared with reported C-S and C=S bond lengths in the literature are found to lie almost directly half-way.

The significance of crystallisation mechanisms and kinetics in directing crystallisation pathways of molecules and the factors affecting the formation of crystals have been reviewed in detail by various researchers [23]. In this case, while we expect the generation of crystals of the redox active macrocycle **[6]**, a degratation product **[8]** is observed instead. The generation of two different analogues of **[8]** i.e. X=S and O, indicate that the crystalisation process does indeed involve degradation of the macrocycle ring and rearrangement of the dmit/dmid systems for coordination to the cobalt centre. This is further confirmed by the fact that in the generation of both of these products, the same starting material i.e. the S_4N_2 thione macrocycle **[4]** was used. It is possible that the rearrangement of the macrocycle to form the dmit/dmid ligand systems involve the solvent in someway in the case of **[B]** although no evidence for this is accessible.

3.4 Conclusion

In the literature, a common reaction is described for the elimination of a thione group from a 4,5-dithiolate-1,3-dithiole-2-thione system using CpCoCOD under specific conditions. This elimination is coupled with the coordination of the CpCo- unit to the thiole sulfurs at positions 1- and 3-. We have applied this reaction to attach the CpCo- group to an [18]ane S_4N_2 macrocycle to form a redox active system. A mixture of the mono- and di-substituted forms [**6**] and [**7**] was observed and the reaction was optimised to give [6] selectively in a 62 % yield. This was done by varying conditions of the reaction i.e. temperature, reaction solvent, the source of the CpCo- unit and the number of added equivalents of the cobalt reagent. Optimum conditions were achieved with 2 equivalents of $CoCo(CO)_2$ in THF for 3 hours under reflux, giving a yield of 63% of [**6**] selectively. The yield of [7] was sufficient only for preliminary characterisation.

Electrochemical and spectroscopic techniques were used to characterise the macrocycle [**6**] fully. Spectroelectrochemical and Electron Paramagnetic Resonance techniques were additionally applied for characterisation of the reduced Co^{II} species [**6**]$^-$. An electrochemically reversible Co^{III}/Co^{II} couple was observed at ΔE_p = –0.29 V for [**6**] and at –0.33 V for [7]. UV-Vis studies showed the presence of a CpCo-dithiolene absorbance for [**6**] and [7] at 675 and 740 nm respectively. These absorbances are attributed to a π-π^* transitions between frontier orbitals showing both metal and ligand character.

Spectroelectrochemical techniques allowed the characterisation of the Co^{II} species [**6**]$^-$ using UV-Vis spectroscopy. An absorbance at 500 nm is observed for the CpCo dithiolene π-π^* transition. Using bulk coulometry we have prepared the Co^{II} species and studied it using epr techniques where an A_{iso}= 39 G was observed indicating a high degree of delocalisation within the system.

Following this attempts to crystallise the new redox active macrocycle failed with evidence observed only for two different analogues {X=S, O} of the degradation product [**8**]. Reasons for the formation of these structures are associated with the instability of the macrocyclic ring. This has been seen previously and is discussed in more detail throughout Chapters 5 and 6.

We therefore conclude that we have successfully prepared and characterised two new redox active macrocycles [**6**] and [**7**] with the former available in sufficient yields to allow guest-binding studies. We have successfully characterised them. Indications from epr experiments are that the macrocycle [**6**] contains a highly delocalised system, including the Cp- ligand, d-orbitals on the cobalt and the dithiolene unit. This feature will serve to enhance communication between the redox active cobalt unit and the host cavity and will contribute to the ability of the system to show a significant electrochemical and spectroscopic response upon binding of a guest metal ion.

3.5 Experimental

Reported in this section are experimental details of the reaction involving CpCoCOD, which resulted in a mixture of [**6**] and [**7**] and the best yielding reaction involving $CpCo(CO)_2$ for the preparation of [**6**]. All other variations are reported in Table 3.1. Work-up and purification methods are identical to those reported here in all cases. Electrochemical studies were carried out under conditions described in Chapter 2.

Preparation of $[NBu_4][BF_4]$ and $[NBu_4][PF_6]$ electrolytes

120 ml tetrafluoroboric acid (50 %) in 500 ml water was mixed together with approximately 660ml of tetrabutyl ammonium hydroxide (40 %). The mixture was stirred until the pH was between 5 and 7. The resultant precipitate of $[NBu_4][BF_4]$ was collected as a white solid and washed with cooled deionised water. The product was recrystallised 3 to 4 times from a 1:1 ratio of high purity water (600 ml) and methanol (600 ml).
The $[NBu_4][PF_6]$ electrolyte was prepared in an identical manner.

Preparation and separation of a mixture of the mono- and di- substituted CpCo- macrocycles [6] and [7]

The [18]ane S_4N_2 thione macrocycle [**4**] (0.26 g; 4.3×10^{-4} moles), was dissolved in 20 ml of toluene and allowed to stir under an inert atmosphere of N_2. To the reaction flask was added a 10 ml toluene solution of 0.20 g (8.6×10^{-4} moles) of CpCoCOD. The reaction mixture was heated to reflux for 48 hours, 40 ml of dichloromethane added and the mixture heated to reflux again. Hot filtration delivered a dark green

filtrate. The filtrate was brought to dryness *in vacuo* and the resultant green solid was re-dissolved in CH_2Cl_2. Dry flash chromatography on silica, eluting with CH_2Cl_2 delivered a dark green solution. The volume was reduced to 90-100 ml and stored in a freezer at –20 °C for four days. A light green solid of [7], was collected by filtration, in 10 % yield. The dark green filtrate was reduced to 20-25 ml, hexane was layered on and this was stored in a freezer at –20 °C overnight. Complex **[6]** was collected by filtration as a dark green / black solid in 8 % yield.

For [6] : Calculated C, 44.1; H, 3.2; N, 3.7 % for $C_{28}H_{24}S_8N_2Co_2$. Found C, 41.1; H, 3.5; N, 3.8:. IR (KBr) ν(C-H) 3448(w), ν(py C-C) 1638(s), ν(C=C) 1451, ν(C-S) 1384(m), ν(C=S) 1061(s) cm^{-1}. UV-Vis [THF] 263 (ε = 28134), 280 (ε = 27724), 373 (ε = 11747), 428 (ε = 3835), 674 (ε = 4958) nm. FAB-MS [3-NOBA]: m/z = 683 $[M^+]$ D.

For [7] : Calculated C, 42.2; H, 2.8; N, 4.1 %. for. $C_{28}H_{24}S_8N_2Co_2$. Found C, 37.5; H, 2.8; N, 4.00. IR: [KBr] ν(C-H) 3448(w), ν(py C-H) 1638(s), ν(Cp C-H) 1571(s), ν(C=C) 1450(m) cm-1. UV: 275 (ε = 23137), 382 (ε = 20342), 740 (ε = 14942) nm. FAB-MS [3-NOBA]: m/z = 763 $[M^+]$ D.

Selective preparation of the mono substituted macrocycle [6]

The [18]ane S_4N_2 thione macrocycle **[4]** (3.47 g; 5.7 x 10^{-3} moles), was dissolved in 50 ml of THF. The solution was stirred under an inert atmosphere of N_2. Following the addition of a 10 ml solution of $CpCo(CO)_2$ (2.07 g; 1.2x10^{-3} moles), the reaction mixture was heated to reflux for three hours. Hot filtration gave a dark green filtrate, which was brought to dryness *in vacuo*. Column chromatography on silica eluting with 2:1 Hexane:CH_2Cl_2, gave a dark green solution. This was reduced to 40ml in vacuo and stored in a freezer at -20°C for four days. A light green solid of **[6]** was collected by filtration in 62% yield.

Calculated C, 44.1; H, 3.2; N, 3.7 % for $C_{28}H_{24}S_8N_2Co_2$. Found C, 42.8; H, 3.3; N, 3.7. Electrospray MS $[CH_2Cl_2]$ m/z = 683, (M^{2+}) = 681. IR (KBr) ν(C-H) 3448(w),

ν(py C-C) 1638(s), ν(C=C) 1451, ν(C-S) 1384(m), ν(C=S) 1061(s) cm^{-1}. UV-Vis [THF] 263 (ε = 28134), 280 (ε = 27724), 373 (ε = 11747), 428 (ε = 3835), 674 (ε = 4958) nm.

3.6 References

1 (a) R. M. Izatt, K. Pawlak, J. S. Bradshaw, *Chem. Rev.*, 1995, **95**, 2529; (b) H. P. Hopkins Jr., A. B. Norman, *J. Phys Chem.*, 1980, **84**, 309; (c) A. K. Srivastava, B. Tiwari, *J. Elctroanalytical. Chem.*, 1992, **325**, 301; (d) R. M. Izatt, J. S Bradshaw, S. A. Nielsen, J. D. Lamb, J. J. Christensen, D. Sen, *Chem. Rev.*, 1985, **85**, 271.

2 V. S. Ijeri, A. K. Srivastava, *Eur. J. Inorg. Chem.*, 2001, 943

3 F. C. J. M van Veggel, W. Verboom, D. N. Reinhoudt, *Chem. Rev.*, 1994, **94**, 2, 279 and *references therein*

4 L. S. W. L. Sokol, L. A. Ochrymowyc, D. B. Rorabacher, Inorg. *Chem.*, 1981, **20**, 3189

5 F. C. J. M van Veggel, W. Verboom, D. N. Reinhoudt, *Chem. Rev.*, 1994, **94**, 2, 279 and *references therein*

6 M. Kodama, E. Kimura, *J. Chem. Soc., Dalton Trans.*, 1980, 2536

7 (a) H. J. Buschmann, *Inorg. Chim. Acta.*, 1985, **108**, 24; (b) D. Siswanta, K. Nagatsuka, H. Yamada, K. Kumajura, H. Hisamoto, Y. Shichi, K. Toshima, K. Susuki, *Anal. Chem.*, 1996, **68**, 4166].

8 R. E. Williams, P-J. Holt, N. C. Bruce, C. R. Lowe, *Heavy metals.* 2000, 213

9 K. S. Bang, M. B. Nielsen, R. Zubarev, J. Becher, *J. Chem. Soc., Chem Commun.*, 2000, **3**, 215

10 B. Girmay, J. D. Kilburn, A. E. Underhill, K. S. Varma, M. B. Hursthouse, M. E. Harman, J. Becher and G. Bojesen, *J. Chem.Soc., Chem Commun*, 1989, 1406

11 A. R. Siedle, *J. Organomet. Chem.*, 1976, **120**, 369-374

12 M. Kajitani, R. Ochiai, R. Kikuchi, M. Okubo, T. Akiyama, A. Sugimori, *Polyhedron,* 1990, **9**, 8, 1123.

13 M. Kajitani, T. Akiyama, A. Sugimori, K. Hirakata, Y. Hoshina, Y. Satsu, G.P. Sato, K. Shimizu, *J. Electroanal. Chem.* **1988**, 251, 421-428

14 I. Piljac, M. Tkalcec, B. Grabaric, *Anal. Chem.* 1975, **47**, 8, 1369

15 R. E. Dessy, R. Kornmann, C. Smith, R. Hayter, *J. Chem. Soc.*, 1966, **88**, 5112

16 J. A. McCleverty, N. M. Atherton, J. Locke, E. J. Wharton and C. J. Winscom, *J. Am. Chem. Soc.*, 1967, **89**, 6082

17 G. B. Carpenter, G. S. Clark, A. L. Rieger, P. H. Rieger, D. A. Sweigart, *J. Chem. Soc. , Dalton Trans*, 1994, **20**, 2903

18 V. Illiev, L. Prakhov, A. Andreev, E. Ignatek, G. Schultz-Ekloff, *Hetergenous Catalysis*, 1987, 6th, Pt 2, 79

19 R. Williams, E. Billig, J. H. Waters, H. B. Gray, *J. Am. Chem. Soc.*, 1966, **88**, 43

20 (a) A. Davidson, N. Edelstein, R. H. Holm, A. H. Maki, *J. Am. Chem. Soc.*, 1963, **85**, 2029; (b) A. Davidson, N. Edelstein, R. H. Holm, A. H. Maki, *J. Am. Chem. Soc.*, 1963, **85**, 3049; (c) H. B. Gray, R. Williams, I. Bernal, E. Billig, *J. Am. Chem. Soc.*, 1962, **84**, 3596; (d) A. H. Maki, N. Edelstein, A. Davidson, R. H. Holm, A. L. Balch, *J. Am. Chem. Soc.*, 1964, **86**, 4580

21 R. E. Dessy, R. Korumann, C. Smith and R. Hayter, *J. Am. Chem. Soc.* 1968, **90**, 2001; R. E. Dessy, F. E. Stary, R. B. King, M. Waldrop, *J. Am. Chem. Soc*, 1966, **88**, 471

22 M. Fourmigue, V. Perrocheau, Acta. Crystallogr., Sect. C (Cr. Str. Comm), 1997, **53**, 1213

23 D. J. W. Grant, Theory and origin of polymorphism, in: H. G. Brittain (Ed.), Polymorphism in Pharmaceutical Solids, Vol. 95, Marcel Dekker, New York, 1999, pp. 1-33; N. Rodriguez-Hornedo, D. Murphy, *Significance of controlling crystallisation mechanisms and kinetics in pharmaceutical systems, J. Pharm. Sci.*, 1999, **88**, 651-660

Chapter Four

Complexation Studies of [6]

Complexation Studies of Guest Metal Ions with the Cobalt Macrocycle [6]

4.0 Introduction

Interest in the co-ordination chemistry of soft donor systems has focused on the reactivity of metal complexes. This finds application in two areas: (1) practical industrial applications involving sensor technology and (2) a fundamental comprehension of how biomolecular systems function for example, metalloenzymes and metal-containing redox proteins. Both of these areas pose very interesting chemical challenges and an overview of both will be given in this report; however the level of detail given regarding biomolecular science will be limited, as it is out with the scope of this work. Instead, focus is made on the industrial science – both fundamentals and applications – and the potential impact of developing a system, capable of showing a specific electrochemical or optical change upon complexation of transition metal ions to the guest-binding site of a redox active chromophore-containing macrocycle.

Co-ordination of thioethers typically stabilises the lower oxidation-state of metal ions and where relevant, the lower spin-state as well. These general properties derive largely from two characteristics of thioether ligands: their π–acidity and their inability to stabilise positive charge effectively, both of which have been discussed previously in Chapter 1. On further consideration of the complexation that these types of soft-donor can take part in, several, often strongly connected factors should be taken into account, which influence the stability and selectivity of the final product. The first of these is donor type. It is already clear that the kind of donor employed in a macrocyclic system has a big influence on the complexation behaviour of the ligand. A large amount of work has been done on the hard donor

systems, which incorporate ether oxygens into the cyclic framework [1]. Such hard donor systems most favourably combine with hard ions, for example alkali/alkaline earth or lanthanide ions, according to the 'hard and soft acid-base' principle [2]. Thus complexation of solely oxygen crown ethers e.g. [18]ane O_6 crown ether, with Na^I, Ca^{II}, and K^I, tend to result in a high stability constant, K_s [3]. Soft and borderline cations (Cu^{II}, Ag^I, Co^{II}, Ni^{II} etc) typically combine less favourably with the hard ether oxygen, thereby resulting in lower stability constants. On the other hand, such soft cations interact favourably with 'soft' donor atoms like sulfur and aromatic nitrogen. Stepwise substitution of nitrogen and sulfur for oxygen in these hard donor systems has been carried out and the stability constants for the resultant complexes measured [4]. One such study was the substitution of two sulfur donor atoms for two ether oxygens in the [18]ane O_6 crown ether, where it was found that the pure oxygen crown complex with Ag^I had $\log K_s = 1.6$ (in H_2O). However the substitution of two sulfur atoms increased the stability constant of the Ag^I complex dramatically to $\log K_s = 4.34$ (in H_2O).

In some early structural work on macrocyclic thioethers, a curious property was revealed. Most sulfur donor atoms of uncomplexed ligands tend to point out of the plane of the cavity of the ring [5, 6, 7]. As a result of this 'exo-dentate' orientation [8] (which contrasts with that more commonly seen in oxa [O] and aza [N] macrocycles) there is an energy penalty for ring binding [9] and some crown thioethers tend to bridge metal ions rather than form monometallic complexes. The factors controlling such conformations within these ligands have been extensively studied. Analysis of the structures of [12]ane S_4 [10], [15]ane S_5 [11], [18]ane S_6 and other macrocyclic thioethers revealed a striking pattern. In practically every crown thioether, all of the C-S linkages adopt the gauche conformation, which results in exodentate orientation.

In oxa-crowns, by contrast, the C-O bonds prefer the anti- conformation. This difference arises largely from the different 1,4-interactions in gauche C-C-E-C and E-C-C-E units (E = O, S), which combine in oxa crowns to give anti C-O and gauche C-C bonds, but in thio crowns give the opposite: gauche C-S and anti C-C bonds.

For molecules such as [14]ane S_4 and [12]ane S_4, this tends to give a quadrilateral structure with the sulfur atoms at the corners. The resulting conformation does not favour chelation, as it necessitates a complete conformational rearrangement to turn the donor atoms "right-side in". Conformational analysis therefore reveals why [14]ane S_4 shows little macrocyclic effect (i.e. its binding affinity only barely exceeds that of the acyclic ligand) and why Rosen and Busch [12] in their work found that [12]ane S_4 more often bridges rather than chelates metal ions [13]. This discussion applies to those systems, which can rearrange freely and for which a variety of different binding modes can be proposed for metal ions. However, for the system under investigation in this chapter, the monosubstituted CpCo- [18]ane S_4N_2 macrocycle [**6**], the rigidity of the backbone will also have a significant role in determining the actual binding mode of the metal ion.

Throughout this work therefore, a question repeatedly pondered is that of the mode of binding of the metal ion i.e. whether a bridging or a cavity-binding mode is favoured for a particular metal. It can be considered that the free ligand cavity possesses 6 'exo-dentate' donor atoms. It must be remembered that, as has been observed by previous workers in this field, bridging mode binding may take place rather than direct cavity-binding.

Considering the mixed S-N donor system used for complexation studies in the course of this work, Figure 4.1, two physicochemical indicators can be identified which might be expected to show metal ion complexation. Firstly, the CpCo-dithiolene moiety of the macrocycle [**6**] shows a strong absorption in the visible spectrum. This can be attributed, as already described in Chapter 3, to a $\pi^* \leftarrow \pi$ transition within the frontier orbitals which contain both metal and ligand character. Complexation of a transition metal ion to the macrocyclic cavity may significantly alter the energy gap between the ground and excited states and thus be expected to alter the position of the CpCo-dithiolene absorbance.

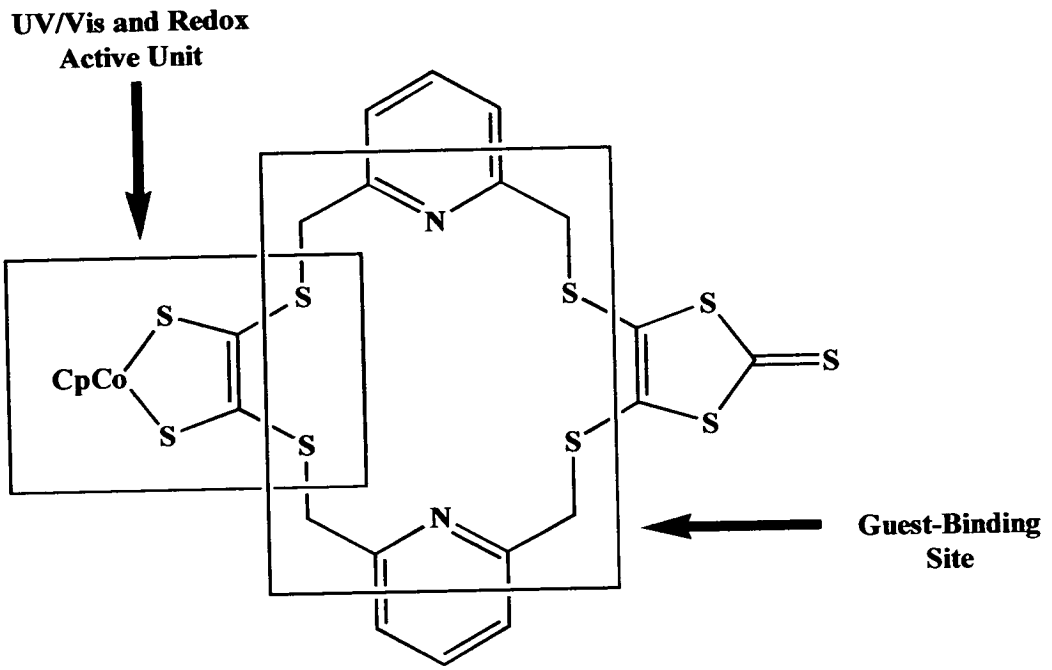

Figure 4. 1 Key groups involved in the complexation studies of soft transition metals to the mono-substituted CpCo- [18]ane S_4N_2 macrocycle [**6**]

Another indicator is the redox potential of the redox active $CpCoC_2S_4$- unit. The free ligand [**6**], shows a reversible Co^{III}/Co^{II} reduction at –0.34 V. Due to the extensive electron delocalisation occurring between the redox active unit and the cavity sulfur atoms, complexation of a transition metal ion to the cavity might be expected to alter the electron density. In doing so the redox potential of the Co^{III}/Co^{II} couple would also be expected to change and it is this deviation from the Co^{III}/Co^{II} reduction at – 0.34 V that is under investigation in this work.

In this chapter we discuss some preliminary results based on some complexation studies of a variety of soft metal ions with the monosubstituted CpCo- [18]ane S_4N_2 macrocycle [**6**] using these physicochemical indicators, as well as assessing the potential of this ligand system to applied sensing technology through potentiometric complexation work.

4.1 Outline of Results

Section 4.2 deals with the complexation of metal ions with the CpCo- [18]ane S_4N_2 macrocycle [**6**]. The results in this section include UV-Vis and electrochemical data. The first section deals with the complexation of Ag^I whilst the second section involves a discussion on complexation studies carried out with the post transition metal ions Hg^{II}, Cd^{II} Sn^{II} and Pb^{II}. The final section deals collectively with the transition metal ions Fe^{II}, Ni^{II}, Co^{II} and Cu^{II}. In all sections, a discussion of the most likely mode of complexation/interaction of the particular ion or group of ions to the macrocycle [**6**] is given.

4.2 Complexation studies of the monosubstituted $CpCo^{III}$-[18]ane S_4N_2 macrocycle [6]

4.2.1 Complexation of Ag^I to the monosubstituted CpCo- [18]ane S_4N_2 macrocycle [6]

4.2.1.1 Introduction

Complexation studies described in this chapter relate solely to the monosubstituted CpCo- [18]ane S_4N_2 macrocycle [**6**]. By introducing the sulfur atoms, it was anticipated that the selectivity towards Ag^I would be greatly enhanced compared with oxa and aza macrocycles. It has been shown in previous studies that thioether containing macrocycles have demonstrated a particular affinity for Ag^I [14, 15, 16, 17, 18] and can show selectivity in systems where several other metal ions are present e.g.

Pb^{II} [19]. In the case of 16- and 17-membered rings containing thioether donor atoms, stability constant differences of approximately 10^3-10^4 in favour of Ag^I over Pb^{II} were reported. For this reason, complexation studies of Ag^I were attempted initially.

4.2.1.2 Complexation of Ag^IBF_4 with [6] in THF

A complexation study was carried out in THF to assess the binding of Ag^I to the cavity of [**6**]. The results of the UV-Vis study are shown in Figure 4.2.

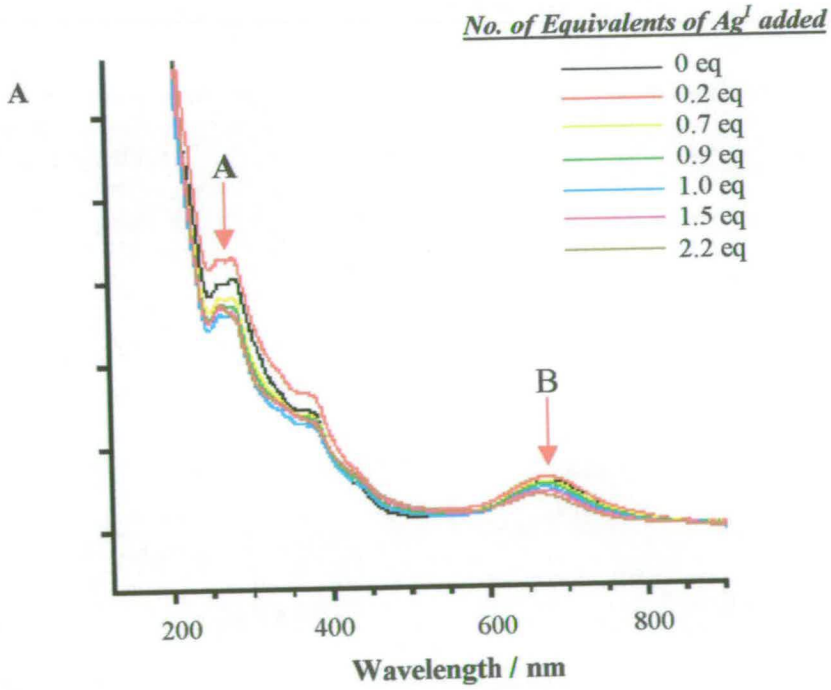

Figure 4.2 UV-Vis-spectra of the monosubstituted CpCo- [18]ane S_4N_2 macrocycle [**6**] in THF upon addition of 2.2 equivalents of Ag^IBF_4.

The band at 675 nm (Figure 4.2), upon sequential addition of Ag^I to a solution of **[6]**, shows a pronounced change in intensity. We attribute this to an interaction of the metal ion with the macrocycle **[6]**. In addition to a drop in absorbance by 32 %, there is a shift to higher energy of the CpCo-dithiolene $\pi^* \leftarrow \pi$ transition with increasing complexation of the guest metal ion species. A shift in the wavelength of 18 nm (385 cm^{-1}) from 675 nm to the longer wavelength, 693 nm, is indicative of an alteration in the energy levels involved in the transition which gives rise to the absorbance. Such a change in the electron density of the CpCo-dithiolene unit can be attributed to the complexation of a guest metal ion to the cavity.

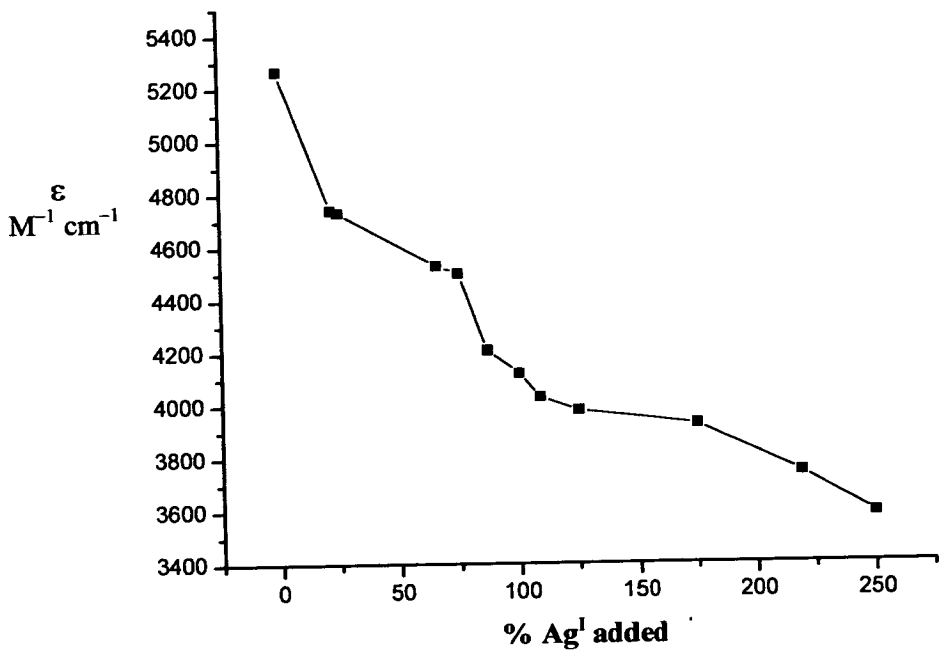

Figure 4. 3 Binding efficiency of the monosubstituted CpCo- [18]ane S_4N_2 macrocycle **[6]**. ε values are measured for A_{664} nm.

A plot of the decrease in absorbance against the concentration of Ag^IBF_4 added is shown in Figure 4.3. Due to the uncertainties in the points it is not clear whether the plot indicates a linear relationship and thus whether the added silver titrates into the macrocycle. The continuation of the decrease in absorption beyond a 1:1 ratio of the

metal ion to the macrocycle **[6]** however, suggests that this is not the case and that equilibrium exists involving bound and unbound Ag^I.

Electrochemical studies of the complexation of the Ag^I by the monosubstituted CpCo- [18]ane S_4N_2 macrocycle **[6]** were carried out in THF. On sequential addition of Ag^I to the macrocycle, the results as shown in Figure 4.4 were observed.

In this study, a new reduction was observed at –1.29 V. A very slight shift to more negative potential was also observed for the Co^{III}/Co^{II} redox potential from the original potential at –0.34 V to –0.37 V.

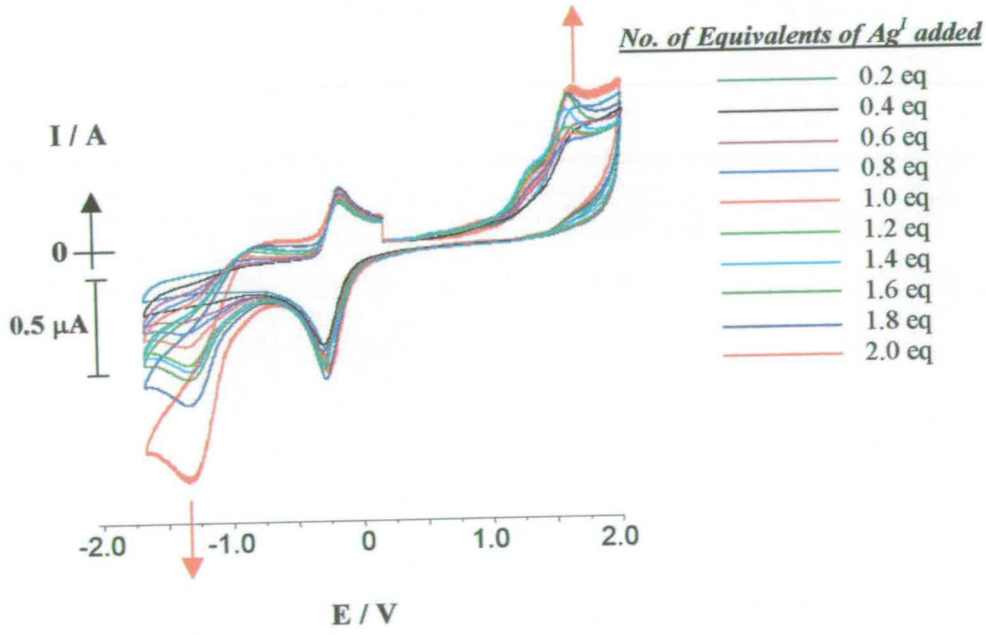

Figure 4. 4 Electrochemical study of the addition of Ag^I to the monosubstituted CpCo- [18]ane S_4N_2 macrocycle **[6]**. Study carried out in THF and followed by Cyclic Voltammetry

The new reduction at –1.29 V increases with increasing Ag^I concentration and is thought to be due to the reduction of bound Ag^I within the cavity of the macrocycle. The reduction of the 'bound' Ag^I species is diffusion controlled and is found at a

much lower potential than that observed for the reduction of 'free' Ag^I metal ions, solvated in THF. In the coordination of the Ag^I by the macrocycle **[6]** the Ag^I appears to be stabilised. This is seen by the shift in potential to a lower value, i.e. from +0.50 V for solvated Ag^I to –1.29 V.

A key feature in this study, Figure 4.4, is the lack of any reduction or stripping signal for the reduction or oxidation of free Ag^I ions of metallic Ag respectively. This is despite an excess of Ag^I being present in solution at the end of the experiment. Further studies were carried out to identify the reason behind this and the reaction mechanism involved. One experiment, which was carried out involved the sequential addition of the monosubstituted CpCo- [18]ane S_4N_2 macrocycle **[6]** to a solution of free silver ions. The results are shown in Figure 4.5.

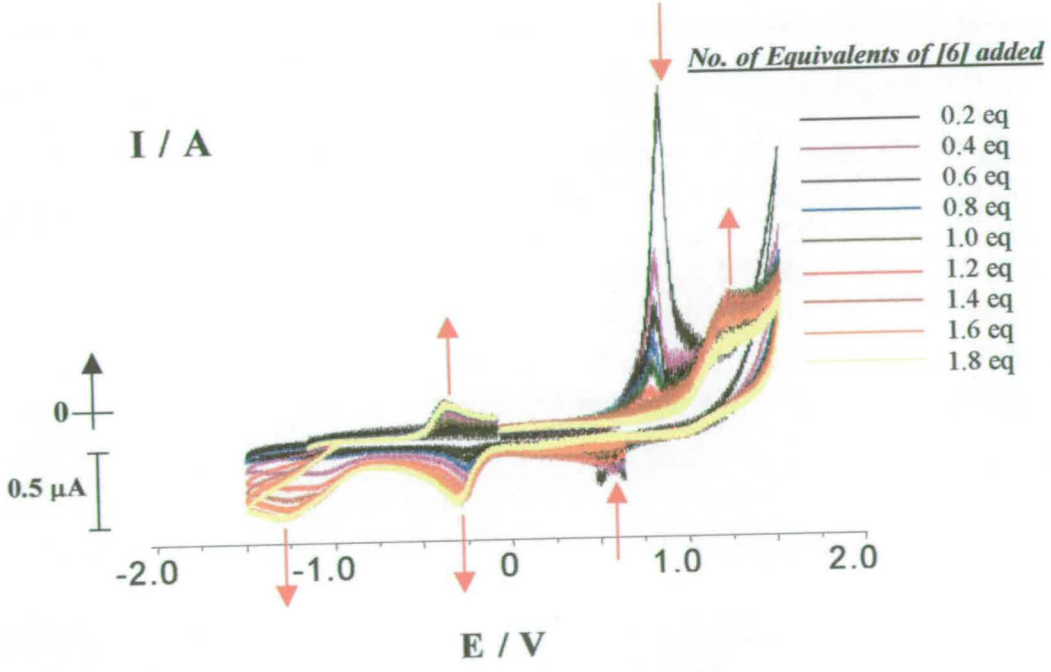

Figure 4. 5 Electrochemical study of the addition of the monosubstituted CpCo- [18]ane S_4N_2 macrocycle **[6]** to free Ag^I in THF followed using Cyclic Voltammetry

The most noticeable feature is that, in the absence of the macrocyclic ligand **[6]**, the Ag^I ions are free to under-go electrochemical processes at the electrode surface. This is seen as a reduction-wave at +0.50 V and an associated stripping peak at +0.95 V, features not seen in the previous complexation experiment (Figure 4.4). With the sequential addition of the macrocycle **[6]** to the solution of Ag^I, we find the gradual decrease in the size of both the characteristic Ag reduction and Ag stripping peak referred to previously. It is apparent from these experiments that the order of addition of **[6]** and Ag^I to the solution plays a crucial role in the resultant voltammogram observed. For example after addition of 0.6 equivalents of **[6]** to the Ag^I solution, appreciable free Ag^I reduction and stripping peaks are apparent (Figure 4.5). After addition of 1.6 equivalents of Ag^I to the **[6]** solution however, an approximately corresponding ratio of **[6]** and Ag^I is present but no peaks due to free Ag^I can be observed (Figure 4.4).

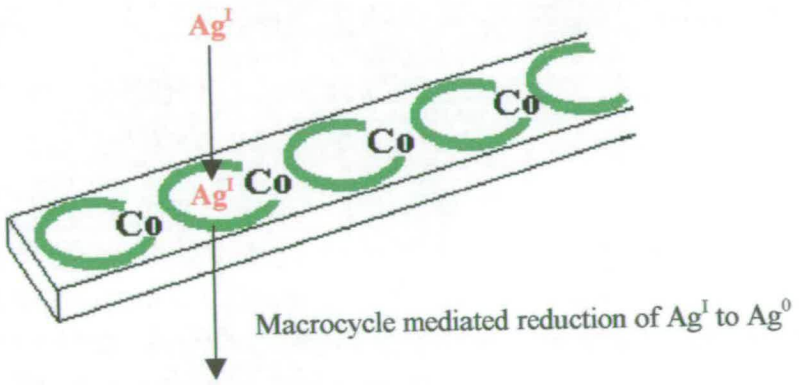

Figure 4. 6 Schematic of the macrocycle mediated reduction of Ag^I and excess Ag^I

It is evident that these results cannot be interpreted purely in terms of the quantities of species present in solution. This suggests that where **[6]** is the only species initially present in solution, the macrocycle is adsorbing onto the surface of the

electrode, blocking any access for free Ag^I ions to get to the electrode (Figure 4.5). Instead the Ag^I are forced to bind to the macrocycle cavity, through which reduction eventually occurs via a macrocycle-mediated (cavity-mediated) mechanism. That this reduction involves the cavity centre is suggested by the correspondence of the reduction peaks at –1.29 V in Figures 4.4 and 4.5, which suggests that the Ag^I is in the same environment when reduced. The reduction is more difficult due to the stabilising effect that the macrocyclic ring has on the Ag^I. This is seen from the lower reduction potential observed as a narrow reduction peak at –1.29 V compared with the reduction potential of the free Ag^I ion seen at +0.5 V. To be noticed from our results is the lack of any increase in the Co^{III} reduction peak despite Ag^I uncomplexed in solution having a reduction potential which is more positive than the $Co^{III} + e^- \rightarrow Co^{II}$ reduction process. This supports the conclusion that the reduction occurs through a macrocycle-mediated process.

Where Ag^I is initially present, addition of **[6]** would not be expected to initially form a surface bound layer as complexation can preferentially occur with the Ag^I present in solution. In the case of the second experiment involving addition of **[6]** to a solution of Ag^I, Figure 4.4, along with changes in E_{red} and E_{ox} for Ag, a parallel increase in the intensity of the bound Ag^I reduction at –1.29 V was observed. The increase of this reduction confirms this signal as macrocycle-mediated reduction of Ag^I at the electrode surface.

Closer examination of the cyclic voltammograms in Figures 4.4 and 4.5 indicates a distinct lack of a return oxidation peak following the mediated reduction. It is interesting that the Ag^I oxidation occurs at a much more positive potential than the reduction peak. This is consistent with the Ag^I stripping peak potential being sufficiently positive of the plating peak for macrocycle-mediated oxidation to be thermodynamically unfavourable. The increase in the narrow oxidation peak at +1.2 V is thought to be due to the re-oxidation of the Ag^0 species through a similar mediated process, as a peak at 1.2 V is seen for the oxidation of free **[6]** and this grows on further addition of Ag^I, Figure 4.4.

The proposed macrocycle-mediated mechanism involved in the study of Ag^I may therefore be summarised as follows. With the surface-adsorbed layer of macrocycle **[6]** on the surface of the electrode, straightforward reduction and oxidation processes for the free Ag^I cannot take place. Instead, the metal ion cannot be reduced until the macrocycle **[6]** has been reduced. In a similar way, the reduced metal ion cannot be re-oxidised until the macrocycle has been re-oxidised.

From the cyclic voltammetric results, Figure 4.4, we can see that more than one equivalent of Ag^I is added to the system, but that the macrocycle-mediated reduction continues to increase. Following the addition of 1 equivalent of the Ag^I ion to the CpCo macrocycle **[6]**, reduction of the Ag^I ion in solution, occurring at –1.29 V, appears to be mediated through Ag^I bound within the cavity of **[6]** as shown in Figure 4.6. To this point, the characteristic features of the cyclic voltammetry studies carried out, all indicate adsorption of the macrocycle onto the surface of the electrode and macrocycle-mediated reduction of the Ag^I ions at the surface of the electrode.

To summarise at this point, the first characteristic is the observation that the cobalt reduction and oxidation peak are both narrow indicating a surface bound species. The second, is the observation of new oxidation and reduction peaks a ~ -1.29 V (reduction) and ~ +1.20 V (oxidation) which, coupled with the increase in both of these peaks beyond 1 equivalent, without any evidence for any free Ag^I peaks appearing, indicates the surface macrocycle-mediated processes. Finally, the reduction at ~ -1.29 V is at a very low potential which, coupled with the fact that the oxidation of the metal does not occur until the macrocycle is itself oxidised at +1.2 V, indicates a complete surface coverage of the electrode with macrocycle **[6]**. This means that no bare surface is available for free Ag redox reactions to occur.

Further confirmation of the interaction of Ag^I with the macrocycle **[6]** comes from the study of the interaction of Ag^I with CpCodmit **[8]**, which is essentially identical to the macrocyclic system **[6]**, but lacks the macrocyclic cavity. This study was

carried out using electrochemistry and involved $Ag^{I}BF_4$ in THF. The first noticeable feature is the absence of the oxidation at +1.2 V, Figure 4.7, which can be assigned to the pyridyl group of the macrocycle.

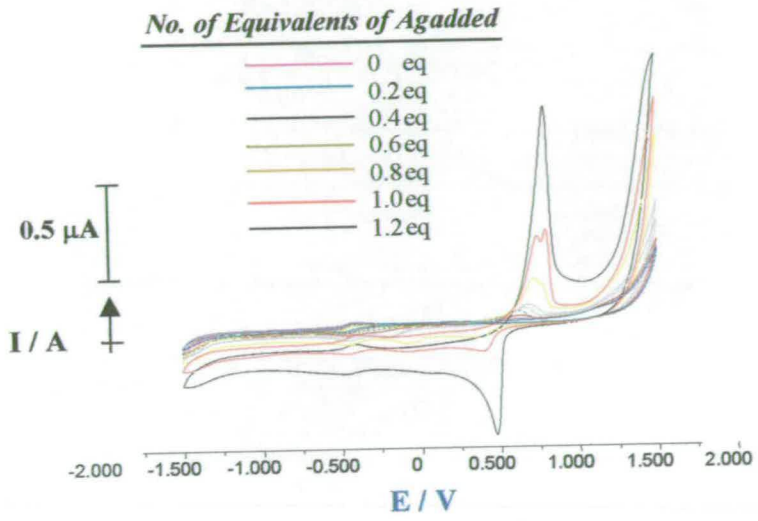

Figure 4. 7 Cyclic Voltammetric study of the complexation of Ag^{I} with CpCodmit [**9**] through addition of Ag^{I} to a solution of [**9**] in THF.

With sequential additions of Ag^{I}, no new peak appears at –1.29 V indicating the absence of a peak previously attributed to macrocycle-mediated reduction. Instead of macrocycle-mediated reduction of Ag, we see instead the normal reduction peak and stripping peak for Ag at +0.5 V and +0.95 V respectively. This adds further strength to our proposal that the shift in the Ag^{I} reduction potential is due to the complexation of Ag^{I} to the cavity of [**6**] adsorbed onto the electrode of [**6**] and that a macrocycle-mediated mechanism for the Ag^{I} is occurring.

4.2.1.3 Complexation of $AgClO_4$ with [6] in DMF

To determine the effects of solvent on the coordinating ability of the macrocycle [**6**] to the metals, the complexation of Ag^I to [**6**] was also attempted in dimethylformamide, DMF. The experiments were carried out in an identical manner to that described in the case of those carried out in THF.

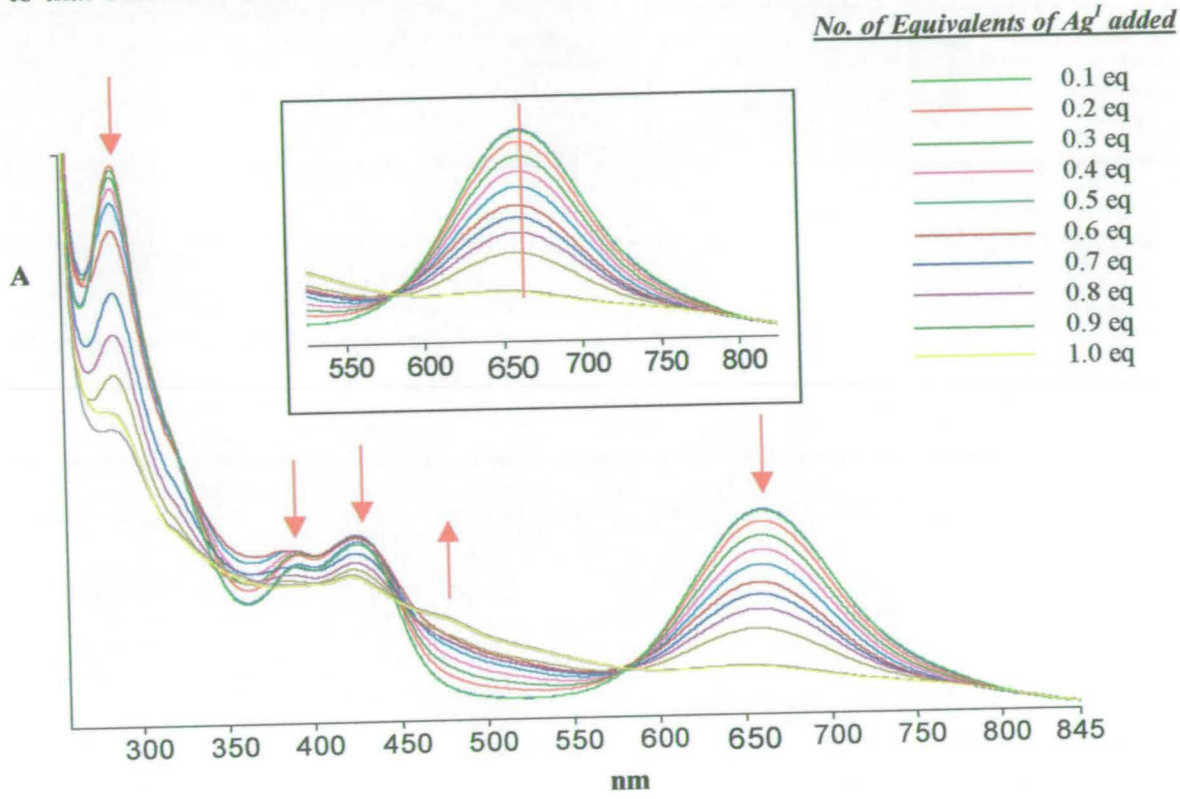

Figure 4.8 Complexation study of Ag^ICIO_4 to the monosubstituted CpCo- [18]ane S_4N_2 macrocycle [**6**] using Ultra-Violet/Visible Spectroscopy in DMF. Two mechanisms are involved. (i) Addition of 0 - 0.5 equivalents where the 664 nm absorbance decreases by approximately half the initial intensity and (ii) addition of 0.6 - 1.0 equivalents. Each stage of the complexation leads to a clear but different set of isosbestic points indicating two distinctive stages in the complexation of Ag^I to the macrocyclic cavity [**6**]

In the UV-Vis experiment carried out in DMF there is a shift in wavelength observed within the absorbance due to the CpCo-dithiolene unit at 664 nm, Figure 4.8). This is comparable to the shift observed in the complexation in THF where, upon addition of 2.15 equivalents of Ag^{I}, a shift of 18 nm (385 cm^{-1}) to a higher energy was observed. In this case the shift is 20 nm (469 cm^{-1}) from 664 to 644 nm. This is a significant shift and coupled with the extremely large variations in intensity, both the absorbance at 664 nm and the new absorbance at 445 nm indicates a large perturbation in the electron density of the CpCo-dithiolene unit. We take this as evidence of guest complexation to the cavity of **[6]**. The new absorbance observed at 445 nm is thought to be due to a $\pi^{*}\leftarrow\pi$ transition within the CpCo-dithiolene unit of the system complexed to the Ag^{I} ion. Presumably the interaction of the Ag^{I} with the Co^{III} pulls electron density away from the cobalt centre affecting the intensity of the CpCo-dithiolene transition.

The collapse of this CpCo-dithiolene absorbance at 664 nm was in this case observed to proceed to completion with 1 equivalent of $Ag^{I}ClO_4$ added. Any further additions of Ag^{I} showed no further changes in the intensity of this absorbance indicating complete interaction of the ion with **[6]**. This enhancement in the binding of Ag^{I} to the cavity of **[6]**, is thought to be due to the stabilising effect of the DMF towards any resultant complex formed. In comparison with the studies carried out in THF the complexation in DMF proceeds through two clear stages. The first involves addition of the $Ag^{I}ClO_4$ salt from 0 - 0.5 equivalents where the absorbance at 664 nm was found to decrease by approximately half the initial intensity. The second completed this process and involved additions of $Ag^{I}ClO_4$ from 0.6 - 1.0 equivalents. Each stage of the complexation led to a clear but different set of isosbestic points indicating two distinctive stages in the complexation of Ag^{I} to the macrocyclic cavity.

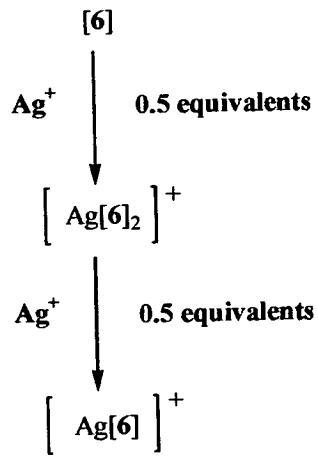

Scheme 4.1 Proposed reaction scheme for the complexation of $Ag^{I}ClO_4$ to [6] in DMF

For the UV-Vis results in Figure 4.8, each spectral change is as a result of the addition of 0.1 equivalents of Ag^{I} ions to the monosubstituted species [6] in DMF. Closer consideration of the absorbances observed at 375 and 425 nm indicates that up to 0.5 equivalent additions causes little change in the intensity of these particular absorbances. Each addition following 0.5 equivalents causes the absorbances to decrease in intensity gradually. From the results indications are that the mechanism is not an equilibrium but instead a titration mechanism indicating a very strong interaction between Ag^{I} and [6].

This suggests that addition of 0 - 0.5 equivalents of Ag^{I} gives a species $Ag^{I}[6]_2$. Further addition of Ag^{I} breaks this species apart and allows the species (Ag^{I}[6]) to form. This could be a reasonable mechanism to explain the observation of two isosbestic points and is outlined in Scheme 4.1.

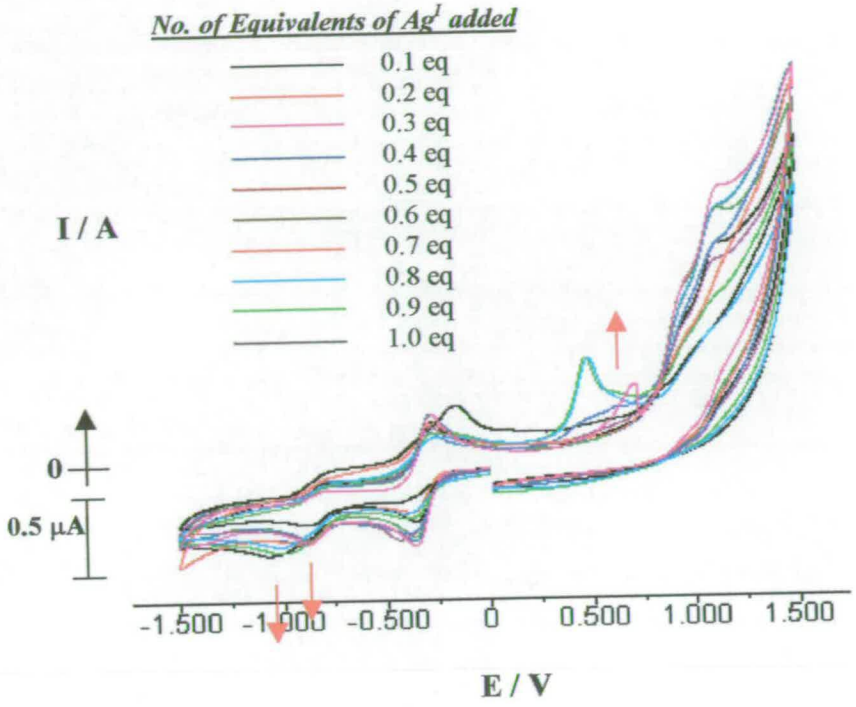

Figure 4. 9 Cyclic Voltammetric study of the complexation of Ag^I to the macrocycle **[6]** in DMF

Cyclic voltammetric studies were also carried out in DMF. A new reduction peak was observed between –0.85 V and –1.10 V and is explained in a similar manner to that described in the THF studies, as follows. The reduction at –0.85 V increases with each addition of Ag^I made up to the addition of 0.5 equivalents. As 0.5 equivalents of Ag^I are added, the observed potential of –0.85 V for the reduction of the bound Ag^I species shifts to a lower potential of –1.05 V indicating a change in the environment of the bound metal ion, to a more stable environment. A mechanism may be proposed, where the addition of 0.5 equivalents leads to the formation of a sandwich type structure. Further addition of 0.5 equivalents results in the overall formation of the 1:1 complex, which would be consistent with the results of the electrochemical studies (Figure 4.9) leading to reduction of the Ag^I at even lower potentials i.e. –1.10 V

The presence in some of the voltammograms, of a possible stripping peak for Ag^0 from the surface of the Pt electrode, could be due to the involvement of the solvent, DMF. It is thought that the DMF must be able to compromise the integrity of the adsorbed layer on the surface of the electrode at high-added Ag^I concentrations, allowing access for the Ag^I ions to the surface and a normal stripping peak to be observed. This will be discussed in more detail at the end of the chapter.

4.2.1.4 Conclusions

The development of the redox active macrocycle **[6]** as an ion sensor was proposed based on the presence of two in-built physical properties (spectroscopic and electrochemical activity) involved with the CpCo-dithiolene unit. These properties made the system ideal for monitoring of the complexation of transition metal ions to the macrocyclic cavity. From the results presented in this section the success of these UV-Vis and redox 'handles' is clear with direct responses observed with each addition of Ag^I made.

In the Cyclic Voltammograms observed in the case of THF using Ag^IBF_4, we find that, as well as the previously observed Co^{III}/Co^{II} redox couple, a reduction potential at approximately –1.29 V gradually grows in with increasing concentration of Ag^I ions in solution. This potential is attributed to the reduction of Ag^I, mediated through surface adsorbed macrocycle. This has been shown through the lack of any stripping peak for uncomplexed Ag in the case of complexation of Ag^I to **[6]**. Addition of **[6]** to a solution of Ag^I on the other hand shows a significant Ag^0 stripping peak, which gradually decreases in intensity as the macrocycle covers the surface of the electrode once again. The inequivalence of the two experiments provided strong evidence that there is surface bound layer of **[6]** mediating the electrochemical processes occurring.

In DMF, there are two distinctive stages in the complexation mechanism from 0 – 0.5 equivalents and 0.6 - 1.0 equivalents both of which appear to form different Ag^{I} complexes at the surface of the electrode capable of undergoing macrocycle-mediated reduction. The complexation is complete following addition of 1 equivalent of $Ag^{I}ClO_4$. The details of the two stages involved in the complexation however are yet to be determined.

Complexation studies involving Ag^{I} have been previously reported in the literature involving thioether macrocyclic ligands. Based on the electrochemical and the UV-Vis results obtained, we can monitor a similar affinity of the Ag^{I} ion for the macrocyclic cavity of **[6]**.

4.2.2 Complexation study of late transition and main group metal ions Cd^{II}, Hg^{II} Sn^{II} and Pb^{II} to the monosubstituted CpCo- [18]ane S_4N_2 macrocycle [6]

4.2.2.1 Introduction

Complexation studies discussed to this point have involved only Ag^{I}. The mechanism proposed for the reduction and oxidation of the bound metal ion, involves a macrocycle-mediated mechanism through the macrocycle **[6]**, occurring as a result of a layer of macrocycle adsorbed onto the electrode. In terms of the UV-Vis results the most illuminating results have been those carried out in DMF. This section considers the detection by coordination of the environmentally important, late transition metal ions such as Cd^{II}, Pb^{II}, Sn^{II} and Hg^{II}. Following the results of the Ag^{I} complexation studies it was decided to carry out these complexations in DMF also.

Based on the literature, it is evident that a considerable number of complexes have been made with six-donor macrocycles of these late transition metal ions. The macrocycles reported include both soft and mixed hard and soft donor systems. One such example is the complex of Pb^{II} to a mixed sulfur-nitrogen macrocycle, which in this particular complex shows suitable dimensions for the complexation of the metal ion [20, 21]. Also reported for the complexation of Pb^{II} is a 22-membered macrocycle incorporating O_4N_2, $O_2S_2N_2$ and S_4N_2-donor sets [20], complexes of Cd^{II} with 1,3 alternate calix[4]arenes [22] and of Hg^{II} to crown ether macrocycles [23]. More recently the preparation and characterisation of the complex of Hg^{II} and 3,6,16-trithia-6,11,19-triazabicyclo[6,6,6]icosane has also been carried out and stability constants calculated [24]. Complexes of Cd^{II} have also been reported for diimine complexes of the type $[CdL(H_2O)_2][ClO_4]_2$ {L = a diimine ligand} [25].

Based on the industrial importance of detecting these metal ions and also the fact that a number of these ions have been previously complexed using similar donor systems i.e. S_4N_2, it was decided to study these with the macrocyclic ligand **[6]**.

4.2.2.2 Complexation results of Cd^{II}, Hg^{II}, Sn^{II} and Pb^{II} to the monosubstituted CpCo- [18]ane S_4N_2 macrocycle [6] in DMF

These experiments were carried out in DMF in an identical manner to that described in the Experimental Section, Section 4.6. The results of the complexation of **[6]** with Cd^{II} are presented in Figure 4.10A. From the complexation study, we see that the addition of 1 equivalent of Cd^{II} does indeed show a decrease in the absorbance at 664 nm. A slight shift ($\leq$ 3 nm; 66 cm^{-1}) is also seen to higher energy indicative of an interaction with the metal ion in the cavity of the macrocycle.

Considering also the complexation of Pb^{II} to **[6]** we see the results presented in UV-Vis spectra in Figure 4.10B. Once again there is a drop in the intensity of the

absorbance due to the $\pi^* \leftarrow \pi$ transition within the CpCo-dithiolene group observed at 664 nm, however in this case no shift is observed in the wavelength.

A

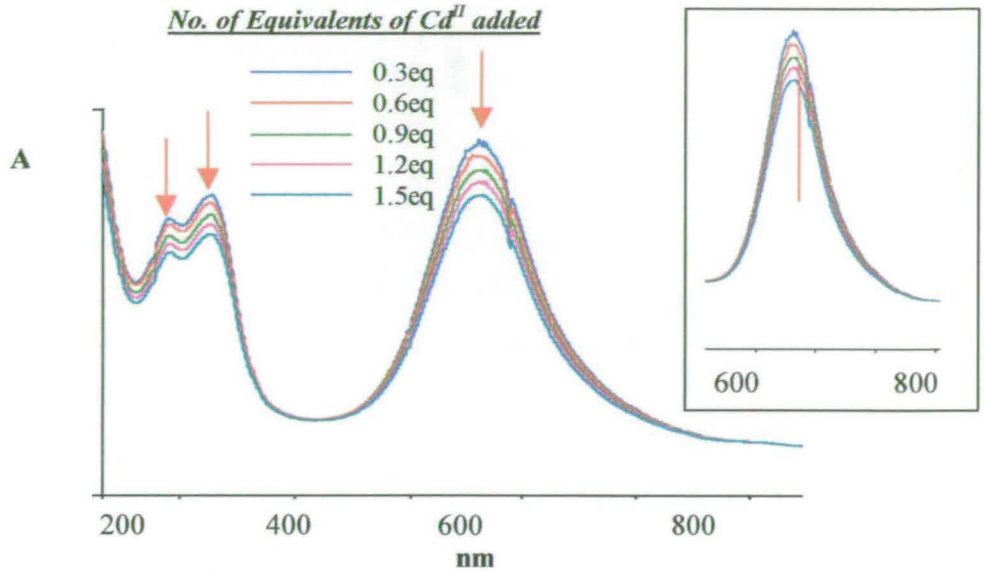

B

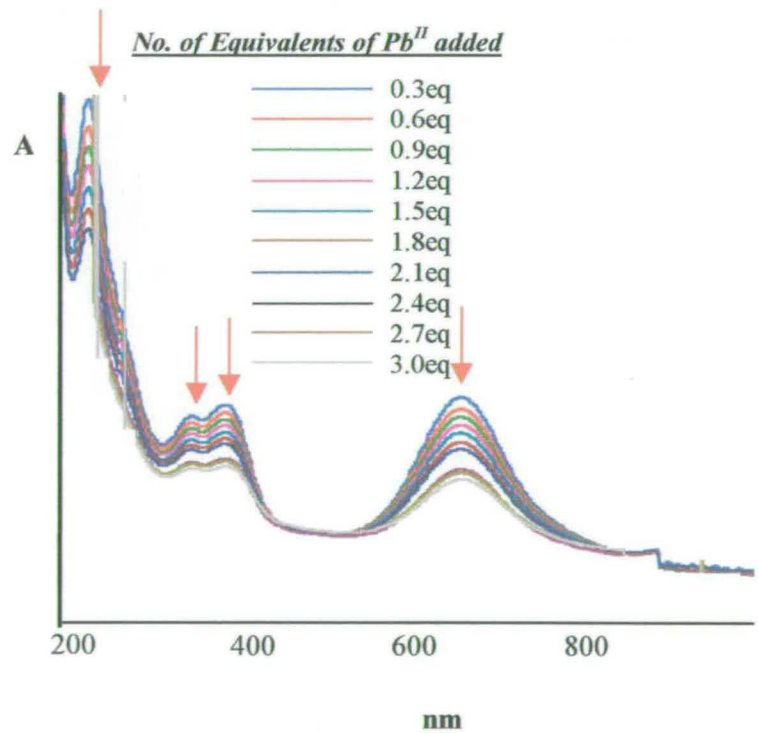

Figure 4. 10 **[A]** Complexation of Cd^{II} to the monosubstituted CpCo- [18]ane S_4N_2 macrocycle **[6]** in DMF followed by UV-Vis spectroscopy. **[B]** Complexation of Pb^{II} to monosubstituted CpCo- [18]ane S_4N_2 macrocycle **[6]** in DMF followed by UV-Vis spectroscopy

Complexation studies of the interaction of Hg^{II} with the macrocycle **[6]** were also carried out and once again the overall decrease in absorbance intensity with increasing [Hg^{II}] was observed, Figure 4.11. The results of the complexation study in UV-Vis for Hg^{II} show that the decrease in absorbance observed at 664 nm, is comparable to that observed for Cd^{II} above.

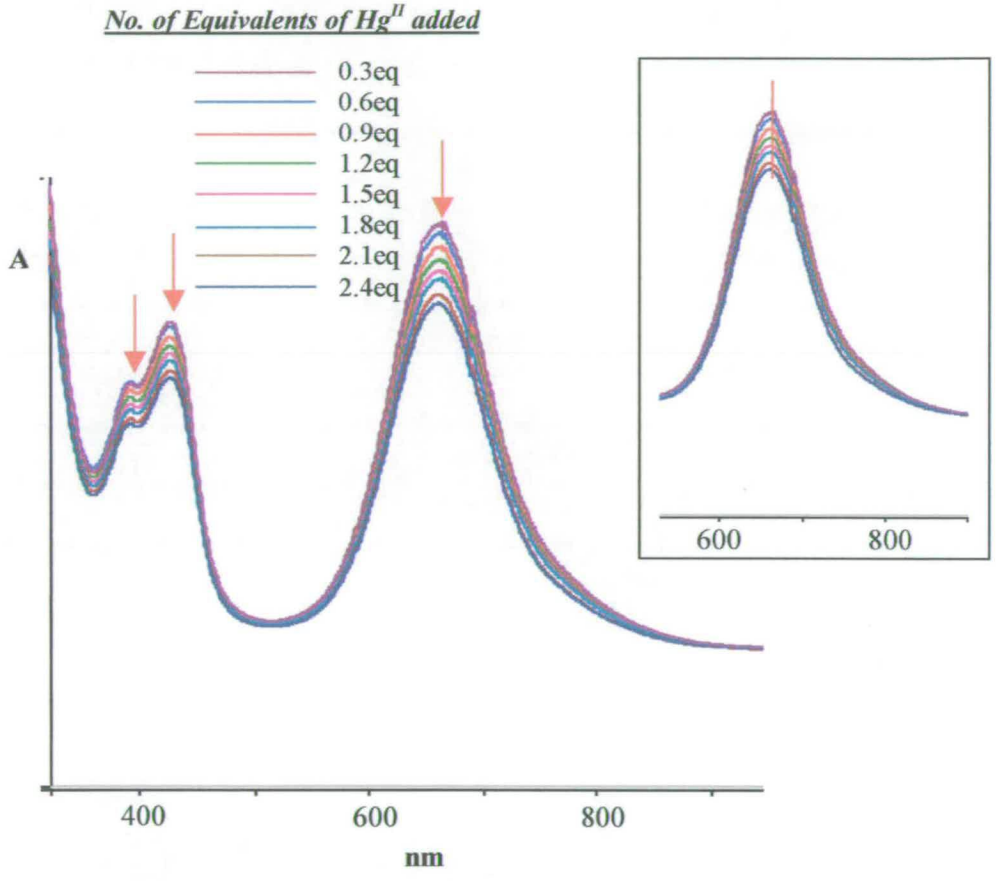

Figure 4. 11 Complexation of Hg^{II} to the monosubstituted CpCo- [18]ane S_4N_2 macrocycle **[6]** in DMF followed by UV-Vis spectroscopy

To give further insight of the mode of interaction of these ions with the macrocycle **[6]**, electrochemical studies were carried out. The electrochemical studies included cyclic voltammetric and differential pulse voltammetric studies. These results are presented in Figure 4.12, 4.13, 4.14 and 4.15.

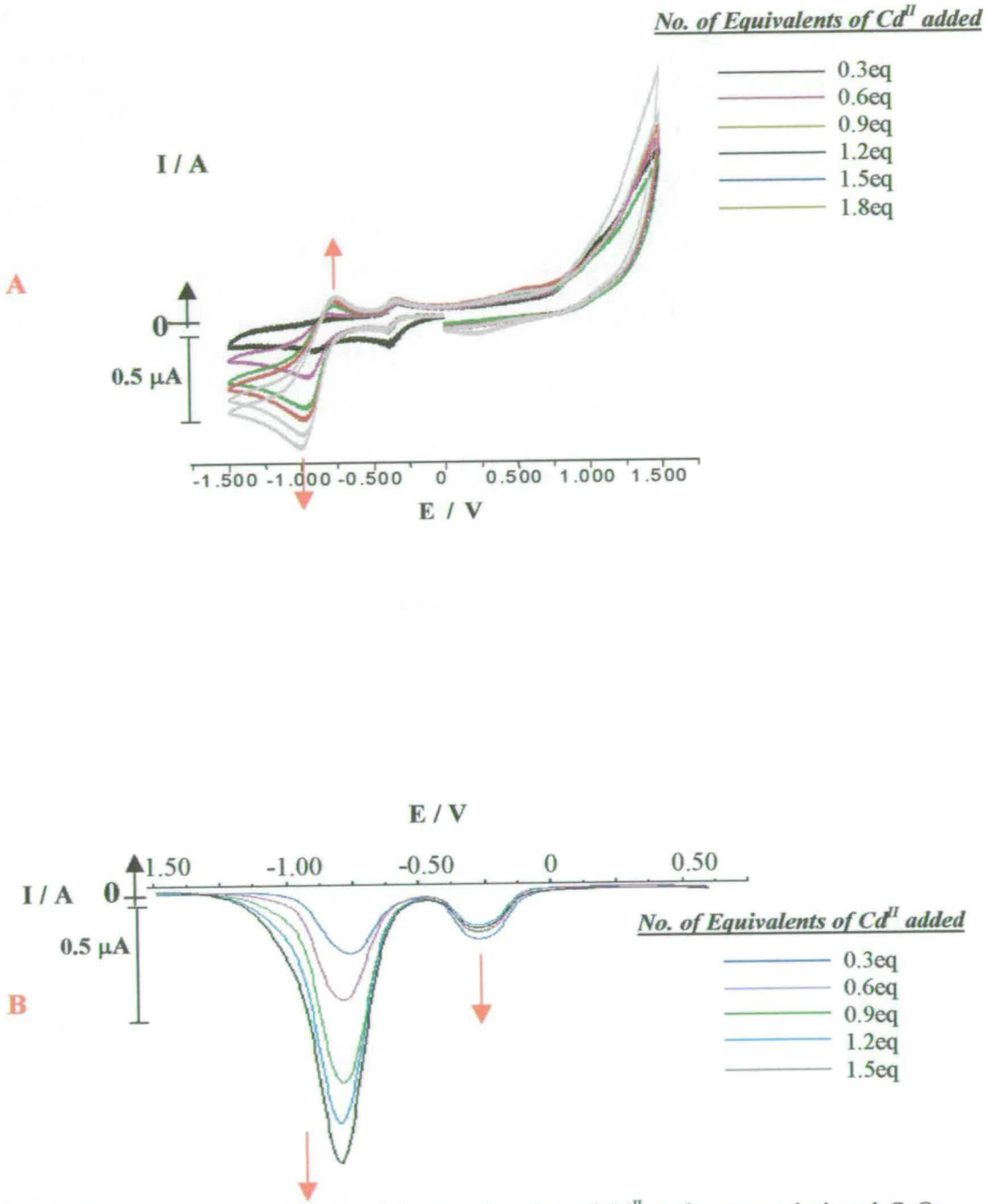

Figure 4. 12 Electrochemical study of the complexation of Cd^{II} to the monosubstituted CpCo-[18]ane S_4N_2 macrocycle [**6**] in DMF followed using Cyclic Voltammetry [**A**] and Differential Pulse Voltammetry [**B**].

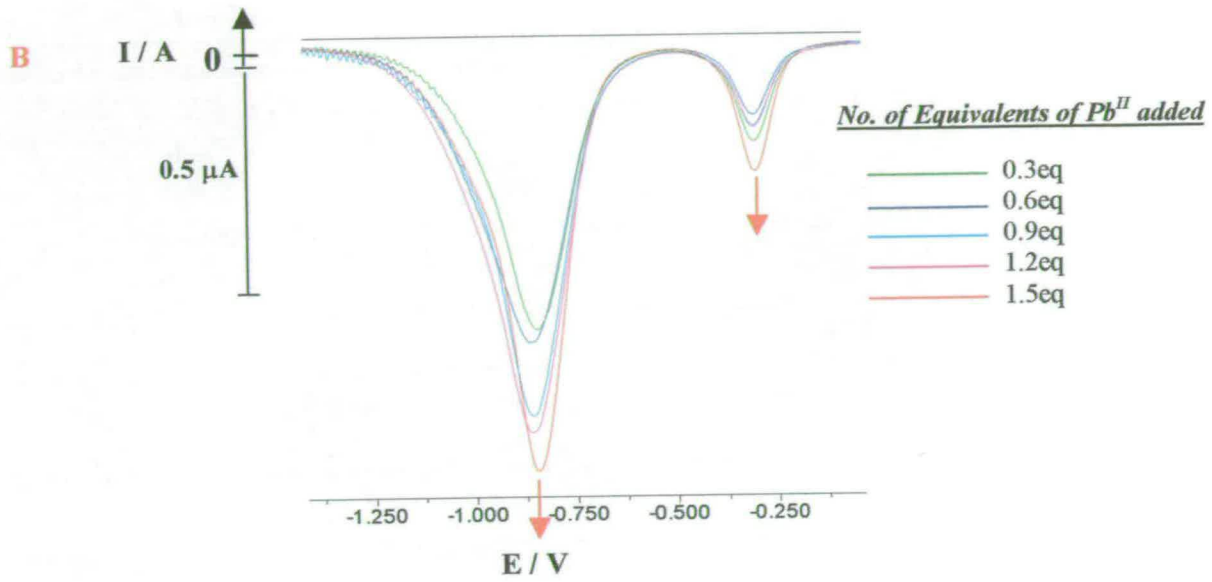

Figure 4. 13 Cyclic Voltammetry (**A**) and Differential Pulse Voltammetry study (**B**) of the complexation of Pb^{II} with the monosubstituted CpCo- [18]ane S_4N_2 macrocycle [**6**] in DMF.

Initially CV studies were carried out on the complexation of Cd^{II} to [**6**], Figure 4.12A. In addition to the CV results observed differential pulse studies were also carried out and are reported in Figure 4.12B. A slight variation in the reduction potential of the Co^{III}/Co^{II} couple at –0.34 V was observed although the variation was not significant. It should be noted that no redox reaction is observed for Cd^{II} in DMF within the experimental electrochemical window.

Also observed in the differential pulse study Figure 4.12B, as in the case of the cyclic voltammogram, is a reduction at a potential of –0.80 V. This signal is seen to increase with increasing addition of the Cd^{II} ions.

Results of the electrochemical study into the interaction of Pb^{II} with the macrocycle [**6**], are shown in Figure 4.13A and B. Observed in these studies, is an increase in signal intensity at –0.87 V in both types of electrochemical study and also the

Co^{III}/Co^{II} reduction observed again at –0.34 V. Once again in the case of the complexation, no redox chemistry for the free Pb^{II} ions is observed within this electrochemical window studied.

When we move on to consider the Hg^{II} complexation to the monosubstituted CpCo-[18]ane S_4N_2 macrocycle **[6]**, Figure 4.14, we once again find a new signal at –0.85 V, which, by comparison of the relative peak height of the new reduction at –0.85 V with that of the 1-electron process occurring for the Co^{III}/Co^{II} couple at –0.37 V, we attribute to the 2-electron, macrocycle-mediated reduction of Hg^{II}, Figure 4.14A. After 0.6 equivalents of Hg^{II} is added to the system a slight change (increase) in the mediated reduction is observed. It should be noted that Hg^{II} in DMF does not undergo redox reactions within the electrochemical window studies for these experiments.

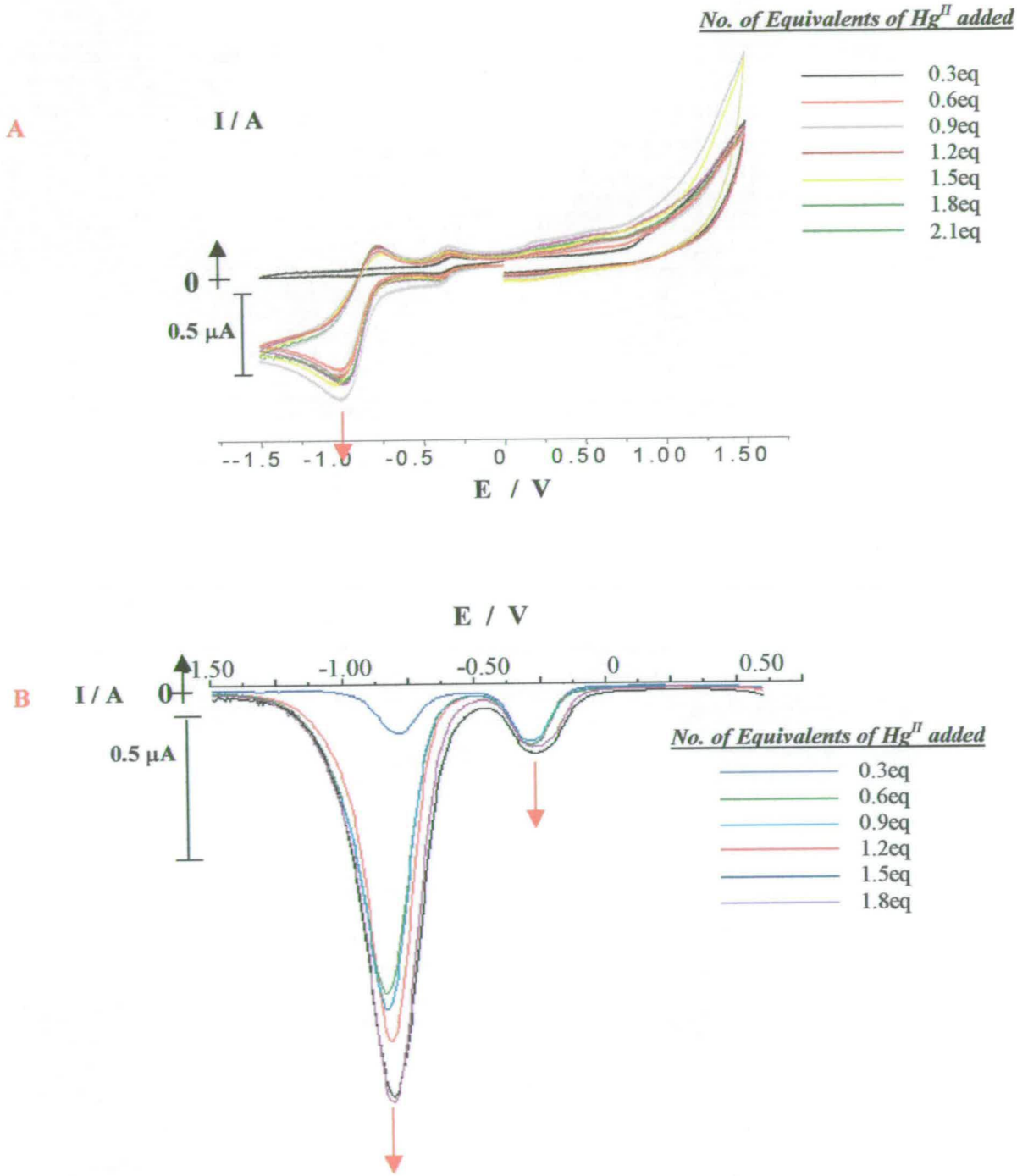

Figure 4. 14 Complexation of Hg^{II} to the monosubstituted CpCo- [18]ane S_4N_2 macrocycle **[6]** in DMF followed by Cyclic Voltammetry **[A]** and Differential Pulse Voltammetry **[B]**

A

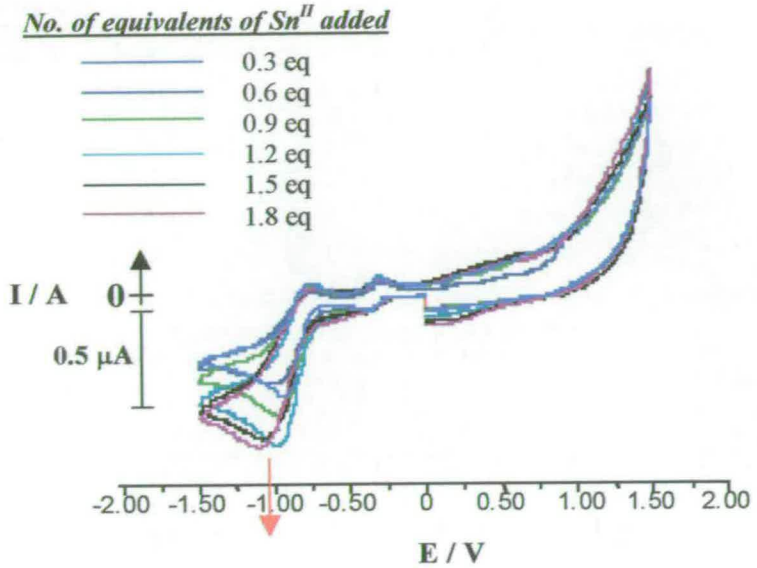

B

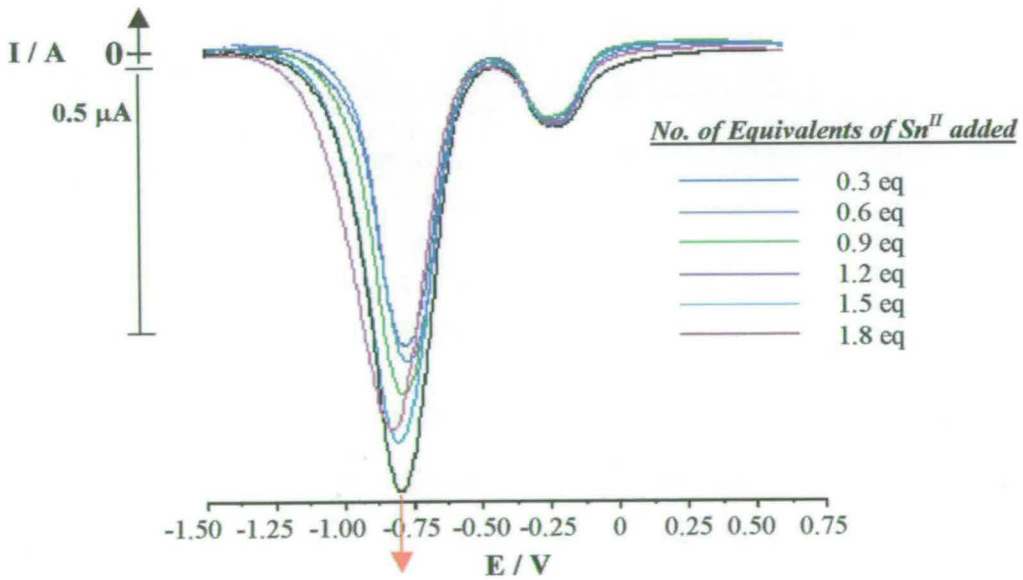

Figure 4. 15 **A** : Cyclic Voltammogram of the complexation of Sn^{II} to **[6]**. **B** : Differential Pulse study of the complexation of Sn^{II} to **[6]**

Also studied using electrochemical studies, was the complexation of Sn^{II} to the macrocycle [**6**]. Once again, following the complexation with Cyclic Voltammetry, a new reduction potential is found to appear between –0.85 V and –1.1 V. The peak position however seems to shift slightly beyond 1 equivalent of Sn^{II} added (Figure 4.15A). Also observed is a feature seen previously; an increase in the reductions intensity with increasing concentration of Sn^{II} ions to the solution. We assign the new reduction to a macrocycle-mediated reduction of Sn^{II} as seen previously for the other metal ions.

In the differential pulse study carried out, once again we see a gradual increase in the reduction potential at –0.85 V due to the macrocycle-mediated reduction of the bound Sn^{II} ions. The results are in comparison with the results obtained for the complexation studies carried out for Hg^{II}, Pb^{II} and Cd^{II}.

4.2.2.3 Conclusions

In all the experiments carried out, involving the complexations the results appear to be similar, with a new reduction appearing at approximately –1.0 V. The reductions in all cases were seen to increase continuously with increasing concentration of metal ions added to the system and coupled with the position, shape and heights of the peaks, indications are once again that a macrocyclic-mediated process occurs for the reduction and oxidation of the metal ion at the electrode surface. A clear example of this is the observation of a very clear second reduction at –0.80 V in the case of Cd^{II}, Figure 4.12 where, once again, a surface bound layer of macrocycle [**6**] is thought to have adsorbed onto the surface of the electrode meaning the only mechanism by which reduction and oxidation of the metal ion species under investigation can occur is through a mediated process at the macrocyclic cavity. With increasing intensity of the reduction peak, no change is observed in the height of the very small return oxidation indicating that the reduction has occurred through

a surface mediated process which resulted in the formation at the surface of a layer of the reduced species. It is not until oxidation of the macrocycle occurs that we see re-oxidation of the reduced species seen as a variation in the intensity of the macrocyclic oxidation signal.

An alternative mechanism to explain the reduction at –0.85 V observed in the case of the Hg^{II} studies, is based on the variations in the intensity of the signal as a result of varying concentrations of Hg^{II} added to the system and makes use of a different mode of complexation. After 0.6 equivalents is added to the system only a slight increase in this reduction signal is observed (Figure 4.14). A common feature among sulfur ligands where complexing to mercury is the preference of the ion to form a bridging $[ML_2]^{II}$ system [26]. It is possible that the limiting value of 0.6 equivalents may indicate formation of a 1:2 Hg^{II}:**[6]** system. A wide variety of chemical environments for these metals are possible and this may be seen in the slight shifts observed in the mediated reduction potentials e.g. Figure 4.15 for Sn^{II}. Unfortunately however, no precipitates formed for the complexations carried out and therefore no analysis could be obtained on the resultant species.

In the UV-Vis spectroscopic studies, the uniform decrease in the extinction coefficient with no clear indication of any shift in the wavelength has been considered. While no conclusive mechanism has been found to explain the observed results and explain the interaction of the metal ion with the ligand, some possibilities have come to light. They include firstly the possibility of aggregation of the ligand molecules around the metal ion, causing an overlap of the transition dipoles and resultant decrease in the extinction coefficient. The second possibility, which has been debated, is the exodentate binding of the metal ion at a close distance to the chromophoric unit. Such binding would also be considered to decrease the extinction coefficient through the static electric field created. Both of these mechanisms will be discussed in more detail at the end of the chapter, Section 4.4.3.2.

When we consider most of the electrochemical studies carried out here, we find that the cyclic voltammograms show a back oxidation peak via oxidation of the macrocycle. This is due to the deposition of metal onto the electrode surface, which is difficult to remove. The extensive shift in the potential to the oxidation potential of the macrocycle and no re-oxidation peak at −1.0 V is indication of this deposited metal and the difficulty associated with oxidising the reduced material.

In general also, we have found that the peak height of the macrocycle-mediated reduction of these M^{II} ions gives a good indication of the number of electrons involved in the electrochemical process at that potential. This is a feature, which will be discussed in more detail when we come to consider other metal ions.

4.2.3 Complexation study of the transition metal ions, Ni^{II}, Fe^{II}, Cu^{II}, and Co^{II} to the monosubstituted CpCo - [18]ane S_4N_2 macrocycle [6]

4.2.3.1 Introduction

To date a common theme has been observed involving the complexation of Ag^{I} and the heavy metal ions Pb^{II}, Hg^{II}, and Cd^{II} to the macrocycle [**6**]. The scheme has been proposed as involving a macrocycle mediated process whereby the reduction and re-oxidation of the metal ions occurs through an adsorbed layer of the macrocycle [**6**] at the electrode surface. Considering the common features observed in these heavier metal ions, studies were expanded to incorporate Fe^{II}, Co^{II}, Cu^{II} and Ni^{II}.

4.2.3.2 Complexation study of Ni^{II} to the monosubstituted CpCo-[18]ane S_4N_2 macrocycle [6]

4.2.3.2a Introduction

The complexation of Ni^{II} to sulphur donors is well known and several systems have been reported in the literature. The coordinating ability of the monosubstituted macrocycle to this species is discussed in more detail in the final discussion at the end of this chapter.

4.2.3.2b Complexation with $Ni^{II}(ClO_4)_2$ with the monosubstituted CpCo- [18]ane S_4N_2 macrocycle [6] in THF

The complexation study of Ni^{II} with the monosubstituted CpCo- [18]ane S_4N_2 macrocycle [**6**] was carried out in both THF and DMF using $Ni^{II}(ClO_4)_2$. The results of the UV-Vis study carried out in THF are shown in, Figure 4.16. The most noticeable difference between this UV-Vis study of Ni^{II} complexation and those of Ag^{I} and Fe^{II} is the lack of any obvious change in either the intensity or the wavelength of the transition absorbance at 675 nm.

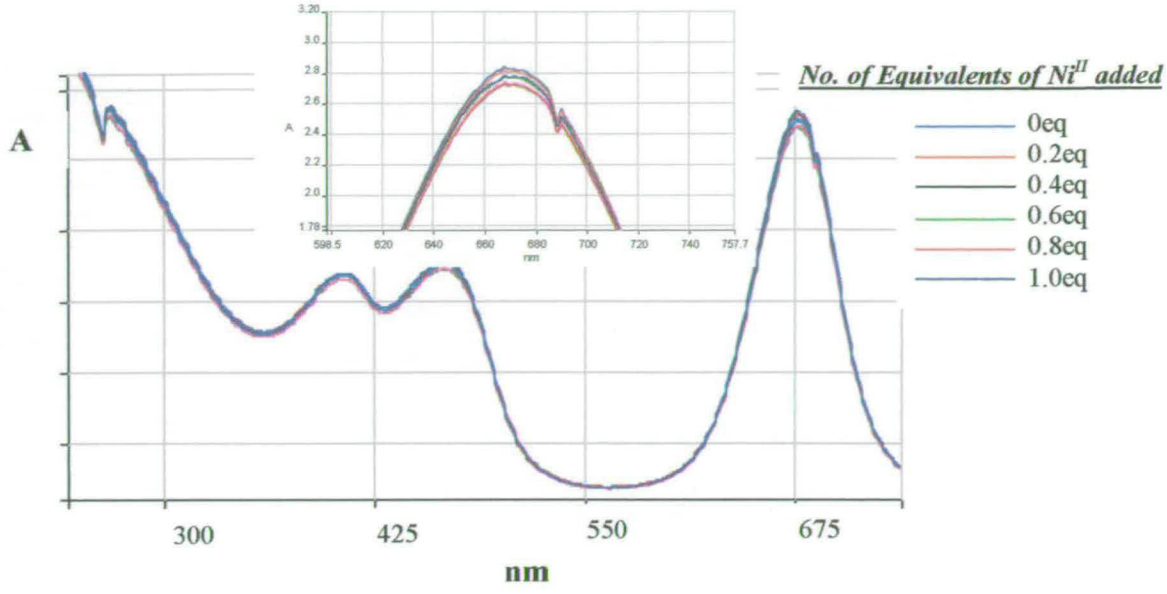

Figure 4. 16 UV-Vis complexation study of Ni^{II} to the monosubstituted CpCo- [18]ane S_4N_2 macrocycle [**6**] carried out in THF. The insert is an expanded image of the top of the absorbance at 675 nm

On consideration of the cyclic voltammetric studies observed in THF, it is likely that a reaction is occurring in the case of Ni^{II}. The reaction does however appear to be proceeding via a different slightly different mechanism compared to those electrochemical studies carried out for Ag^{I}, Fe^{II}, Pb^{II}, Hg^{II}, Sn^{II} and Cd^{II}. It should be noted also that, oxidation or reduction processes for the free Ni^{II} species under these experimental conditions is not observed within the electrochemical window studied.

An increase in the size of the Co^{III} reduction peak at –0.34 V was observed, Figure 4.17. Should both the 1-electron reduction of Co^{III} and the 2-electron reduction of Ni^{II} be taking place at this potential, we would expect that the peak height be approximately three times the size of the initial Co^{III}/Co^{II} reduction when only [**6**] is present. Comparing the cyclic voltammogram of 0.1, 0.5 and 1.0 equivalent addition in Figure 4.17, we can see that the processes at –0.34 V do indeed correlate to a 3-electron process. In this case, no new reduction peak was observed at lower potential

(in contrast with the other metal ions discussed to date) but instead simply an increase in the Co^{III} reduction peak past 1 equivalent is observed. This indicates a reduction process of the Ni^{II} mediated through the cobalt centre of **[6]** adsorbed at the electrode surface and not a macrocycle mediated process.

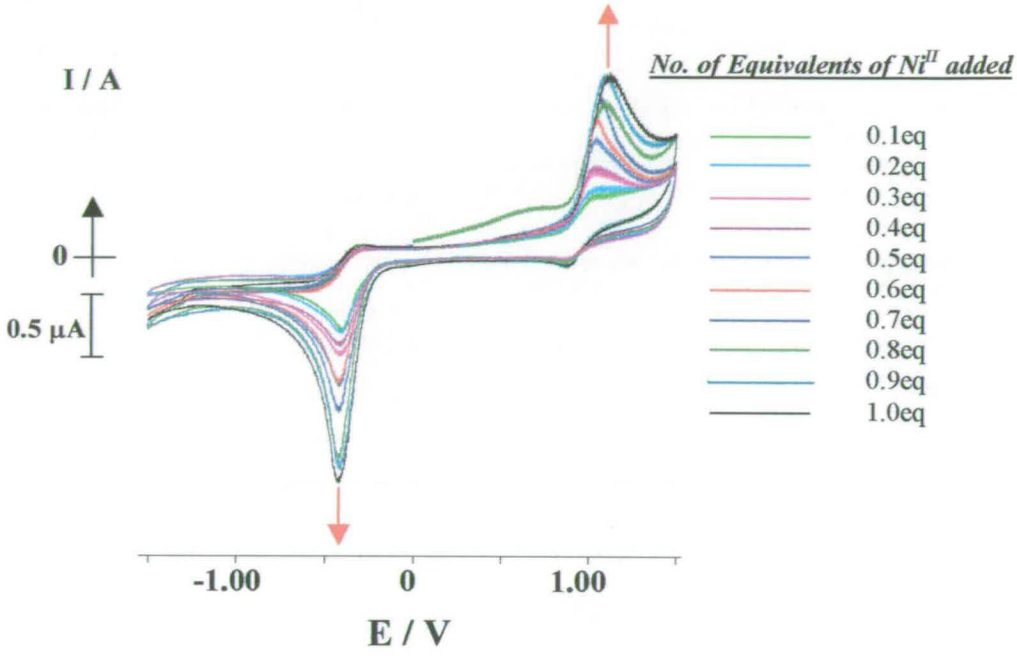

Figure 4. 17 Complexation of Ni^{II} with the monosubstituted CpCo- [18]ane S_4N_2 macrocycle **[6]** in THF. Sweeping negative in each scan

The cobalt-mediated reduction of the Ni^{II} results in Ni^{0}, which appears to be re-oxidised via a catalytic macrocycle-mediated oxidation back to Ni^{II} as seen by an increase in the oxidation at +1.2 V observed.

The reduced return oxidation peak for the Co^{III}/Co^{II} couple also indicates that re-oxidation from Co^{II} to Co^{III} has already taken place before the sweep reaches that potential. This is consistent with mediated reduction of Ni^{II}.

.

In order to confirm that the re-oxidation of Co^{II} to Co^{III} is coupled to the 2-electron Ni^{II} reduction, electrogeneration at –0.40 V in THF of a solution of **[6]** was carried out to give a solution of the reduced macrocyclic species $[\mathbf{6}]^{-}$. Ensuring complete lack of any oxygen, 0.1 equivalent portions of the Ni^{II} species were added to the solution. The addition was monitored using UV-Vis and cyclic voltammetric techniques.

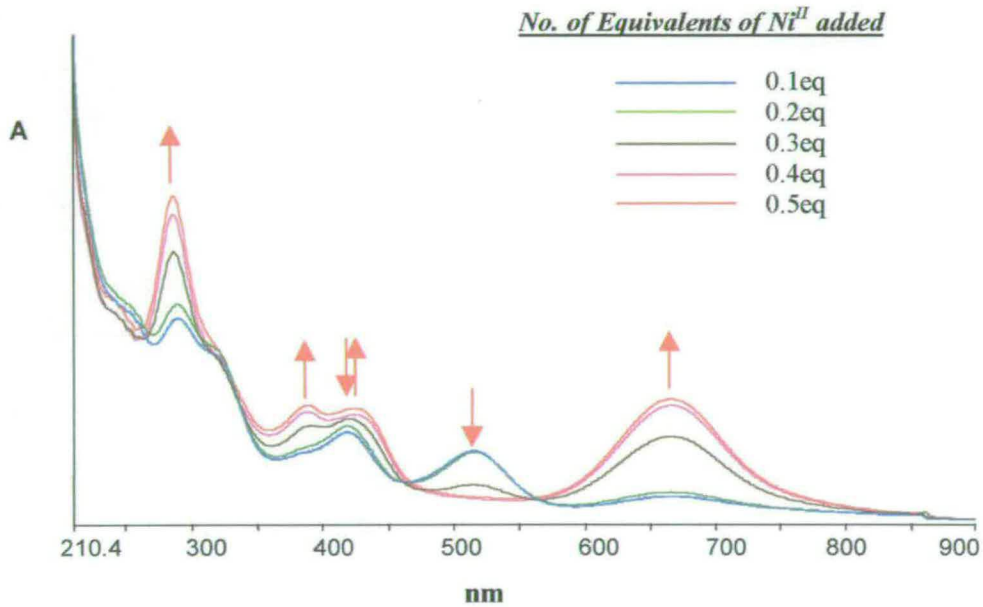

Figure 4. 18 UV-Vis study of the complexation of $Ni^{II}ClO_4$ to the reduced monosubstituted $CpCo^{II}$- [18]ane S_4N_2 macrocycle $[\mathbf{6}]^{-}$ in THF

Following the addition of 0.5 equivalent of the Ni^{II} salt to the electrogenerated Co^{II} species $[\mathbf{6}]^{-}$, the Co^{II} centre was found to have completely converted back to its oxidised Co^{III} form, Figure 4.18, hence the reduced back-peak for the oxidation of Co^{II} to Co^{III}, Figure 4.17. Coupled with the cyclic voltammetry results and the regeneration of the $CpCo^{III}$-dithiolene absorbance at 675 nm, Figure 4.18, we see the re-development of the two $\pi^{*}\leftarrow\pi$ macrocyclic transitions at 375 and 425 nm.

4.2.3.2c Complexation of Ni^{II} with the monosubstituted CpCo- [18]ane S_4N_2 macrocycle [6] in DMF

An identical complexation study to that described in 4.2.3.2b was carried out in DMF as in the case of Ag^{I} previously. The experiment was carried out in an identical manner to that described for THF with 0.1 equivalent additions made to the macrocycle [**6**]. What was observed however was quite different to the THF studies.

As with the case of the Ag^{I} studies in DMF, there is a significant reduction in the intensity of the absorbance at 664 nm. In contrast to the results observed for the Ag^{I} complexation, only a very small shift in the wavelength is observed for the CpCo-dithiolene transition.

The distinct difference in the UV-Vis results compared with those obtained for THF is thought to be as a result of solvent effects. It is postulated that the complex formed between Ni^{II} and the macrocycle [**6**] is made more stable, possibly through coordination of the DMF solvent molecules than in THF, where little or no changes were observed in the intensity of the same absorbance. For this reason it is further proposed that Ni^{II} complexes with the macrocycle [**6**] in this case.

A

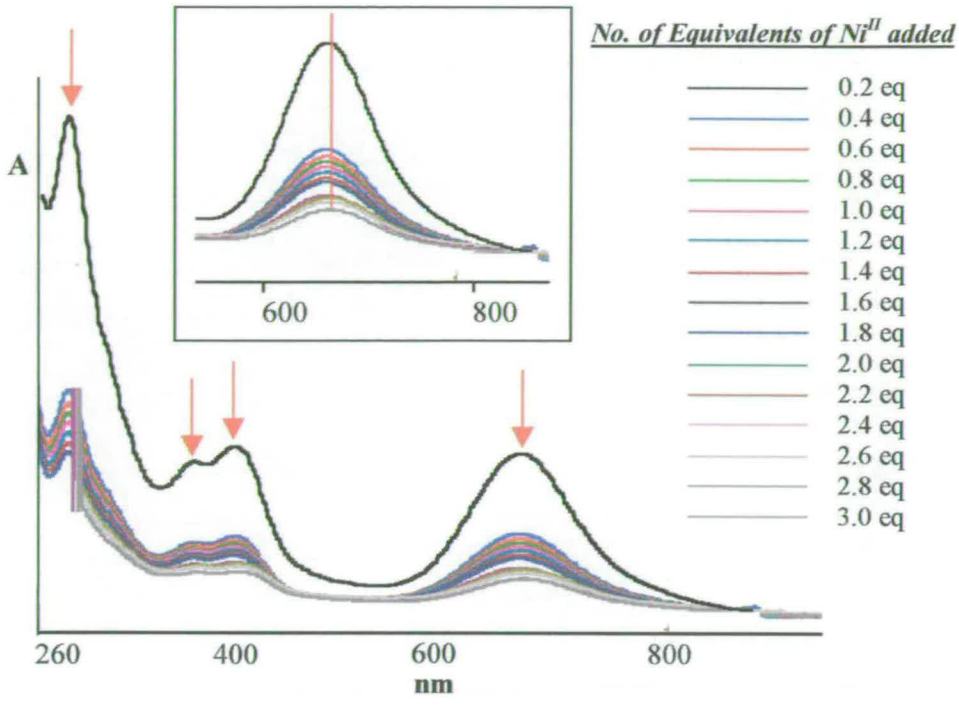

B

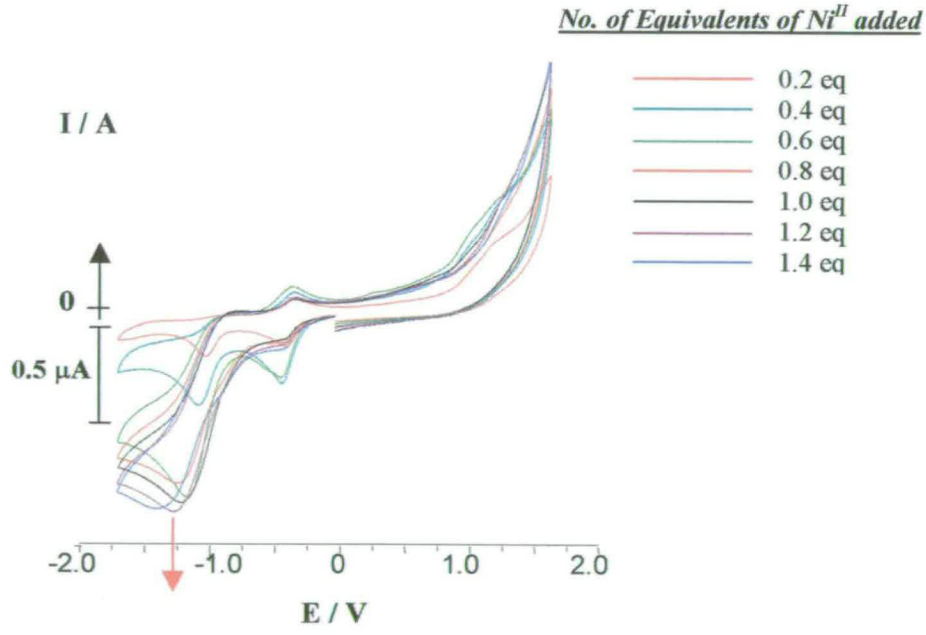

Figure 4. 19 **A :** UV-Vis Complexation of Ni^{II} to the monosubstituted CpCo- [18]ane S_4N_2 macrocycle **[6]** in DMF. **B** : Cyclic Voltammetry study of the complexation of Ni^{II} to the monosubstituted CpCo- [18]ane S_4N_2 macrocycle **[6]** in DMF

In the electrochemical results, Figure 4.19B, we find that there is a new reduction signal observed at –1.10 V. This is contrary to the results observed in the case of THF and is once again thought to be due to the complexation of Ni^{II} in the macrocycle [**6**]. With the increase in the intensity of the new reduction signal past 1 equivalent once again the process is attributed to a macrocycle-mediated reduction of the stabilised Ni^{II} species. With the process involving a 2-electron process it is expected again that a 2:1 ratio is observed for reductions at –1.1 V to the Co^{III}/Co^{II} reduction at –0.34 V for equimolar concentrations of Ni^{II} and [**6**]. This however is not the case. The mechanism looks to be more complicated possibly involving disruption of the surface bound film of [**6**] by DMF.

4.2.3.3 Complexation study of Fe^{II} to the monosubstituted CpCo-[18]ane S_4N_2 macrocycle [6]

4.2.3.3a Introduction

There have been a number of studies carried out on thiolates [27] because of their relevance as model compounds for Fe-S proteins. Sulfur donor complexes of iron are found generally in bioinorganic chemistry in proteins such as rubredoxin [1 Fe] including tetrahedral type complexes such as $[Fe(SPh)_4]^{2-}$ and ferredoxins [clustered Fe], for example $[Fe_4(SPh)_{10}]^{2-}$.

Nitrogen donor macrocycles incorporating iron guest ions are also extremely important in biology forming the basic structure of porphyrins [28]. As a result of the importance of these complexes, other N_4 macrocyclic complexes have also been intensively studied. Based on these literature reports, the complexation of Fe^{II} to the cavity of the mixed donor macrocycle [**6**] should prove interesting.

4.2.3.3b Complexation study of Fe^{II} to monosubstituted CpCo- [18]ane S_4N_2 macrocycle [6] in DMF

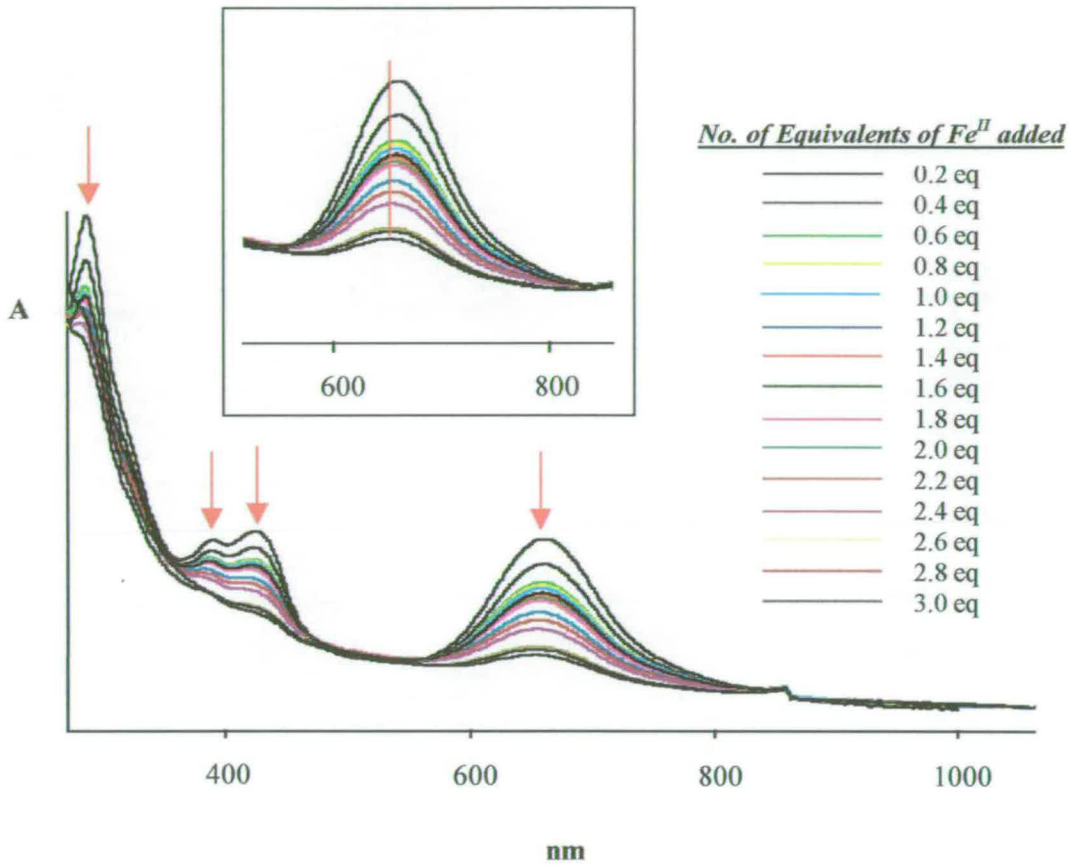

Figure 4. 20 Complexation of Fe^{II} to the monosubstituted CpCo- [18]ane S_4N_2 macrocycle [**6**] in DMF. Study followed by UV-Vis spectroscopy

Attempts were made to complex the Fe^{II} ion to the monosubstituted CpCo- [18]ane S_4N_2 macrocycle [**6**]. Due to the exceptionally good solubility of the reagents and products in DMF, it was decided that DMF should be employed as the solvent system here also.

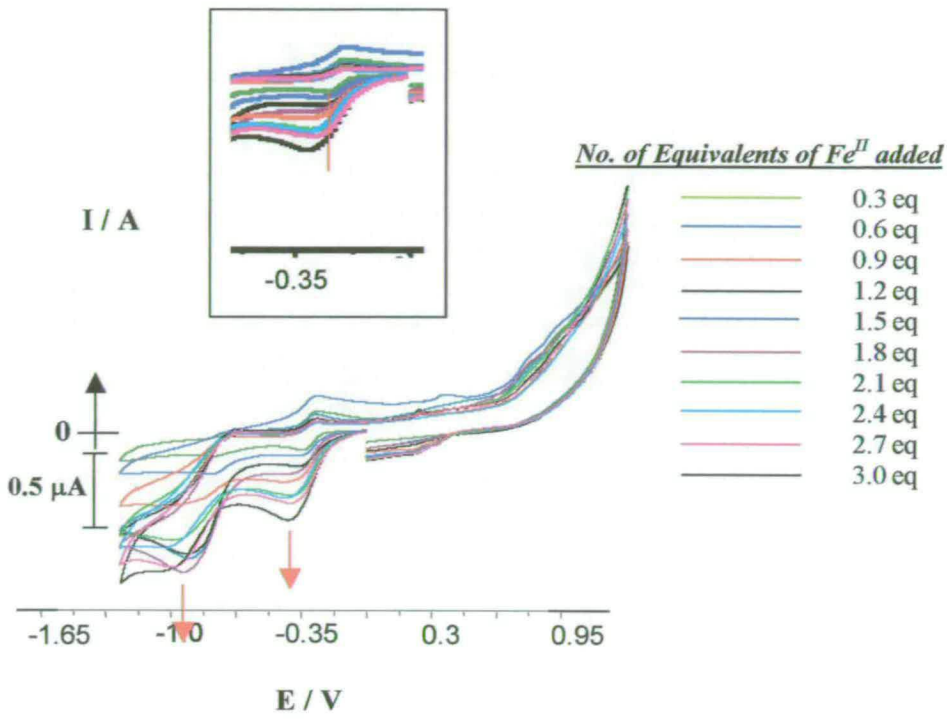

Figure 4. 21 Cyclic voltammetric study of the complexation of Fe^{II} to the monosubstituted CpCo- [18]ane S_4N_2 macrocycle **[6]** in DMF

In the case of the cyclic voltammetric studies carried out, the reduction associated with the Co^{III}/Co^{II} couple at –0.34 V was found to increase with increasing quantities of Fe^{II} added to the system. Coupled with the increase in the reduction at lower potential of –0.8 V the results may be compared with those of Ag^{I}. The results of the Ag^{I} complexation showed that adsorption of a thin layer of macrocycle onto the electrode surface is occurring through which the Fe^{II} is reduced to Fe^{0}. This is further clarified by the lack of any noticeable stripping peaks for the free Fe species as observed in the case of the Ag^{I} complexation study and also the increase in the intensity of the new reduction signal past 1 equivalent. As such, a macrocycle-mediated reduction of the Fe^{II} ion is again proposed.

Following the addition of 1 equivalent and the corresponding increase of the reduction observed at –0.80 V for the reduction of the Fe^{II} through a macrocycle mediated process, an increase in the Co^{III}/Co^{II} redox couple is observed. This increase is due to the reduction of uncomplexed Fe^{II} mediated through the Co^{III} centre.

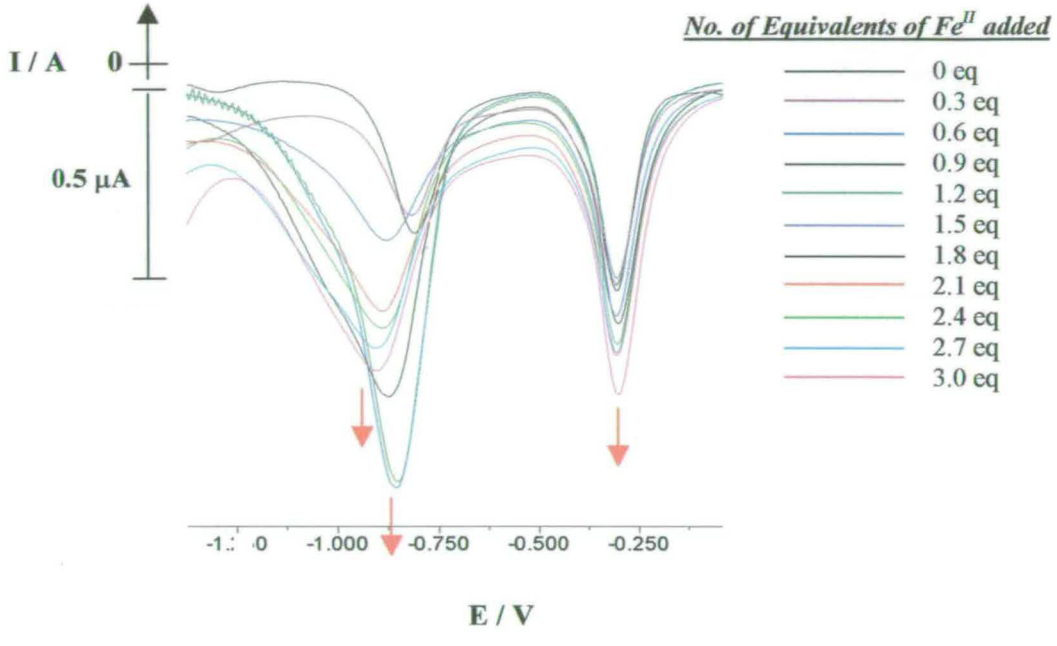

Figure 4. 22 Differential Pulse study of the complexation of Fe^{II} to the monosubstituted CpCo-[18]ane S_4N_2 macrocycle **[6]** in DMF

Further evidence for the characterization of this new reduction as a reduction peak for Fe^{II} lies in the actual electron process occurring in the reduction of Fe^{II} to Fe^0. Reduction of Fe^{II} to Fe^0 involves a 2-electron process. The mediated-reduction peak at –0.8 V would therefore be expected to be twice the intensity of that of the cobalt reduction at –0.34 V. Examination of the results in Figure 4.21 clearly confirms this

to be the case, with the two reduction peaks at –0.8 V and –0.34 V in a 2:1 ratio where 1 equivalent of Fe^{II} has been added.

Considering the results of the differential pulse potentiometry, Figure 4.22, we find that a new reduction signal appears at approximately -0.83 V with addition of up to 0.6 equivalents of $Fe^{II}(ClO_4)_2$. From this point, with the addition of up to 1.5 equivalents of $Fe^{II}(ClO_4)_2$, the reduction potential shifts to a more negative potential at –0.87 V. From the addition of 1.5 to 2.1 equivalents, this reduction peak shifts once again to a potential of –1.03 V.

Similar results are observed in the cyclic voltammograms presented in Figure 4.21. In the case of these studies, we see once again a variation in the reduction potential observed at –0.83 V. The reason for the variations in the potential of these mediated reductions is thought to be due to the differences in the energetics of the bound species. These alterations cause shifts in the reduction potential from –0.83 V to approximately –1.0 V indicating identical interactions of the metal ions with the macrocycle [**6**] to that observed in the Differential Pulse studies.

4.2.3.3c Conclusions

In a similar scheme to that proposed for the initial complexation of Ag^{I} to the macrocyclic cavity of the monosubstituted CpCo- [18]ane S_4N_2 macrocycle [**6**], the Fe^{II} is also thought to undergo macrocycle-mediated reduction process at the electrode surface. In this case, the reduction is a 2-electron process ($Fe^{II} - Fe^{0}$), seen by the 2:1 ratio of the reductions at ~ –1.00 V and –0.34 V.

4.2.4 Complexation study of Co^{II} and Cu^{II} to the monosubstituted CpCo- [18]ane S_4N_2 macrocycle [6].

4.2.4.1 Introduction

The complexation studies described in this section include those of Co^{II} and Cu^{II} to [**6**]. The studies were carried out in an identical manner to those for the previous metal ions. Complexation of Co^{II} to macrocycles has been reported in the literature and in some cases we see some intriguing features of macrocyclic chemistry including rearrangement of the macrocyclic ring to give an optimum metal binding cavity.

One macrocycle which is comparable to our system [**6**] is the [18]ane S_6 system which forms a complex with $Co^{II}(picrate)_2$ [29]. The Co^{II} ion is coordinated solely by thioether groups to yield a rare example of low-spin (tetragonally distorted) octahedral complex; Co-S_{eq} = 2.25 and 2.29 Å, Co-S_{ax} = 2.48 Å. More common are the complexes of Cu^{II}, which form readily by coordination with a hexadentate ligand. A typical example is the picrate salt of the [18]ane S_6 thiocrown ether. More recently complexes of Ni^{II}, Co^{II}, Cu^{II}, Zn^{II}, Mn^{II} and Ag^{I} with a variety of macrocyclic polyethers including dicyclohexano [18]ane crown ether have been reported [30]. In a potentiometric study of the Cu^{II} and Ag^{I} complexes, results indicate 1:1 complex formation between the metal ion and crown ether macrocycle. Noticeable from the literature is the lack of any reports of S_4N_2 donor macrocycles binding to Cu^{II} and Co^{II}.

4.2.4.2 Complexation studies of Co^{II} and Cu^{II} to the monosubstituted CpCo- [18]ane S_4N_2 macrocycle [6] inTHF

As in the case of the previous complexations (Section 4.2.1, 4.2.2 and 4.2.3), studies in THF involving Co^{II} and Cu^{II} were initially carried out. Addition of 0.2 equivalent-portions of guest-ion, were made to a THF solution of the ligand [**6**] (Section 4.5). UV-Vis results are reported below for each of the Co^{II} (Figure 4.24) and Cu^{II} (Figure 4.25) ions.

As is clear from both the complexation of Co^{II} ($CoCl_2$) (Figure 4.23A) and Co^{II} ($Co(BF_4)_2$) (Figure 4.23B), there is little variation in absorbance with increased quantities of Co^{II} ions added to the system. This is comparable to the results obtained for the Ni^{II} complexation studies carried out Section 4.2.3.2. However, the lack of any change in the electrochemical cyclic voltammograms further substantiated a lack of interaction of the ion with the macrocycle [**6**] either directly in solution or at the electrode surface.

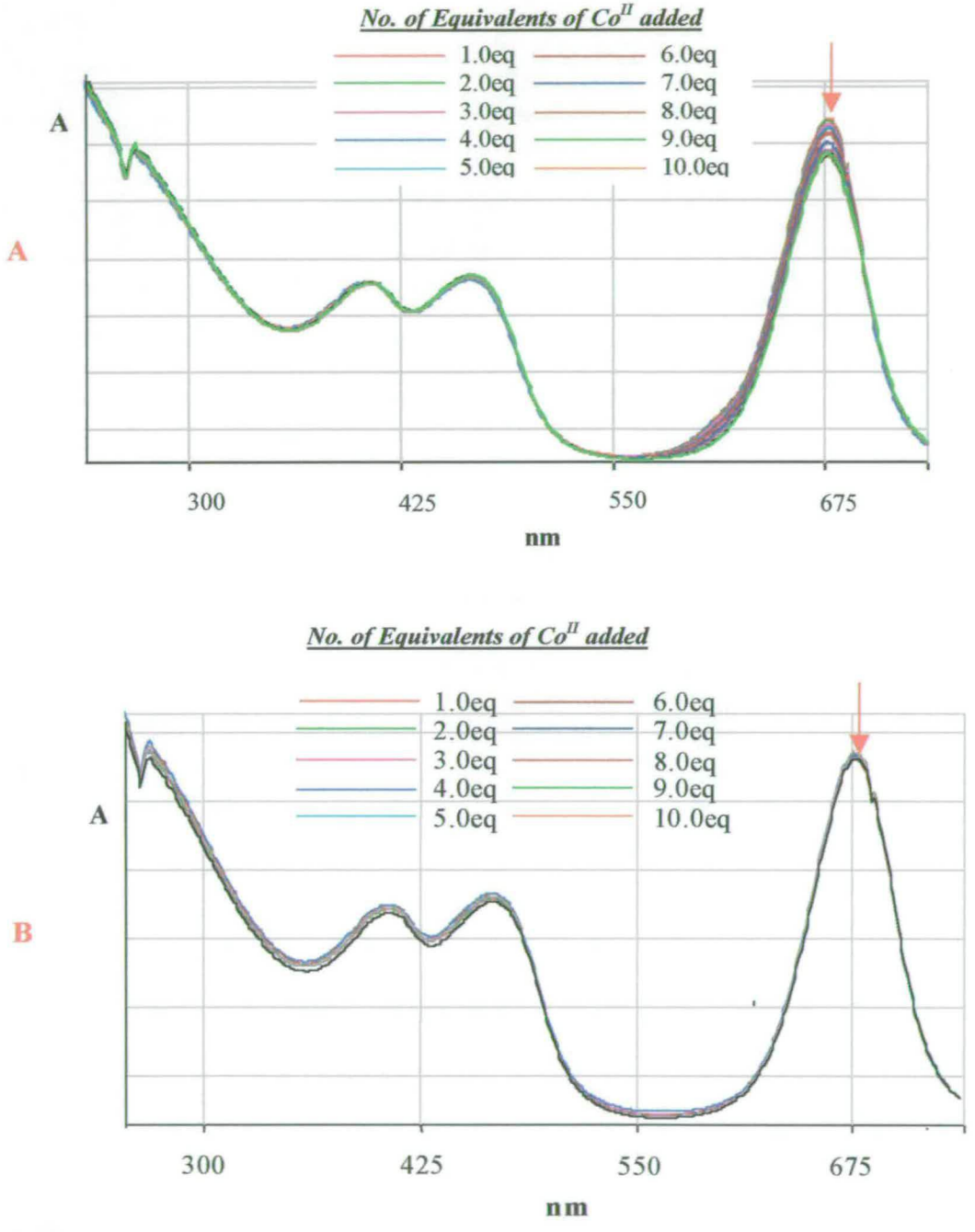

Figure 4. 23 [**A**] Complexation study of $Co^{II}Cl_2$ to the monosubstituted CpCo- [18]ane S_4N_2 macrocycle [**6**] in THF. [**B**] Complexation study of $Co^{II}(BF_4)_2$ to the monosubstituted CpCo- [18]ane S_4N_2 macrocycle [**6**].

There are a number of possible reasons for this and mainly they deal with the size of the ion and the size of the cavity of **[6]**. Also needing consideration is the flexibility of the macrocyclic ligand **[6]**.

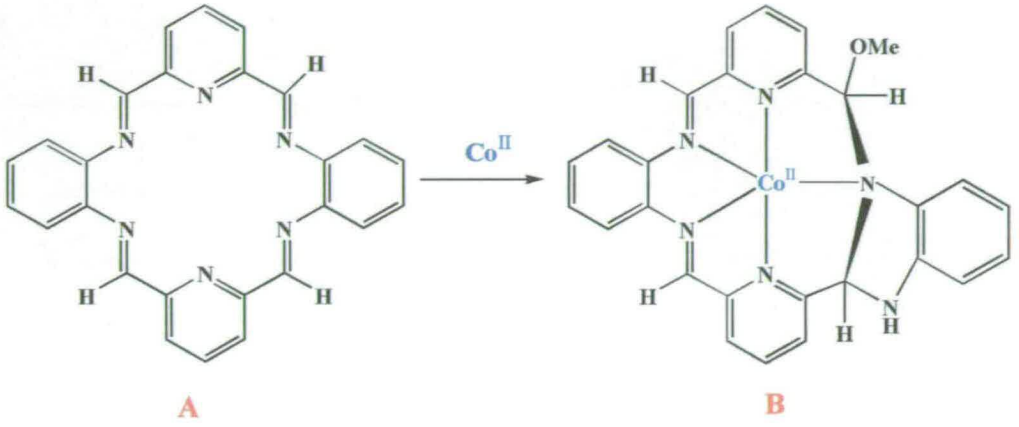

Scheme 4. 2 Ring contraction of the hexaaza-macrocyclic ligand **[A]** with the addition of Co^{II} to give the complex **[B]**

When we consider the reported complexes in the literature, we find that Co^{II} usually binds successfully to hexadentate macrocycles with some rearrangement of the macrocyclic backbone. In the case of the 18-membered hexa-aza macrocycle shown in Scheme 4.2, for example, the cavity is found to be too large for complexation of a first row transition metal ion. In such cases, addition of Co^{II} causes a ring contraction of A to give B, Scheme 4.2. The contraction is made possible by a distortion from planarity of the ligand upon addition of methanol followed by an intramolecular attack of the amine on the imine to generate the smaller 15-membered macrocycle.

As mentioned previously, there is a lack of any reports for complexation of Co^{II} to the cavity of any macrocycles analogous to **[6]** and as such, the results obtained in this study were unsurprising.

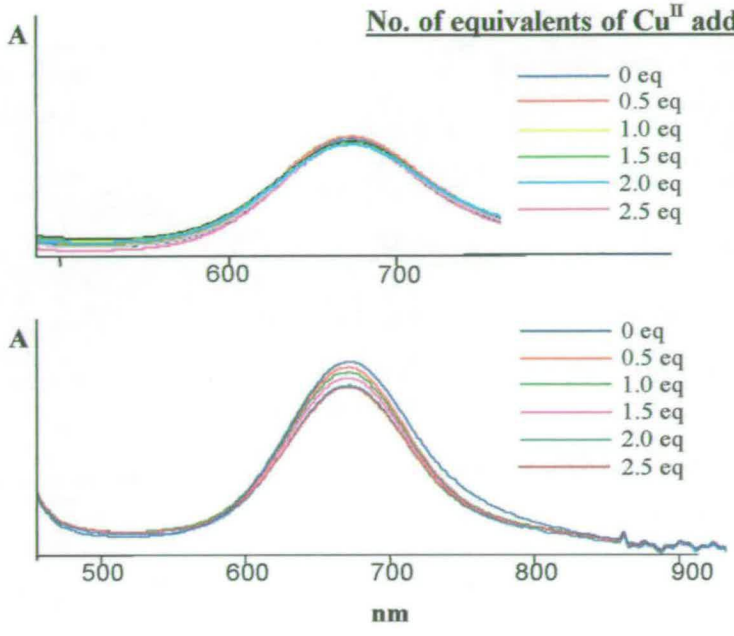

Complexation of $Cu^{II}(OAc)_2$ to the macrocyclic cavity of [**6**] in THF. Shown is the sequential addition of 2.5 equivalents of the metal

Complexation of $Cu^{II}(BF_4)_2$ to the macrocyclic cavity of [**6**] in THF. Shown is the sequential addition of 2.5 equivalents of the metal

Figure 4. 24 Comparison of the CpCo-dithiolene absorbance at 675 nm for the complexation of $Cu^{II}(OAc)_2$ and $Cu^{II}(BF_4)_2$ with the monosubstituted CpCo- [18]ane S_4N_2 macrocycle [**6**]

In comparison to Co^{II} studies, the geometry within the cavity of [**6**] seems to slightly favour Cu^{II} over Co^{II}. This interaction of Cu^{II} (Figure 4.24), though minimal in the bulk solution, appears to occur due to the known ability of Cu^{II} to adapt to any geometric environment [31] e.g. in phthalocyanines and cyclam- macrocyclic cavities.

In the case of the electrochemical studies, once again a new reduction is observed to increase at –1.45 V in the case of Cu^{II}. As with previous complexation studies with Ag^{I}, Fe^{II}, Ni^{II} and the heavy metal ions Pb^{II}, Hg^{II} and Cd^{II}, the macrocycle [**6**], is thought to be adsorbed at the surface of the electrode. The reduction observed at –1.45 V is attributed to the macrocycle-mediated reduction of the Cu^{II} ion with the height of the new reduction peak equivalent to a 2-electron process ($Cu^{II} + 2\ e^{-} \rightarrow$

Cu^0). Variations in the macrocycle oxidation peak at +1.2 V are attributed to the re-oxidation of the Cu^0 to Cu^{II} once again via a macrocycle-mediated process.

In Figure 25B, $Cu^{II}BF_4$ is cycled at 20 mV s^{-1} in THF. The purpose of this experiment is to determine the reduction and oxidation potential of the free Cu^{II} species. Reduction of Cu^{II} ($Cu^{II} + 2e^- \rightarrow Cu^0$) is seen at approximately 0 V (however this value is difficult to measure) while the stripping peak of Cu^0 ($Cu^0 \rightarrow Cu^{II} + 2e^-$) is observed at +0.98 V. Considering the results observed in Figure 4.25A, we find that at concentrations of Cu^{II} greater than 1 equivalent these redox reactions become evident.

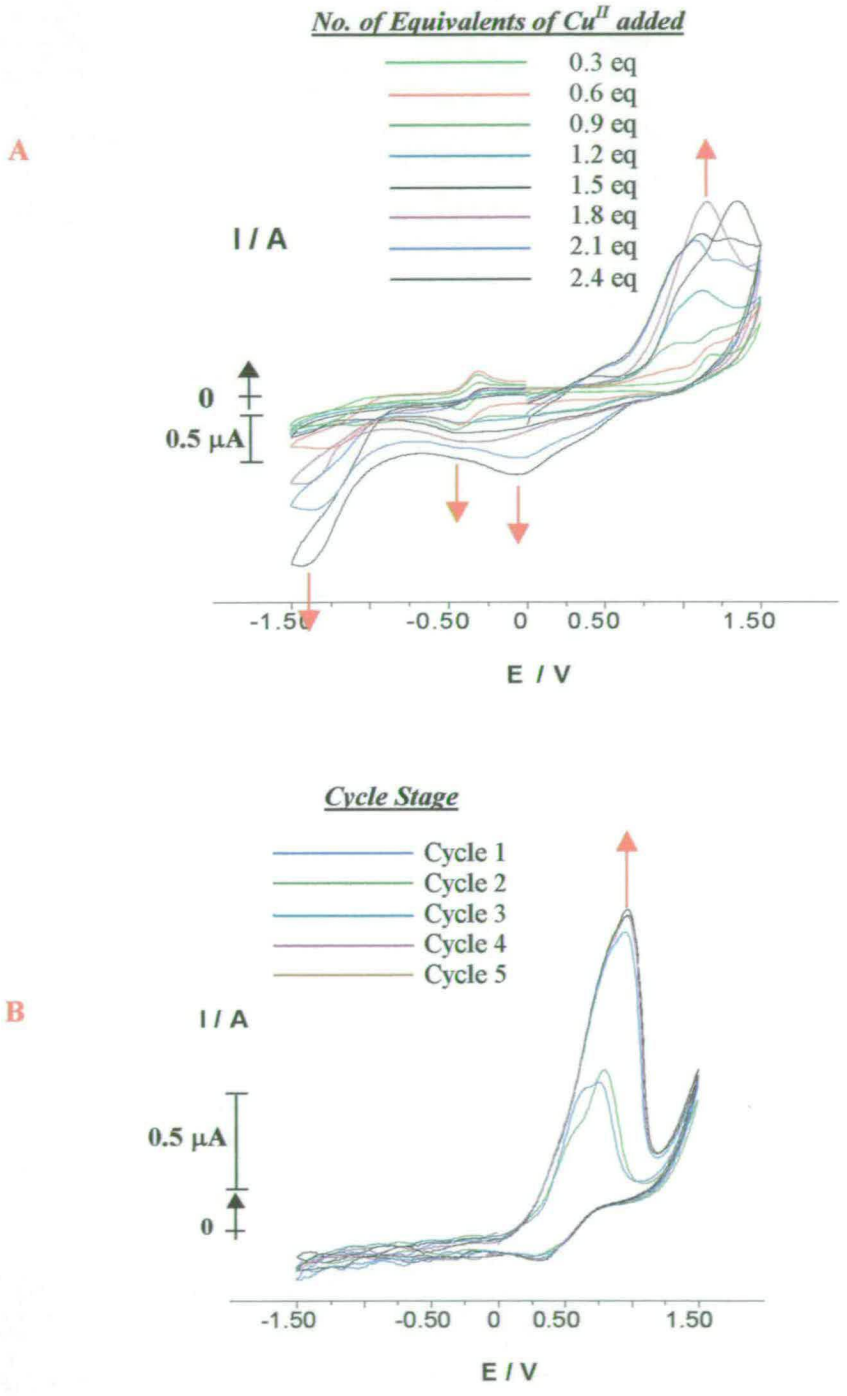

Figure 4. 25 [**A**] Complexation study of the addition of $Cu^{II}(BF_4)_2$ to the monosubstituted CpCo-[18]ane S_4N_2 macrocycle [**6**] to 2.4 equivalents. [**B**] $Cu^{II}(BF_4)_2$ cycled at 20 mV s^{-1} in THF. Both were followed by Cyclic Voltammetry

4.2.4.3 Complexation of $Cu^{II}(BF_4)_2$ to the monosubstituted CpCo-[18]ane S_4N_2 macrocycle [6] in DMF

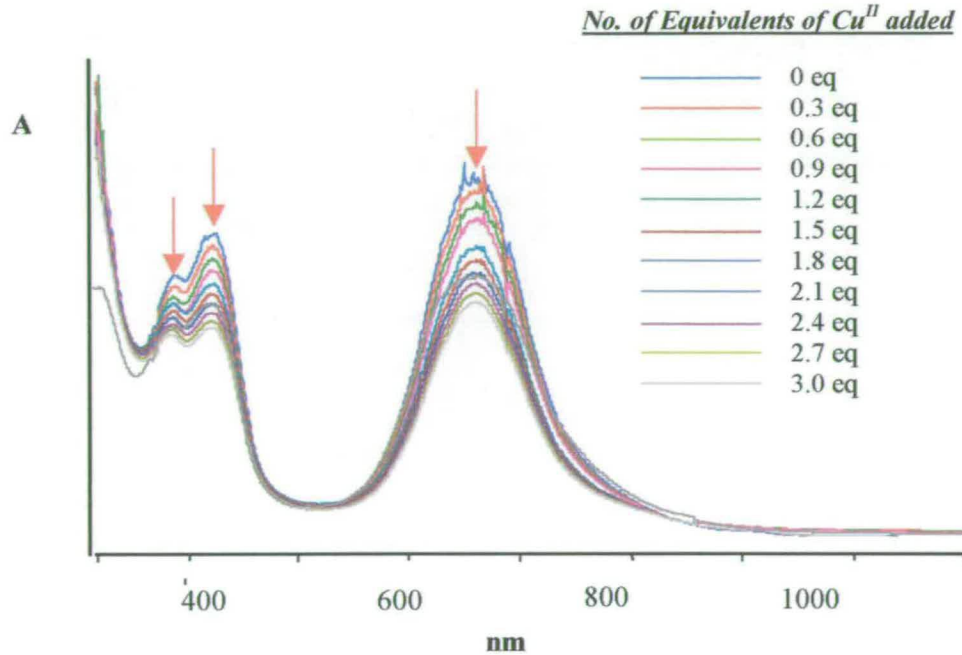

Figure 4. 26 Complexation of $Cu^{II}(BF_4)_2$ to the monosubstituted CpCo- [18]ane S_4N_2 macrocycle [**6**] in DMF followed by UV-Vis spectroscopy

From the results observed previously in DMF for other metals, it was thought that, as in the case of the Ag complexation studies, further information on the mechanism of binding of Cu^{II} could be obtained by carrying out the complexation of $Cu^{II}(BF_4)_2$ in DMF. $Cu^{II}(BF_4)_2$ was used as the Cu^{II} ion source. The UV-Vis experimental results are shown in Figure 4.26.

From these complexation results we find that, as with several previous complexation studies, a decrease in all absorbances was observed. This once again is indicative of a similar type of interaction as that observed in the case of the main group ions with the macrocycle [**6**] (Section 4.2.2) and will be full discussed in Section 4.4.3.2.

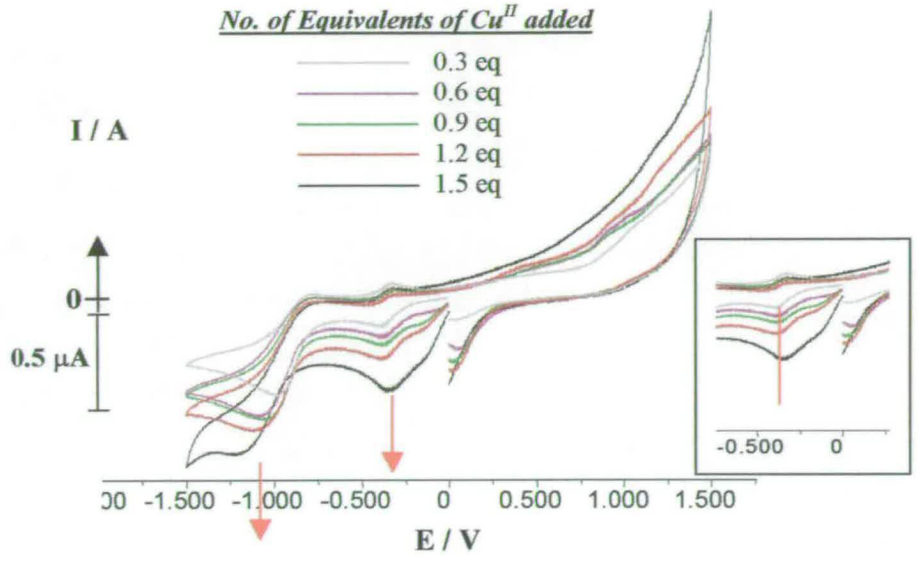

Figure 4. 27 Complexation study of Cu^{II} with monosubstituted CpCo- [18]ane S_4N_2 macrocycle **[6]** in DMF followed by cyclic voltammetry

From the cyclic voltammogram presented in Figure 4.27, an increase in the intensity of the Co^{III}/Co^{II} reduction signal is observed with increasing concentration of Cu^{II} added to the system. A new reduction observed at approximately -1.18 V is also observed. While there is no indication of an oxidation peak at lower potentials, an increase in the macrocycle oxidation at approximately +1.2 V is observed although it is not a distinct peak.

When we examine the differential pulse potentiometry presented in Figure 4.28 a new reduction is clear at approximately –0.90 V. As increasing quantities of the ion species was added to the solution, this reduction was seen to shift to lower potentials up to –1.18 V. The variation in these reduction potentials is thought to be due to the metal ion present in a variety of chemical environments in the course of the mediated reduction process. While the reduction potentials observed for the macrocycle-mediated reduction of Cu^{II}. Is observed to be in similar environments shifting from

approximately –0.90 V to –1.18 V, there is a reduction in the peak height of the reduction as the concentration of added Cu^{II} is added.

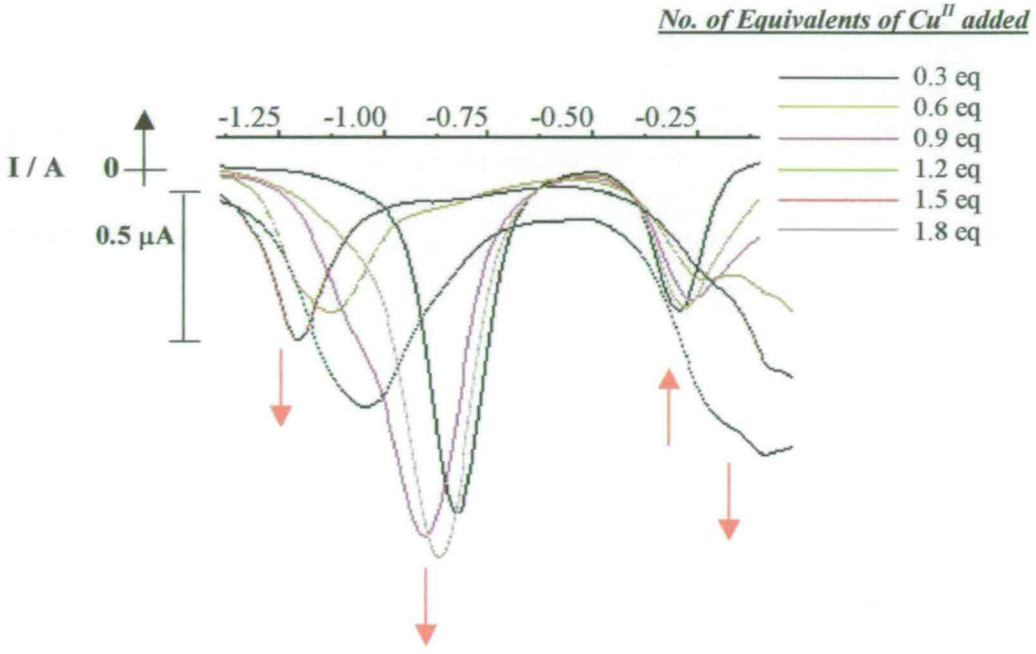

Figure 4. 28 Differential Pulse Voltammetry study of the reaction of Cu^{II} with the macrocycle [6]

The results obtained for both the cyclic voltammogram and the differential pulse studies are similar to those observed for the Fe^{II} complexation discussed previously. Macrocycle-mediated reduction of the bound Cu^{II} was observed at approximately –1.18 V and no return oxidation peak was observed. It should be remembered however that the oxidation may take place outside the given electrochemcial window.

Changes in the reduction process of the Co^{III}/Co^{II} couple are also seen. In a comparison of the results presented for the cycling of $Cu^{II}BF_4$ in THF and those results presented here, we find that the new reduction increasing at 0.5 V is indeed

due to the reduction of free Cu^{II} ($Cu^{II} + 2e^- \rightarrow Cu^0$). It is thought therefore that once again the solvent is compromising the integrity of the surface adsorbed macrocycle layer, allowing free Cu^{II} access to the Pt electrode surface and redox processes to occur for the ions at concentrations greater than 1 equivalent. A final consideration in the case of this study is the ratio of the reduction at –0.90 V to that of the Co^{III} reduction observed at –0.34 V. Following the addition of 1 equivalent of Cu^{II} to the reaction mixture, the ratio of these peaks is 2:1 indicating, as expected, that the reduction at –0.90 V is due to the macrocycle-mediated reduction of Cu^{II}.

With a drop in each of the absorbances observed in the UV-Vis experiment, Figure 4.26, there appears to be a more considerable interaction with the macrocycle in DMF than was the case in THF from the UV-Vis and the electrochemical studies Figure 4.24.

4.3 Complexation studies of the reduced monosubstituted $CpCo^{II}$- [18]ane S_4N_2 macrocycle $[6]^-$

4.3.1 Introduction

Based on the complexation results of Ag^I, Fe^{II}, Co^{II}, Cu^{II}, Ni^{II} ions and the late transition metals Hg^{II}, and Cd^{II} and the heavy metal ions Sn^{II} and Pb^{II}, to the monosubstituted CpCo- [18]ane S_4N_2 donor macrocycle **[6]** previously discussed, studies were carried out to determine the interaction of the Co^{II} reduced species $[\mathbf{6}]^-$, with the same metal ions.

4.3.2 Results and Discussion of complexations to $[6]^-$

As discussed, in each of these complexations, the UV-Vis spectrum was obtained after each addition of the metal ion was made. In each of the spectra obtained, the starting and finishing UV-Vis absorbance of the $\pi^*\leftarrow\pi$. CpCo-dithiolene based transition of both **[6]** and $[\mathbf{6}]^-$ macrocycles were measured. Normalising the results, the % change in the re-oxidation of Co^{II} to Co^{III} was determined. These results have been tabulated in Table 4.1.

From the results presented, we see that in some cases, the absorbances due to the $\pi^*\leftarrow\pi$ transition at 664 nm ([**6**]) increases with increasing concentrations of the metal ion under investigation. At the same time the absorbance due to a $\pi^*\leftarrow\pi$ transition with the $CpCo^{II}$-dithiolene unit at 515 nm in $[\mathbf{6}]^-$ is found to decrease with each addition. The extent to which these changes actually occur, varies from metal to metal but from the results collected, two distinct groups of metals are obvious, one of which causes re-oxidation of the Co^{II} centre to Co^{III} and the other causing little or no oxidation at the Co^{II} site.

Table 4. 1 Degree of change in the CpCo-dithiolene absorbance at 664 nm in **[6]** and 515 nm in $[\mathbf{6}]^-$. Values are taken from studies carried out in DMF.

Metal Ion	No. of Added Eq.	E^0M^{n+} /V	% Rise in A_{664} in **[6]**	% Drop in A_{515} in $[\mathbf{6}]^-$
Ag^I	1	+0.50	65	100
Co^{II}	0.5	-0.18	40	75
Cu^{II}	0.5	+0.14	45	80
Ni^{II}	0.5	ND	100	100
Pb^{II}	4	ND	0	9
Hg^{II}	4	ND	0	8
Cd^{II}	4	ND	0	9
Fe^{II}	0.5	-0.10	90	100

Note **ND** indicates Not Detected in the electrochemical window; E^0M^{n+} Reduction potentials of the metal ions measured DMF

For the complexation of these metal ions to the reduced macrocycle $[\mathbf{6}]^-$, complete re-oxidation is observed in the case of Ag^I, Ni^{II} and Fe^{II} only, where the quantity of metal ions added to the system is as given in Column 2 of Table 4.1. In the case of Co^{II}, Cu^{II}, Pb^{II}, Hg^{II} and Cd^{II}, complete re-oxidation of $[\mathbf{6}]^-$, as shown by the results presented in Columns 3 and 4, is not achieved either at 0.5 equivalents of added metal ions or any quantity up to the number of equivalents shown in Table 4.1. It is thought that, as the reduced species $[\mathbf{6}]^-$ is re-oxidised and **[6]** re-formed, competitive binding of the metal ions between the two systems takes place. As a result of this, despite the reduction of the absorbance at 515 nm and initial increase in the absorbance at 664 nm due to the re-oxidation of $[\mathbf{6}]^-$ to **[6]**, there is a parallel process occurring involving complexation of any free metal ions in the solution to **[6]**. Where this occurs, a parallel drop in the absorbance at 664 nm, similar to that

reported previously in this chapter is observed. For this reason, complete re-generation of the absorbance at 664 nm due to the macrocycle [**6**] by these metal ions, is never observed.

In terms of the actual re-oxidation process, it would be expected that metal ions with redox potentials more positive than the Co^{III}/Co^{II} redox potential i.e. –0.34 V, would be capable of the re-oxidation of the Co^{II} centre back to the Co^{III} state. Considering the results in Table 4.1 there are two distinct groups; the transition metal ions and the heavy metal ions Pb^{II}, Cd^{II} and Hg^{II}. This is as expected, as all of the transition metals studied have reported redox potentials more positive than –0.34 V. The late transition metal ions are seen to undergo redox reactions at potentials lower than the Co^{III}/Co^{II} redox potential at –0.34 V.

Considering firstly the case of the transition metal ions, the extent to which re-oxidation of the Co^{II} site takes place varies with each metal as seen in Table 4.1. This is not completely understood, however it is thought to be due to the binding capacity of the macrocycle [**6**] to the guest metal ions with the cavity of [**6**]. Successful binding may allow for electron transfer to occur, making re-oxidation of the Co^{II} centre possible. An example of this re-oxidation by the first row transition metal ions is given in Figure 4.36 where the chosen metal is Ni^{II}. As can be seen by this example, the Ni^{II} is the sole oxidising species for the re-oxidation of Co^{II}-Co^{III}. In the case of the other transition metal ions, similar quantities of the metal ion under investigation do indeed cause re-oxidation of the Co^{II} centre, but to varying extents depending on the metal ion. These quantities are detailed in Table 4.1.

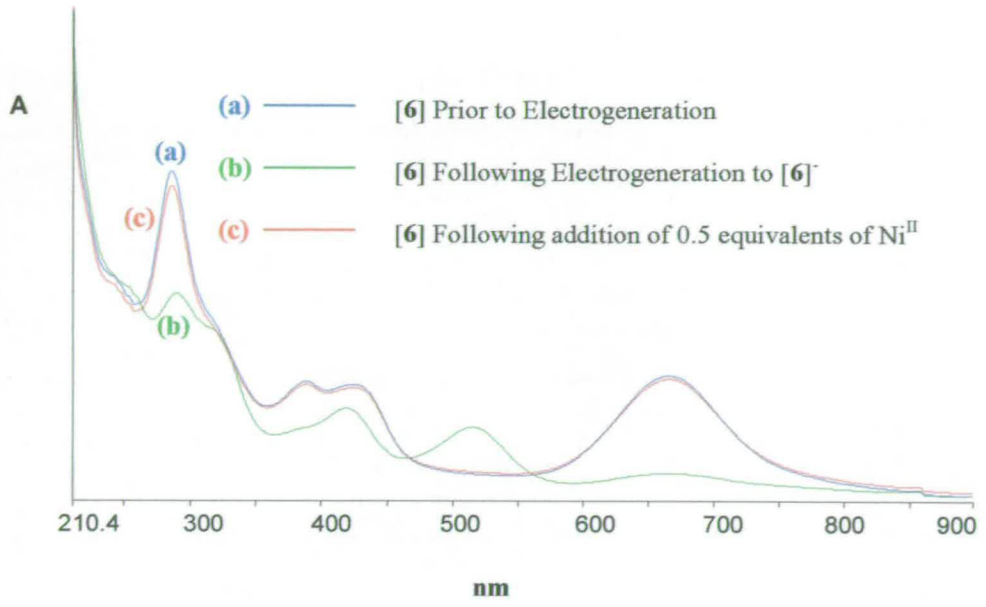

Figure 4. 29 An example of the re-oxidation of the Co^{II} centre of $[\mathbf{6}]^-$ to Co^{III} by 0.5 equivalents of Ni^{II}. Similar effects are seen for the other 1st row transition metal ions.

One of the most interesting aspects of these studies involves the lack of any re-oxidation of the Co^{II} centre by the main group ions. The fact that little or no re-oxidation occurs through interaction of these ions with the macrocycle [**6**], means that a comparison can be made between studies involving [**6**] and $[\mathbf{6}]^-$ with identical quantities of metal ions. The differences in binding of the metal ions to the macrocyclic cavities of [**6**] and $[\mathbf{6}]^-$ can therefore be investigated. These results will be discussed in detail below.

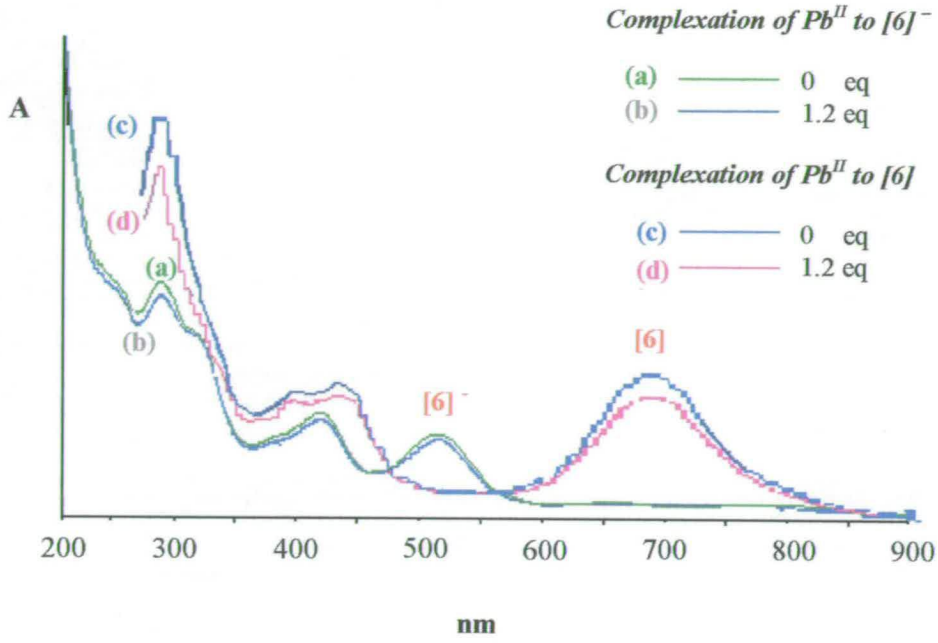

Figure 4.30 Comparison of the interaction of 1.2 equivalents of Pb^{II} with the macrocycle **[6]** and $[\mathbf{6}]^-$Results are identical to those observed for Cd^{II} and Hg^{II}.

When we compare the interaction of Cd^{II}, Hg^{II} and Pb^{II} with the reduced macrocycle $[\mathbf{6}]^-$ we find evidence of an interaction of each of the metal ions with the cavity. This is observed through a decrease in the absorbance intensity of the $\pi^* \leftarrow \pi$ transition at 515 nm, but the change in extinction coefficient occurs to a lesser extent than that observed for changes in the band at 664 nm when a similar quantity of metal is added to the macrocyclic system **[6]**. As all metal ions showed similar changes only one example is given for Pb^{II}.

4.4 Discussion

4.4.1 Geometric Considerations

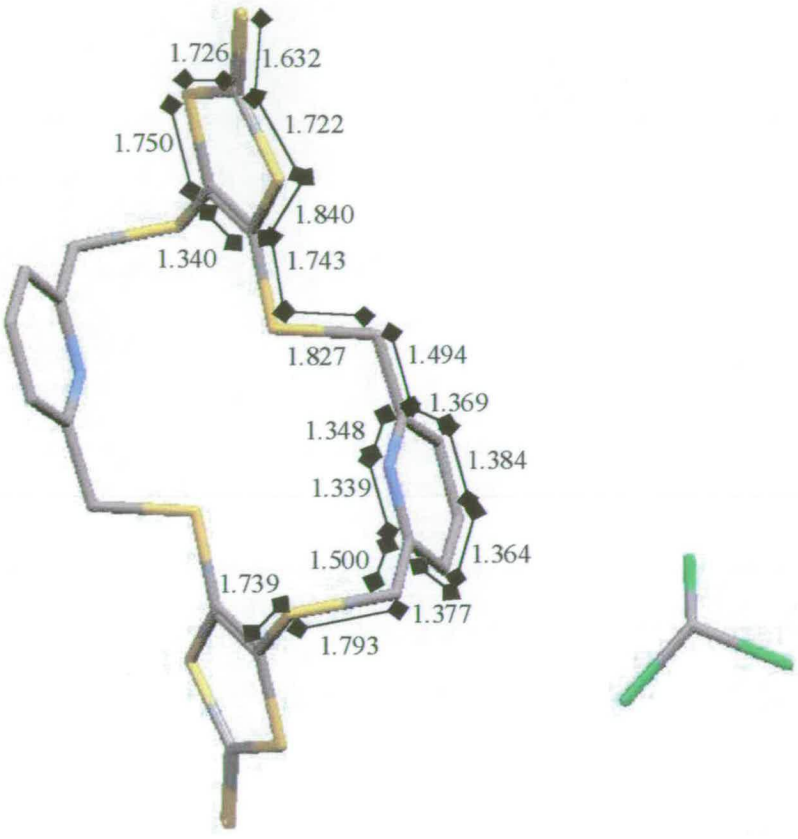

Figure 4.31 Crystal structure of the S_4N_2 donor macrocycle **[4]**, Chapter 1. Indications of bond lengths are given for the macrocyclic backbone.

Macrocycle design for selective guest complexation takes into account a number of geometric considerations. In terms of metal coordination chemistry, optimal binding takes into consideration the ability of the donor atoms to assemble in a favourable geometrical arrangement about the metal. Optimal metal-ligand interactions should

also be achieved without the introduction of unfavourable steric interactions within the ligand framework.

Generally, in simple macrocyclic systems involving identical donor atoms such as the tetraaza-macrocycles, the most easily determined parameter is the radius of the cavity. The radius of the cavity can then be matched up directly with known metal ionic radii in selecting appropriate combinations of metal ions and ligands. For systems where mixed donor atoms are involved, the determination of cavity size is more complicated. Also for **[6]**, significant deviations from planarity must also be considered along with the presence of unsaturated bonds.

In the case of the macrocyclic system **[6]**, no crystal structure could be obtained, probably due to instability of **[6]** in solution over long periods of time. For this reason, geometric considerations are taken from the precursor S_4N_2 donor macrocycle **[4]** to deduce the binding capacity of the various metal ions to the macrocyclic cavity. Figure 4.31 shows the bond lengths of the macrocyclic backbone. In Figure 4.32 the inter-cavity distances are indicated while the angles indicating displacement of the donor atoms from the plane of the macrocycle are also shown.

Angle of Displacement from plane of macrocyclic cavity

A	74.8 °	(C-S_2-CH_2; CH_2-S_4-C)
B	83.0 °	(C-N_1-C; C-N_2-C)
C	55.4 °	(CH_2-S_3-C; C-S_1-CH_2)

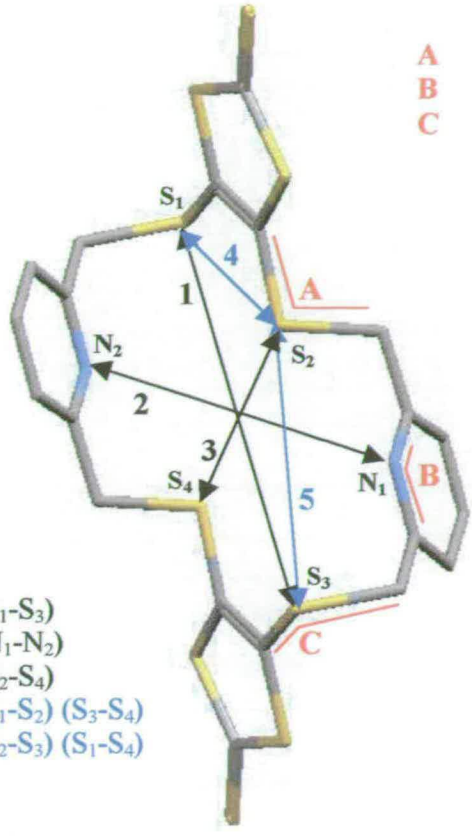

Inter Cavity Distances

1	8.515 Å (S_1-S_3)
2	5.860 Å (N_1-N_2)
3	3.410 Å (S_2-S_4)
4	3.317 Å (S_1-S_2) (S_3-S_4)
5	5.574 Å (S_2-S_3) (S_1-S_4)

Figure 4. 32 Crystal structure of the free S_4N_2 donor macrocycle [**4**]. Indications of intercavity distances and displacement angles from the plane of the macrocycle for key donor atoms are given

The macrocycle in question [**4**] has inter-cavity distances of 5.86 Å from N_1–N_2 and a distance of 3.41 Å from S_2–S_4 and 8.52 Å for the second S_1–S_3. With the centre of inversion, the angles of displacement from the plane of the macrocyclic ring, defined as the least squares plane of best fit through CH_2-S4-C and C=C-S4 are seen to be 74.8 ° for the donor atoms S_2 and S_4, 83.0 ° for N_1 and N_2 and 65.4 ° for S_1 and S_3.

Taking into account these measurements, the macrocyclic backbone does possess a certain degree of flexibility. This flexibility is vital if the macrocyclic cavity is to be able to arrange itself into an optimum environment to coordinate to metal ions of

various sizes. Two such situations are possible. In the first case, the guest metal ion is too large for the cavity. In such cases, we would expect to find the metal ion sitting above or below the donor set. An extension of this coordination mechanism leads to a second structural motif, in which two of the macrocyclic ligands sandwich the metal ions. This has previously been referred to in Section 4.0 involving the discussion of thioether macrocycles [5, 6, 7, 14, 15, 16, 17, 18]. In the second case the metal ion may be too small for the bonding cavity of the macrocycle. In such cases, only some of the donor atoms may be bonded to the metal ion or, in more extreme cases if disparity between the hole-size and the size of the cation, two or more metal ions may be incorporated. Also possible for this situation is the exodentate binding of the metal ion to some of the donor atoms facing out of the cavity of the macrocycle.

The binding efficiency of the macrocycle, as already mentioned, takes into account the flexibility of the macrocyclic backbone. This flexibility can be judged by considering the angle of displacement of the donor atoms from the plane of the macrocycle. This angle of displacement through the plane of the macrocycle can vary from a large value (as reported in Figure 4.32), at which the cavity distances of S_1-S_3, S_2-S_4 and N_1-N_2 move from a maximum to an angle of zero where donor atom distances are at a minimum. (The distances S_1-S_2, S_3-S_4, S_1-S_4 ad S_2-S_3 would not be expected to change considerably due to the rigid nature of this area of the macrocycle). This flexibility can present a series of optimum cavity distances to which the various metal ions (of varying ionic radii, r_i) may bind effectively. Considering the reasonable flexibility of the overall macrocyclic backbone, the cavity of the macrocycle may conceivably rearrange therefore to incorporate the metal ion.

Coupled with the dimensions of the binding cavity and the flexibility of the backbone, account should be taken of the metal ion characteristics, including the ionic radii, r_i. Considering r_i of the metal ions and based on the measurements taken from the crystal structure of **[4]** detailed above, conclusions can then be drawn on the metal ion which would be most likely to coordinate easily to the cavity. The metal ion ionic radii and other metal ion characteristics are detailed in Table 4.2 .

When we consider r_i we find two distinct groups of ions. Those with $r_i > 0.90$ Å and those with $r_i < 0.90$ Å. Based on the inter-cavity distances, we would propose that the metal ions with $r_i > 0.90$ Å would bind most efficiently to the cavity. This is not to say that those metals with r_i, <0.90 Å would not bind, rather that the stability of the resultant complex would be greatly diminished. Indeed from the results to date, we see significant interaction of the transition metal ions with the macrocycle **[6]**. Further analysis of the binding efficiency of **[6]** to the metal ions studied is given later in the discussion. However, as well as ionic radii and cavity size, consideration is also made of the optimum bond lengths for each of the metal ions and a question raised as to whether the macrocycle can re-arrange to create an optimum coordination environment for which to stabilise the metal.

A series of CSD searches was carried out in order to determine the optimum bond lengths for M-N and M-S bonds for each of the metal ions studied, where the metal ions were defined as having 4-sulfur and 2-nitrogen donor atoms in their coordination sphere. The results are described in Table 4.2 where the optimum bond length ranges are reported along with the number of complexes from which these ranges are determined. These reports were examined and the most prevalent M-N and M-S bond lengths determined for macrocyclic complexes of each of the metal ions. Table 4.2 details these optimum bond length ranges for each of the metal ions.

Table 4.2 Results of the CSD search on six-donor macrocyclic complexes of Ag^{I}, Fe^{II}, Ni^{II}, Co^{II}, Cu^{II}, Cd^{II}, Pb^{II} and Hg^{II} where the macrocycle has been defined as having 4 sulfurs and 2 nitrogen donor atoms.

M^{n+}	M^{n+} / r_i / Å	M-N / Å	M-S / Å	No. of complexes
Ag^{I}	1.26	2.40-2.60	2.87-2.95	139
Fe^{II}	0.74	1.96-2.02	2.19-2.54	36
Ni^{II}	0.69	1.95-2.15	2.32-2.56	121
Co^{II}	0.72	1.84-2.00	2.45-2.65	25
Cu^{II}	0.72	1.80-2.05	2.28-2.90	29
Hg^{II}	1.10	2.35-2.60	2.70-3.15	13
Cd^{II}	0.95	2.41-2.57	2.65-2.80	16
Pb^{II}	1.20	2.51-2.68	2.73-2.89	31

Note r_i indicates the Ionic Radius

CSD reports show that these optimum bond lengths for Ag-N and Ag-S bonds are of the order of 2.50 Å (Ag-N bond) and 2.95 Å (Ag-S bond). From the results of the complexation studies carried out here in the case of **[6]**, we see results, which suggest the selective binding of Ag^{I}.

Moving on to consider the results of the late transition metal and main group metal ions, CSD searches once again showed the likelihood of forming a six-donor (4-sulfur and 2 nitrogen) complex of **[6]** to the respective metal ion. Bond lengths of a similar magnitude to those observed for Ag^{I} were reported, Table 4.2. Ag^{I} seems to bind in such a way as to directly perturb the orbitals of the chromophore. From the literature it has been observed that compounds, which bind Ag^{I} easily, also appear to show a particular affinity for Pb^{II}. In this case, the late transition metal ions appear to interact with the macrocycle through a different mechanism where a uniform drop in

the extinction coefficients of the UV-Vis bands is observed. A proposal for mechanisms by which the late transition metal ions interact with **[6]** is discussed in Section 4.4.3.2.

Comparison is also made of the bond-lengths of sulfur and nitrogen bonds to Ag^{I} and the late transition metal ions. We find that the overall distance from sulfur to diagonally opposite sulfur would be only slightly greater for Ag^{I} than for any of the heavier metal ions. In fact the same distance for the heavier metal ions would be only 0.3 and 0.4 Å shorter. This tends to indicate that with extra stabilisation by co-ordinating solvent molecules, complexes of the late transition metal ions may exist.

For the remainder of the transition metal ions, CSD searches for Fe^{II} revealed that the optimum Fe-N and Fe-S bond lengths for these types of systems were in the range of 1.96-2.02 Å and 2.19-2.54 Å respectively. CSD searches on Ni^{II} gave a range of optimum lengths from 1.95–2.15 Å for a typical Ni-N bond and 2.32–2.56 Å for a Ni-S bond. These results for nickel however, are representative of a number of systems, which have the capacity to be far more flexible in terms of their coordinating ability to the guest metal ion. In our case the backbone of the ligand is comparatively rigid which may cause the observed lack of coordination of these ions to the cavity observed in THF. In each of these metals, the reported bond-lengths are substantially smaller than those reported for either Ag^{I} or the late transition metal ions. As the flexibility of the backbone is limited, it is proposed that the binding of the metal ion to the cavity is hindered, unless stabilized by a solvation sphere.

Similarly, when we consider the electrochemical and UV-Vis spectroscopic results for the transition metal ion studies carried out in DMF, we see quite complicated spectra and cyclic voltammograms for these metals indicating a wide variety of coordination environments being adopted in a bid to stabilise the metal ion. In contrast to the results observed for Ag^{I} binding, results for Fe^{II} and Ni^{II} are clearer. This is due to the fact that Ni^{II} (Section 4.2.3.2) does not bind to the cavity of **[6]**. As a result, complexation studies carried out in THF involving Ni^{II}, show only cobalt

mediated reduction peaks. In contrast, Fe^{II}, as discussed previously in Section 4.2.3.3, shows peaks for both cobalt and macrocycle mediated processes. Electrochemical features of the complexation studies are discussed in more detail below, Section 4.4.3.1.

In the CSD searches carried out for Co^{II} the bond lengths observed were 1.84–2.00 Å for Co-N and 2.45-2.65 for a Co-S. In the case of Cu^{II}, the ranges were 1.80-2.05 and 2.28-2.90 Å. Generally, the smaller ionic radii values means, that the macrocyclic backbone will once again have to pucker considerably more in order to accommodate the ion efficiently. The UV-Vis results indicate little or no interaction with the macrocycle in THF. In DMF however, we observe a greater stability of the resultant complexes formed. This may be due to the ability of the solvent molecules to add extra stability to the complex by coordination. This is also a potential explanation for the clear interaction of Ni^{II} with **[6]** in DMF where no direct interaction with the cavity of **[6]** occurs in THF.

The most promising results throughout this work have been for the complexation of Ag^{I}. In the development of any sensory device, one of the most vital properties is the selectivity. In this work, we have shown that the macrocyclic ligand **[6]** shows a high degree of selectivity towards Ag^{I}, presumably due to the macrocyclic characteristics described here. Other considerations involving hard-soft donor systems are discussed below (Section 4.4.2).

It can be seen from this discussion that the binding of a metal ion to a cavity depends on

(a) the size of the macrocyclic cavity
(b) its ability to rearrange in order to incorporate a variety of metal ions
(c) the size of the guest metal ion

4.4.2 Hard-Soft Donor Systems

As discussed previously, coordination of thioethers typically stabilises the lower oxidation states of metal ions and when relevant, the lower spin-state as well [32]. These properties derive from two key characteristics of thioether ligands. The first of these properties involves the π-acidity of thioether ligands and the second, their inability to stabilise positive charge effectively.

It has already been discussed that donor type i.e. Hard or Soft, is pre-requisite in the determination of the complexation behaviour of the ligand towards metal ions [33]. From literature, it has been found that hard donor systems (i.e. predominantly oxygen containing) most favourably combine with hard ions e.g. alkali/alkaline earth or lanthanide ions according to the hard and soft acid-base principle [33] where the stability constants K_s of these complexes are very high. From this hard and soft acid-base principle, it has been found that soft cations interact more favourably with 'soft' donor atoms like sulfur and aromatic nitrogens.

Considering the donor atoms incorporated into **[6]**, and the results described here, the first row, divalent transition metal ions are characteristically border-line and as such would be expected to coordinate poorly to the cavity of the macrocycle **[6]**. In contrast, Ag^{I}, Cd^{II}, Sn^{II}, Hg^{II} and Pb^{II} are all part of the second and third row transition metal series or the post transition metal series and are, by comparison to their first row counterparts, much softer in nature. As a result of this difference in the hard-soft nature of the atoms, we can once again make a clear distinction between the two groups of metal ions i.e. those of the 1st row series and those of the 2nd and 3rd row and post transition metal series. The macrocycle **[6]** was designed with a particular attention being paid to the preparation of a soft donor macrocycle. In the complexation studies carried out here, we have seen a system capable of the selective binding of the softer metal ions studied.

UV-Vis studies of the interaction of the metal ions of the first row transition metal series with the macrocycle **[6]** in THF show little interaction with the macrocycle **[6]** compared with that observed with metal ions such as Ag^{I}. When we consider the same complexation studies carried out in DMF we find a far great interaction occurring between the macrocycle and the metal ions. As discussed throughout the chapter, the stabilising effect of coordinating solvent molecules may also add sufficient 'hard'-donor character to the 1st row transition metal ions to stabilise complexes of the type $[\mathbf{6}]M^{n+}$.

When the binding capacity of the soft donor macrocycle is coupled with the geometric characteristics of both the macrocycle and the metal ion the optimum conditions for the binding appear to favour the successful interaction of the late transition metal ions and heavy metal ions.

4.4.3 Binding Energetics

4.4.3.1 Redox Active Macrocycles and Mediated Redox Reactions

From the outset, the main aim of this project was to develop a new redox active, soft donor macrocycle, which is capable of showing a degree of selectivity towards metal ions. While straightforward complexation of the metal ions to the macrocyclic cavity had been anticipated, some of the results of the complexation studies observed were quite different.

Starting with the electrochemical results, no shift in the Co^{III}/Co^{II} redox couple was observed – a potential key indicator of complexation to the cavity of **[6]**. Instead, and in almost all cases, a new reduction peak was observed to increase in peak height at approximately –1.0 V with increasing quantities of metal ions added. The value of this reduction potential varied depending on the metal under investigation and the results can be seen in Table 4.3. The observation of this new reduction, led to the conclusion that the reduction and oxidation of the metal ion was mediated by the macrocycle. Indeed further studies, in particular in the case of the Ag^{I} complexations carried out, gave evidence for a surface adsorbed layer of the macrocyclic ligand **[6]**, which appears to mediate the reduction and oxidation processes of metal ions which would normally occur at the bare electrode surface. The observed new redox peaks positions support the proposal of a macrocyclic-mediated mechanism for the reduction and oxidation of the guest metal ion under investigation. In some cases (e.g Ni^{II}), the reduction potential of the metal appeared to favour a cobalt centre-mediated reduction process seen by an increase in the reduction peak height of the Co^{III}/Co^{II} redox couple.

In the case of the macrocycle-mediated redox processes, the increase in the peak height observed at ~ -1.0 V continues past 1 equivalent. The ratio of the heights of

this reduction peak to the Co^{III}/Co^{II} reduction peak is indicative of the number of electrons involved in the mediated process. For example, from a comparison of the relevant intensities in the case of Cd^{II} complexation to [**6**], the peak height of the second reduction occurring at –0.8 V following 0.6 equivalent addition and that of the Co^{III}/Co^{II} reduction peak are seen to be in a ratio of 2:1. This is consistent with the macrocycle-mediated process arising as a result of the $2e^-$ reduction of Cd^{II} to Cd^0.

When we consider the electrode potentials of the reduction of the free metal ions, we find a widely varying range of potentials. These potentials, when compared with the new reduction potentials of the metal ions through the mediated processes discussed previously, indicate the difficulty that the ion has in gaining access to the electrode surface in order to undergo electrochemistry at the electrode surface. One example of this involves the reduction of free Ag^I normally found at +0.50 V. Once bound to the macrocycle [**6**], the reduction of the ion shifts to –1.29 V where it undergoes macrocycle-mediated reduction. No evidence for reduction at +0.50 V is observed even in cases where an excess of Ag^I is present in solution. Instead, the layer of surface bound macrocycle is thought to block the electrode surface to the free metal ions. This means that the macrocycle has to undergo reduction before the metal ion can easily undergo reduction through the macrocycle-mediated process. The reduction potentials of the new reduction processes are found at significantly lower potentials than that associated with the free metal ion.

This shift in potential from the free ion potentials to those of the macrocycle-mediated potentials at ~ -1.0 V, indicates the stabilising effects on the metal ions, of the macrocyclic complexation. This has been seen before for polyamine or imine macrocycles where the coordination of 4 non-tethered nitrogen donor units has a far smaller stabilizing effect on the metal ion than that of the closed tetraazamacrocyclic unit and the potentials of the latter are far lower than those of the former [34].

Table 4. 3 Comparison of reduction potentials and macrocycle-mediated reduction potentials for the respective metal ions

M^{n+}	$E^{\theta}_{M^{n+}}$ / V	$\Delta E^{\theta}_{Co^{III/II}}$ / V	$E^{\theta}_{[6]/M^{n+}}$ / V	K
Ag^{I}	0.53	-0.16	-1.29	1.86×10^{30}
Fe^{II}	-0.08	-0.21	-0.80	5.25×10^{26}
Ni^{II}	ND	0	-1.1	-
Co^{II}	-	-	-	-
$*Cu^{II}$	-0.10	+0.06	-1.18	$4.54 \times 10^{45*}$
Hg^{II}	ND	0	-0.85	-
Cd^{II}	ND	0	-0.80	-
Pb^{II}	ND	0	-0.87	-
Pb^{II}	ND	-	-1.1	-

Note Values quoted are those measured during the complexation studies carried out in DMF. * In the case of Cu^{II}, $E^{\theta}_{M^{n+}}$ was difficult to measure accurately, hence K for this metal is not reliable.

$E^{\theta}(M^{n+})$ is the standard reduction potential of the M^{II} species; $\Delta E^{\theta}_{(Co^{III/II})}$ is the shift in potential of the Co^{III}/Co^{II} couple as a result of the metal ions added. $E^{\theta}_{[6]/M^{n+}}$ is the reduction potential observed for the macrocycle mediated reduction of the metal ion at the electrode surface. **ND** indicates that no redox chemistry was observed for the metal ions species in the given electrochemical window under the conditions studied. K is the association Constant for the metal interaction with the macrocycle

Further indications of the lack of any direct interaction of the metal ions with the electrode surface, except through the mediated processes already described, comes from the distinct lack of any stripping peaks observed in the course of the electrochemical studies. This is the case up to and past 1 equivalent addition and can

only be due to the inhibiting effect of the macrocycle adsorbed onto the surface of the electrode.

In a comparison of E^{θ}_{Mn+} and $E^{\theta}_{[6]/Mn+}$ a theoretical approach to the determination of the associated constant K of the metal with the macrocycle [**6**] may be developed. Using the specific example of Ag^{I}, there is a significant difference between the reduction of the free metal at +0.50 V and the reduction of the bound metal ion at – 1.29 V. This is also the case generally, and in general since

$$\Delta G_1^{\theta} = -nFE^{\theta}(M^{n+})$$

is the free energy change for the reaction

$$ne^{-} + M^{n+} \Leftrightarrow M \qquad \mathbf{A}$$

and

$$\Delta G_2^{\theta} = -nFE^{\theta}_{[6]/M^{n+}}$$

is the free energy change for the reaction

$$ne + [6]M^{n+} \Leftrightarrow M + [6] \qquad \mathbf{B}$$

so for the process

$$[6] + M^{n+} \overset{K}{\longleftrightarrow} [6]M^{n+}$$

the Free Energy Change, ΔG^{θ} is

$$\Delta G^{\theta} = \Delta G_1^{\theta} - \Delta G_2^{\theta}$$

where K is the association constant for **[6]** and M^{n+}

$$\Delta G^{\theta} = nF(E^{\theta}_{[6]/M^{n+}} - E^{\theta}_{M^{n+}})$$

and since

$$\Delta G^{\theta} = -RT \ln K \quad \text{where K = Association Constant}$$

then

$$\ln K = \frac{nF}{RT}(E^{\theta}_{M^{n+}} - E^{\theta}_{[6]/M^{n+}}) \qquad \textbf{Equation 4.1}$$

So applying this equation to the determination of the association constant K, for Ag^{I} complexation to **[6]**, K_{AgI} is calculated as being 1.86 x 10^{30}. Similarly through measurement of $E^{\theta}_{[6]/Mn+}$ and E^{θ}_{Mn+} for each of the other metals, the association constants for the complexation of these metals to **[6]**, may be determined and in the case of Fe^{II} and Cu^{II} these results are presented in Table 4.3.

The UV-Vis results suggest that DMF is able to more efficiently stabilise any complexes formed between some metal ions and **[6]**. However, in the electrochemical studies interactions observed between the metal ion and **[6]** in THF, were clean with a gradual increase in peak height as a result of the addition of metal ions to the reaction mixture e.g. Ag^{I}. In the case of complexation studies carried out in DMF, the results were comparatively varied, with the reduction potential of the bound metal ion shifting in redox potential by as much as ±0.4 V.

One explanation for this difference involves the integrity of the surface adsorbed macrocycle layer. It is thought that the greater solvating power of the DMF molecules may compromise this layer allowing pockets of bare electrode to be seen

by the metal ions in solution. As a result of this, the metal ions can be observed in several forms involving free metal ions, the macrocycle or a mixture of macrocycle and solvent molecules. Clear examples of this are seen in the case of Ag^{I}, Fe^{II} (Figure 4.22) and Cu^{II} (Figure 4.25) where the reduction potentials vary within a range of approximately ±0 0.4 V

Electrochemical results involving the reduced macrocyclic species $[\mathbf{6}]^{-}$ are also interesting. Taking into account the reduction potential at –0.34 V for the Co^{III}/Co^{II} redox processes, we would expect the oxidation process $Co^{II} \rightarrow Co^{III} + 1e^{-}$ to occur at approximately –0.28 V and to be greatly enhanced due to the increased concentration of the Co^{II} species in solution following electrogeneration. Instead, no difference was observed. As we have already discussed (Section 4.2.4), this observation is as a result of the ability of the metal ions with reduction potentials more positive than –0.34 V to re-oxidise the Co^{II} centre to Co^{III} before the electrochemical re-oxidation of the Co^{II} site can take place. This re-oxidation occurs to varying extents depending on the metal ion studied and is discussed in more detail in Section 4.3.

4.4.3.2 Ionic Effects in the UV-Vis Spectra

4.4.3.2a Variations in ε for complexations with [6]⁻

Considering the results observed in the case of the complexation studies of [**6**]- with given metal ions an increase, of variable extents, was observed in the absorbance at 664 nm (due to [**6**]), which there was a drop observed in the absorbance in 515 nm (due to [**6**]⁻). The extent of this change is dependent on the metal under investigation however the magnitude of the drop in these absorbances is dependent on the square of the frequency and is larger at lower frequency.

Thus, at 515 nm (due to [**6**]⁻) there would be expected to be about half as much drop in the absorbance compared to that at 664 nm (due to [**6**]). Also to be considered is that the band at 515 nm for [**6**]⁻ has a much smaller area than that at 664 nm for [**6**]. The overall change in area of each appears therefore, in the case of Pb^{II} (Figure 4.13), to be roughly as expected. Any further reduction in the absorbance due to [**6**]⁻ may arise from screening of the Pb^{II} electric field by the negative charge on the chromophore itself. The results presented here then do not indicate that [**6**]⁻ interacts less favourably with Pb^{II}, but reflect other reasons that the change in extinction coefficient due to the presence of the metal ion, is smaller than that observed for [**6**].

4.4.3.2b Ionic Effects on Chromophore Activity in the UV-Vis Spectra

We have seen variations in the macrocyclic absorbances due to interaction of the metal ions with the macrocycle [**6**].⁻ The most interesting of these interactions involved the late transition metal ions i.e. Hg^{II}, Cd^{II}, Pb^{II} and Sn^{II}. In each of these

cases, we observed a gradual drop in the extinction coefficient at each of the absorbance wavelengths with increasing concentration of the metal ions added.

As already mentioned briefly in Section 4.2.2, this drop in the absorbance intensity of the macrocyclic ligand is due to the way in which the metal ion interacts with the macrocycle. From a survey of the literature, two mechanisms have been considered although neither mechanism has yet been proven.

The first of these mechanisms is based on a feature observed by Abkowitz *et al,* in which the degree of molecular association or aggregation of a copper phthalocyanine dye in benzene and THF was studied [35]. Dimerisation of the Pc was found to occur resulting in a significant drop in the observed extinction coefficient. Coupled with this drop in the extinction coefficient, broadening of the absorbance band was also seen indicating interaction of the transition dipoles through aggregation of the chromophoric units. While the studies carried out in the case of the late transition metal ions did not indicate any 'obvious' broadening effects due to aggregation of the chromophoric units, a decrease in the extinction coefficients for each of the absorbances due to **[6]**, comparable to the decrease in extinction coefficients observed for the copper phthalocyanine, was clearly observed.

A second proposal was made, involving the mode of binding of the metal ion to the macrocycle. It has already been discussed that in some cases where optimum binding conditions are not achieved through complete binding of the metal ion to the cavity, the metal ion will bind/tether itself to the donor atoms in an exodentate manner. The main group ions, are thought to undergo this exodentate binding by tethering themselves to the donor atoms of the macrocycle however in doing so they do not have sufficient orbital overlap with the chromophoric unit to cause a shift in the absorbance. However, it does have sufficient effect, through the generation of a static electric field, on the extinction coefficient of the absorbance transitions, causing them to decrease with increasing concentration of the metal ions in solution.

A 1st order perturbation theory calculation was carried out by Dr. Philip Camp, at the University of Edinburgh, which considered a di-cationic species at a distance of 5 Å from the chromophore. It was calculated that the static electric field effect on the chromophore brought about by such an interaction could result in an extinction coefficient of approximately 40 % of its original value. Clearly, this calculation is only a starting point for future, more exact and detailed calculations, but it does strongly suggest the effect of the presence of the metal ion on the extinction coefficients of [**6**]. This electric field effect is almost identical to that observed in the case of the late transition metal ions studied here where due to the size of the metal ion, it is held at a distance from the donor cavity. In contrast, Ag^{I} is clearly capable of binding more closely to the donor atoms, which sees the ion achieving optimum conditions within the cavity of the macrocycle of [**6**]. In doing so, it is thought that the metal ion has sufficient orbital overlap with the chromophoric unit to cause significant perturbations in position and intensity of the absorption bands.

Due to time limitations, calculations could not be carried out in order to determine whether the explanation resulting from this 1st order perturbation theory calculation is indeed correct, however it is hoped, as mentioned, that calculations will be carried out at a later date in order to clarify the results.

4.4.4 Molecular Mechanics

As has been discussed throughout this section, macrocycle design for selective guest complexation takes into account a number of geometric considerations. Some of these considerations are explainable through the application of molecular mechanics. Several reviews [36, 37, 38] have been published, which describe in detail, the procedures used in the application of molecular mechanics to macrocycle design and related concepts to macrocycle-guest interactions.

One important objective of the molecular mechanics approach is to design macrocycles which are pre-organised and which should therefore accept one guest ion and reject others from a series where the guests have similar characteristics and dimensions. Since the molecular mechanics procedure allows one to vary the numerical values of parameters in a systematic manner, information concerning the importance of and optimum values for these parameters in host-guest interactions can be obtained.

It is, of course, desirable to check the predictions of the molecular mechanics calculations against experimental data. However, in the case of these studies, time limitations meant that no such theoretical studies could be carried out. It is however suggested that such calculations should be undertaken in order to determine the selectivity of the macrocycle **[6]** for Ag^{I} over a series of transition metal ions based on the affinity of the system for the metal ion, based on the experimental results discussed previously in the chapter, Section 4.1.

4.5 Conclusions

There were two physicochemical indicators within the CpCo- S_4N_2 donor macrocycle **[6]** identified, which were thought to be capable of showing metal ion complexation to the system. These were both based on the CpCo- dithiolene moiety of the macrocycle **[6]**, which shows a strong absorption in the visible spectrum at 664 nm attributed to a $\pi^* \leftarrow \pi$ transition within the frontier orbitals containing both metal and ligand character. Firstly, complexation of a transition metal ion to the macrocyclic cavity was expected to alter the position and/or the intensity of this CpCo-dithiolene absorbance. Secondly, due to the extensive electron delocalisation occurring between the redox active unit and the cavity sulfur atoms, complexation was expected to alter the electron density and therefore the redox potential of the Co^{III}/Co^{II} couple at –0.34 V.

The choice of the metals used in the complexation studies described in this chapter, took into account several factors. Firstly, a wide variety of sizes were involved, varying the ions from Fe^{II} and Ni^{II} to Hg^{II}, Pb^{II} and Ag^{I}. These variations allowed for a study of the ability of the cavity to discriminate between ions of varying size. It also allowed examination of the flexibility of the cavity to pucker in order to coordinate ions of different sizes. A variety of borderline and soft metal ions were studied to allow an investigation of the ability of the macrocycle to discriminate between hard and soft guests. Finally, a variety of metals were chosen because of the impact that developing a selective ionic sensor would have on both the scientific and industrial community. Fe^{II} and Cu^{II} centres are found throughout current biological and biotechnological research. Ag^{I} is used extensively in photographic applications.

In summarising the results of the UV-Vis results for each of the metal studied, Table 4.4, some conclusions are drawn. It is concluded that

(a) Selective binding of **[6]** to the metal ion Ag^{I}, is observed where the interaction involves an orbital interaction of the metal ion with the chromophoric unit.

(b) DMF always promotes a more efficient interaction of the metal ion with the macrocycle **[6]**.

Table 4. 4 Comparison of final results for the UV-Vis experiments carried out

Metal Studied	DMF	THF
Ag^{I}	O	E
Cd^{II}	E	ND
Hg^{II}	E	ND
Sn^{II}	E	ND
Pb^{II}	E	ND
Fe^{II}	E	ND
Ni^{II}	E	N
Co^{II}	ND	N
Cu^{II}	E	N

Note : **O** indicates interaction of the metal with the chromophore through direct orbital interaction. **E** indicates an electrostatic interaction with the metal ion tethered to the chromophore but where no orbital interaction occurs, **N** indicates no significant interaction of the metal with the chromophore. **ND** indicates that this study was not under-taken.

In the case of all the other metals studied, interaction is believed to occur through the tethering of the metal ion to the chromophore but without any orbital interaction. Such tethering to the chromophoric unit is thought to be exodentate based on the geometric considerations previously discussed, Section 4.4.3.2b.

Following the complexation studies of Ag^{I} to the macrocycle [**6**], the appearance of a new band at 515 nm is observed. This band has, as previously discussed, been attributed to the complexation of the metal ion with the macrocyclic cavity. Bearing in mind this new band at 515 nm and the selectivity of the macrocycle towards Ag^{I}, it is conceivable that a new selective sensory device may be developed for the detection of Ag^{I}. This may be brought about through simple monitoring the new absorbance at 515 nm and would be effective even in comparison with other late transition metal ions such as Pb^{II}.

The selective extraction of transition metal ions in particular the more environmentally harmful metals Hg^{II}, Sn^{II}, Pb^{II} and Cd^{II}, is a topic of enormous commercial interest. From the results presented here, the redox macrocycle [**6**] has been seen to be selective towards Ag^{I} while having a particular affinity for the detection of the main group ions also. This is seen as a clean gradual increase in the reduction potential of the bound metal ion at $\sim$ -1.0 V coupled with very strong variations in the UV-Vis spectra for the relevant study in particular Ag^{I}.

Following an analysis of the geometric features of the macrocycle backbone and cavity through a series of CSD searches and crystal structure analysis, the likelihood of the metals binding to a system such as that described in [**6**], was examined. The geometric considerations are given in Table 4.2 and Figure 4.31 and 4.32. We have found that the largest of the ions in terms of ionic radii, Ag^{I}, appears to give best coordination results for the ligand system [**6**]. This can be attributed to the optimised geometry and co-ordinating ability of the cavity donor atoms of the macrocycle. It has also been noticed that, due to the rigidity of the macrocyclic backbone, puckering of the ring to accommodate the smaller metal ions is not wholly possible. Instead, by using a more coordinating solvent such as DMF, it is possible that the partially complete coordination spheres become filled and the metal complexes become stabilized.

Considering the results of the complexation studies for all the metals studied, UV-Vis spectra were found to show a significant decrease in the UV-Vis absorbances. No shift in the wavelength was observed for Pb^{II}, Hg^{II}, Cd^{II} and other metal ions in DMF, however a significant effect on the extinction coefficient of the chromophoric unit was found to occur. Calculations are currently being carried out to conclude the actual mode of interaction of these metal ions with [**6**]. The mechanism is thought to involve either the aggregation of the macrocycle ligands around the metal ions, or to involve a static electric field, which in turn affects the chromophore ultimately reducing the extinction coefficient of the macrocyclic ligand absorbances.

Ag^{I}, in contrast, showed a dramatic shift in the wavelength of the CpCo-dithiolene absorbance. This is thought to be due to the selectivity that is known of thioethers for Ag^{I} and hence the selective binding of the metal ion to the cavity of the macrocycle. Due to time limitations the development of this system and its selectivity for Ag^{I} could not be extended further.

With the added insolubility of [**6**] in H_2O the application of this system is clear. Clearly the macrocycle adsorbs very well to the electrode surface and shows excellent selectivity toward binding of Ag^{I}. In dispersing the macrocycle on a Indium Tin Oxide electrode we would be able to use the electrochemical and spectroscopic handles of the macrocycle to probe for metal ions within a variety of media and ultimately in the solid state eliminating any involvement of solution work (unless required).

Throughout this work, the aim has been to develop a system, which is capable of showing a direct physical response, in this case spectroscopic or electrochemical, upon interaction with a guest transition metal ion. The studies carried out in this work have lead to the proposal of some interesting mechanisms involving mediated redox processes and static electric field effects on the chromophoric unit. Only very basic, preliminary calculations have been mentioned in this discussion. A series of

molecular mechanical calculations are due to be carried out to complete the complexation work in the near future.

In conclusion therefore, we have proven the success of the designs described in Chapter 3, in the development of a new soft-donor redox-active macrocycle capable of binding soft metal ions. Through a wide variety of binding studies, the capability of this new redox active macrocycle [**6**], in binding guest transition metal ions has been established and the selectivity of the ligand toward Ag^{I} observed.

4.6 Experimental

UV-Vis spectroscopic and electrochemical methods were carried out in the manner described in Chapter 2, (Section 2.2.2).

Complexation studies of [6]

0.2 mM solutions of the macrocycle [**6**] in THF and DMF were prepared. In each case the solutions contained 0.5 M $TBABF_4$, which acts as a background electrolyte for the electrochemical studies. The solvent employed was distilled and dried before use and was continually de-gassed throughout the experiments carried out in order to eliminate any presence of O_2. Once the macrocyclic solution was prepared, the experiments were commenced. Addition was made of even portions (0.1 eq, 0.2 ml) of the transition metal salt dissolved in the given degassed solvent (also containing 0.5 M $TBABF_4$). The electrochemical cell used was as described in Section 2.2.2. Following each addition of the metal ion salt, equilibration was allowed for 30 minutes. Following each UV-Vis study, the quantity of sample used for the study was reintroduced to the bulk solution whereupon electrochemical measurements were performed.

Complexation studies of [6]$^-$

The complexation studies of the reduced macrocycle [**6**]$^-$ were carried out in an identical manner to those described above for [**6**]. In this case however all complexation studies were carried out in THF and under an inert atmosphere. Electrolyte concentrations were maintained at 0.5 M $TBABF_4$. 20 ml of 2 mM [**6**]$^-$ was generated *in-situ*, by electrogeneration of 20 ml of [**6**] at –0.4 V. Following electrogeneration, 0.1 equivalent portions of the metal ions were then added to the macrocycle to the limiting value described in Table 4.1. Following each addition,

equilibration was allowed for 30 minutes before the cyclic voltammogram and UV-Vis spectra were obtained. Dry N_2, distilled solvents and inert atmospheres in the UV-Vis spectrometer were all used in order to eliminate any presence of O_2.

4.7 References

[1] S. Searles Jr., M. Tamres, *The Chemistry of the Ether Linkage*, Eds., S. Patai, John Wiley and Sons, London, 1967, 243

[2] T. –L. Ho, *Hard and Soft Acids and Bases, Principle Organic Chemistry*, Academic Press, New York-San Francisco-London, 1977

[3] J. J.Christensen, D. J. Eatough, R. M. Izatt, *Chem. Rev.*, 1974, **74**, 351

[4] H. K. Fresndorft, *J. Am. Chem. Soc*, 1971, **93**, 600

[5] R. E. DeSimone, M. D. Glick, *J. Am. Chem. Soc.*, 1976, **98**, 762

[6] N. K. Dalley, J. S. Smith, S. B. Larson, K. L. Matheson, J. S. Christensen, R. Izatt, *J. Chem. Soc., Chem. Commun.*, 1975, 84

[7] N. K. Dalley, S. B. Larson, J. S. Smith, K. L. Matheson, R. M. Izatt, J. J. Christensen, *J. Heterocycl. Chem.*, 1981, **18**, 463

[8] (a) R. E. DeSimone, M. D. Glick, *J. Am Chem. Soc*, 1975, **97**, 942; (b) R. E. DeSimone, T. M. Tighe, *J. Inorg. Nucl. Chem.*, 1976, **38**, 1623, (c) R. M. DeSimone, M. D. Glick, *J. Coord. Chem.*, 1976, **5**, 18

[9] (a) N. K. Dalley, in *Synthetic Multidentate Macrocyclic Compounds*, R. M. Izatt, J. J. Christensen, Eds., Academic, New York 1978, 207; (b) I. Goldberg In *Chemistry of Ethers, Crown Ethers, Hydroxyl Groups and their Sulphur Analogues*, S. Patai, Eds., Wiley: New York, 1980; Part 1, Suppl. E., 175

[10] J. R. Hartman, B. M. Foxman, S. R. Cooper, *J. Am. Chem. Soc.*, 1987, **109**, 4238

[11] J. R. Hartman, R. E. Wolf Jr., B. M. Foxman, S. R. Cooper, *J. Am. Chem. Soc.*, 1983, **105**, 131

[12] W. Rosen, D. H. Busch, *J. Am. Chem. Soc.*, 1969, **91**, 4694, *Inorg. Chem.*, 1970, **9**, 262

[13] D. B. Rorabacher, M. J. Martin, M. J. Koenighauer, M. Malik, R. R. Schroeder, J. F. Endicott; L. A. Ochrymowyc, in *Copper Coordination*

Chemistry : Biomedical and Inorganic Perspectives; K. D. Karlin, J. Zubieta, Eds.,; Academic Press : Guilderland NY; 1983, 167

[14] R. M. Izatt, J. S. Bradshaw, S. A. Nielsen, J. D. Lamb, J. J. Christensen and D. Sen, *Chem. Rev.*, 1985, **85**, 271

[15] R. M. Izatt, K. Pawlak, J. S. Bradshaw and R. L. Brunening, *Chem. Rev.*, 1991, **91**, 1721

[16] L. F. Lindoy, in *Cation Binding by Macrocycles*, eds. Y. Inoue and G. W. Gokei, Marcel Dekker, New York, 1990, pp. 599

[17] A. J. Blake and M. Schroder, *Adv. Inorg. Chem.*, 1990, **35**, 1

[18] S. R. Cooper and S. C. Rawle, *Struct. Bonding* (Berlin), 1990, **72**, 1

[19] K. R. Adam, D. S. Baldwin, P. A. Duckworth, L. F. Lindoy, M. McPartlin, A. Bashall, H. R. Powell, P. A. Tasker, *J. Chem. Soc., Dalton Trans.*, 1995, **7**, 1127

[20] D. Moras, R. Weiss, Bull. Soc. Chim. Fr, 1972, 549

[21] M. Herceg and R. Weiss, *Bull. Soc. Chim. Fr.*, 1972, 549

[22] R. J. W. Lugtenberg, R. J.M. Egberink, J. F. J. Engbersen and D. N. Reinhoudt, *J. Chem. Soc., Perkin Trans. 2*, 1997

[23] R. Iwamoto, H. Wakano, *Bull. Chem. Soc. Japan.*, 1973, **46**, 1114

[24] C. A. Sharrad, L. Grondahl, L. R. Gahan, *J. Chem. Soc., Dalton Trans.*, 2001, **19**, 2937

[25] L. Valencia, H. Adams, R. Bastida, D. E. Fenton, A. Macias, *Inorg. Chim. Acta*, 2001, **317**, 1-2, 45

[26] F. J. Lalor, H. Hartigan, *unpublished results*

[27] R.H. Holm et al , *J. Am. Chem. Soc.*, 1986, **108**, 5607

[28] A. P. B. Lever, H.B. Gray, Eds., *Iron Porphyrins*, Vols, 1, 2, Addison-Wesley, Reading, Massachusetts 1983

[29] M. –A. Ahearn, J. Kim, A. J. Leong, L. F. Lindoy, O. A. Matthews and G. V. Meehan, *J. Chem. Soc., Dalton Trans.*, 1996, 3591

[30] M. Wen, M. Munakata, Y. Suenaga, ,*Inorg Chim Acta*, 2002, **332**, 18-24

[31] P. Tasker, L. Cronin, N. Robertson, D. White, *J. Chem. Soc. Chem. Comm.*, 1998

[32] S. G. Murray, F. R. Hartley, *Chem. Rev.*, 1981, **81**, 365

[33] T.–L Ho., *Chem. Rev.*, 1975, **75**, 1; T.–L. Ho, *Hard and Soft Acids and Bases Principle in Organic Chemistry*, Academic Press, New York-San Francisco-London, 1977

[34] R. Kowallick M. Neuburger, M. Zehnder, *Helv. Chim. Acta*, 1997, **80**, 3, 948

[35] M. Abkowitz, A. R. Monahan, J. Chem. Phys, 1973, 58, 6, 2281; A. R. Monahan, J. A. Brado, A. F. DeLuca, J. Phys., Chem., 1978, 76, 3, 446

[36] Y. Murakami, O. Hayashida, Proc. Natl. Acad. Sci. U. S. A. 1993, **90**, 4, 1140

[37] G. A. Ozin, S. Ozkar, Chem. Mater. 1992, **4**, 3, 511-21

[38] P. D. J. Grootenhuis, J. Eerden, P. J. Dijkstra, S. Harkema, D. N. Reinhoudt, . J. Am. Chem. Soc. 1987, **109**, 26, 8044

Chapter Five

Photochemical Reactions

Photochemical Reactions

5.0 Introduction

There is an activation energy associated with all chemical reactions and for this reason no chemical transformations are possible without some input of external energy. Depending on the size of this activation barrier and indeed the energy of the resultant product the reaction pathway may take several different forms.

If we consider the example outlined in Figure 5.1, which uses a thermal energy source, we see that heating molecules of A to form molecules of the type B, is more likely to lead to the isolation of C. The latter transformation has a lower activation energy barrier (E_2-E_1) and C is also the most stable of the three states.

In order of increasing energy, molecules tend to have translational, rotational, vibrational and electronic excited states. The transition of an atom or molecule from an electronic ground state to an electronic excited state requires the absorption of near IR, visible and near UV light. Photochemistry can then occur as a result of chemical transformation induced by transition to the excited state. In comparison with translational, vibrational and rotational energy levels, which are very closely spaced, the electronic levels in a molecule are generally widely spaced in terms of energy.

Use is made of these large energy differences in photochemistry, where direct absorption of a photon of high energy (in the UV-Vis region of the spectrum), produces electronically excited molecules, without significant excitation of the various rotational and vibrational levels, thus avoiding thermally induced fragmentation reactions.

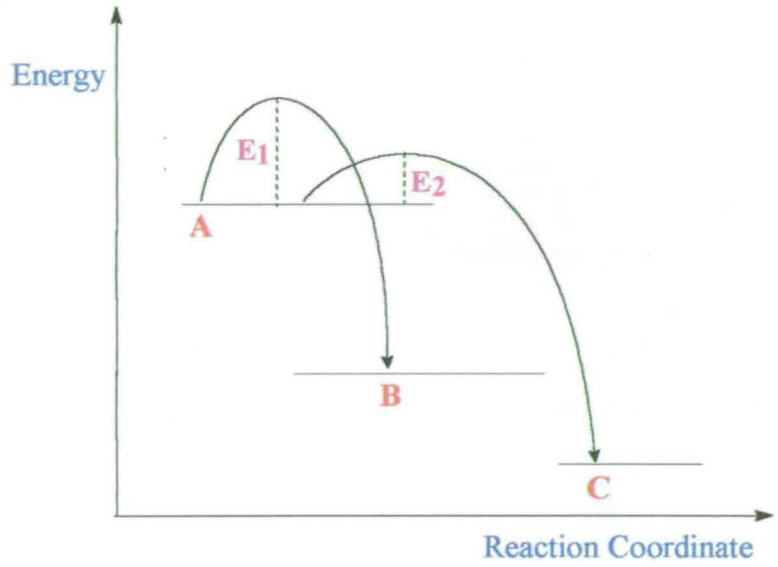

Figure 5.1 Diagram showing the thermal transformations of A to B with the higher activation energy E_1, and the competing transformation of A to C with the lower activation energy E_2

In general, a photochemical reaction may occur upon the absorption of a photon of radiation by the species in question. Absorption is a prerequisite for excitation to occur and whole molecules in the UV have a very high density of states with very high numbers of vibrational and rotational lines indicating that photons are absorbed. Not all photons are necessarily absorbed by all molecules and in some cases, molecules are completely unaffected by the powerful beam possessing high-energy photons. Absorption occurs when the energy of the incoming photon exactly matches the energy difference between two energy levels of the molecule, i.e. E_2-E_1 = hυ.

The light source used in a photochemical experiment is determined by the absorption spectrum of the molecule under study. The most widely used sources are those based

on mercury. The lamps are also dependable and capable of supplying a steady illumination of both ultraviolet and visible light covering the range from 200 nm to 750 nm and above. In using such a light source, i.e. a continuum light source, optimisation of absorption can occur. Internal conversion then provides the S_1 excited state rapidly, from which reactions can occur.

Three main types of mercury lamp exist and are designated as low, medium and high pressure where each type has unique spectral characteristics. The low-pressure or resonance lamp has a mercury vapour pressure of 0.005 - 0.1 Torr and operates at room temperature. The emission from these lamps is mainly at 253.7 and 185.9 nm, which correspond to transitions

$$Hg(^3P_1) \longrightarrow Hg(^1S_0) + h\upsilon$$

and

$$Hg(^1P_1) \longrightarrow Hg(^1S_0) + h\upsilon'$$

The high-energy emissions at 184.9 nm, are usually not transmitted unless an ultra-pure quartz reactor (Suprasil) is used as glass absorbs the emitted Hg radiation.

Medium pressure lamps operate at 1-10 atm and at relatively high temperatures. Consequently the lamp requires a few minutes to warm up to its operational temperature. The emission from these lamps is usually a weak continuum with the superimposition of spectral lines. The higher operating pressures and temperatures result in diminished intensity of the 253.7 and the 184.9 nm lines. They are also extremely useful for the excitation of organic compounds due to the matching of these lines to typical absorption bands of organic compounds.

High-pressure lamps operate at about 200 atm however the large increase in pressure and in working temperature introduces many more spectral lines and so a stronger continuum is obtained with broadening of the principle emission lines. Emission from these lamps is very weak below 280 nm.

5.1 Fate of Electronically Excited Molecules[1]

According to quantum mechanics, energy absorbed by a molecule may contribute to vibrational, rotational or electronic excitation. As the energy levels for vibrational, translational and rotational excitation are very close, molecules in the ground electronic state are really a collection of species with different rotational and vibrational levels at room temperature. Electronic excitation can, and does, occur from any of these levels.

The mass of an electron is much smaller than that of any nucleus hence the initial step in the electronic excitation of a molecule takes place without changes in the position of the atoms. Vertical excitation is said to have occurred. If the lifetime of the excited species is long enough, relaxation back to the singlet ground state, S_0, may occur. This is a simple photochemical reaction and can possibly lead to a different molecule e.g. a *cis-trans* isomerization in an alkene.

Instead of molecular rearrangements or reactions occurring following excitation, energy could instead be lost, returning the molecule to the first excited state S_1. This is called *internal conversion.* The loss of heat is directly proportional to the energy required for excitation to occur, i.e. the difference in energy of the excited energy level and the final energy level. The overall process is a conversion of light to heat.

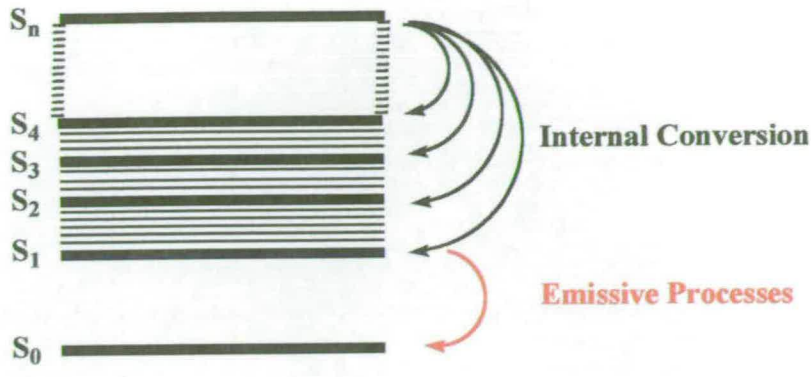

Figure 5.2 Vibrational levels involved in internal conversion and emissive process

Following excitation from S_0 to an excited state S_n, internal conversion occurs to bring the molecule back to the S_1 level i.e. the vibrational levels provide a 'ladder' down which the molecule is able to internally convert to the S_1 state. The energy gap between S_1 and S_0 is generally too large for internal conversion to occur and therefore, emissive processes occur from $S_1 \rightarrow S_0$. An example of such an emissive process is the luminescence process occurring from the singlet excited state S_1, which is called *fluorescence*.

If the electron undergoes *intersystem crossing* i.e. a transition from the excited singlet state, S_1, to a thermodynamically favoured excited triplet state T_1, then three choices again become possible for returning to the ground state. It can (a) lose energy thermally (although in this case the energy levels are too widely spaced for this to rapidly occur and lifetimes may be up to 1s), (b) lose energy in the form of a photon (in this case called *phosphorescence*) or (c) undergo photochemical reaction.

Intersystem-crossing is actually a violation of the spin selection rules and is often not efficient. It can be enhanced by spin-orbit interaction between an excited molecule (in the singlet state) and an atom of high atomic number. This effect is called the

Heavy-Atom Effect. The use of chlorinated solvents in the course of this work in the form of CH_2Cl_2, proves very useful for efficient *intersystem crossing* to occur.

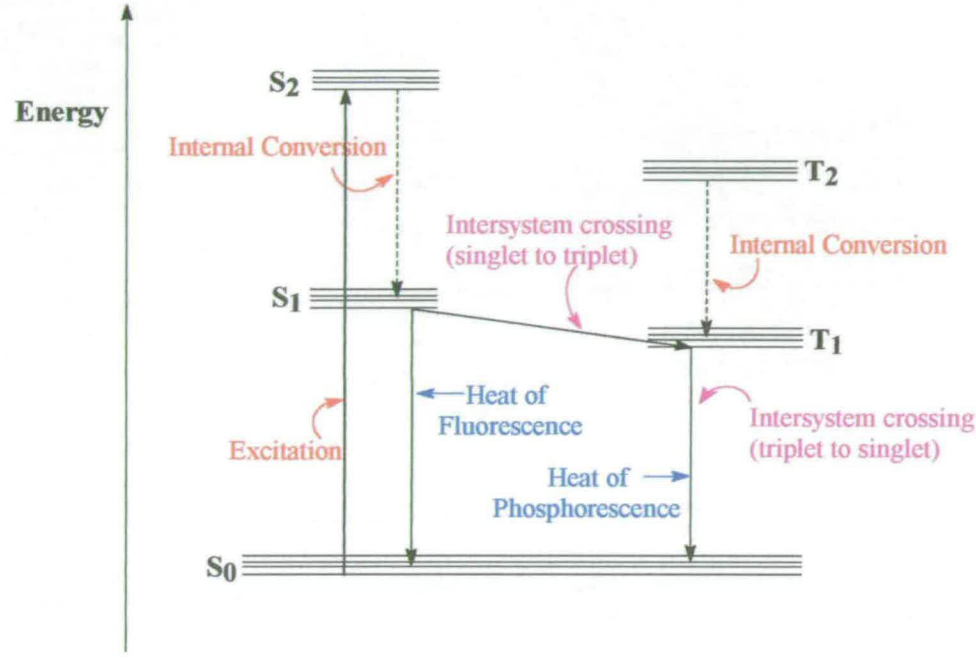

Figure 5.3 A Jablonski Diagram showing the excitation of a molecule A from its ground state (S_0) to a variety of excited states via photochemical processes

Multi relaxation processes are also possible in such systems. Such processes include *spin-lattice*, *spin-spin* relaxation and *spin-orbit* coupling (also referred to as *jj* coupling). In the case of *spin-lattice* relaxation, energy is given up to the surroundings e.g. by collision with other molecules in solution. In the case of *spin-spin* relaxation, the energy is transferred to other spin systems within the molecule.

5.2 Experimental Considerations

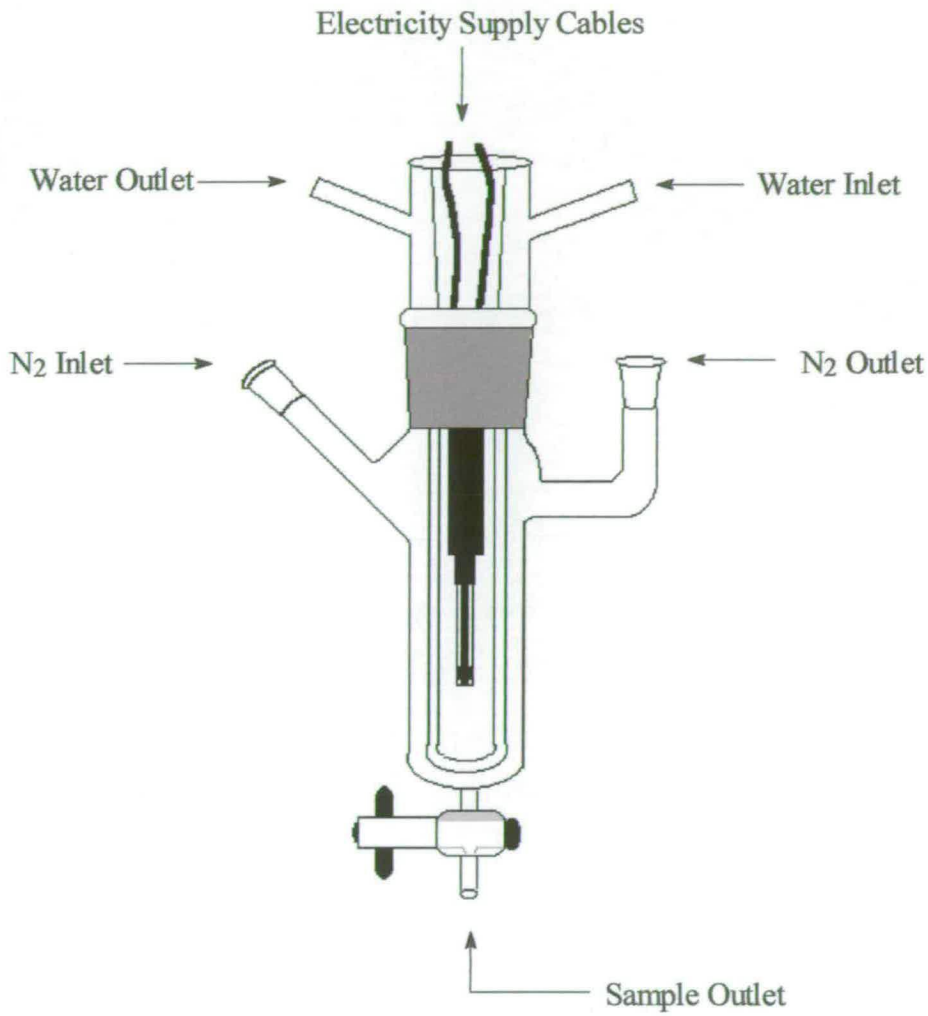

Figure 5.4 Immersion apparatus for solution phase photochemistry

Preparative organic photochemistry can be carried out using two methods. The first, involving a system of lamps surrounding the solution of the compound to be irradiated, is not used and will not be discussed here. The second experimental set-up, and the one adopted here, involves the solution of the compound completely

surrounding the irradiating lamp in a reactor described in Figure 5.4. This method allows for a more efficient and economical use of the lamp output.

The lamp is contained in a double-walled immersion well constructed of quartz, which is optically transparent down to 200 nm. The double surface of the immersion well allows the solution of the compound to be insulated from the heat of the medium-pressure arc lamp by circulation of cooling water.

The outer vessel of the reactor is usually made of Pyrex and can be varied in size and also in the number of outlets and inlets attached to it. Variations in reactor design allow for experiments to be carried out under aerobic or anaerobic conditions and also under constant, low or high temperature conditions.

Mercury lamps provide a highly versatile and convenient method of irradiation in synthetic, solution-phase, organic photochemistry. In the experiments discussed in this chapter, a medium pressure mercury lamp was used in an experimental set-up identical to that described in Figure 5.4 unless otherwise stated.

5.3 Theoretical background to deprotection of [5]

5.3.1 Introduction

It has been proposed [2], that 1,3-dithiole-2-ones of the general formula [O=$CS_2C_2R_2$] {R = alkyl} readily undergo photochemical decarbonylation reactions upon irradiation in solution with medium-pressure mercury lamps. The rearrangement has been proposed to be most efficient in chlorinated solvents such as CCl_4 or CH_2Cl_2 and results in the formation of a dithione [$(S=C)_2C_2R_2$] moiety, which is highly reactive towards transition metal units. The reaction is described below (Scheme 5.1).

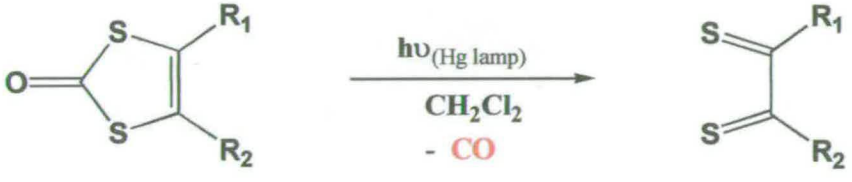

Scheme 5.1 General scheme for the irradiation of 1,3-dithiol-2-ones with a medium pressure Hg lamp

In the course of this project, the [18]ane S_4N_2 ketone macrocycle **[5]** has been prepared, Figure 5.5. The peripheral part of this macrocycle **[5]** is identical to that in the reaction above and as such may be a suitable candidate to undergo similar decarbonylation reactions. This type of reaction, makes feasible the *in-situ* formation of the [18]ane S_4N_2 tetrathione macrocycle **[9]**, which could be reacted directly with a metal salt of the type $[ML_1L_2]^{2-}$, to ultimately yield a redox active macrocycle.

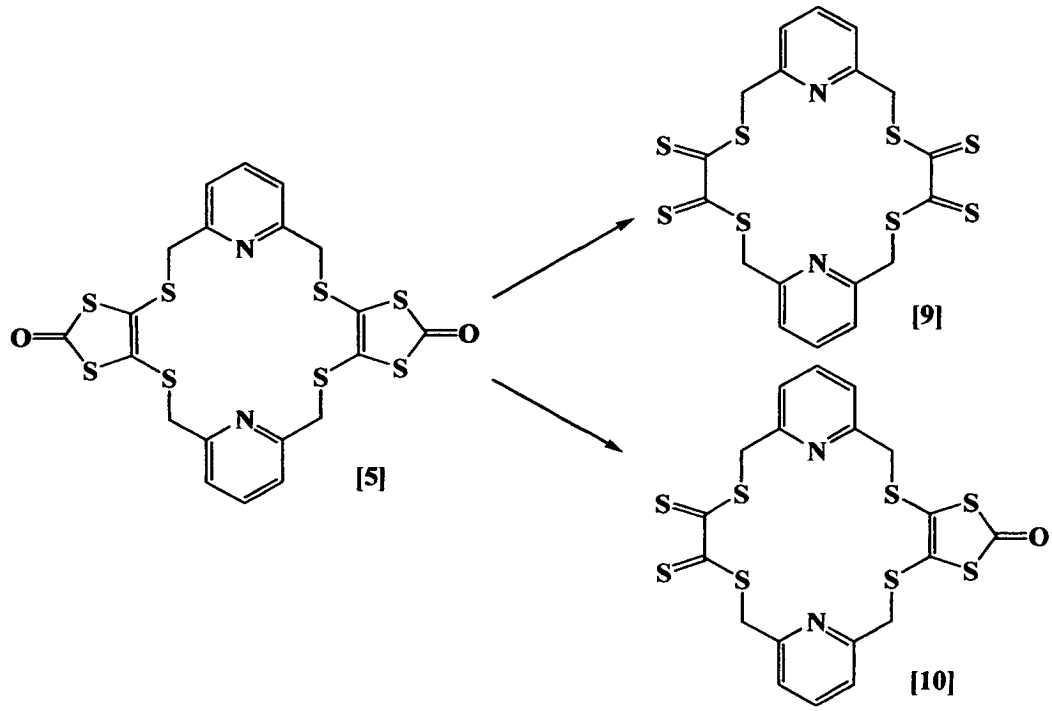

Figure 5.5 Irradiation of the [18]ane S_4N_2 ketone macrocycle **[5]** to give the tetrathione macrocycle **[9]** and the mono-deprotected macrocycle **[10]**

When a carbonyl group is electronically excited, non-productive events can occur, such as luminescence or non-radiative energy transfer which returns the starting molecule to the ground state. Productive reactions may take many forms. The simplest is referred to as a *Norrish Type I* reaction [3] Figure 5.2, which involves a decarbonylation mechanism in which the bond adjacent to the carbonyl is broken and a pair of radicals is formed.

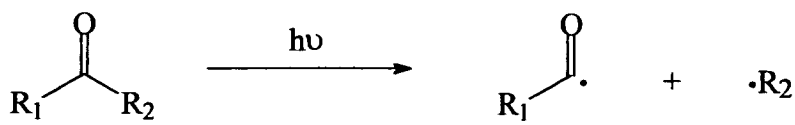

Scheme 5.2 Initial mechanistic step in a *Norrish Type 1*, decarbonylation reaction

Radical reactions follow, and succeeding events depend very much on the conditions used in the irradiation. For 1,3-dithiole-2-ones, a decarbonylation mechanism according to Scheme 5.3 may result.

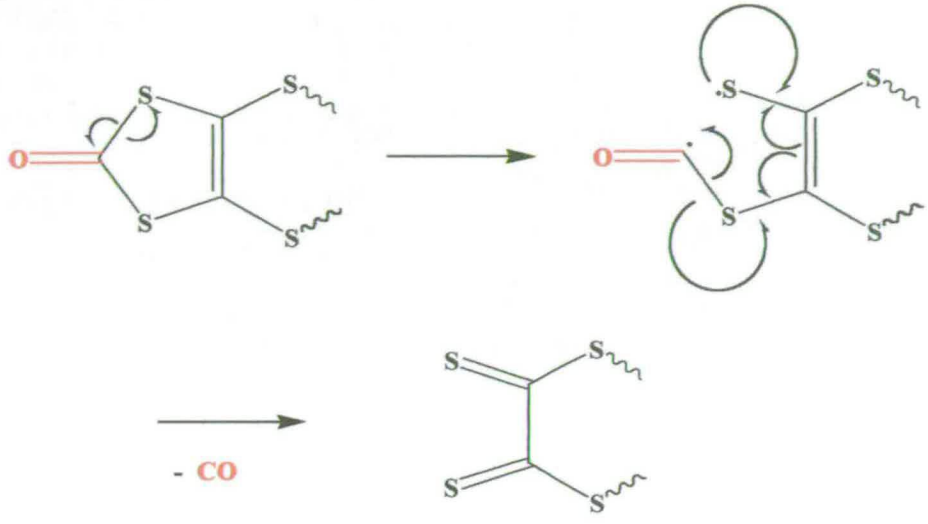

Scheme 5.3 A possible mechanism for the photochemically induced decarbonylation of the bis ketone macrocycle **[5]** via a *Norrish Type 1* route [3]

Depending on the extent of the reaction, one or two carbonyl groups are eliminated to give **[10]** or **[9]** respectively. As a direct result of the presence of the resultant thione sulfurs, the system is made highly reactive towards metal-ligand systems of the type $[ML_1L_2]$ {M = redox active metal; L_1 and L_2 = semi-labile ligands capable of displacement by the nucleophilic thione groups}.

In the case of the non-macrocyclic system following decarbonylation, the repulsion between the lone pairs on the two thione sulfurs, coupled with the lack of a rigid backbone, allowed for free rotation about the C-C single bond. This free rotation resulted in a *trans* conformation and the degree of electron pair repulsion is minimised.

In the case of the macrocycle [5], the final product juxtaposes two highly co-ordinating thione groups in a *-cis* conformation, with the help of the, *in-situ* rigid macrocyclic framework.

5.3.2 Metal Coordination to the decarbonylated macrocycle

5.3.2.1 Coordination of $Na_2[Ni(mnt)_2].xH_20$

Nickel dithiolene complexes have been well researched in the literature and the extent of their application is wide ranging based on the properties they possess. Extensive delocalisation is among the most important of these, incorporating empty d-orbitals on the metal and the coordinated dithiolene ligands. Applications of these systems include the area of nonlinear optics [4], based on the presence of an intense low energy absorption band. Also, based on the ease with which changes can be made to the electronic nature of the central metal, they are ideal candidates to act as precursors for the synthesis of a wide variety of sulfur based materials [5].

As discussed in the previous section, irradiation of the [18]ane S_4N_2 ketone macrocycle [5] leads to the decarbonylation of the peripheral ketone moieties, yielding highly co-ordinating thione-based sulphur atoms.

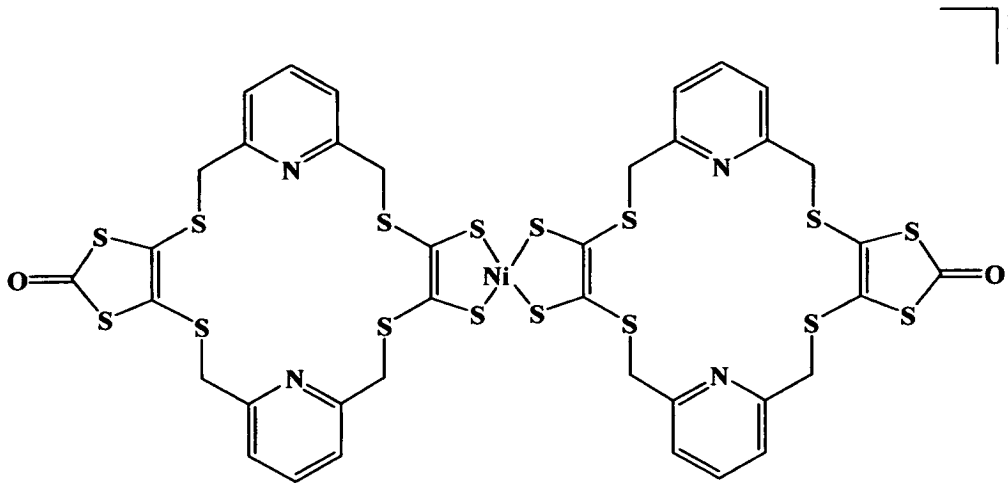

[11]

Figure 5.6 Product of the irradiation of the [18]ane S_4N_2 ketone macrocycle [5] and reaction with $Na_2[Ni(mnt)_2]xH_20$ {mnt = $[S_2C_2(CN)_2]^{2-}$

Irradiation of the ligand was carried out in dichloromethane under a continuous N_2 flow for 0.5 hours. Upon addition of 2 equivalents of a methanol solution of the $Na_2[Ni(mnt)_2]xH_2O$ salt, a dark solid was collected which proved to be that of the dimacrocyclic-Ni species, Figure 5.6. The proposed structure of this product indicates that the product of the initial radiation is the mono deprotected macrocycle **[10]**.

This new redox-active system, **[11]**, has been characterised in full including mass spectrometry (Appendix 3.1) and UV-Vis spectral analysis, Figure 5.7. The yield of the product is low (32 %) and this coupled with time limitations meant that no complexation studies with transition metal ions were carried out. However, the considerable potential of such a system in (a) the detection of transition metal ions by coordination of the guests to either or both cavities and (b) a wide variety of studies on the guest-guest interactions, if any, promoted by the highly delocalised

Ni-dithiolene units is obvious. The versatility of this reaction in the preparation of a wide variety of redox active macrocycles is clear when one considers the incorporation a number of different redox active metals, in place of the Ni, to the highly reactive thione sulfurs.

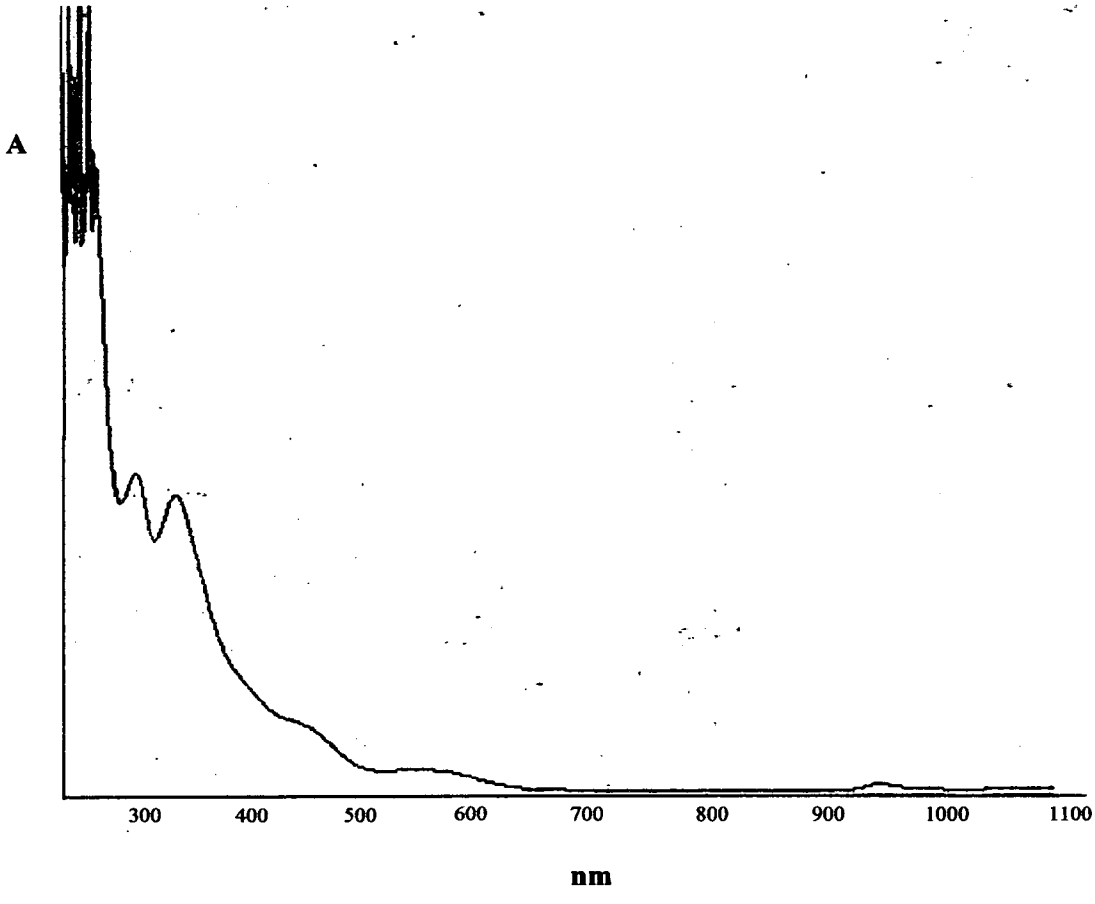

Figure 5. 7 UV-Vis spectrum of the product of the irradiation of the [18]ane S_4N_2 ketone macrocycle [5] and reaction with $Na_2[Ni(mnt)_2]xH_2O$ [11]

There are significant benefits in developing a simple procedure towards the preparation of Ni-dithiolene compounds which (a) have the ability to exist in several well defined oxidation states (b) have distinctive low energy bands, a property which has been developed in the area of non-linear optics and finally (c) depicts a system

which is tuneable both in terms of the redox behaviour and the position of the low energy HOMO to LUMO transition

Considering the incomplete decarbonylation reaction following irradiation for 30 minutes, it is clear that a longer irradiation exposure time could lead to enhanced decarbonylation. Irradiation of the ligand was therefore carried out for a total of 2 hours.

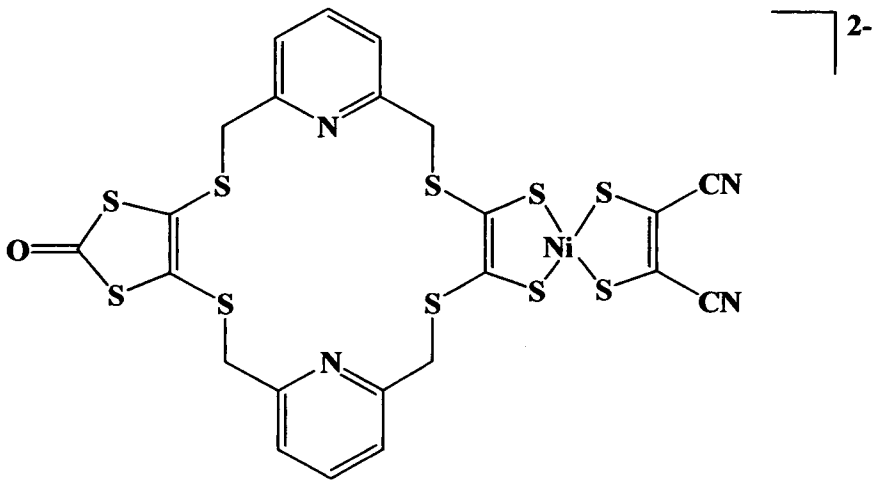

[12]

Figure 5.8 Product **[12]** of the irradiation of the bis ketone macrocycle **[5]** for 2 hours and reaction with $Na_2[Ni(mnt)_2]$

In this case, addition of a methanol solution of $Na_2[Ni(mnt)_2].xH_2O$ drop-wise to the irradiated ligand gave the mono-substituted $[Ni(mnt)(macrocycle)]^{2-}$ **[12]** as a dark green solid in 36 % yield. Microanalysis showed that the redox active system was present as the sodium salt $Na_2[Ni(mnt)(macrocycle)]$, Figure 5.8. A second material isolated from the reaction mixture was the non-decarbonylated system containing a Ni^{II} ion within the cavity of the macrocyclic ring **[13]**. No clear reason for the presence of this system has been identified but is possibly caused by incomplete

decarbonylation. Alternatively, the longer irradiation time may result in degradation of much of the ligand and thus a smaller quantity of [**10**] is available for complexation to the Ni centre.

Table 5.1 Comparison of the UV-Vis absorbances of [**12**] with that of the starting material $Na_2[Ni(mnt)_2]$

Assignment	**$Na_2[Ni(mnt)_2]$ / nm**	**[12] / nm**
(dithiolene based) $\pi \rightarrow \pi^*$	270.63, (ε = 25,687),	254.35, (ε = 22,352)
	315.42, (ε = 19,342)	331.23, (ε = 18,766)
		375.21, (ε = 17,998)
		465.32, (ε = 21,687)
(M-dithiolene based) $\pi \rightarrow \pi^*$	905.12, (ε = 12,473)	920.4, (ε = 12,156)
Unassigned transitions	1041.76, (ε = 8,545)	1025.7, (ε = 8,825)

Mass spectrometric (Appendix 3.1) and elemental analysis indicated the successful preparation of the mono-substituted $[Ni(mnt)(macrocycle)]^{2-}$ [**12**] Figure 5.8. The significant changes in the characteristic macrocyclic-based $\pi^* \leftarrow \pi$ transitions and those of the typical, low wavelength Ni dithiolene $\pi^* \leftarrow \pi$ transitions over a range from 920.4 nm (ε = 12,473 M^{-1} cm^{-1}), is further evidence the formation of [**12**]. By a comparison of the UV-Vis absorbances of the Ni-dithiolene starting material $Na_2[Ni(mnt)_2]$, with those of the product Table 5.1, the nature of the product [**12**] is confirmed.

Despite the successful preparation of this product, the yield was considerably low (36 %). No complexation studies were carried out, however the significance of these systems and their potential as ion sensors is clearly evident.

5.3.2.2 Reactions involving $[NEt_4]_2[Pd(dmit)_2]$ and $[NEt_4]_2[Zn(dmit)_2]$

5.3.2.2a Introduction

With the success of the decarbonylation reaction using Hg medium-pressure irradiation, the procedure was further developed to attempt the incorporation of a variety of other metals into the macrocyclic system.

5.3.2.2b Results and Discussion

Pd^{II}, $[NEt_4]_2Pd(dmit)_2$ and Zn^{II}, $[NEt_4]_2Zn(dmit)_2$ were chosen as possible convenient sources of metal units. The experimental procedure was carried out as in the case of nickel (Section 5.3.2.1), however no precipitate apart from recovered starting metal salts, was observed at any stage in the reaction. Mass spectrometry gave no evidence for the presence of any metal complexed macrocyclic system within the reaction mixture.

Closer examination of representative UV-Vis data from each of these reactions Figure 5.9, indicates that little or no reaction occurred. Instead, it was found that the isolated products were shown by elemental analysis and Mass Spectrometry to be identical to the starting materials.

The preference for the thione sulfurs for nickel over palladium or zinc may be explained as follows. Pd is present in the second row transition metal series and as such complexes involving Pd are very kinetically stable. In any attempt to exchange ligands bound to the metal, the existing bonds first need to be broken and the energy required to do this is high. In the course of this work then, the coordination of either of the deprotected species [**9**] or [**10**] to the $[Pd(dmit)_2]^{2-}$ species will involve the

initial cleaving of the existing Pd-S bonds. The energy barrier to the cleaving of these bonds means that the overall reaction and formation of the new redox active macrocycle is kinetically disfavoured.

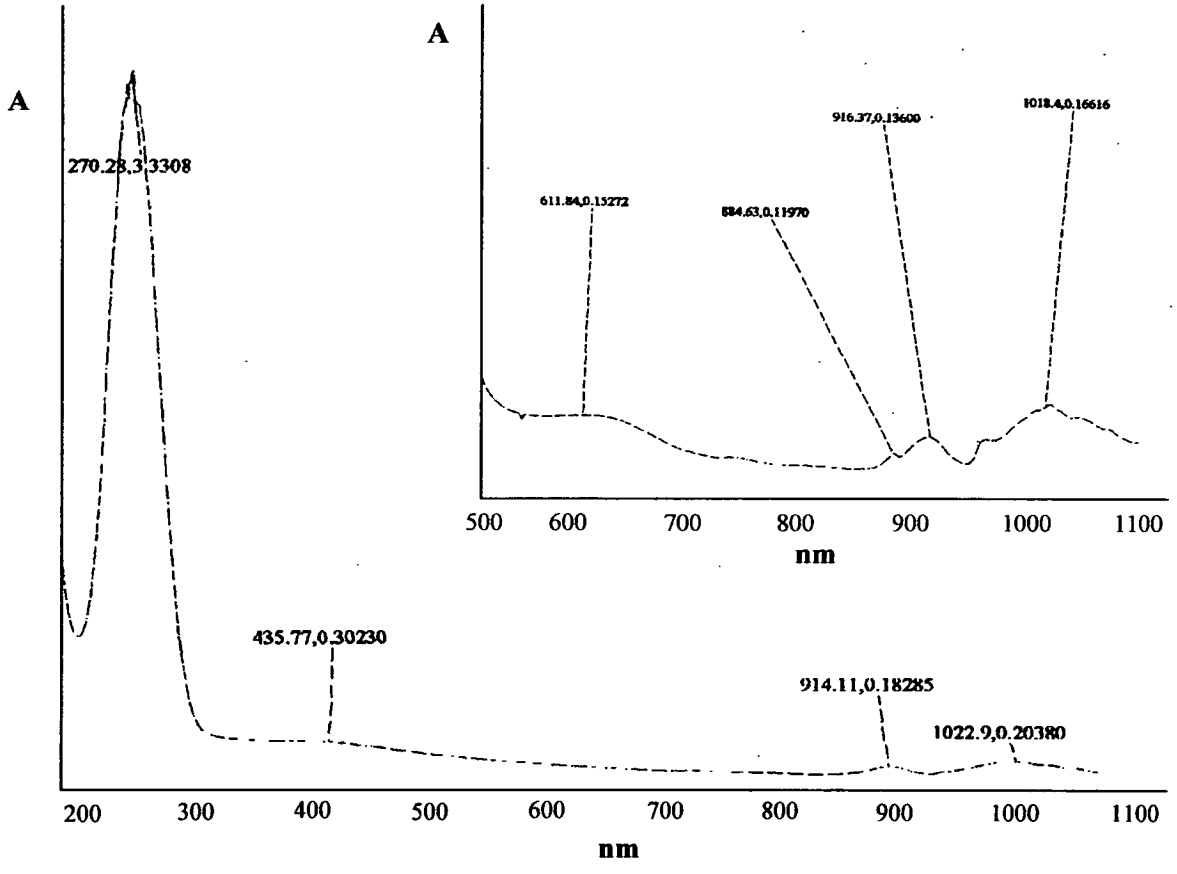

Figure 5. 9 UV-Vis spectrum of the product of the irradiation of the [18]ane S_4N_2 ketone macrocycle [5] and reaction with $[NEt_4]_2Pd(dmit)_2$

If we move our attention to Zn, the extent to which Zn-dithiolene complexes have been reported in the literature is minimal. Possibly the most commonly known form of Zn-dithiolene complexes is the starting material, $[Zn(dmit)_2]^{2-}$, used in this reaction. Considering the lack of literature references for these species, indications

are that an inherent instability of these types of Zn-dithiolene complexes exists and inhibits the overall reaction from taking place.

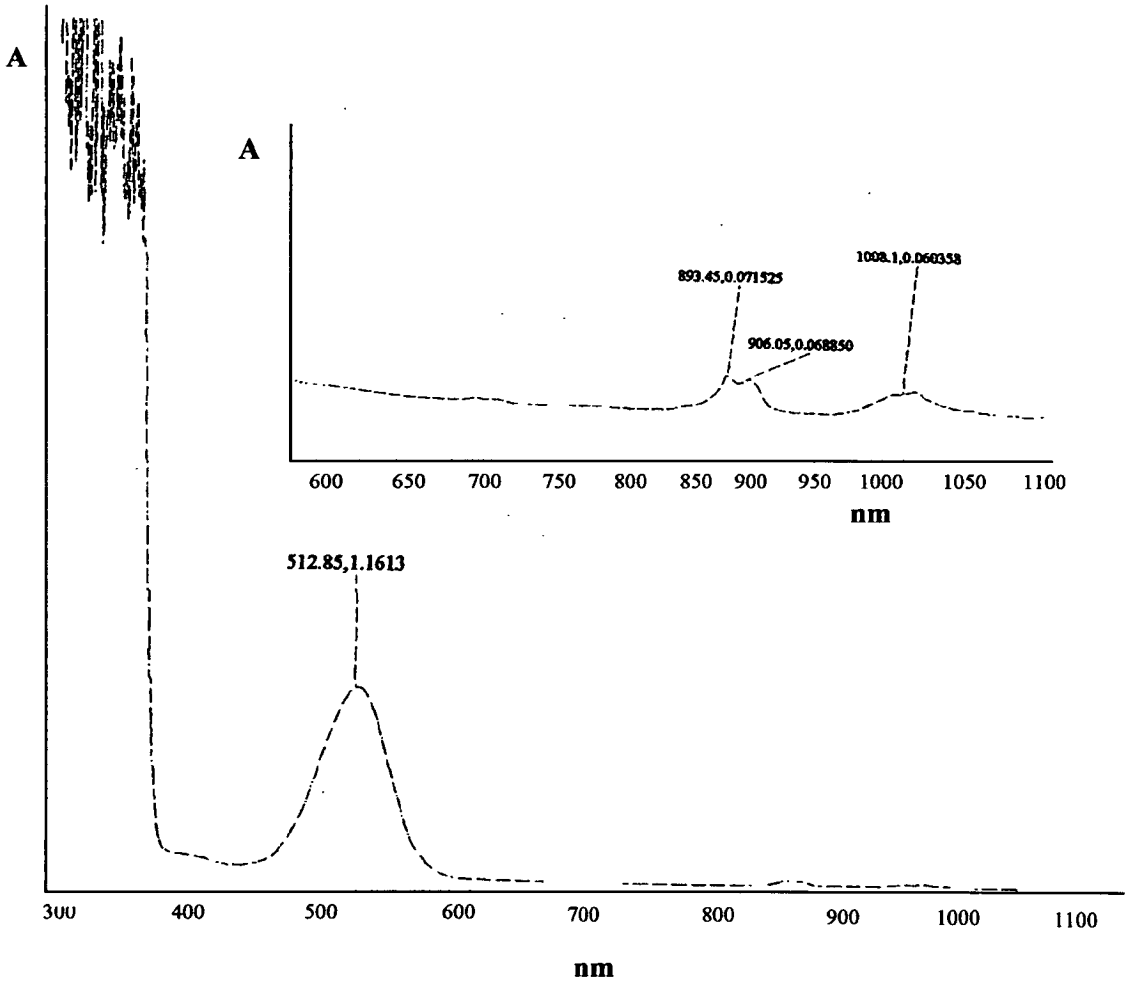

Figure 5. 10 UV-Vis spectrum of the product of the irradiation of the [18]ane S_4N_2 ketone macrocycle [5] and reaction with $[NEt_4]_2Zn(dmit)_2$

5.4 Conclusions

In our attempts to prepared new redox active macrocycles, the most important step has proven to be the route chosen to deprotect the macrocycle at the thione or ketone carbons. The route described in detail in this chapter, involves photochemical irradiation and decarbonylation of [18]ane S_4N_2 ketone macrocycle [**5**] in CH_2Cl_2. The photochemical irradiation of these systems is simple and effective with minimal environmental impact as carbon monoxide is the only side-product of the reaction.

Preliminary experiments using this method have proven very successful. The reaction of the deprotected product ([**10**]) with a transition metal salt $[M(L)_2]^{2-}$, has also proven successful with the preparation of the mono-substituted (mnt)Ni-macrocycle [**12**] and also the bismacrocyclic Ni(macrocycle)$_2$ system, [**11**] through coordination of the thione sulfurs to the coordination sphere of the metal, M.

With the success of this reaction in the deprotection of the bisketone macrocycle, this step may, in principle, be utilised in the general development of a variety of redox active macrocycles. With the redox active units incorporated in [**11**] and [**12**] and the metal-dithiolene absorbances observed in the near-IR, the potential of these systems as redox-active or spectroscopic ion sensors in detecting transition metal ions is considerable. Projects are currently underway in refining and optimising the decarbonylation step and the preparation of a wide variety of new redox active systems is underway.

5.5 Experimental

Irradiation Experiments were carried out using a Medium Pressure Hg lamp with Quartz Reactor assembly. Irradiation experiments were carried out in all cases in a dichloromethane solution of the [18]ane S_4N_2 ketone macrocycle [**5**]. Irradiation times varied and are described below with each individual experiment. Unless otherwise stated all reactions were carried out under an inert atmosphere

Preparation of the [18]ane S_4N_2 ketone macrocycle [5] [6].

Benzoyl ester derivative of the 1,3-dithiol-2-thione-4,5-dithiole dianion [**1**][6], {1.00 g; 2.46 mmol} was dissolved in 13ml of CH_2Cl_2 and to the solution was added a suspension of $Hg(OAc)_2$ {1.96 g; 6.15 mmol} in 16 ml acetic acid. The reaction was stirred for 40 minutes at room temperature. The resultant yellow precipitate was filtered and discarded. To the filtrate was added 50 ml of CH_2Cl_2. The organic phase was then washed with four 75 ml aliquots of distilled water. Neutralisation was then carried out with two 75 ml aliquots of a saturated sodium hydrogen carbonate solution. Finally the organic phase was washed with two 75 ml aliquots of distilled water. The organic phase was dried over $MgSO_4$, reduced to half the volume *in vacuo* at which point a large quantity of EtOH was layered on top and the solution placed in the freezer. After 48 hours pale yellow crystals of the benzoyl derivative of the 1,3-dithiol-2-one-4,5-dithiolate dianion [**2**] (i.e. the dmid ester) were collected in 78 % yield.

To a stirred suspension of the 1,3-dithiol-2-one-4,5-dithiole [**2**] (dmid ester) [6] {0.21 g; 0.54 mmol) in 36 ml of EtOH, was slowly added a 3ml solution of NaOMe {0.06 g; 1.09 mmol in MeOH). The reaction mixture was allowed to stir for 30 minutes or until all the solid material has dissolved. This dark 'blood-red' solution was added drop-wise to a solution of bis(bromomethylpyridine) {0.15 g; 0.54 mmol} in 32 ml

of EtOH, over a 12 hour period. The resultant pale yellow precipitate was filtered and collected. Recrystallisation from hot CH_2Cl_2 and washing with Et_2O resulted in a yield of 63 % of the [18]ane S_4N_2 ketone macrocycle [**5**]. FAB MS [CH_2Cl_2] m/z = 570.49. Calculated 42.12 %C, 2.53 %H, 4.91 %N for $C_{20}H_{14}N_2O_2S_8$. Found 42.80 %C, 2.40 %H, 4.80 %N. UV-Vis (Appendix >>>)

Irradiation of the [18]ane S_4N_2 ketone macrocycle [5]

The quartz reactor (Figure 5.4) was charged with a solution of the [18]ane S_4N_2 ketone macrocycle [**5**] {0.14 g; 0.39 mmol} in 100 ml of CH_2Cl_2. The medium pressure quartz lamp was immersed into the solution within its sealed system and the condenser and N_2 started. Irradiation was carried out for 30 minutes. The resultant sample was syringed in equal quantities, under N_2, to three different round bottom flasks, each of which was under a dynamic N_2 flow. Subsequent reactions with a variety of metal salts are described below.

(i) Reaction with $[NEt_4]_2[Zn(dmit)_2]$

To the 33 ml portion of the irradiated sample was added a 2 ml acetone solution of $[NEt_4]_2[Zn(dmit)_2]$ {0.12 g; 2 equivalents}. The addition was made drop-wise and the reaction was allowed to stir for 30 minutes before being filtered. The filtrate was found to be a deep red colour and was rotary evaporated to 5 ml. An equal quantity of hexane was layered on top allowing recovery of 0.10 g of the starting material $[NEt_4]_2[Zn(dmit)_2]$. Calculated 36.98 %C, 4.16 %H; 4.31 %N for $C_{40}H_{54}N_4S_{18}Zn_2$. Found 36.64 %C, 5.46 %H, 3.81 %N. UV-Vis [$(CH_3)_2CO$] 512.9 (ε = 18,564 M^{-1} cm^{-1}), 894.5 (ε = 7,580 M^{-1} cm^{-1}), 904.7 (ε = 12,098 M^{-1} cm^{-1}), 1016.2 (ε = 9,713 M^{-1} cm^{-1}) nm. FAB Mass Spectrometry - no identifying peaks found only matrix observed

(ii) Reaction with $Na_2[Ni(mnt)_2]xH_2O$[7] : Preparation of the bicyclic system [(macrocycle)$_2$Ni] [11]

To a 33 ml portion of the irradiated sample was added a 2 ml MeOH solution of $Na_2[Ni(mnt)_2]$ {0.06 g; 2.0 equivalents}. The addition was made drop-wise and the reaction was allowed to stir for 30 minutes before being filtered. A pale brown precipitate of [**11**] was collected in 32 % yield, upon filtration of the reaction mixture. Upon rotary evaporation of the filtrate to 5 ml and addition of EtOH, a green solid was collected which gave identical analysis to the starting material $Na_2[Ni(mnt)_2]xH_2O$. FAB Mass Spectrometry m/z 1152 D. Calculated 38.00 %C, 2.33 %H, 4.67 %N for [**11**] $C_{38}H_{28}N_4S_{16}O_2NiNa_2$. Found 38.21 %C, 2.41 %H, 4.82 %N.

(iii) Reaction with $[NH_4]_2[Pd(mnt)_2]$ [7]

To a 33 ml portion of the irradiated sample was added drop-wise, a 2ml MeOH solution of {0.085 g; 0.26 mmol} of $[NH_4]_2[Pd(mnt)_2]$. No precipitate was seen to form and no colour change occurred. Precipitate formed on the addition of hexane was collected as a purple-red solid. FAB Mass Spectrometry m/z = 751, 614, 596 D. UV-Vis [MeOH] 270.3, 435.8, 914.1, 1022.9 nm. Calculated 33.50 %C, 2.70 %H, 10.20 %N for $C_{23}H_{22}N_6S_{10}OPd$. Found 22.51 %C, 1.78 %H, 19.81 %N. The resultant filtrate of this precipitation was also analysed. FAB Mass Spectrometry m/z = 404, 327, 281 D. UV-Vis (MeOH) 270.3 (ε = 25,342 M^{-1} cm^{-1}), 435.8 (ε = 21,265 M^{-1} cm^{-1}), 884.7 (ε = 7,698 M^{-1} cm^{-1}), 914.1 (ε = 11,576 M^{-1} cm^{-1}), 958.4 (ε = 10,548 M^{-1} cm^{-1}), 1022.9 (ε = 9,348 M^{-1} cm^{-1}) nm.

Preparation of the monosubstituted Na_2[(mnt)Ni(macrocycle)] [12]

The quartz reactor was charged with a 100 ml of CH_2Cl_2 solution of the [18]ane S_4N_2 ketone macrocycle [**5**] {0.15 g; 0.27 mmol). The medium-pressure quartz lamp was immersed into the solution within the sealed system and the condenser and N_2 started. Irradiation was carried out for 2 hours. The resultant sample was syringed,

under N_2, into a round bottom flask. To the irradiated sample was added drop-wise a 2 ml CH_2Cl_2 solution of $[NBu_4]_2[Ni(mnt)_2]$ {0.51 g; 0.53 mmol} and the reaction allowed to proceed for 30 minutes. A yellow precipitate formed. The reaction mixture was rotary evaporated to 5 ml and the product **[12]** isolated as a yellow solid in 36 % yield. Electrospray Mass spectrometry m/z = 740.2 (M^+); 739.0 (M^+-1); 699.34 and 669.09 D. Calculated 35.06 %C, 1.78 %H, 7.10 %N for $C_{23}H_{14}N_4S_{10}NiONa_2$. Found 35.30 %C, 2.06 %H, 6.69 %N. UV-Vis 254.4, 331.2, 375.2, 465.3, 920.4, 1025.7 nm. Also isolated from further recrystallisations of the filtrate was the starting material, the [18]ane S_4N_2 ketone macrocycle **[5]**, in 7 % yield.

5.6 References

1 C. E. Wayne, R. P. Wayne, Photochemistry, Oxford Chemistry Primers, Oxford Science Publications, Oxford University Press, 1996

2 K. Hartke, T. Kissel, J. Quante, R. Matusch, *Chem. Ber.*, 1980, **113**, 1898

3 J. Kagan, '*Organic Photochemistry, Principles and Applications*', Academic Press Inc., San Diego, 1993; W. M. Horspool, '*Synthetic Organic Photochemistry*', Plenum Press, 1984

4 C. S. Winter, S. N. Oliver, J. D. Rush, C. A. S. Hill, A. E. Underhill, *Mol. Cryst. Liq. Cryst,* 1993. **235**, 181

5 R. S. McLean, *Abstr. Pap. Am. Chem. S.*, 1992, **204 5-TECH**, Part 1

6 N. Svenstrup, J. Becher, *Synthesis*, 1995, 215

Chapter Six

Routes to Redox-Active Macrocycles

Other attempted routes to alternative redox-active macrocycles

6.0 Introduction

To this point in the project the use of the well established dmit and dmid precursors {$[C_3S_5]^{2-}$ [**1**] and $[C_3S_4O]^{2-}$ [**2**]} have been employed. From these precursors, [18]ane S_4N_2 thione and ketone macrocyclic ligands, [**4**] and [**5**], have been prepared. While the donor sites of these systems are ideal for the complexation of transition metal ions, the development of a versatile route to the coordination of a redox-active unit to the peripheral parts of the macrocycles has proven complex.

Direct attachment of the Cp-Co unit by reaction of $CpCo(CO)_2$ with the [18]ane S_4N_2 thione macrocycle [**4**] has been discussed in considerable detail in Chapter 3. The decarbonylation reaction of the [18]ane S_4N_2 ketone macrocycle [**5**] to expose two or four highly reactive thione groups has also been developed and is discussed in Chapter 5. In parallel with these studies, a considerable amount of work was carried out to develop other methods to the preparation of a wide range of redox active macrocycles. Some of the more interesting results observed are reported in this chapter.

6.1 Deprotection of the [18]ane S_4N_2 thione and ketone macrocycles [4] and [5] and reaction with transition metal salts

6.1.1 Introduction

For the attachment of a redox active unit to the peripheral areas of the [18]ane S_4N_2 thione and ketone macrocyclic ligands **[4]** and **[5]**, deprotection is initially required. Deprotection of analogous precursors, has most commonly been carried out with base which acts as a nucleophile deprotecting at the ketone or thione carbon. This was discussed in more detail in the introduction, in Section 1.1.1.3b.

6.1.2 Results and Discussion

The deprotection of the thione and ketone groups of the [18]ane S_4N_2 macrocycles **[4]** and **[5]**, was initially attempted with tetramethylammonium hydroxide $[NMe_4]OH$. The reactions were carried out using varying quantities of base and in each case, were immediately followed by reaction of the assumed now deprotected species with a transition metal salt of the type $[L_nMX_m]^{2-}$ {L = dppe, bipy, *p*-cymene; n = 1, 2; X = Cl; m = 2}. The metal salts used in these reaction were $[(p\text{-cymene})RuCl_2]_2$, $[(bipy)_2RuCl_2]xH_2O$, $[Cp_2TiCl_2]$, and $[(dppe)NiCl_2]xH_2O$.

The envisaged mechanism for this reaction was to deprotect at the ketone or the thione groups to form the tetrathiolate macrocycle, Figure 6.1. Reaction with the metal salts would then occur via nucleophilic displacement of halide ligands from the metal co-ordination sphere using the deptrotected thiolate sulfurs.

For each of the metal salts investigated, the result was the same. It was observed that attack at the thione **[4]** / ketone **[5]** carbon was not occurring to any measurable extent, but instead the base deprotection appeared to preferentially attack at the CH_2 group adjacent to sulfur in the macrocyclic ring, resulting in the abstraction of a proton, Figure 6.2.

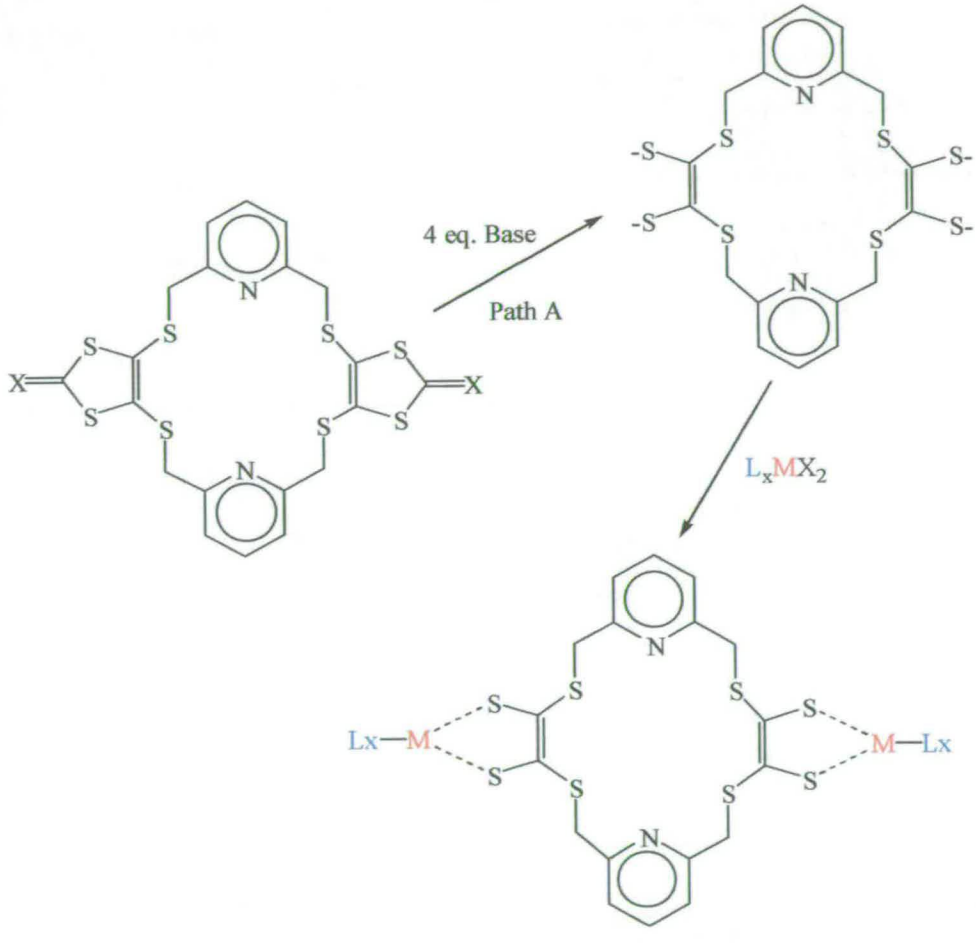

Scheme 6.1 Attempted base-deprotection of the [18]ane S_4N_2 thione (X = S) and ketone (X = O) macrocyclic ligands **[4]** and **[5]**, followed by reaction with metal salts, $[L_xMX_m]^{n-}$

The product in each of the base deprotection, following degradation of the macrocyclic ring, is the dmit and dmid dianions **[1]** and **[2]**. After addition of the $[L_nMX_m]^{2-}$ the only identifiable product of the reaction is found to be the

$[dmitML_x]^{n-}$ or $[dmidML_x]^{n-}$ derivative. The lack of evidence for the presence of dmit or dmid dianions [1] and [2] in the mass spectrum of the starting macrocyclic ligands, [4] and [5] effectively rules out the possibility of impure starting materials. Test reactions were also carried out by reaction of the dmit dianion with the same metal salts. Analysis of the resultant products confirmed similar products from both reactions.

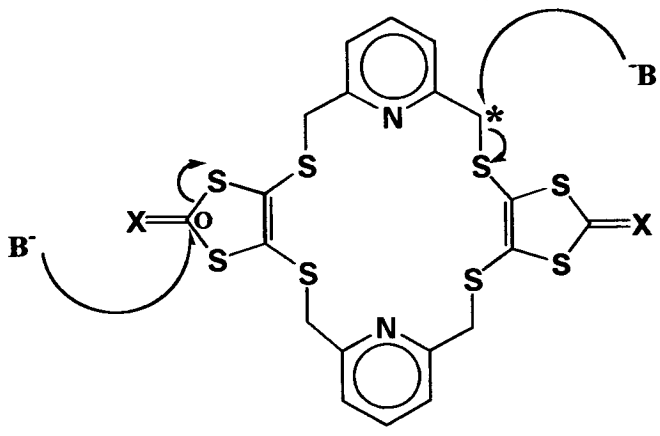

Figure 6.1 Mechanism for attempted nucelophilic base attack in the deprotection of the macrocyclic ring (O) with the actual observed reaction (*)

For example, if we consider the results of the reaction of the $[(bipy)_2RuCl_2].2H_2O$ compound with the TMAOH-deprotected [18]ane S_4N_2 thione macrocycle [4], we find evidence in the ^1H NMR and mass spectrum for the $[(bipy)_2Ru(dmit)]$ species [16]. Elemental analysis of this product was largely consistent with the $[(bipy)_2Ru(dmit)]$ product [16], although no further purification was attempted as this complex has already been described in the literature.

Similar reactions were carried out with NaOMe. In these cases, the results were identical to those observed with TMAOH with deprotection evidently again occurring at the macrocyclic ring.

A number of attempts to carry out deprotection with Cs_2CO_3 in MeOH were also carried out, however, in these cases no deprotection appeared to occur, either at the carbonyl/thione carbon or at the macrocyclic ring. This may be due to solubility problems, hampering the progress of the reaction.

Reactions carried out with $[Cp_2TiCl_2]$ and the [18]ane S_4N_2 thione macrocycle also involved preliminary base deprotection. The results of the analyses on these products were not easy to explain with extremely complex ^1H NMR data and indecipherable elemental analyses. The results are described in the experimental section.

Despite the successful deprotection of dithiolenes referred to in the literature (see Section 1.1.1.3b), from the results observed in the course of these reactions, base deprotection of the [18]ane S_4N_2 donor macrocycles [**4**] and [**5**] was unsuitable, attacking instead at the more susceptible CH_2 group next to the ring sulfur atom.

6.2 Reactions using the tetrathiaoxalate dianion $[NEt_4]_2$[tto] [3]

6.2.1 Introduction

As a result of the problems associated with base deprotection of the macrocyclic ligands [**4**] and [**5**], routes were explored, which eliminated the need for the involvement of a base. One such route, which has been developed in the course of this work is the photochemical decarbonylation experiment described in Chapter 5.

However, also attempted were routes using the highly reactive tetrathiaoxalate dianion [**3**].

Preparation of the precursor [**3**], was carried out according to the literature preparation[1], however the method described was found to be difficult to reproduce in some details. By making some significant changes to the preparative scheme introduced by Rauchfuss involving the more reactive intermediate Na_2S_2, we have successfully developed a reproducible and effectively higher yielding route to the reactive $[tto]^{2-}$ precursor $[C_2S_4]^{2-}$ [**3**]. The complete preparative route is outlined in the experimental section.

6.2.2 Attempted cyclisation of the $[NEt_4]_2[tto]$ [3] precursor with bis(bromomethyl)pyridine

Using the $[tto]^{2-}$ dianion [**3**], cyclisation with bis(bromomethyl)pyridine in a 1:1 ratio was attempted, however no evidence for the [18]ane S_4N_2 tetrathione macrocycle [**9**] was obtained, Scheme 6.2. On consideration of the precursor, the obvious repulsion between the negative charges on the thiolate sulfurs and the added repulsion between the lone-pairs of the thione sulphurs, forces the molecule to preferentially exist in a *trans-* conformation with respect to these groups. This may suggest why cyclisation of $[tto]^{2-}$ with bis(bromomethyl)pyridine has proven difficult, with formation of oligomeric species perhaps occurring instead.

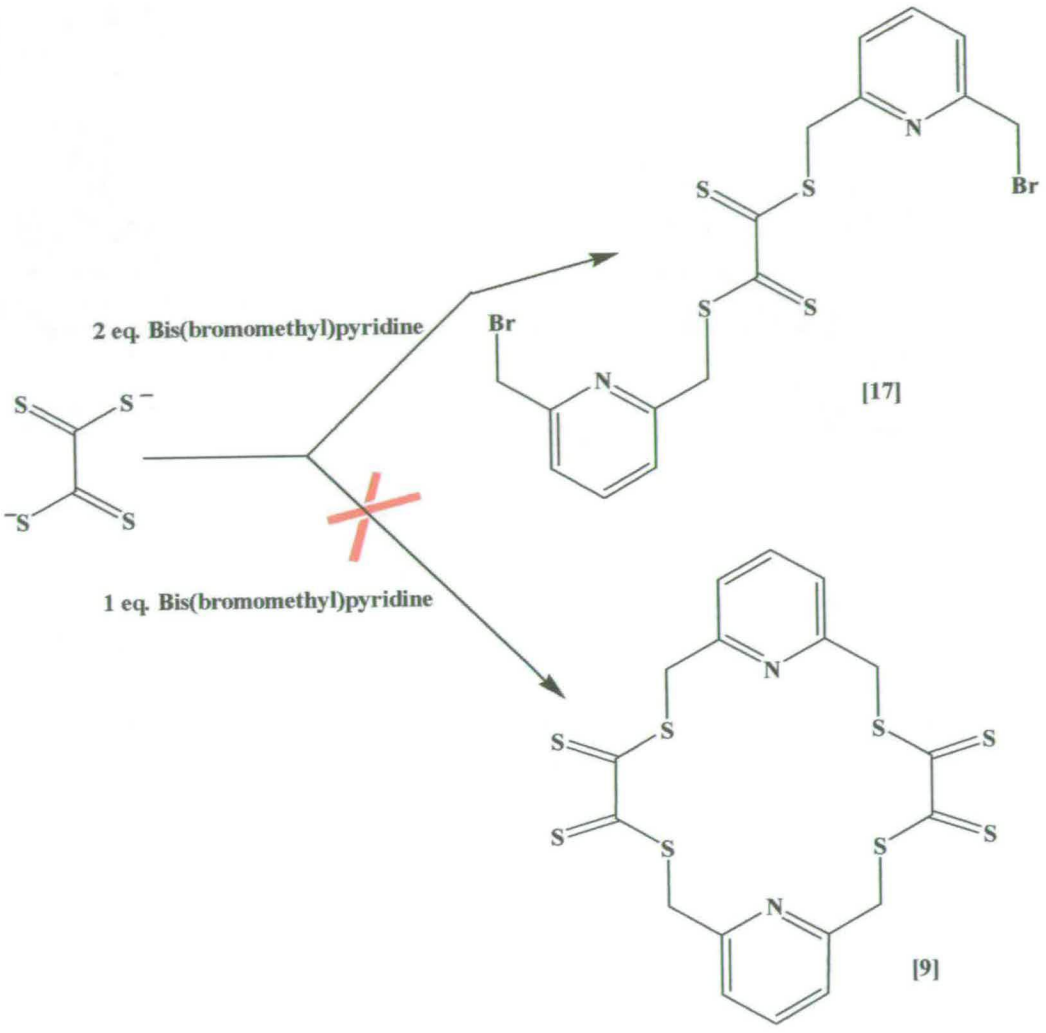

Scheme 6.2 Reaction of the $[tto]^{2-}$ dianion [**3**] with 1 and 2 equivalents of bis(bromomethyl)pyridine. Formation of $[(C_2S_4)(CH_2(C_5H_4N)CH_2Br)_2]$ [**17**]

We have, however, successfully reacted the $[tto]^{2-}$ dianion [**3**] with 2 equivalents of bis(bromomethyl)pyridine to form $[(C_2S_4)(CH_2(C_5H_4N)CH_2Br)_2]$ [**17**], Scheme 6.2. We expect that this system again exists with the thione groups and hence the CH_2-Br groups in a *trans*- conformation. Attempts to cyclise [**17**], with either another

equivalent of $[tto]^{2-}$ [**3**] or an equivalent of the dmit dianion [**1**], have failed, most likely for the same reasons as described before.

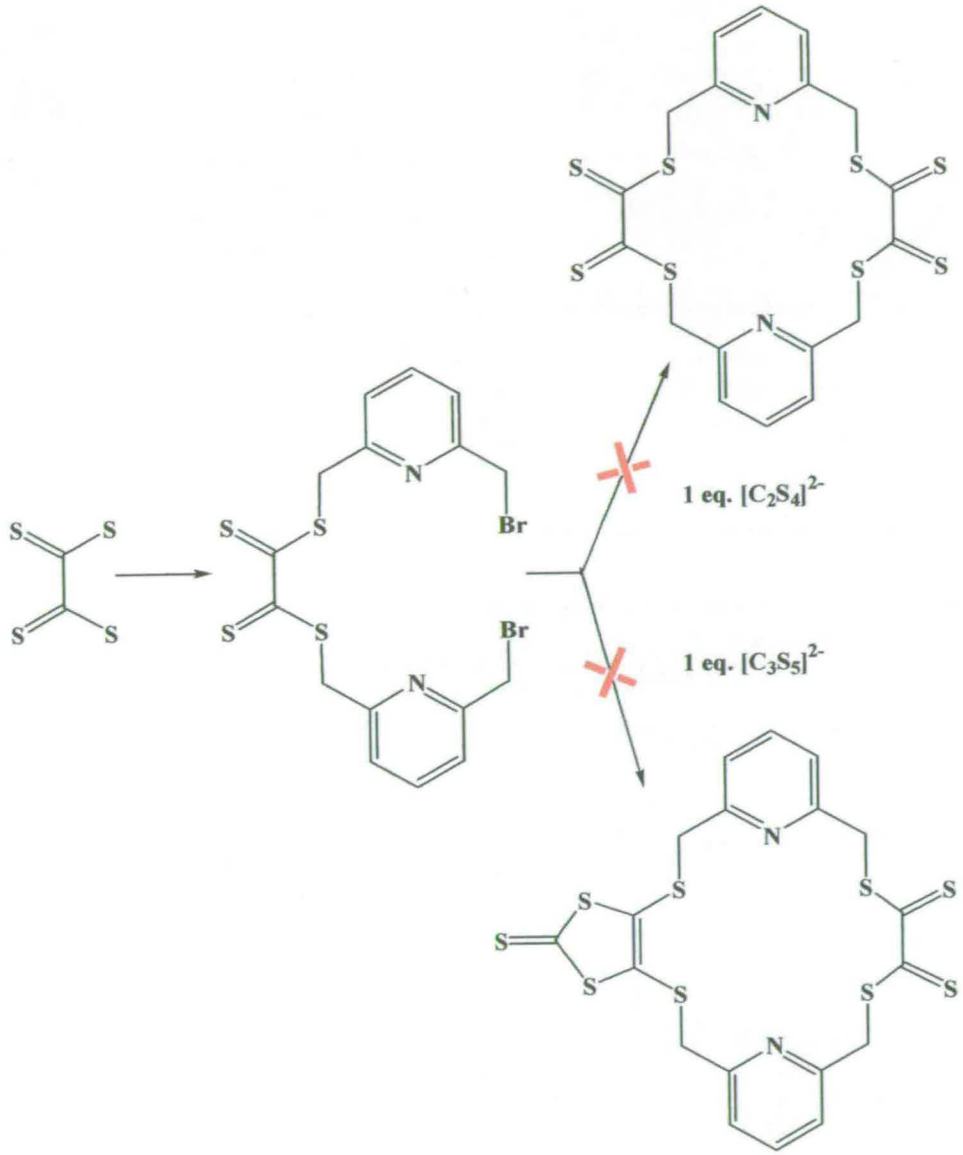

Scheme 6.3 Attempted cyclisations of $[(C_2S_4)(CH_2(C_5H_4N)CH_2Br)_2]$, [**17**], with $[C_2S_4]^{2-}$ [**3**] and $[C_3S_5]^{2-}$ [**1**]

By reaction of [**17**] with CpCoCOD, we have successfully prepared the cobalt derivative [$CpCoC_2S_4(CH_2(C_5H_4N)CH_2Br)_2$] [**18**]. In doing so we have forced the thione groups to form a *cis-* conformation, while also achieving a similar conformation with the CH_2-Br groups. Cyclisation should be straight forward. For unknown reasons however, attempts at cyclisation of this molecule have also proved unsuccessful.

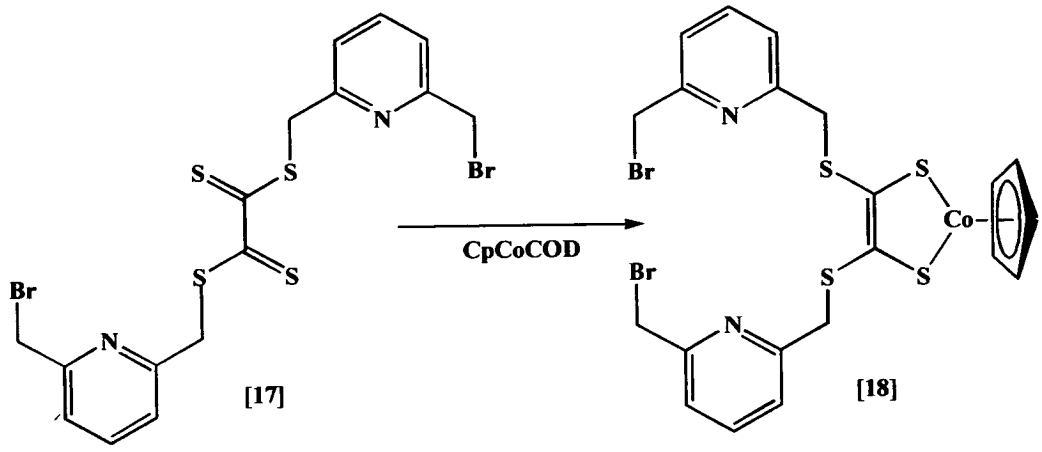

Scheme 6.4 Preparation of the cobalt derivative [$CpCoC_2S_4(CH_2(C_5H_4N)CH_2Br)_2$], [**18**]

With equal coordinating properties observed for CpCodmit and the ligand species [**17**], it is possible that any attempts to cyclise the species [**18**] with $[C_3S_5]^{2-}$ may have led to competition between both ligand systems {[**1**] and [**17**]} for the cobalt centre.

6.2.3 Attempted cyclisation of $[C_3S_5][(CH_2(C_5H_4N)CH_2Br)_2]$, [19]

Following the preparation of $[(C_2S_4)(CH_2(C_5H_4N)CH_2Br)_2]$, [**17**], and observing the cyclisation problems associated with the conformation of the molecule, it was proposed that the formation of the dmit analogue, $[(C_3S_5)(CH_2(C_5H_4N)CH_2Br)_2]$, [**19**], would force the CH_2-Br groups into a *cis*- conformation, making cyclisation of the system with [**3**] more favourable.

The formation of the $[(C_3S_5)(CH_2(C_5H_4N)CH_2Br)_2]$ [**19**], was successful by the reaction of the dmit dianion [**1**] with 2 equivalents of bis(bromomethyl)pyridine in methanol.

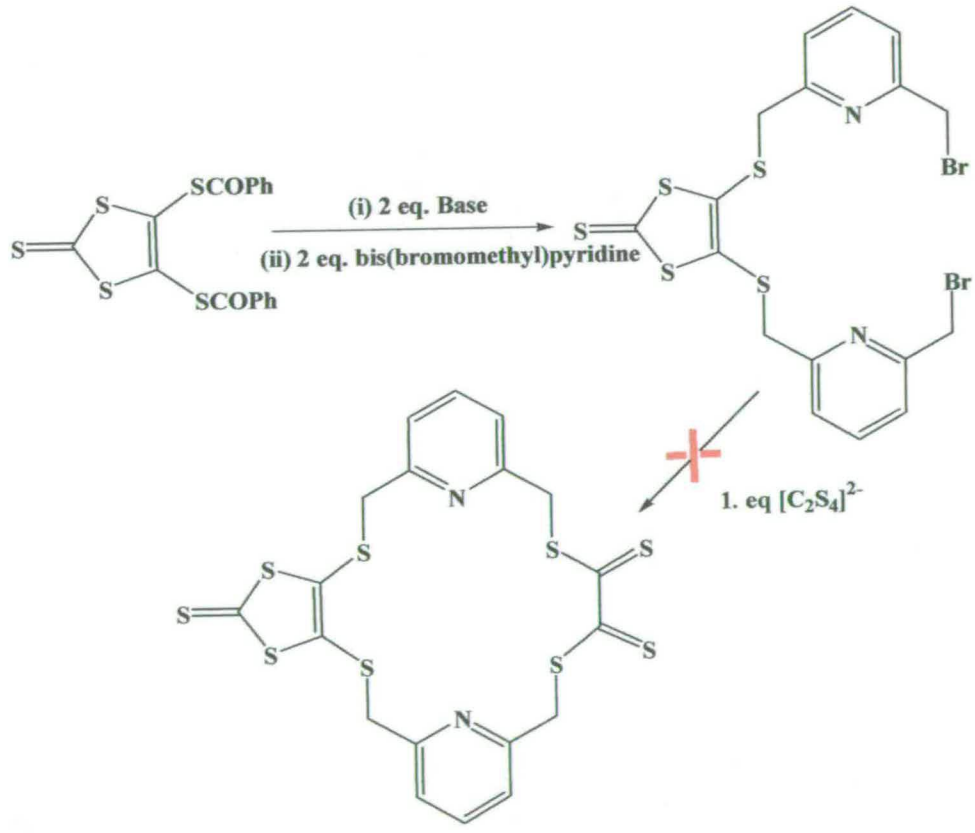

Scheme 6.5 Attempted cyclisation $[(C_3S_5)(CH_2(C_5H_4N)CH_2Br)_2]$ [**19**] with $[C_2S_4]^{2-}$ [**3**]

Also successfully prepared was the keto analogue $[(C_3S_4O)(CH_2(C_5H_4N)CH_2Br)_2]$ **[20]**, by reaction of **[19]** with $Hg(OAc)_2$ in CH_2Cl_2/AcOH. Attempts to cyclise **[20]** with an equivalent of **[3]** were, however, unsuccessful. This was again assumed to be as a result of the conformational difficulties of the $[tto]^{2-}$ **[3]** molecule.

6.3 Attempted *in-situ*, 'one-pot' cyclisation from $[(C_2S_4)(CH_2(C_5H_4N)CH_2Br)_2]$ [17] with $[ML_2]^{2-}$ salts

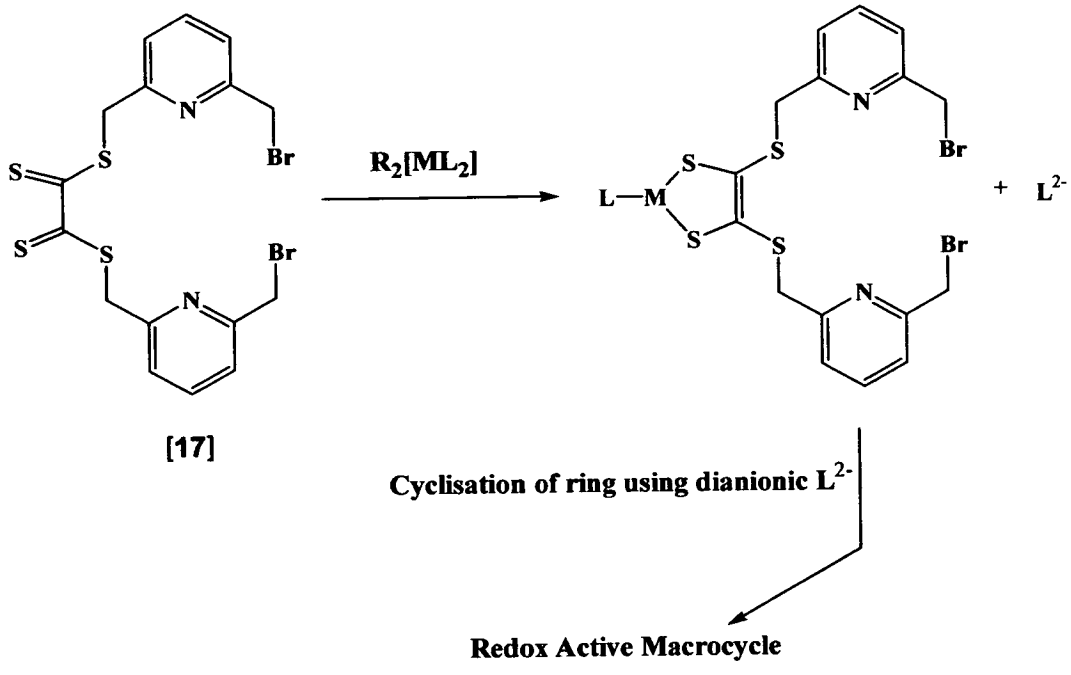

Scheme 6.6 Attempted route for the in-situ cyclisation of $[(C_2S_4)(CH_2(C_5H_4N)CH_2Br)_2]$ **[17]**, with metal salts $R_2[ML_2]$ {R = Na^+, $[NBu_4]^+$, $[NC_5H_5Et]_+$; M = Ni^{II}, Pd^{II}; L = $[mnt]^{2-}$$[dmit]^{2-}$}

Having observed the success of the reaction of the 2:1 bis(bromomethyl)pyridine : tto adduct with CpCoCOD, attempts were made to develop and expand this reaction to incorporate several other redox active metal units using metal salts of the general type $R_2[ML_2]$ {M = Ni, Pd; L = $[mnt]^{2-}$, $[dmit]^{2-}$; R = Na^+, $[NBu_4]^+$, $[C_5H_5NEt]^+$}.

Difficulties were observed with the cyclisation of $[CpCoC_2S_4(CH_2(C_5H_4N)CH_2Br)_2]$ **[18]** with $[C_2S_4]^{2-}$ **[3]**. As a result it was proposed that complexation to incorporate the redox unit followed by *in-situ* cyclisation of the macrocycle may be achievable.

The proposal involved the reaction of the ligand **[17]** with a metal salt of the type $[ML_2]^{2-}$, where the ligand coordinated to the metal via sulphur-metal bonds. By coordination to the metal of the highly reactive thione groups of the ligand **[17]**, the CH_2-Br groups would be forced into a cis- conformation with simultaneous elimination of an L^{2-} ligand from the metal coordination-sphere, which in turn would complete the cyclisation by reaction at the CH_2-Br carbons.

The reactions were carried out with $Na_2[Ni(mnt)_2]xH_2O$, $[NBu_4]_2[Ni(mnt)_2]$, $[NBu_4]_2[Pd(dmit)_2]$ and $[C_5H_5NEt]_2[Ni(dmit)_2]$. No decipherable peaks were observed in the mass spectrum in the case of the reaction with $Na_2[Ni(mnt)_2]$. In this case, coordination of the $[(C_2S_4)(CH_2(C_5H_4N)CH_2Br)_2]$ ligand **[17]** to the Ni, displaces an $[mnt]^{2-}$ ligand which, through rotation about its C-C axis, attains the more favourable *trans*-conformation of the sulfur atoms. The *trans*- geometry may make completion of the cyclisation process difficult.

Considering the free rotation with the $[mnt]^{2-}$ ligand, a second Ni species $[NBu_4]_2[Ni(dmit)_2]$ was used where the more rigid $[C_3S_5]^{2-}$ dianionic ligand would be displaced. Once again however no peaks were observed for any decipherable products. In this case, we may speculate that only oligomeric and/or polymeric materials are formed. No reaction was seen to occur in the case of the Pd salt. In the case of the Pd work, kinetic effects may once again be acting (see Chapter 5). Cleavage of the Pd-S bonds of the $[Pd(dmit)_2]^{2-}$ ligand is first of all required,

however as Pd is a second row transition metal, bond of this type are quite strong indicating a high energy barrier to the cleavage of the bond which is necessary before the coordination of the ligand [17] can take place.

6.4 Attempted stepwise preparation of the [18]ane S_4N_2 tetrathione macrocycle [9]

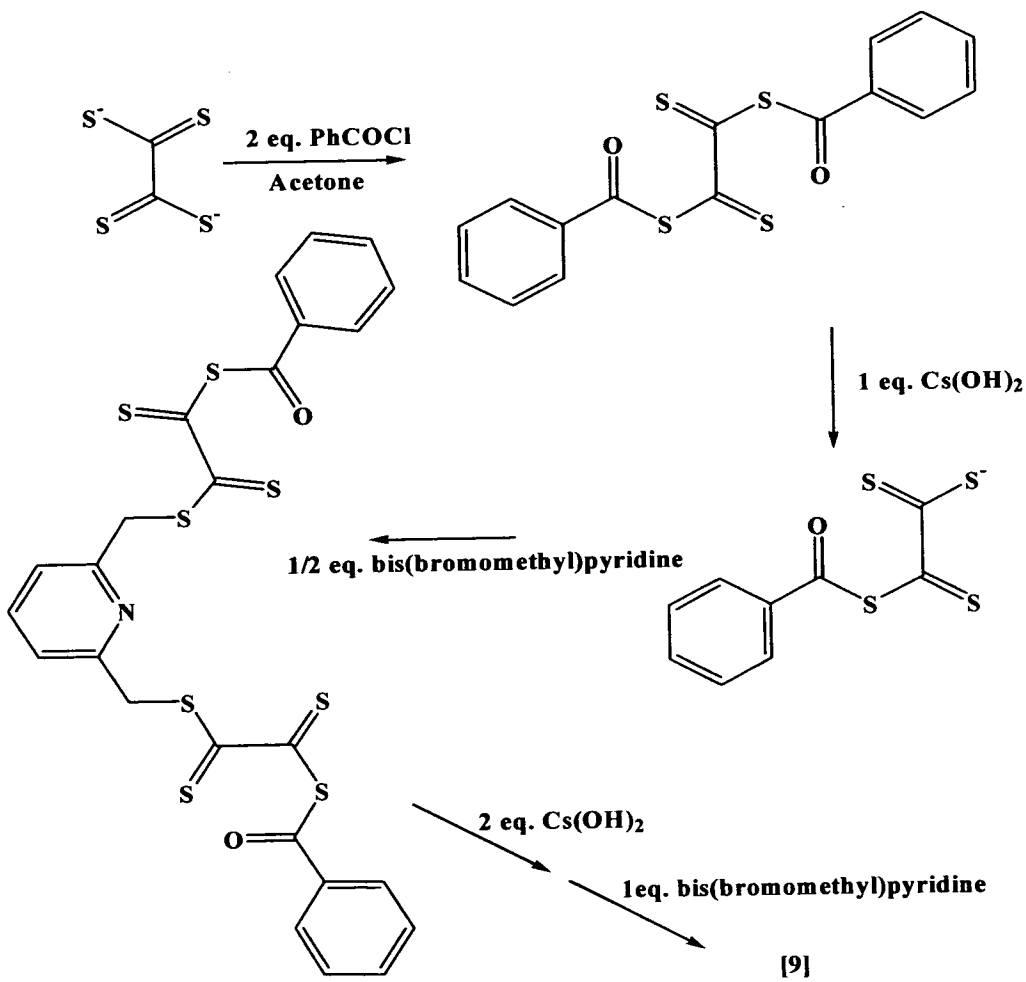

Scheme 6.7 Attempted cyclisation from the $[tto]^{2-}$ precursor [3] to prepare the tetrathione macrcycle [9]

As the more straight-forward routes to the cyclisation of the $[tto]^{2-}$ dianion were unsuccessful, it was thought that a stepwise approach, beginning from the acylated product, may be more productive as the instability of $[tto]^{2-}$, **[3]** in solution may have been a problem.

In a similar manner as the derivatisation of the dmit dianion **[1]**, bezoylation of the $[C_2S_4]^{2-}$ species **[3]**, was carried out successfully to form $[C_2S_4(COPh)_2]$. From this the selective mono-deprotection of one of the protected sulphur atoms was carried out using 1 equivalent of $Cs(OH)_2$. Reaction of the mono-deprotected species was then carried out with half an equivalent of bis(bromomethyl)pyridine to attempt to form the 2:1 tto:bis(bromomethyl)pyridine species **[17]**. Evidence for this species was seen in mass spectrometry however, purification proved difficult.

Using the impure sample of **[17]**, 2 equivalents of $Cs(OH)_2$ were added to deprotect the two benzoyl groups. This was followed by attempted cyclisation with bis(bromomethyl)pyridine to form the tetrathione macrocycle. While evidence of the final macrocycle was seen in the mass spectrum, once again isolation of the species could not be achieved, most likely due to the presence of oligomeric species.

6.5 Conclusions

In an attempt to attach redox active units to the [18]ane S_4N_2 donor macrocycle **[4]** a number of methods have been attempted. The standard method of deprotection of 1,3-dithiole-2-one species to give dithiolene ligands, has been to react them with base (either TMAOH, NaOMe or $Cs(OH)_2$). Under similar reaction conditions using the starting macrocyclic ligands **[4]** or **[5]** problems arise in which the base preferentially abstracts a proton from the macrocyclic ring in preference to attack at the thione or ketone carbons.

In order to eliminate the need for the use of a base deprotection, the preparative conditions[1] of the $[NEt_4]_2[tto]$ **[3]**, were implemented. The incorporation of this precursor into a macrocyclic system would allow for the highly reactive thione sulphurs to coordinate readily to metal species thereby incorporating them into the system as the redox centres. A large number of routes were attempted to cyclise the $[tto]^{2-}$ dianion **[3]** with bis(bromomethyl)pyridine in the process of which we have successfully prepared two systems which may have promise as complexing ligands. The first is the $[(C_2S_4)(CH_2(C_5H_4N)CH_2Br)_2]$, **[17]** and the second, the dmit analogue $[(C_3S_5)(CH_2(C_5H_4N)CH_2Br)_2]$ **[19]**.

It was attempted to cyclise $[(C_2S_4)(CH_2(C_5H_4N)CH_2Br)_2]$, **[17]** with $[dmit]^{2-}$ **[1]** and $[tto]^{2-}$ **[3]**, however analyses showed no evidence for the formation of the cyclic product. Attempts to carry out an *in-situ* cyclisation of the ligand **[17]** with $[ML_2]^{2-}$ salts, however these reactions also formed only oligomeric and polymeric materials.

Attempts to cyclise the $[tto]^{2-}$ precursor were also carried out by initially benzoylating the $[tto]^{2-}$ dianion **[3]** and from there, carrying out selective deprotections with $Cs(OH)_2$ and reactions with bis(bromomethyl)pyridine. While there is evidence for this sequence of reactions actually working, the isolation of the

relevant materials from the oligomeric mixture has, unfortunately, proven very difficult.

While some progress was made with these routes, in particular those involving the ligands $[(C_2S_4)(CH_2(C_5H_4N)CH_2Br)_2]$ **[17]** and $[(C_3S_5)(CH_2(C_5H_4N)CH_2Br)_2]$ **[19]**, due to time limitations work was not completed in this area. The most successful routes for the deprotection of the thione and ketone groups are those involving Hg irradiation (Chapter 5). Alternatively, the route described in Chapter 5 for the *in-situ* deprotection of the thione/ketone groups, though limited to the incorporation of CpCo- units is highly successful for the preparation of redox active macrocycles.

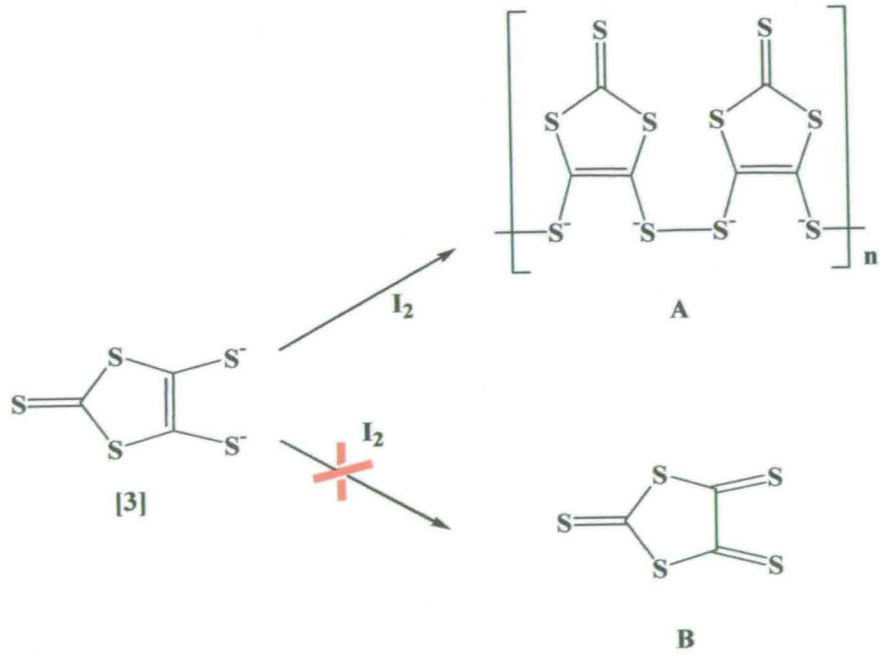

Figure 6.2 Oxidation of the dmit dianion **[1]** which favours the formation of an oligomeric species **[A]** over a bisthione species **[B]**

The unsuccessful cyclisations of the ligands $[(C_2S_4)(CH_2(C_5H_4N)CH_2Br)_2]$, **[17]** with $[tto]^{2-}$ **[3]** are attributed to the very large repulsive force between the thione

sulfurs and also between the negatively charged thiolate sulfurs of [**3**]. These repulsive forces enforce a *trans-* geometry on the system, making attack of both thiolate sulfurs at the CH_2-Br carbons on the same molecule of [**17**] or [**18**], very unlikely. More probable, in this case is the formation of oligomeric species.

Coupled with this repulsive force between the lone-pair orbitals on the thione sulfurs, is an intrinsic instability within any species of the form $[R_2S_2C_2(=S)_2]$ where the thiones groups have a *cis-* geometry. This instability may make it almost impossible to isolate species of this type which include the [18]ane S_4N_2 tetrathione macrocycle [**9**]. An example is the oxidation of the dmit dianion [**1**] shown in Figure 6.2.

In the example described in Figure 6.2 the oxidation of the product to the oligomer [**A**] is favoured over the formation of the bisthione product [**B**] due to ability of the system to avoid a compound, which holds the thione sulfurs in the unfavoured *cis-* geometry

While the isolation of these types of species may be impossible, it is clear from the work described in Chapter 5, that *in-situ* use of these compounds is possible.

6.6 Experimental

6.6.1 Introduction

All reactions were carried out in distilled solvent and under an inert atmosphere unless otherwise stated.

6.6.2 Experimental

Preparation of the dmit [1] and dmid [2] dianions and the [18]ane S_4N_2 donor macrocycle [4] and [5]

The preparation of the dmit and dmid dianionic species [**1**] and [**2**] respectively, were carried out as described in the literature[2]. The formation of the [18]ane S_4N_2 thione macrocycle [**4**] followed another literature preparation [3]. The keto derivative [**5**] was made using an identical route to [**4**] using the dmid dianion [**2**] in place of the dmit dianion [**1**].

Deprotection of the [18]ane S_4N_2 thione and ketone macrocyclic ligands [4] and [5] and reaction with $[(p\text{-cymene})RuCl_2]_2$, $[(bipy)_2RuCl_2]xH_2O$, $[Cp_2TiCl_2]$, and $[((dppe)NiCl_2]xH_2O$

1. [18]ane S_4N_2 thione macrocycle [4]

a. Reaction with $[(p\text{-cymene})RuCl_2]_2$: To a stirred solution of the [18]ane S_4N_2 thione macrocycle [**4**] {0.10 g; 0.17 mmol} in 40 ml of ethanol was added a 1 ml solution of 4 equivalents of TMAOH {0.11 g; 0.66 mmol}. The reaction mixture was

allowed to stir until all solid material was completely dissolved. To the resultant yellow solution was added 1 equivalent of [(*p*-cymene)$RuCl_2$]$_2$, drop-wise, overnight. The resultant brown precipitate was filtered and collected (54 mg). Calculated 43.20 %C, 3.98 %H, 2.65 %N for $C_{38}H_{42}Cl_2N_2Ru_2S_8$. Found 34.91 %C, 3.17 %H, 0.39 %N. FAB MS m/z = 461 D. ^{1}H NMR [$CDCl_3$] δ_H = 1.28 [($C\underline{H}_3$)$_2$CHPh(CH_3)]-Ru; 6H, d), 2.65 ([(CH_3)$_2$C$\underline{H}$Ph(CH_3)]-Ru; 1H, sept), 7.18 ([(CH_3)$_2$CH$C_6\underline{H}_4$(CH_3)]; 4H, ABBA quartet), 2.31 ([(CH_3)$_2$CHPh($C\underline{H}_3$)]-Ru; 3H,s) ppm.

b. Reaction with [(bipy)$_2$RuCl$_2$].2H$_2$O : To a stirred solution of the [18]ane S_4N_2 thione macrocycle **[4]** {0.10 g; 0.17 mmol} in 40 ml ethanol, was added 4 equivalents of [NMe_4]OH {0.11 g; 0.67 mmol} in 1 ml MeOH. To the resultant red solution was added [(bipy)$_2$RuCl$_2$].2H$_2$O {0.17 g; 0.33 mmol} drop-wise, over-night. After 24 hours the dark brown/purple precipitate was collected (23 mg) by filtration. Calculated 51.91 %C; 3.44 %H; 8.35 %N for $C_{58}H_{46}N_{10}S_8Ru_2$. Found 44.37 %C; 3.29 %H; 9.05 %N. FAB MS m/z = 609.3. 639, 714, 742, 790 D.

c. Reaction with [(Cp)$_2$TiCl$_2$] : To a stirring suspension of the [18]ane S_4N_2 thione macrocycle **[4]** {0.10 g; 0.17 mmol) in 20 ml THF, was added 4 equivalents of TMAOH {0.11 g; 0.67 mmol} in 1 ml MeOH. To the resultant red solution was added a solution of [(Cp)$_2$TiCl$_2$] in 30 ml THF and the reaction mixture was allowed to reflux. Reflux was maintained for three hours after which the resultant red reaction mixture was observed. The reaction was allowed to cool and a precipitate was seen to form which was collected as a red solid and analysed Calculated 52.39 %C; 3.91 %H; 3.22 %N for $C_{38}H_{34}N_2S_8Ti_2$. Found 39.99 %C; 2.72 %H; 3.22 %N. FAB MS m/z = 514, 728, 893, 1003 1130, 1258 D. ^{1}H NMR [$CDCl_3$] δ_H = 1.60 (2H, s); 4.05 (5H, m); 6.45 (10H, m); 7.23 (2H, m) ppm.

2. [18]ane S_4N_2 ketone macrocycle [5]

a. Reaction with [(dppe)NiCl$_2$]$_5$H$_2$0 : The [18]ane S_4N_2 ketone macrocycle **[5]** {0.02 g; 0.04 mmol} was suspended in 50 ml of distilled EtOH. To the solution was

added 4 equivalents of tetramethylammonium hydroxide TMAOH {0.03 g; 0.15 mmol). To the resultant yellow solution was added dropwise, an ethanol solution of 2 equivalents of [(ddpe)$NiCl_2$] {0.06 g; 0.07 mmol; 25 ml EtOH}. The reaction was allowed to continue overnight. After 24 hours the reaction mixture was found to be a brown/black colour with no precipitate formed. Rotary evaporation to approximately 3 ml gave no further evidence for precipitation.

b. Reaction with [(bipy)$_2$RuCl$_2$].xH$_2$0 : To a stirring solution of the [18]ane S_4N_2 ketone macrocycle **[5]** {0.05 g; 0.09 mmol}in 50 ml of EtOH was added 4 equivalents of [NMe_4]OH {0.06 g; 0.37 mmol} in 2 ml MeOH. Deprotection was allowed to continue until all solid material was dissolved. To the resultant yellow solution was added 2 equivalents of [(bipy)$_2$$RuCl_2$].x$H_2$0 in 100 ml EtOH. The addition was made drop-wise, overnight. After 24 hours the reaction mixture was filtered and the volume of the filtrate reduced to 35 ml. An equal volume of hexane was added and the reaction mixture was stored over night at –20 °C. The resultant precipitate was filtered off and collected as a brown solid (43 mg). Calculated 51.91 %C; 3.44 %H; 8.35 %N for $C_{58}H_{46}N_{10}S_8Ru_2$. Found 43.69 %C; 3.14 %H; 8.60 %N. FAB MS m/z = 609, 766, 856, 1049 D.

c. Reaction with [(p-cymene)RuCl$_2$]$_2$: To a suspension of the [18]ane S_4N_2 ketone macrocycle **[5]** {0.05 g; 0.08 mmol} in 40 ml THF was added 4 equivalents of [NMe_4]OH {0.06 g; 0.35 mmol} in 2 ml MeOH. To the resultant yellow reaction mixture was added drop-wise, 1 equivalent of a methanol solution of [(*p*-cymene)$RuCl_2$]$_2$ {0.06 g; 0.18 mmol}. Upon complete addition of the ruthenium salt, the resultant red reaction mixture showed no indication of precipitate formation. The volume was reduced by half and was kept at –20 °C overnight. The pale precipitate collected by filtration in 14 % yield was analysed. Calculated 43.20 %C, 3.98 %H, 2.65 %N for $C_{38}H_{42}Cl_2N_2Ru_2S_8$. Found 34.42 %C, 3.23 %H, 0.24 %N.

Attempted cyclisation of the $[tto]^{2-}$ dianion [3] with bis(bromomethyl)pyridine

To a stirring solution of the bis(bromomethyl)pyridine {0.06 g; 0.2 mmol} in 40 ml MeOH was added dropwise a solution of $[tto]^{2-}$ [3] {0.100 g; 0.2 mmol) in 40 ml MeOH. A yellow/orange material was found to precipitate. This was collected by filtration (10 mg). Calculated 41.98 %C, 2.72 %H, 5.44 %N for $C_{18}H_{14}S_8N_2$. Found 41.17 %C, 5.25 %H, 5.47 %N. FAB MS m/z = 514, 520, 531, 589, 616, 744 D.

Preparation of $[(C_2S_4)(CH_2(C_5H_4N)CH_2Br)_2]$ [17] by reaction of $[tto]^{2-}$ [3] with 2 equivalents of bis(bromomethyl)pyridine.

To a stirring solution of bis(bromomethyl)pyridine {0.43 g; 1.0 mmol} was added dropwise a solution of the $[tto]^{2-}$ dianion, [3] {0.56 g; 2.0 mmol in 40 ml MeOH}. The orange precipitate was collected in 56 % yield by filtration. Calculated for $C_{16}H_{14}S_4N_2Br_2$ 36.78 %C, 2.68 %H, 5.36 %N. Found 37.00 %C, 2.63 %H, 4.81 %N. FAB MS [THIO-THF] m/z = 433, 523, 541 (M^+) D.

Preparation of $[CpCoC_2S_4(CH_2(C_5H_4N)CH_2Br)_2]$ [18]

A mixture of $[(C_2S_4)(CH_2(C_5H_4N)CH_2Br)_2]$ [17] {0.15 g; 0.28 mmol} and $CpCo(CO)_2$ {0.17 g; 0.30 mmol} in 50 ml THF was allowed to stir for 30 minutes. The green-brown mixture was then refluxed for 30 minutes, whereupon a brown dark precipitate was seen to form. Stirring was continued for a further 30 minutes at which point the resultant green precipitate of [18] was filtered off and collected in 54 % yield. Calculated for $C_{21}H_{19}N_2S_4Br_2Co$. 39.01 %C, 2.94 %H, 4.33 %N. Found 39.49 %C, 3.17 %H, 4.52 %N. FAB MS [NOBA-DMF] m/z = 661 (M^+), 681, 756 D.

Attempted cyclisation of $[(C_2S_4)(CH_2(C_5H_4N)CH_2Br)_2]$ [17] with 1 equivalent of $[tto]^{2-}$ [3]

To a 100ml round bottom flask was added simultaneously a MeOH solution of $[tto]^{2-}$ [3] {0.11 g; 0.28 mmol in 60 ml MeOH} and a THF solution of $[(C_2S_4)(CH_2(C_5H_4N)CH_2Br)_2]$ [17] {0.16 g; 0.28 mmol in 60 ml THF}. The reaction mixture was seen to go a pale yellow colour however analysis showed no evidence for the cyclised product. Calculated 41.98 %C, 2.72 %H, 5.44 %N for $C_{18}H_{14}S_8N_2$. Found 36.53 %C, 4.56 %H, 1.71 %N

***In-situ*, 'one-pot' cyclisation from $[(C_2S_4)(CH_2(C_5H_4N)CH_2Br)_2]$ [17] with $[ML_2]^{2-}$ salts**

a. **Reaction with $Na_2[Ni(mnt)_2]$** : Addition of the salt $Na_2[Ni(mnt)_2]$ {0.06 g; 0.15 mmol in 20 ml THF} to a solution of $[(C_2S_4)(CH_2(C_5H_4N)CH_2Br)_2]$ [17] {0.008 g; 0.15 mmol in 20 ml THF) gave a red solution with a pale precipitate. The reaction was allowed to stir under N_2 overnight after which the precipitate was filtered, and collected which was analysed to be recovered starting material. FAB MS [THF-NOBA] m/z = 547, 582, 601 D.

b. **Reaction with $[NBu_4]_2[Ni(dmit)_2]$** : Addition of the salt $[NBu_4]_2[Ni(dmit)_2]$ {0.04 g; 0.04 mmol in 20 ml THF} to a solution of $[(C_2S_4)(CH_2(C_5H_4N)CH_2Br)_2]$ [17] {0.02 g; 0.04 mmol in 20 ml THF) gave a green solution with a pale precipitate. The reaction was allowed to stir under N_2 overnight after which the precipitate was filtered, collected (0.04 mg) and submitted for analysis. No decipherable peaks apart from matrix were observed in the mass spectrum (FAB MS) obtained.

c. **Reaction with $[NBu_4]_2[Pd(dmit)_2]$** : Addition was made of $[NBu_4]_2[Pd(dmit)_2]$ {0.15 g; 0.15 mmol in 20 ml THF}drop-wise to a solution of $[(C_2S_4)(CH_2(C_5H_4N)CH_2Br)_2]$, [17] {0.08 g; 0.15 mmol in 20 ml THF}. The reaction mixture was stirred over 12 hours and the orange precipitate was filtered off and

collected. Analysis showed the product to be recovered starting material. FAB MS [THF-NOBA] m/z = 864, 800, 754, 725 D.

d. Reaction with $[Et\text{-}C_5H_5NEt]_2[Ni(dmit)_2]$: Addition was made of $[Et\text{-}C_5H_4NEt]_2[Ni(dmit)_2]$ {0.10 g; 0.15 mmol in 20 ml THF}drop-wise to a solution of $[(C_2S_4)(CH_2(C_5H_4N)CH_2Br)_2]$, [17] {0.08 g; 0.15 mmol in 20 ml THF}. The reaction mixture was allowed to stir over 12 hours and the deep red precipitate (73 mg) was filtered off. Analysis showed the precipitate to be recovered starting material. No decipherable peaks were observed in the mass spectrum (FAB MS) apart from matrix.

Preparation of $[(C_3S_5)(CH_2(C_5H_4N)CH_2Br)_2]$, [19] from the reaction of the $[dmit]^{2-}$ dianion [1] with 2 equivalents of bis(bromomethyl)pyridine.

To a stirred solution of the bis(bromomethyl)pyridine {0.66 g; 3.0 mmol in 50 ml MeOH} was added dropwise a solution of the $[dmit]^{2-}$ dianion [1] {0.51 g; 1.5 mmol (previously deprotected with NaOMe {0.13 g; 3.0 mmol}) in 50 ml MeOH}. A yellow precipitate of $[(C_3S_5)(CH_2(C_5H_4N)CH_2Br)_2]$ [19], formed and was collected in 25 % yield. Calculated 36.04 %C; 2.48 %H; 4.95 %N for $C_{17}H_{14}S_5Br_2N_2$. Found 36.63 %C; 2.39 %H; 4.62 %N. FAB MS (NOBA-THF) m/z 566, 547 (M^+) D.

Attempted cyclisation of $[(C_3S_5)(CH_2(C_5H_4N)CH_2Br)_2]$ [19] with 1 equivalent of the $[tto]^{2-}$ dianion [3]

A MeOH solution of $[tto]^{2-}$ [3] {0.06 g; 0.15 mmol in 30 ml MeOH} was added dropwise to a stirred solution of $[(C_3S_5)(CH_2(C_5H_4N)CH_2Br)_2]$, [19]. The resultant red-orange solution yielded a pale precipitate. Calculated 40.82 %C; 2.51 %H; 5.01 %N for $C_{19}H_{14}S_9N_2$. Found 35.26 %C; 2.24 %H; 4.00 %N. FAB MS [NOBA-THF] m/z = 766, 749, 666, 624 D.

Stepwise addition from the benzoylated derivative of $[NEt_4]_2[tto]$, [3]

1. Benzoylation of $[tto]^{2-}$ [3] to give $[(C_2S_4)(COPh)_2]$, [21]

To a MeOH solution of the $[tto]^{2-}$ dianion [**3**] {0.30 g; 0.73 mmol in 20 ml MeOH} was added 2 equivalents of benzoyl chloride {0.17 ml; 1.46 mmol}. The mixture was found to form a yellow precipitate almost immediately. The precipitate of $[(C_2S_4)(COPh)_2]$ [**21**] was filtered off and collected in 73 % yield. Calculated 41.34 %C; 3.45 %H for $C_{10}H_{10}S_4O_2$. Found 41.12 %C, 3.21 %H. FAB MS [THIO-CH_2Cl_2] m/z = 312 (M^+), 290, 185 D.

2. Reaction of the partially hydrolyzed benzoylated product $[(C_2S_4)(COPh)_2]$ [21] with 0.5 equivalents of bis(bromomethyl)pyridine

Addition of a MeOH solution of $Cs(OH)_2$ {0.03 g; 0.50 mmol in 3 ml MeOH} was made to a MeOH suspension of the benzoylated product $[(C_2S_4)(COPh)_2]$ [**21**] {0.35 g; 0.001 mmol}. This solution was added dropwise to a stirring solution of bis(bromomethyl)pyridine {0.13 g; 0.5 mmol in 15 ml MeOH}. A yellow precipitate was collected (21 mg) and analysed by mass spectrometry (FAB MS), however no peaks were observed other than matrix.

Calculated 48.43 %C, 2.75 %H, 2.26 %N for $C_{25}H_{17}S_8NO_2$. Found 43.25 %C, 2.63 %H, 1.97 %N.

3. Reaction of the product of step 2, with 1 equivalent of bis(bromomethyl)pyridine

Deprotection of the assumed product from Step 2, $[(COPh)(C_2S_4)]_2[(CH_2C_5H_4NCH_2)]$, [**22**] {0.08 g; 0.13 mmol in 10 ml MeOH} with 2 equivalents of NaOMe {0.01 g; 0.26 moles in 10 ml MeOH} was carried out under N_2. The reaction mixture was then added drop-wise to a MeOH solution {0.04 g; 0.13 mmol in 20 ml}. A red-orange precipitate was collected (40mg). Calculated 44.57 %C, 2.59 %H, 5.19 %N for $C_{20}H_{14}S_8N_2$. Found 37 %C, 2.21 %H, 3.72 %N.

6.7 References

1 J. C. Lodmell, W. C. Anderson, M. F. Hurley and J. Q. Chambers, *Anal. Chim. Acta,* 1981, **129**, 49

2 N. Svenstrup, J. Becher, *Synthesis*, 1995, 215

3 B. Girmay, J.D. Kilburn, A.E. Underhill, K.S.Varma, M.B..Hursthouse, M.E. Harman, J. Becker,G. Bojesen, *J. Chem. Soc., Chem. Com.* 1989, 1406

Appendices

Appendix 1 Crystal Structure Details

Appendix A1.1 CpCo[dmit] [8] - $P2_1/c$

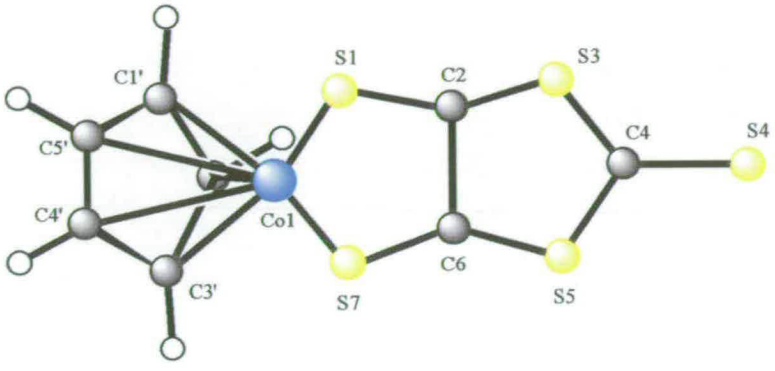

Table A1.1.1 Crystal data and structure refinement for [CpCo(dmit)] **[8]** (P21/c)

Empirical Formula	$C_{16}H_{10}Co_2S_{10}$
Formula weight	640.70
Wavelength	0.71073 A
Temperature	150(2) K
Crystal system	Monoclinic
Space group	P21/c
Unit cell dimensions	a = 5.8934(2) A $\alpha = 90^o$ b = 7.8204(3) A $\beta = 97.119(3)^o$ c = 23.1984(11) A $\gamma = 90^o$
Volume	1060.94(7) A^3

Z	2
Density (calculated)	2.006 Mg/m^3
Absorption coefficient	2.551 mm^{-1}
F(000)	640
Crystal description	Green plate
θ range for data collection	2.75 to 29.12°
Index ranges	-7<=h<=7, -10<=k<=10, -31<=1<=31
Reflections collected	14358
Independent refelctions	2834 [R(int) = 0.0820]
Scan type	θ-ϕ
Absorption correction	Sortav (Tmin = 0.762, Tmax = 0.85)
Solution	Direct (SIR92)
Refinement type	Full-matrix least-squares on F^2
Program used for refinement	SHELXL-97
Hydrogen atoms placement	Geometric
Hydrogen treatment	Riding
Data / restraints / parameters	2834 / 0 / 127
Goodness-of-fit on F^2	0.998
Conventional R [F.4sigma (F)]	R1 = 0.0426 [1868 data]
Weighted R (F^2 and all data)	WR2 = 0.0914
Final Maximum delta / sigma	0.001
Weighting scheme	Calc $w=1/\{\s^2(Fo^2) + (0.0.0361P)^2 + 0.0000P\}$ where $P = (Fo^2 + 2Fc^2) / 3$
Largest diff. Peak and hole	0.736 and –0.633 $e.A^{-3}$

Table A1.1.2 Selected bond lengths [Å] and angles [°] for [CpCo(dmit)] [**8**] (P21/c)

Co(1) - C(5')	2.024(4)
Co(1) – C(1')	2.030(4)

Co(1) – C(4')	2.033(4)
Co(1) – C(2')	2.036(4)
Co(1) – C(3')	2.042(4)
Co(1) – S97)	2.1223(9)
Co(1) – S(1)	2.1273(10)
S(1) – C(2)	1.709(3)
C(2) – C(6)	1.381(4)
C(2) – S(3)	1.732(4)
S(3) – C(4)	1.728(3)
C(4) – S(4)	1.657(4)
C(4) – S(5)	1.728(3)
S(5) – C(6)	1.739(3)
C(6) – S(7)	1.704(3)
C(1') – C(2')	1.407(5)
C(1') – C(5')	1.417(6)
C(2') – C(3')	1.400(5)
C(3') – C(4')	1.379(5)
C(4') – C(5)	1.383(6)
C(5') – Co(1) – C(1')	40.91(19)
C(5') – Co(1) – C(4')	39.85(17)
C(1') – Co(1) – C(4')	68.06(18)
C(5') – Co(1) – C(2')	67.91(17)
C(1') – Co(1) – C(2')	40.50(16)
C(4') – Co(1) – C(2')	67.69(15)
C(5') – Co(1) – C(3')	66.63(16)
C(1') – Co(1) – C(3')	67.43(15)
C(4') – Co(1) – C(3')	39.55(15)
C(2') 0 Co(1) – C(3')	40.15(14)
C(5') – Co(1) – S(7)	152.73(16)
C(1') – Co(1) – S(7)	153.78(15)

C(4') – Co(1) - S(7)	113.90(13)
C(2') – Co(1) – S(7)	114.26(11)
C(3') – Co(1) – S(7)	96.99(10)
C(5') – Co(1) – S(1)	102.68(14
C(1') – Co(1) – S(1)	103.79(12)
C(4') – Co(1) – S(1)	132.40(12)
C(2') – Co(1) - S(1)	136.03(11)
C(3') – Co(1) – S91)	169.21(11)
S(7) – Co(1) – S(1)	93.44(4)
C(2) – S(1) – Co(1)	103.29(12)
C(6) – C(2) – S(1)	119.4(3)
C(6) – C(2) – S(3)	116.4(3)
S(1) – C(2) – S(3)	124.21(18)
C(4) – S(3) – C(2)	97.26(16)
S(4) – C(4) –S(3)	123.9(2)
S(4) – C(4) 0 S(5)	122.52(18)
S(3) - C(4) – S(5)	113.5(2)
C(4) – S(5) – C(6)	97.61(16)
C(2) – C(6) – S(7)	120.8(3)
C(2) – C(6) – S(5)	115.2(3)
S(7) – C(6) – S(5)	124.01(18)
C(6) - S(7) – Co(1)	102.97(10)
C(2') – C(1') – C(5')	106.8(3)
C(2') – C(1') – Co(1)	70.0(2)
C(5') – C(1') – Co(1)	69.3(2)
C(3') – C(2') – C(1')	107.3(3)
C(3') – C92') – Co(1)	70.2(2)
C(1') – C(2') – Co(1)	69.5(2)
C(4') – C(3') – C(2')	109.3(3)
C(4') – C(3') – Co(1)	69.9(2)

C(2') – C(3') – Co(1)	69.7(2)
C(3') – C(4') – C(5')	108.0(4)
C(3') – C(4') – Co(1)	70.6(2)
C(5') – C(4') – Co(1)	69.7(2)
C(4') – C95') – C(1')	108.6(4)
C(4') – C(5') – Co(1)	70.4(2)
C(1') – C(5') – Co(1)	69.8(2)

Appendix A1.2 CpCo[dmit] [8] – Pbcn

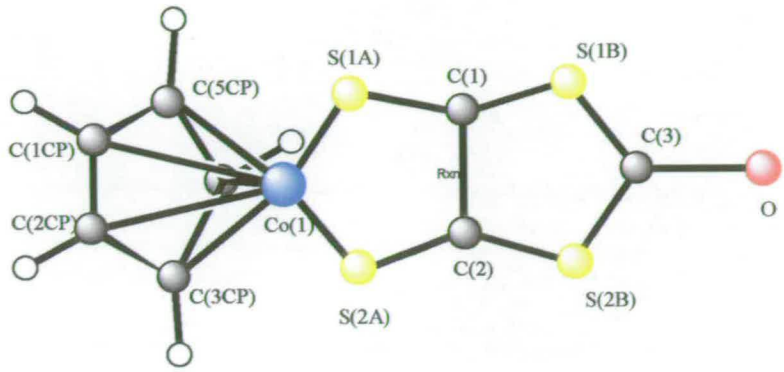

Table A1.2.1 Crystal data and structure refinement for [CpCo(dmit)] **[8]** (Pbcn)

Empirical Formula	C8 H5 Co O S4
Formula weight	304.29
Wavelength	1.54184 A
Temperature	150 (2) K
Crystal system	Orthorhombic
Space group	Pbcn
Unit cell dimensions	a = 17.807(4) A $\alpha = 90^{o}$ b = 7.9654(16) A $\beta = 90^{o}$ c = 14.290(3) A $\gamma = 90^{o}$
Volume	2026.9(7) A^3
Number of reflections for cell	42 $(20 < \theta < 22^{o})$
Z	8
Density (calculated)	1.994 Mg / m^3
Absorption coefficient	20.644 mm^{-1}
F(000)	1216
Crystal description	Dark Needle

Crystal size	0.78 x 0.16 x 0.08 mm
θ range for data collection	4.97 to 69.95°
Index ranges	0<=h<=21, 0<=k<=9, 0<=1<=17
Reflections collected	2790
Independent refelctions	1812 [R(int) = 0.0276]
Scan type	ω - θ
Absorption correction	Psi-scans (Tmin=0.08, Tmax=0.77)
Solution	Direct (sir97)
Refinement type	Full-matrix least-squares on F^2
Program used for refinement	SHELXL - 97
Hydrogen atoms placement	Geometric
Hydrogen treatment	Riding
Data / restraints / parameters	1812 / 0 / 128
Goodness-of-fit on F^2	1.053
Conventional R [F.4sigma (F)]	R1 = 0.0741 [1180 data}
Weighted R (F^2 and all data)	WR2 = 0.2185
Extinction coefficient	0.00028(10)
Final Maximum delta / sigma	0.000
Weighting scheme	Calc w=1/{\s^2(Fo^2) + (0.1198P)^2 + 8.1328P} where P = (Fo^2 + 2Fc^2) / 3
Largest diff. Peak and hole	1.122 and –1.430 e.A^{-3}

Table A1.2.2 Selected bond lengths [Å] and angles [°] for [CpCo(dmit)] **[8]** (Pbcn)

Co(1) – C(3CP)	2.024(11)
Co(1) – C(2CP)	2.039(12)
Co(1) – C(1CP)	2.039(10)
Co(1) – C(5CP)	2.034(9)
Co(1) – C(4CP)	2.046(9)

Co(1) – S(2A)	2.125(3)
Co(1) – S(1A)	2.137(3)
C(1) – C(2)	1.347(13)
C(1) – S(1A)	1.717(8)
C(1) – S(1B)	1.755(10)
S(1B) – C(3)	1.7575(12)
C(2) – S(2A)	1.698(9)
C(2) – S(2B)	1.755(8)
S(2B) – C(3)	1.777(11)
C(3)-O(3)	1.213(11)
C(1CP) – C(2CP)	1.395(18)
C(1CP) – C(5CP)	1.404(15)
C2CP) – C(3CP)	1.413(17)
C(3CP) – C(4CP)	1.392(14)
C(4CP) – C(5CP)	1.423(13)
C(3CP) – Co(1) – C(2CP)	40.7(5)
C(3CP) – Co(1) – C(1CP)	67.5(5)
C(2CP) – Co(1) – C(1CP)	40.0(5)
C(3CP) – Co(1) – C(5CP)	40.7(5)
C(2CP) – Co(1) – C(5CP)	67.9(4)
C(1CP) – Co(1) – C(5CP)	40.3(4)
C(3CP) – Co(1) – C(4CP)	40.0(4)
C(2CP) – Co(1) – C(4CP)	68.1(4)
C(1CP) – Co(1) – C(4CP)	68.0(4)
C(5CP) – Co(1) – C(4CP)	40.8(4)
C(3CP) – Co(1) – S(2A)	97.2(3)
C(2CP) – Co(1) – S(2A)	112.4(4)
C(1CP) – Co(1) – S(2A)	150.6(4)
C(5CP) – Co(1) – S(2A)	157.3(3)
C(4CP) – Co(1) – S(2A)	117.0(3)

C(3CP) – Co(1) – S(1A)	168.5(3)
C(2CP) – Co(1) – S(1A)	138.1(5)
C(1CP) – Co(1) – S(1A)	105.3(4)
C(5CP) – Co(1) – S(1A)	100.9(3)
C(4CP) – Co(1) – S(1A)	129.7(3)
S(2A) – Co(1)- S(1A)	93.02(11)
C(2) – C(1) – S(1A)	120.4(8)
C(2) – C(1) – S(1B)	117.9(7)
S(1A) – C(1) – S(1B)	121.7(5)
C(1) – S(1A) – Co(1)	102.4(3)
C(1) – S(1B) – C3	96.1(5)
C(1) – C(2) – S(2A)	121.1(7)
C(1) – C(2) – S(2B)	116.8(7)
S(2A) – C(2) – S(2B)	122.1(5)
C(2) – S(2A) – Co(1)	103.1(3)
C(3) – S(2B) – C(2)	96.8(5)
O(3) – C(3) – S(2B)	123.4(8)
O(3) – C(3) – S(1B)	124.1(9)
S(2B) – C(3) – S(1B)	112.5(5)
C(2CP) – C(1CP) – C(5C)	108.8(10)
C(2CP) – C(1CP) – Co(1)	70.0(6)
C(5CP) – C(1CP) – Co(1)	69.6(5)
C(1CP) – C(2CP) – C(3CP)	107.1(10)
C(1CP) – C(2CP) – Co(1)	70.0(7)
C(3CP) – C(2CP) – Co(1)	69.1(6)
C(4CP) – C(3CP) – C(2CP)	109.3(11)
C(4CP) – C(3CP) – Co(1)	70.8(6)
C(2CP) – C(3CP) – Co(1)	70.2(7)
C(3CP) – C(4CP) – C(5CP)	107.7(10)
C(3CP) – C(4CP) – Co(1)	70.0(5)

C(5CP) – C(4CP) – Co(1)	70.0(5)
C(1CP) – C(5CP)- C(4CP)	107.7(10)
C(1CP) – C(5CP) – Co(1)	69.8(6)
C(4CP) – C(5CP) – Co(1)	69.9(6)

Appendix 1.3 Dmid ester [2]

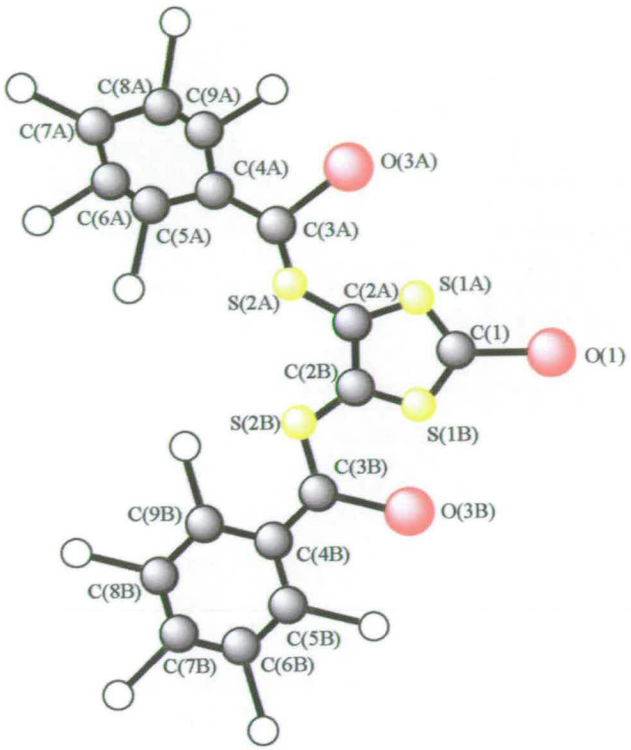

TableA1.3.1 Crystal data and structure refinement for dmid ester [2]

Empirical Formula	$C_{17}H_{10}O_3S_4$
Formula weight	390.49
Wavelength	0.71073 A
Temperature	150(2)
Crystal system	Monoclinic
Space group	C2/c
Unit cell dimensions	a = 35.6157(14) A $\alpha = 90^o$ b = 5.1975(2) A $\beta = 115.9840(10)^o$ c = 19.1419(7) A $\gamma = 90^o$

Volume	3185.2(2) A^3
Number of refelctions for cell	7372 ($2 < \theta < 27.5^o$)
Z	8
Density (calculated)	1.629 Mg / m^3
Absorption coefficient	0.610 mm^{-1}
F(000)	1600
Crystal description	Colourless block
Crystal size	0.48 x 0.16 x 0.16 mm
θ range for data collection	1.27 to 26.42°
Index ranges	-44<=h<=44, -3<=k<=6, -23<=1<=23
Reflections collected	9386
Independent refelctions	3275 [R(int) = 0.0202
Scan type	ϕ to ω scans
Absorption correction	Sadabs (Tmin = 0.641, Tmax = 0.935)
Solution	Direct (SHELXL – 97 (Sheldrick, 1990))
Refinement type	Full-matrix least-squares on F^2
Program used for refinement	SHELXL – 97
Hydrogen atoms placement	Refined freely
Hydrogen treatment	3275 / 0 / 258
Data / restraints / parameters	0.955
Goodness-of-fit on F^2	R1 = 0.0273 {2813 data]
Conventional R [F.4sigma (F)]	wR2 = 0.0695
Weighted R (F^2 and all data)	0.00049(17)
Final Maximum delta / sigma	0.000
Weighting scheme	Calc w=1/{\s^2(Fo^2) + (0.0.0460P)^2 + 0.0000P} where P = (Fo^2 + 2Fc^2) / 3
Largest diff. Peak and hole	0.384 and –0.300 e.A^{-3}

Table A1.3.2 Selected bond lengths [Å] and angles [°] for the dmid ester [2]

C(1) – O(1)	1.2067(19)
C(1) – S(1A)	1.7610(16)
C(1) – S(1B)	1.7794(16)
S(1A) – C(2A)	1.7410(15)
C(2A) – C(2B)	1.345(2)
C(2A) – S(2A)	1.7491(15)
S(2A) – C(3A)	1.8279(16)
C(3A) – O(3A)	1.1947(19)
C(3A) – C(4A)	1.485(2)
C(4A) – C(5A)	1.382(2)
C(4A) – C(9A)	1.390(2)
C(5A) – C(6A)	1.384(2)
C(6A) – C(7A)	1.383(2)
C(7A) – C(8A)	1.380(2)
C(8A) – C(9A)	1.384(2)
S(1B) – C(2B)	1.7527(15)
C(2B) – S(2B)	1.7531(15)
S(2B) – C(3B)	1.7939(15)
C(3B) – O(3B)	1.2059(18)
C(3B) – C(4B)	1.485(2)
C(4B) – C(9B)	1.393(2)
C(4B) – C(5B)	1.397(2)
C(5B) – C(6B)	1.378(2)
C(6B) – C(7B)	1.390(2)
C(7B) – C(8B)	1.382(2)
C(8B) – C(9B)	1.388(2)
O(1) – C(1) – S(1A)	124.30(13)
O(1) – C(1) – S(1B)	122.32(13)
S(1A) – C(1) – S(1B)	113.38(9)

C(2A) – S(1A) – C(1)	95.79(7)
C(2B) – C(2A) – S(1A)	118.35(11)
C(2B) – C(2A) – S(2A)	125.35(12)
S(1A) – C(2A) – S(2A)	116.30(9)
C(2A) –S(2A) – C(3A)	98.68(7)
O(3A) – C(3A) – C(4A)	125.25(14)
O(3A) – C(3A) – S92A)	120.70(12)
C(4A) – C(3A) – S(2A)	114.05(11)
C(5A) – C(4A) – C(9A)	119.41(15)
C(5A) – C(4A) – C(3A)	123.38(14)
C(9A) – C(4A) – C(3A)	117.21(15)
C(4A) – C(5A) – C(6A)	120.53(16)
C(7A) – C(6A) – C95A)	119.90(17)
C(8A) – C(7A) – C(6A)	119.89(16)
C(7A) – C(8A) – C(9A)	120.31(16)
C(8A) – C(9A) – C(4A)	119.97(16)
C(2B) – S(1B) – C(1)	95.76(7)
C(2A) – C(2B) – S(1B)	116.68(11)
C(2A) – C(2B) – S(2B)	118.58(11)
S(1B) – C(2B) – S(2B)	124.74(9)
C(2B) – C(2B) – C(3B)	104.65(7)
O(3B) – C(3B) – C(4B)	123.82(14)
O(3B) – C(3B) – S(2B)	122.30(12)
C(4B) – C(3B) – S(2B)	113.85(11)
C(9B) – C(4B) – C(5B)	119.46(14)
C(9B) – C(4B) – C(3B)	122.98(14)
C(5B) – C(4B) – C(3B)	117.56(14)
C(6B) – C(5B) – C(4B)	120.40(15)
C(5B) – C(6B) – C(7B)	119.91(15)
C(8B) – C(7B) – C(6B)	120.11(15)

C(7B) – C(8B) – C(9B)	120.25(15)
C(8B) – C(9B) – C(4B)	119.84(14)

Appendix 2.1 Dissociation of $Ag^{I}X$

For the Dissociation Constant of

$$Ag^{+} + X \Leftrightarrow AgX^{+}$$

where $K = \dfrac{a_{Ag^{+}} + a_{X^{-}}}{a_{AgX}}$

Here K is the Diffusion Coefficient and a is the activity of the ionic species in solution. Relating the electrochemical potential for this species to the activity of the ionic species in solution we find that

$$E = E^{\theta} + \frac{RT}{F} \ln K \frac{a_{AgX}}{a_{Ag^{+}} + a_{X^{-}}}$$

From this we get that

$$E = E^{\theta} + \frac{RT}{F} \ln K + \frac{RT}{F} \ln a_{AgX} - \frac{RT}{F} \ln a_{X^{-}}$$

We know that E^{ϕ} for the new couple when

$$a_{AgX} = a_{X^{-}} = a_{Ag^{+}} = 1$$

Therefore

$$E^{\theta}_{AgX/Ag} = E^{\theta}_{Ag/Ag^{+}} + \frac{RT}{F} \ln K$$

Where E^{θ} (Ag/Ag^{+}) is the electrode potential before addition of the ligand species X; E^{θ} (AgX/Ag) is the elecrode potential after addition of the ligand species X; R is gas constant; T is the temperature (K); F is the Faraday constant and K is the dissociation constant for the reaction described.

Appendix 3.1 **Mass Spectrum of the product of the irradiation of the [18]ane S_4N_2 ketone macrocycle [5] and reaction with $Na_2[Ni(mnt)_2]xH_20$ [11]**